Use of steel slag for carbon dioxide capture and utilisation

Thesis

Submitted in partial fulfillment of the requirements for the degree of

Doctor of Philosophy

of the

Indian Institute of Technology, Bombay, India

and

Monash University, Australia

by

Raghavendra Ragipani

Supervisors:

Prof. Akkihebbal K. Suresh (IIT Bombay)

Prof. Sankar Bhattacharya (Monash University)

The course of study for this award was developed jointly by
the Indian Institute of Technology, Bombay and Monash University, Australia
and given academic recognition by each of them.
The programme was administered by The IITB-Monash Research Academy

2019

Abstract

Carbon dioxide sequestration via carbonation of steel slags is a promising way of combining two waste products to produce value-added products such as precipitated calcium carbonate (PCC). PCC production via mineral carbonation is a multi-step process, which broadly includes calcium extraction into an aqueous solution and calcium carbonate precipitation. The shortcomings with mineral carbonation are associated with the extraction step and include slow extraction rate, poor extraction efficiency and selectivity of calcium from slag. The major impediments for seeking systematic improvements in these processes include poor understanding of leaching characteristics, the role of independent parameters that influence the dissolution rates, and concomitantly a lack of *a priori* dissolution models for heterogeneous residues such as steel slag.

In this thesis a systematic study has been carried out by generating *a priori* information necessary to determine the mineral carbonation potential, investigate avenues for process intensification of slag dissolution and PCC production, and develop kinetic model for slag dissolution. The work mainly focusses on batch experiments and mathematical modelling to understand the parametric effects on slag dissolution kinetics in various acidic media and PCC production via CO_2 pressure-swing carbonation.

The maximum potential for calcium extraction from BOF slag has been found to be 81.8%, which is in good agreement with the fraction of calcium present as orthosilicates. While mineral phase rich in trivalent elements such as Fe^{3+} and Al^{3+} is scantly leachable, the RO phase — which is a solid solution of FeO–MgO–MnO — has been found to be the main source of impurity in the form of iron and magnesium along with the silica from calcium silicate dissolution. The study proposes a new method to inhibit leaching of RO phase impurities (both Fe and Mg) by sodium molybdate addition to the acidic leaching agent. The proposed method is an alternative to the pH-swing, where only iron impurities are removed after the dissolution step.

The leaching characteristics of BOF slag observed in nitric acid, acetic acid and CO_2 environments show that calcium silicates dissolve congruently without leaving residual silica layer. Despite non-existence of any passivating layer, the increase in particle size resulted in lower calcium extraction efficiency in both nitric acid and acetic acid environments concurring with the observations reported in the literature, which indicates that effect of particle size cannot be singularly used to determine the controlling mechanism. Based on the initial elemental release rates, slag dissolution rate could be described by proton-promoted dissolution mechanism similar to the single (pure) silicates and oxides. The findings from parametric studies on slag dissolution suggest a strong influence of morphological features on relative surface area evolution of calcium due to selective leaching, which in turn was found to influence calcium extraction efficiency with variation in particle size. A surface reaction based kinetic model has been developed by considering the surface area evolution of RO phase globules by *sporulation model* (Adrover et al., 2004) and influence of proton activity described by Langmuir–Hinshelwood type rate law (Kline and Fogler, 1981). The model predictions with best-fit parameters have been found to match with experimental observations closely.

The pressure-swing carbonation experiments confirm high supersaturation with respect to calcite during dissolution step because of unfavourable calcite precipitation kinetics. The results show scope to substantially reduce the water volume and CO_2 pressure required for dissolution. Further, silica was observed to condense on the surface of PCC resulting in silica-PCC composite, which is expected to exhibit better mechanical properties (Lourenço et al., 2013).

Overall, the thesis adds to existing body of scientific knowledge pertaining to mineral carbonation of steel slag in significant ways, including explaining the dissolution characteristics consistent with the slag chemistry, proposing alternative to pH-swing for major impurity removal, demonstrating scope for improving the pressure-swing carbonation efficiency by reducing water requirement, and possibility to further value addition with silica-PCC composite production. The kinetic model brings one step closer to a priori dissolution model and aids in process intensification and reactor development studies.

Contents

List of Figures

List of Tables

Nomenclature

$> MOH$ Representation of surface metal oxide

$> SO^-$ Deprotonated surface oxide

$> SOH$ Representation for oxide at solid-liquid interface attached to the solid

ΔG_r Distance from equilibrium, or chemical affinity

ΔP Drop in reactor CO_2 partial pressure

ϵ Dielectric constant of the medium

η_{Ca} Selectivity of calcium in the leachate

γ Activity coefficient

Ω Solution saturation index

ψ Surface potential

ρ Density of slag particle

pH_{ZPC} pH corresponding to the point of zero surface charge

RO phase Mineral phase containing solid-solution of FeO-MgO-MnO

$\vec{r}, r_+$ Forward reaction rate

A_M Atomic number of element M

C Capacitance of double layer

d_{Ca} depth of calcium leaching; distance between reaction front and intial particle radius

d_{slag} slag diameter

E_a Activation energy

F Faradays constant

$F(D,t)$ Time dependent particle size distribution function

$g(I)$ effect of ionic strength on dissolution rate

I Ionic strength of the solution

K_a Acid dissociation constant

k_x general notation for rate constant

k_H Henry's law constant for CO_2

k_La Gas-liquid mass transfer coefficient

k_{SCa},k_{SFe},k_{SMg} Langmuir constant for dissolution of Ca, Fe and Mg respectively

K_{sp} Solubility product

K_w Water dissociation constant

P_{CO_2} Partial pressure of carbon dioxide

pO_2 Partial pressure oxygen

r reaction rate

$R(D)$ Growth rate pf particles

r_M Rate of dissolution of element M from the slag

r_{sp} Rate of sporulation of RO phase particles

S_{area} Surface area of particle

S_{RO} Surface area of RO phase particle

V_G Gas phase volume in the reactor

V_L Liquid volume in the reactor

X_{Ca} Fraction of calcium extracted

x_{Ca}, x_{Fe}, x_{Mg} mass fraction of calcium, iron and magnesium in slag

[M] Concentration of metal M

APC Air pollution control residue

C_2F Dicalcium ferrite

C_2S Dicalcium silicate

C_3S Tricalcium silicate

$CO_2 \cdot$ Saturated CO_2 concentration at the gas-liquid interface

{M} Activity of metal M

ACC Amorphous calcium carbonate

AOD slag Argon oxygen decarburization slag

BOF slag Basic oxygen furnance slag

CC slag Continuous casting slag

EAF slag Electric arc furnace slag

EDTA Ethylenediaminetetraaceticacid

GBFS slag Granulated blast furnace slag

H/S Acid-to-solid ratio in the slurry mmol/g

IAP Ionic activity product for $CaCO_3$

L/S Liquid-to-solid ratio in the slurry ml/g

LD slag Linz-Donawitz slag (same as BOF slag)

LF slag Ladle furnace slag

MEA	Monoethanolamine
NVT	moles (N), volume (V), and temperature (T)
PCC	Precipitated calcium carbonate
PS	Sample particle size
PSD	Particle size distribution
R	Universal gas constant 8.314 J/mol/K
S/L	Solid loading in the slurry wt%
TBP	Tributyl phosphate
TGA	Thermal gravimetric analysis

Declaration

I declare that this written submission represents my ideas in my own words and where others' ideas or words have been included, I have adequately cited and referenced the original sources. I also declare that I have adhered to all principles of academic honesty and integrity and have not misrepresented or fabricated or falsified any idea/data/fact/source in my submission. I understand that any violation of the above will be cause for disciplinary action by the Institute and can also evoke penal action from the sources which have thus not been properly cited or from whom proper permission has not been taken when needed.

Notice 1

Under the Copyright Act 1968, this thesis must be used only under the normal conditions of scholarly fair dealing. In particular no results or conclusions should be extracted from it, nor should it be copied or closely paraphrased in whole or in part without the written consent of the author. Proper written acknowledgement should be made for any assistance obtained from this thesis.

Notice 2

I certify that I have made all reasonable efforts to secure copyright permissions for third-party content included in this thesis and have not knowingly added copyright content to my work without the owner's permission.

Student Name: Raghavendra Ragipani

IITB ID: 1340240008

Monash ID: 25883186

Chapter 1

Introduction

Iron & steelmaking slags are alkaline solid residues generated during the process of crude steel production from iron ore and scrap metal (Figure 1.1). These residues are rich in Ca, Fe, Mg, Al and Si depending on the metallurgical process which generates the material. Significant amounts of these residues end up in landfills after limited use in cement production and construction industry. Apart from solid waste residues, iron & steel industries also contribute significantly (8–9%) to global anthropogenic CO_2 emissions. India is the third largest producer of crude steel and largest producer of direct reduced iron. Owing to the significant gap between per capita consumption in India (61 kg) and the world average of 208 kg, and sustained growth in crude steel demand, the crude steel production is expected to increase three-fold to 300 MT by 2030–31 (Ministry of Steel, 2017). Consequently, a proportional increase in various slag generation is expected. Presently, utilisation of iron and steel slags and reduction of carbon dioxide emissions are two main challenges for iron and steel industries.

1.1 Steel slag generation and utility

Globally, 70% of the crude steel is produced via basic oxygen furnace (BOF) route and the remaining from electric arc furnace (Figure 1.1). About 200 kg of BOF slag is generated per tonne of crude steel production from pig iron (Das et al., 2007). In major crude steel producing countries such as China and India, the current utilisation of steel slags is below 30% and the rest ends up in landfills (Guo et al., 2018; Chand et al., 2016). Generally, steel slags are used as aggregate in the construction industry and Portland cement production. However, their use in these industries is limited due to volume instability and relatively low

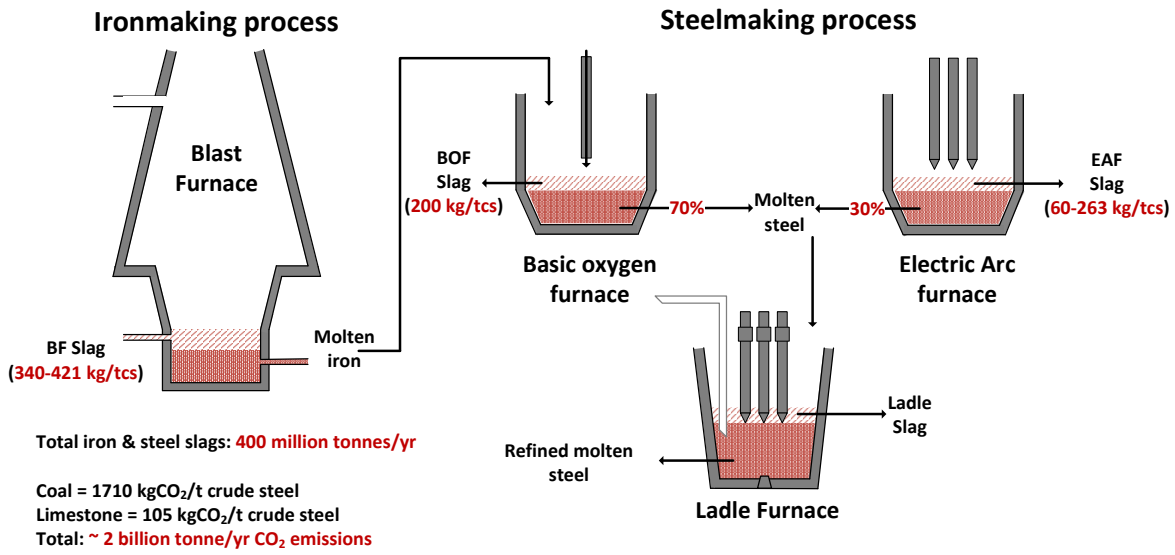

Figure 1.1: Schematic of iron and steel making processes (Data source:Das et al. (2007) and Carpenter (2012))

tricalcium silicate (C_3S) content, respectively (Dippenaar, 2005). Alternatively, steel slags can be used to chemically fix CO_2 as carbonates by a process called mineral carbonation (reaction 1.1), whereby the twin problems of slag utilisation and CO_2 emissions can be simultaneously addressed.

$$2\,CaO \cdot SiO_2 + 2\,H_2O + 2\,CO_2 \longrightarrow 2\,CaCO_3 + H_4SiO_4 \tag{1.1}$$

The carbonation of slag is also known to stabilise heavy metals from leaching and hence improve its utility as an aggregate. Additionally, by selective extraction and carbonation, steel slag can be valorised to value-added products such as precipitated calcium carbonate (PCC).

1.1.1 Precipitated calcium carbonate – production and use

High-purity precipitated calcium carbonate with narrow particle size distribution (0.5–3.5 μm) is used as a filler in printing and writing papers to improve optical properties such as paper brightness, and whiteness. In addition, use of fillers reduce the fibre content required for paper making. Currently, PCC is made from high quality limestone with low

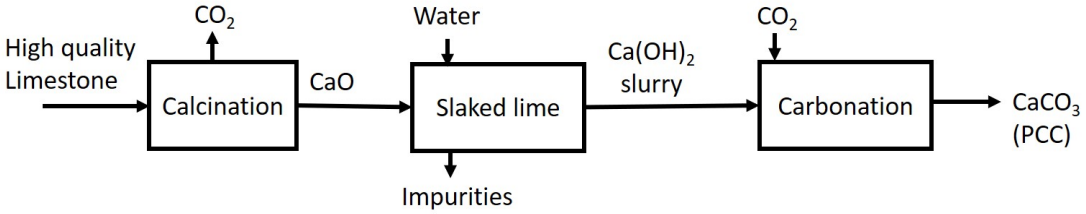

Figure 1.2: Conventional PCC production

Mg and Si content. Typical PCC production process is shown in Figure 1.2. Production of PCC from waste materials such as steel slag is an exciting opportunity with benefits of solid waste minimisation, CO_2 capture and lower reliance on high-quality limestone.

1.1.2 PCC production via mineral carbonation

Several mineral carbonation routes have been proposed with an aim to sequester carbon dioxide as shown in Figure 1.3. Among these, indirect mineral carbonation routes, involving selective calcium leaching and calcium carbonate production, allow PCC production. In addition, the iron-rich residual slag after calcium extraction can be recycled within the iron & steel industry and also has a prospective use in production of cathode precursor material (Shen and Forssberg, 2003; Wu et al., 2011).

Selective extraction of calcium from silicates is known to be a slow process. In order to accelerate the dissolution kinetics, processes using acidic leaching agents, severe particle size reduction, use of complexing additives, mechanical activation of feedstock, and so on are being actively investigated. Use of acidic leaching agents and non-selective leaching typically encountered in steel slag dissolution necessitate use of an intermediate step to swing the pH from acidic to basic conditions, wherein impurities were removed by precipitation besides favouring CO_2 absorption and calcium carbonate precipitation. Although slag-to-PCC generation is demonstrable, the commercialisation of process is limited by energy-intensive steps such as heavy particle size reduction, regeneration and recycling of acidic leaching agent and base used for achieving pH-swing, and lack of proven reactor technology. Major impediments for seeking systematic improvements in the processes include poor understanding of leaching characteristics and mechanistic explanations for the same. Problems with the understanding of steel slag dissolution

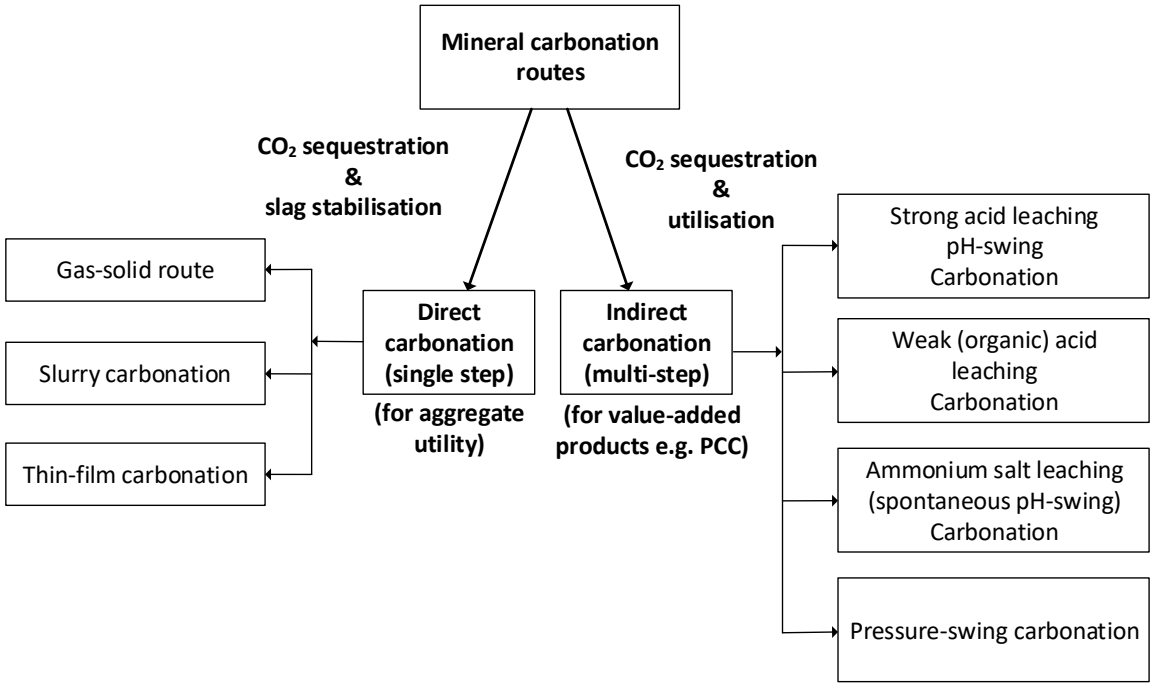

Figure 1.3: Mineral carbonation routes and PCC production

kinetics are associated with the difficulty in identification of the rate controlling step and a lack of kinetic models that consider the heterogeneous nature of steel slag.

1.2 Thesis objectives

The broad aim of the thesis is to undertake a systematic study to understand the dissolution characteristics of BOF slag in various acid environments, and PCC production from steel slag. The objectives involve: a) to characterise the steel slag, identify the leaching chemistry to generate *a priori* knowledge for process intensification and kinetic modelling, b) to investigate the dissolution characteristics of steel slag in various acidic media and CO_2 environment and determine the controlling mechanism and independent parameters that influence the kinetics, c) to model the dissolution kinetics based on *a priori* information generated, and d) investigate the PCC production potential via CO_2 pressure-swing carbonation.

1.3 Thesis organisation

Thesis has eight chapters in total. Chapter 1 is an introduction to the problem statement, describes the motivation, and objectives. In Chapter 2, literature related to various studies on mineral carbonation routes has been discussed at length by identifying the possibilities and problems. Further, current understanding of the mineral carbonation mechanism, factors influencing the dissolution rates and relevant mathematical models to describe the kinetics, progress made in development of mineral carbonation reactors are discussed. Chapter 3 describes the materials and methods employed in the study. In Chapter 4, characterisation studies performed to determine the elemental, mineralogical and physical characteristics of the LD slag used in this study are discussed. Further, relevant leaching characteristics of the slag have been studied to understand the dissolution behaviour, chemistry associated with the slag dissolution, and potential for calcium utilisation and CO_2 sequestration by mineral carbonation. In chapter 5, an extensive parametric study conducted to understand the influence of various operating parameters on calcium dissolution characteristics is discussed. A surface-complexing additive was proposed to reduce iron impurity in the leachate and compared it with the pH-swing method widely reported in the literature. Further, preliminary analysis of slag dissolution kinetics is reported. In chapter 6, production of PCC using pressure-swing carbonation was investigated. An opportunity to produce surface-modified PCC, which is expected to have greater value due to better mechanical properties is reported. In chapter 7, parametric modelling of multi-element dissolution phenomena is presented. Estimation of parameters and model validation are discussed. Chapter 8 summarises the thesis findings and proposes future work.

Chapter 2

Literature Review

The literature review covers extent of worldwide steel slag generation and their potential for carbon dioxide sequestration, various mineral carbonation routes proposed so far and their performance, and current state-of-art of reactor technology. Both the direct and indirect mineral carbonation routes have been extensively reviewed. The present chapter also presents a critical review on current understanding of dissolution mechanism, relevant mathematical models used to describe the dissolution kinetics. The review broadly covers models, which describe a) intrinsic dissolution kinetics, and b) structural aspects that affect the dissolution characteristics of solid particles. Lastly, a summary of the literature with identified gaps is presented.

2.1 Background

The mineral carbonation process was first proposed by Seifritz (1990), where CO_2 disposal by means of abundantly available silicates, which is similar to the natural weathering process, was put forward. It was proposed that the resultant hard water and silica could be safely drained deep into the ocean. Along similar lines, Kojima et al. (1997) suggested that the discharge of soluble bicarbonates into the deep ocean, where the water is undersaturated with respect to calcium carbonate (Stumm and Morgan, 2012), would maximise carbon dioxide sequestration. As shown in the reactions below, discharging onto the surface of the ocean may result in partial sequestration due to equilibration to carbonates and release of CO_2.

$$CaSiO_3(s) + H_2O + 2\,CO_2(g) \longrightarrow Ca^{2+} + SiO_2(s) + 2\,HCO_3{}^-$$

$$Ca^{2+} + 2\,HCO_3{}^- \rightleftarrows CaCO_3(s) + CO_2(g) + H_2O$$

Contrary to the notion of maximising CO_2 sequestration, which has been mentioned earlier,Lackner (2003) suggested that mineralisation of carbon dioxide (also referred to as carbon dioxide mineralisation) to insoluble carbonates is suitable for safe and permanent disposal of CO_2. Further, insoluble carbonates can be easily stored and its environmental impact can be confined to a specific site unlike water-soluble bicarbonates that are drained into the ocean. In addition to these factors, when the possibility of product utilisation is considered, it is preferable to convert CO_2 to carbonates.

Lackner et al. (1995) made an extensive assessment of various mineral feedstocks that are rich in calcium and magnesium oxides, because these elements form stable carbonates and are environmentally neutral. Further, based on the exothermicity of MgO/CaO carbonation, it was suggested that the overall energy requirement would be minimal, and the process was expected to be constrained by slow kinetics (reactions that occur on geological time scales). Kojima et al. (1997) evaluated the rates of CO_2 consumption for various silicates and suggested that increasing the surface area of naturally occurring silicate minerals could accelerate the sequestration and balance the rate of CO_2 generation. Considering thermodynamic constraints, especially for Mg-rich minerals, Lackner et al. (1997) suggested the use of aggressive operating parameters such as temperature, CO_2 pressure, use of acids for dissolution and so on, in addition to the reduction of the grain size to overcome the slow kinetics. Various estimates of power requirements for pulverisation show that the parasitic energy losses because of grinding are as high as 25–50% of the total power consumption (Kakizawa et al., 2001; Penner et al., 2004; Katsuyama et al., 2005), which suggests that heavy particle-size reduction may reduce net CO_2-capture benefits. The problem of accelerating the kinetics is being pursued through selection of feedstocks such as alkaline industry-derived wastes (discussed below) which are more reactive; exploring various mineral carbonation routes and enhancement strategies (discussed in Section 2.2); and improving the current understanding of the dissolution mechanism (discussed in Sections 2.4, 2.5, and 2.6).

Industrial wastes and mineral carbonation potential Calcium based alkaline industry-derived wastes (CAIDW) such as various slags from iron and steel industries, fly ash from power plants, and recycled concrete and waste cement from the construction industry are being investigated for mineral carbonation for the following reasons:

- Industry-derived wastes possess higher reactivity than their natural analogues (Huijgen et al., 2005)
- These industries make a significant contribution to anthropogenic CO_2 emissions, which makes them suitable points of CO_2 source; for instance, iron and steel industries contribute about 6-7% towards total CO_2 emissions (Doucet, 2010)
- There are environmental concerns that are related to heavy metal leaching in landfills (Huijgen and Comans, 2006)
- CO_2 emissions that are associated with the quarrying of natural minerals for mineral carbonation can be avoided Huijgen et al. (2005)

Among various wastes, steel slags from steelmaking industries are being actively investigated for CO_2 mineralisation due to desirable features such as high calcium content (as CaO > 35%), the presence of highly reactive free lime (as high as 12%) (Yildirim and Prezzi, 2011), and consequent high alkalinity. Worldwide annual production of steel slags is as high as 350 million tonnes and could save up to 170 millions tonnes of CO_2 per annum (Doucet, 2010).

2.2 Mineral carbonation routes

This section describes the proposed routes for mineral carbonation. It also describes the reported sequestration capacities, suitable operating conditions, and reaction kinetics and its enhancement.

2.2.1 Direct gas-solid route

Lackner et al. (1995) first described the gas-solid route in which silicates that are rich in alkaline earth metals could be carbonated at a high temperature, because the process is expected to be extremely slow at atmospheric conditions. Carbonation experiments on steel slag (Tian et al., 2013) and air pollution control (APC) residues (Baciocchi et al., 2006; Ghacham et al., 2016) showed that conversion is negligible at temperatures below 300 °C. Further increase in temperature to 400 °C accelerated the rate and resulted in 60 % conversion of the APC residue in 6 hours (Baciocchi et al., 2006). Similarly, in

the case of steel slag, the rate of carbonation increased 70 times when the temperature was increased from 400 to 600 °C (Tian et al., 2013). These experiments demonstrated the strong influence of temperature on the gas-solid reaction kinetics. As the reaction is exothermic, carbonation at elevated temperatures would not be detrimental to the energy economics of the process (Lackner et al., 1995). Zevenhoven and Kavaliauskaite (2004) performed exergy analysis of the process at 350 °C with magnesium-based minerals as feedstock and showed a net heat release of 1.5 kJ per kg of stored CO_2. However, there exists a thermodynamic limit on the maximum carbonation temperature (dependent on CO_2 pressure), because free CO_2 is more stable than carbonates at very high temperatures (Lackner et al., 1995; Zevenhoven et al., 2002). In the case of steel slag that contains C_2F ($Ca_2Fe_2O_5$), C_2S (β-Ca_2SiO_4) and free lime (CaO) at 1 bar CO_2 partial pressure, Santos et al. (2012b) observed an optimal temperature (830–850 °C) that was just below the carbonate decomposition temperature (850 °C). Under these conditions, only free lime was the major reacting component, while the reactivity of other phases such as C_2F was found to be negligible. When the maximum carbonation temperatures of CaO, C_2S, C_2F and MgO under 1 atm CO_2 partial pressure, which are 861, 400, 664 and 400 °C, respectively(Santos et al., 2012b), are taken into account, it appears that complete carbonation of all phases is not feasible at any selected temperature. Thus, the gas-solid route at low CO_2 partial pressure appears to be unsuitable for feedstocks such as steel slag, which contains multiple phases (especially C_2S and C_2F); however, those feedstocks that contain large amounts of free lime or portlandite can be successfully carbonated (Tian et al., 2013). Besides carbonate stability, an increase in temperature was observed to reduce the surface area in steel slag (Yu and Wang, 2011) and APC residue (Prigiobbe et al., 2009) by pore structure modification and sintering (Tian et al., 2014). However such effects were largely noticed during sample pre-heating (Prigiobbe et al., 2009). Whether the rate of surface area modification is fast enough to significantly reduce the rate of carbonation has not been investigated in earlier studies.

The influence of CO_2 partial pressure to enhance carbonation of steel slags and APC residues by the gas-solid route were studied in the range of 0.05–1 atm (Yu and Wang, 2011; Prigiobbe et al., 2009; Tian et al., 2013) and 4–20 bar (Santos et al., 2012b). Under CO_2 partial pressures lower than 1 atm, Tian et al. (2013) reported a modest increase in the extent of carbonation (45.9 to 52.5%) of steel slag with an increase in

CO_2 partial pressure at 600 °C, while experiments by Yu and Wang (2011) did not show a definite trend to conclude any improvement. In the case of the APC residue, Prigiobbe et al. (2009) reported a significant increase in the initial rate of carbonation (till 50% conversion) at 350 °C; however, the overall extent of carbonation was reported to be marginally lower at higher pressure. In contrast to these experimental findings at sub-atmospheric pressures, Santos et al. (2012b) observed a strong effect of CO_2 partial pressure on steel slag carbonation at a low temperature (350 °C), where CO_2 uptake increased 176% when the CO_2 pressure was increased from 4 to 20 bar. However, no appreciable effect of CO_2 partial pressure was observed on the extent of carbonation at a higher temperature of 650 °C. The influence of CO_2 partial pressure on the extent of carbonation is expected to be dependent on the relative importance of surface reaction and diffusional contributions (Bhatia and Perlmutter, 1983). Experiments on pure CaO by Bhatia and Perlmutter (1983) showed that carbonation proceeded through a surface reaction-controlled step followed by a diffusion-controlled step. In the former regime, CO_2 partial pressure showed a linear dependence on the rate of carbonation, while the latter regime, which is expected to be solid-state diffusion, did not show any influence of CO_2 pressure.

Furthermore, several studies showed that gas-solid carbonation can be enhanced by the presence of water vapour (Nikulshina et al., 2007; Reddy et al., 2010; Ukwattage et al., 2013; Ko et al., 2015; Kalinkin et al., 2005; Santos et al., 2012b; Montes-Hernandez et al., 2012) and SO_2 (Tian et al., 2013). In the case of CaO carbonation, Nikulshina et al. (2007) noted that the addition of water vapour resulted in a carbonation rate that was 22 times faster than dry CaO at 400 °C. Reddy et al. (2010) observed that 16% moisture provided the best results for fly ash carbonation at a low temperature of 60 °C. Although moisture was observed to promote carbonation, the mechanism behind the process is not clearly understood. For instance, Kalinkin et al. (2005) and Montes-Hernandez et al. (2012) suggested a catalytic activity of H_2O, while Ukwattage et al. (2013) and Ko et al. (2015) suggested that Ca leaching to the surface is enhanced in the presence of moisture. Santos et al. (2012b) suggested that enhancement in solid-state diffusivity through intermediate hydroxylation could be a major reason, without ruling out the possibility of catalytic activation. Reddy et al. (2010), based on experiments at low temperature (60 °C), attributed the effect to the formation of carbonic acid in the presence

of moisture. Tian et al. (2013) studied the effect of SO_2 on steel slag carbonation and found that the rate of carbonation could be enhanced by SO_2 in the diffusion-controlled regime. The effect was attributed to surface activation in which the rate of carbonation improved by 3.8 times as the concentration of SO_2 increased from 1 to 151 ppm, which led to an overall improvement in the efficiency of carbonation by 7.8%.

Currently, research on gas-solid carbonation is not being actively pursued due to low conversion and uncertainty about economic viability. However, several questions of scientific importance, especially those related to establishing the controlling mechanism and quantifying the influence of various operating parameters, are yet to be answered convincingly.

2.2.2 Direct aqueous route

Direct aqueous carbonation, which is also referred to as slurry carbonation, is a single stage process that involves the absorption of CO_2 into alkaline slag slurry for $CaCO_3$ precipitation. Because of the single stage operation, the process is suitable for permanent sequestration of carbon dioxide without the separation of product ($CaCO_3$) for utilisation (Yuen et al., 2016). Unlike gas-solid carbonation, which is very slow in the carbonation of silicates (Kojima et al., 1997), the aqueous route can potentially reach 100% conversion with dicalcium silicate as feedstock, as has been reported by Shtepenko et al. (2006) and Santos et al. (2009).

The process involves three reaction steps (Yan et al., 2013; Huijgen et al., 2006; Fernández Bertos et al., 2004a) : 1) the dissolution of CO_2 in water; 2) the release of Ca or Mg from solid matrix into the solution, which involves hydration and ionisation (Santos et al., 2013a); and 3) the reaction of Ca or Mg with carbonate or bicarbonate ions to form a carbonate precipitate.

CO_2 absorption:

$$CO_2(g) + H_2O \rightleftharpoons H^+ + HCO_3^-$$

$$HCO_3^- \rightleftharpoons H^+ + CO_3^{2-}$$

Overall carbonation reaction (for calcium silicate):

Dissolution: $CaSiO_3 + 2\,CO_2 + H_2O \rightleftharpoons Ca^{2+} + 2\,HCO_3^- + SiO_2$

Precipitation: $Ca^{2+} + CO_3^{2-} \longrightarrow CaCO_3(s)$

The dissolution reaction, which involves the release of Ca^{2+} or Mg^{2+} from silicates into the solution, is generally favoured under acidic conditions; while the precipitation of carbonate is favourable under basic conditions. Since both these steps occur in a single step, the roles of the solution chemistry and the operating conditions are significant. Optimal conditions for the process, however, appear to differ based on the mineral composition. For instance, experiments that were performed at a sub-atmospheric pressure by using a silicate feedstock showed a carbonation yield that was below 20%, while those feedstocks that contained lime could be carbonated up to 85% (Uibu et al., 2011). The possible reasons for the poor carbonation efficiency of silicates include 1) sub-optimal operating conditions, 2) inert Ca/Mg phases or dispersion of reactive Ca/Mg in less reactive phases, and 3) inhibition of calcium extraction into aqueous solution by a passive layer formation (Bodor et al., 2013; Santos et al., 2012a; Pan et al., 2016).

Parametric studies for optimal conditions

The slurry carbonation process has been extensively investigated in a variety of reactors over a wide range of temperatures (20–225 °C), CO_2 partial pressures (up to 150 bar), and liquid-to-solid ratios (1.5 to 1000 ml/g) to understand carbonation behaviour and determine the favourable conditions. Table 2.1 shows the list of reported studies along with operating parameters.

Effect of temperature Huijgen et al. (2005) investigated the effect of temperature on steel slag carbonation and reported a strong positive effect on the efficiency of carbonation up to 200 °C, which was found to be optimal. Further increase in temperature, however, led to lower extent of carbonation. The presence of an optimal temperature was attributed to the opposing effects of the mineral dissolution rate which increases with temperature and CO_2 solubility and reduces with an increase in temperature (Huijgen et al., 2005; Yan et al., 2015). At higher temperatures, besides the lower solubility of CO_2, thermodynamics of overall carbonation reaction is negatively impacted (Huijgen et al., 2005; Gerdemann et al., 2003). Similar trends of carbonation efficiency with different optimal temperatures were reported for wollastonite (Yan et al., 2013; Huijgen et al., 2006), Mg-silicates(Gerdemann et al., 2003; Yan et al., 2015), and other industrial residues (Chang et al., 2011a; Ukwattage et al., 2016).

Table 2.1: Reported studies on direct aqueous mineral carbonation

Study	**Feedstock**	**Reactor**	**Temp.** [°C]	**Press.**[bar]	**L/S** [ml/g]	**Addtives**
Huijgen et al. (2005)	steel slag	Batch	25–225	1–30	2–20	-
Huijgen et al. (2006)	wollastonite	Batch	25–225	1–40	2–10	-
Béarat et al. (2006)	olivine	Batch	185	135	NS	$0.64\,\mathrm{M}\,NaHCO_3 + 1\,\mathrm{M}\,NaCl$
Gerdemann et al. (2007)	olivine, wollastonite, serpentine	Batch	RT–250	up to 250	6.7	$0.64\,\mathrm{M}\,NaHCO_3 + 1\,\mathrm{M}\,NaCl$
Bonenfant et al. (2008)	EAF slag, LF slag	Batch	20	atm	10	-
Lekakh et al. (2008a)	EAF slag, LMF Slag	Batch	RT	atm	8.33	-
Jarvis et al. (2009)	olivine	Batch	185	135	NS	$0.64\,\mathrm{M}\,NaHCO_3 + 1\,\mathrm{M}\,NaCl, 5.5\,\mathrm{M}\,KHCO_3$
Krevor and Lackner (2009)	serpentine	Batch	120	20	333	NaCl, NH_4Cl, sodium citrate, sodium oxalate, sodium EDTA and sodium acetate.
Chang et al. (2011a)	steel making slags	Batch	40–160	48.2 and 89.6	0–100	-
Chang et al. (2011b)	steel making slags	Bubble column	25	1	10	-
Uibu et al. (2011)	oil shale ash, EAF and LF slags	Batch	RT	atm (15% CO_2)	10	-
Bonfils et al. (2012)	lizardite	Batch	120	20	4 and 333	Sodium oxalate
Bodor et al. (2013)	$Ca_2MgSi_2O_7, Ca_7Mg(SiO_4)_4, Ca_4Si_2O_7F_2$, β-C_2S, γ-C_2S, $Ca_3Mg(SiO_4)_2, Ca_2Fe_2O_5$, BOF, AOD, CC slags, CaO, MgO	Batch	90	20	80	-
Pan et al. (2013)	BOF slag	Rotating packed bed	RT	1 (30% CO_2)	20	Cold rolling water
Yan et al. (2013)	wollastonite	Batch	80–200	20–60	10	-
Santos et al. (2013b)	AOD slag , CC slag	Batch	20–250	0–60	4–40	-
Santos et al. (2014a)	CaO, AOD slag, CC slag, wollastonite, APC residue, BOF slag	Batch	50	1	100	Magnesium chloride hexahydrate
Pan et al. (2014)	steel slag	Batch	40–90	1	2	0–10% NaOH
Bodénan et al. (2014)	peridotites, lherzolite, Ni-pyrometallurgical slag	Batch	180	10–20	11.1	$0.7\,\mathrm{M}\,NaCl, 0.43\,\mathrm{M}\,NaCl + 0.27\,\mathrm{M}\,NaHCO_3$
Yan et al. (2015)	wollastonite, serpentine, olivine	Batch	80–200	20–60	10	0.6 M $NaHCO_3$
Tamilselvi Dananjayan et al. (2015)	coal flyash	Batch	RT	2–10	2–20	-
Pan et al. (2016)	BOF slag	Bubble column	30–70	1	5–20	-
Ukwattage et al. (2016)	BOF slag	Batch	20–80	30	0.25–3	-
Polettini et al. (2016)	BOF slag	Batch	60	5 (40% CO_2)	5	-

NS: Not specified; Temp. = Temperature; Press. = Pressure; L/S = Liquid to solid ratio; RT = Room temperature; atm = atmospheric pressure

Effect of CO_2 partial pressure In general, the CO_2 partial pressure was reported to have a positive influence on the overall carbonation efficiency (Huijgen et al., 2005). As mentioned earlier, at sub-atmospheric conditions, the carbonation yield was a meagre 20% with silicates as feedstock. At elevated CO_2 partial pressures, about 75% of the feedstock could be carbonated within a reaction time of less than an hour (Huijgen et al., 2005). Most studies reported an optimum pressure for carbonation, which varied based on the feedstock and the composition of the carbonating gas. For instance, 9 bar was found be optimum for BOF and CC slags (Huijgen et al., 2005; Santos et al., 2013b), 4 bar for CFA(Tamilselvi Dananjayan et al., 2015) and 15 bar for AOD slag(Santos et al., 2013b). Yan et al. (2013) noted that an increase in the synthetic flue gas pressure from 20 to 60 bar reduced the carbonation efficiency of wollastonite, while pure CO_2 showed the opposite trend. The decrease in the overall extent with increase in pressure, including the case of the synthetic flue gas containing H_2S, was attributed to poor carbonate precipitation efficiency due to the reduction in the slurry pH. On the other hand, the enhancement that was observed at pressures below optimum was attributed to the increased solubility of CO_2 (Huijgen et al., 2005; Santos et al., 2013b), while Huijgen et al. (2005) considered it an improved mass transport effect, and Eikeland et al. (2015) attributed it to a reduction in the pH, which enhances dissolution. However, these effects were not de-convoluted.

Effect of L/S ratio : Several experimental studies showed that decreasing the L/S ratio improved the carbonation efficiency. In the case of steel slag, Huijgen et al. (2005) observed a reduction in carbonation efficiency when L/S was varied from 2 to 20 kg/kg. The authors hypothesised that the improvement in the carbonation efficiency at low L/S was a consequence of higher ionic strength. Similar trends in the carbonation yield were reported for CFA (Ukwattage et al., 2013, 2014) and C_2S (Shtepenko et al., 2006). Béarat et al. (2006) attributed the improvement in carbonation efficiency when solid loading was increased to resultant particle abrasion.

Presence of inert phases

Bodor et al. (2013) experimentally studied the carbonation extent of various synthetic mineral phases that are present in industrial residues such as steel slag. It was observed that, under intense carbonation conditions, the most common mineral phase calcium

silicate C_2S reached a maximum of 87% of conversion. In the case of other (Ca, Mg) silicates, Bredigite showed a near complete conversion while in Åkermanite nearly 40% remained uncarbonated. The Fe-rich calcium silicate phase, Srebrodolskite, was found to be least susceptible and carbonated to only 22% efficiency. Poor reactivity of iron-containing phases, despite milling, was also reported for Portland cement (Shtepenko et al., 2006; Mahoutian et al., 2014), and steel slags (Huijgen et al., 2005; Mahoutian et al., 2014). Mahoutian et al. (2014) reported poor reactivity of aluminium-rich calcium silicate (gehlenite). In addition to these differences in the carbonation susceptibilities of various silicates, the reactivity of the mineral phases was also found to vary across residues, highlighting the complexity that is associated with the materials that contain multiple phases. For instance, merwinite was carbonated reasonably well in CC slag (Santos et al., 2013b), while it remained unreacted in AOD slag (Mahoutian et al., 2014; Santos et al., 2013b). Furthermore, Bodor et al. (2013) noted that a comparison of synthetic minerals and mineral phases present in waste residues showed mixed trends. For instance, Srebrodolskite and C_2S exhibited higher reactivity in industrial residues in comparison to synthetic minerals, while Bredigite, which was the most reactive among the synthesised phases, did not carbonate completely in the AOD slag. The dispersion of reactive phases in an inert material, grain size, secondary mineral precipitation and formation of silica-rich layers were posited to be the reasons for the varying reactivity (Bodor et al., 2013).

Formation of a passivating layer

Several studies have speculated that surface passivation is the major reason that limits 100% carbonation.This hypothesises the formation of a passivating layer such as silica (Béarat et al., 2006; Daval et al., 2011; Andreani et al., 2009; Santos et al., 2014a, 2013a; McKelvy et al., 2006; Julcour et al., 2015; Eikeland et al., 2015), calcite (Tamilselvi Dananjayan et al., 2015; Chang et al., 2012, 2011b; Mo and Panesar, 2013; Pan et al., 2013), or both (Huijgen et al., 2005, 2006; Daval et al., 2009b; Jarvis, 2008). It has been hypothesised that the silica layer forms either by incongruent dissolution, which leads to a residual layer, or by re-precipitation after attaining saturation. Though the silica layer is generally thought to be passive, some studies (Daval et al., 2009a; Béarat et al., 2006) reported the occasional presence of calcite and magnesite within the nano-sized pores

of the silica layer, which indicates that it is permeable to reactive species. Also, when silica is formed by incongruent dissolution, condensation of neighbouring Si-OH groups to Si-O-Si linkages may lead to cracking and coarsening of porosity (Borges et al., 2010; Daval et al., 2009a; Béarat et al., 2006). Nevertheless, the properties of the silica layer may not be ubiquitous, because their nature (formation as silica gel or phyllosilicate) is understood to depend on the parent mineral phase and the operating conditions (Bodor et al., 2013; Bodénan et al., 2014; Daval et al., 2011). Based on the currently available experimental observations, it is suspected that the silica layer plays an important role in passivating the surface (Daval et al., 2011).

Studies that have hypothesised passivation by carbonates referred to surface precipitation of the calcite layer (Shtepenko et al., 2006; Daval et al., 2009b; Chang et al., 2011a) or to pore filling of micro- to nano-sized pores (McKelvy et al., 2006; Huntzinger et al., 2009; Daval et al., 2009b). It was observed that calcite nucleated on the silicate surface as islands and continued to grow and merge into a thick surface layer. However, it was noted that the leaching continues to occur through the fractures (caused due to the accumulation of stress) despite the loss of porosity (Ruiz-Agudo et al., 2013). Stockmann et al. (2014) studied the dissolution of various calcium and magnesium-rich minerals in a calcium-rich leachate and found that the precipitation of a thick layer does not impede the dissolution rates. Further, it is interesting to note that the Mg-silicates exhibit similar carbonation characteristics as Ca-silicates although the magnesite precipitation does not happen on the surface (Huijgen et al., 2006), with the exception of its occasional appearance in the micro-pores of the silica-rich layer, as mentioned previously.

Enhancement of direct aqueous carbonation

In order to enhance the reaction rate and the extent of carbonation, several strategies including the use of additives and the employing of physical and chemical methods to destroy the passivating layer were investigated.

Use of inorganic and organic additives: In the case of Mg-silicate, the addition of inorganic additives such as $NaCl + NaHCO_3$ to the solution enhanced the reaction rate and the overall conversion (O'Connor et al., 2001). Observed enhancement in carbonation was thought to be due to their pH-buffering ability. Liu and Maroto-Valer (2010), in their

study on brine carbonation, observed that 1 M NaCl + 0.6 M $NaHCO_3$ acted as a buffer by resisting pH change at 7.7 for several days (under the tested conditions). Further, the use of only NaCl did not prove to be effective, which confirms any direct influence of alkali cations (McKelvy et al., 2006; Eikeland et al., 2015). Along similar lines, Prigiobbe (2010) suggested that the addition of inorganic salts (NaCl, $NaNO_3$) improved carbonation of APC residues only to the extent of the pH changes that were observed, without any direct influence on the dissolution rates. Other studies, however, suggested that the enhancement may not be entirely due to the pH effect, which was based on the observation that higher partial pressure of CO_2 lowers the pH almost equally in both distilled water and $NaHCO_3$ solution (Chen et al., 2006b). Jarvis et al. (2009) suggested that high bicarbonate activity promoted exfoliation of the passivating layer and enhanced Mg dissolution. In addition, higher carbonate ion concentration (by a factor of 10^5) led to the precipitation of the carbonate at a very low concentration of Mg ions (Chen et al., 2006b; Jarvis et al., 2009). The rate of carbonation reached a plateau at bicarbonate ion concentration above its saturation index (McKelvy et al., 2006; Jarvis et al., 2009). Additionally, a higher concentration of carbonate may negatively affect the CO_2 absorption due to the salting-out effect and may decrease the dissolution rate due to the reduced hydration (Jarvis et al., 2009). Despite the success with Mg-silicates, the extent of the use of bicarbonate additives with Ca-silicates was limited (Gerdemann et al., 2003). In one study by Gerdemann et al. (2003), in which wollastonite was used as feedstock at 150 bar and 185 °C, the use of a bicarbonate buffer solution resulted in lower carbonation rate compared to the rate when distilled water was used. Experiments on wollastonite by Yan et al. (2015) at 40 bar and 150 °C in a bicarbonate solution showed only a marginal improvement in conversion as compared to distilled water.

Based on works related to natural waters and weathering phenomena, it has been long established that organic ligands promote dissolution of silicates by ligand-promoted dissolution in addition to the proton-promoted mechanism. Krevor and Lackner (2009) studied the influence of different organic salts (mentioned in Table 2.1) on silicate dissolution under 120 bar CO_2 pressure and 120 °C; they showed that citrate, EDTA and oxalate enhanced the rate and led to 100% dissolution of the minerals. However, it is not very clear if the enhanced dissolution resulted in overall carbonation efficiency. For instance, Bonfils et al. (2011) reported that earlier observations on the enhancement of carbonation by

using oxalate was observed only in a low solid concentration in which Mg precipitated as oxalate salt instead of carbonate. Further investigations by Bonfils et al. (2012), in which solid by-product of Mg did not form when EDTA and citrate were used, did not yield any significant improvement in carbonation extent; this suggested strong complexation of the Mg ion in an aqueous solution.

Removal of surface passivation: Several studies experimented on physical and chemical ways to remove any passivating layer and to improve the carbonation efficiency. Pan et al. (2014) used 0–10% NaOH as an additive in steel slag carbonation to relegate calcite precipitation and induce aragonite precipitation, which does not cover the surface of the residual slag unlike calcite. However, an improvement in the carbonation was noticed up to 4% NaOH, in which the precipitate contained both calcite and aragonite. Béarat et al. (2006) reported that, in the case of olivine, increasing the solid loading results in mechanical abrasion that is assisted by particle-particle collisions, and promotes carbonation by breaking the passive layer. Based on this lead, Bodénan et al. (2014) and Julcour et al. (2015) demonstrated high carbonation efficiency for olivine mineral carbonation in a stirred bead mill that contained alumina beads as the grinding material. It was shown that the synergistic effect increased the carbonation extent to as high as 78% as against the 7% without the grinding media. Experiments with other Mg-silicates showed improvements of a similar magnitude. Santos et al. (2013a) investigated the effect of ultrasound on direct aqueous carbonation reactions of AOD and CC slags, and observed that the use of ultrasound resulted in carbonation enhancement to the tune of 63% (30 % to 49%) in the case of the AOD slag and 20% (61% to 73%) in the case of the CC slag. The enhancement was thought to be due to the removal of the passive layer. Araizi et al. (2016) studied the effectiveness of ultrasound in the enhancing of the carbonation of APC residues, ladle slag, and cement bypass dust. They found that ultrasound induced a significant reduction in the particle size and improved carbonation only at a high L/S ratio (50–100 kg/kg), while the effect was insignificant at a low L/S ratio (0.2–0.6 kg/kg). It was hypothesised that sonication enhanced CO_2 absorption rate at high L/S ratio due to cavitation phenomenon. Additionally, sonication was shown to result in complete conversion of reactive phases such as lime and portlandite, while non-sonicated samples showed incomplete conversion. The average mean diameter of

the sonicated slurry was lower than non-sonicated slurry leading to higher conversion. In addition, sonication influenced the morphology of the precipitated calcium carbonate (round morphology observed). The study, however, did not attribute the enhancement to the exfoliation of the passive layer.

2.2.3 Thin-film carbonation

Thin-film carbonation emerged as a process route that was based on the optimum L/S that was observed in the direct aqueous route under stationary conditions. Based on gas-solid and direct aqueous carbonation routes, it emerged that water is essential for solvation and hydration reactions (Reddy et al., 2009; Baciocchi et al., 2011; Han et al., 2014); however, excess water was found to be detrimental to CO_2 mass transport and carbonate precipitation (Fernández Bertos et al., 2004a; Shtepenko et al., 2006). Further, optimal humidification is dependent on the heat of the reaction which leads to sample dry-out. In order to maintain the humidification, the ground alkaline reactant is wet to paste and carbonated under humidified CO_2 gas. Typically, the liquid-to-solid ratio is maintained at less than 1.5.

Thin-film carbonation, also referred to as wet carbonation, was mainly investigated for accelerated carbonation of building materials to induce high strength (Fernández Bertos et al., 2004a; Shtepenko et al., 2006) and toxic waste material stabilisation (Fernández Bertos et al., 2004a,b; Gunning et al., 2010). Fernández Bertos et al. (2004a) determined an optimum L/S of 0.06-0.2 kg/kg to achieve high strength in carbonated products. For CO_2 sequestration, thin-film carbonation on steel slags (Zingaretti et al., 2014; Baciocchi et al., 2011, 2015; Polettini et al., 2016), stainless steel slags (Salman et al., 2014; Santos et al., 2013b; Zingaretti et al., 2014; Baciocchi et al., 2009) and other alkaline waste materials (Gunning et al., 2010; Baciocchi et al., 2010) has been extensively investigated.

2.2.4 Indirect mineral carbonation routes

Indirect mineral carbonation is a multi-step dissolution and precipitation process with scope for production of value-added products such as precipitated calcium carbonate (PCC). Lackner et al. (1995) first described the indirect route using hydrochloric acid as a leaching agent. The process involved the leaching of Mg from olivine using HCl to form

magnesium chloride in solution. Further, consumed HCl is regenerated by decomposition of magnesium chloride to magnesium hydroxide precipitate that can be carbonated (as shown in the reaction scheme below).

$Mg_3Si_2O_5(OH)_4 + 6\,HCl \longrightarrow 3\,MgCl_2 + 2\,SiO_2 + 5\,H_2O$ After evaporation,

$MgCl_2 \cdot 6\,H_2O(solid) \longrightarrow Mg(OH)Cl(solid) + HCl(gas) + 5\,H_2O\,(gas)$

$2\,Mg(OH)Cl(solid) \xrightarrow{H_2O} Mg(OH)_2(solid) + MgCl_2\,(aq)$

The process is more complex than direct aqueous carbonation but attractive as the rates of individual steps are expected to be fast. However, recovery and regeneration of acid is a concern (Lackner et al., 1995). In the current section, studies in which various leaching agents such as mineral acids, organic acids, complexing salts and the like were used to assess the overall carbonation potential and generation of PCC are reviewed.

Use of organic acids

Considering the acid dissociation constant (pKa) of organic acids, Kakizawa et al. (2001) proposed the use of acetic acid as a leaching agent because both the dissolution and carbonation reactions are expected to occur spontaneously. Subsequently, several studies (Table 2.2) were conducted to investigate the efficacy of various organic acids, and the influence of the operating parameters on calcium extraction and on calcium carbonate precipitation. Teir et al. (2005, 2007) studied the feasibility of the acetic acid process to produce PCC from wollastonite and steel-making slag. Further, Eloneva et al. (2008a,b, 2009) studied the use of other feedstock materials such as BF slag, EAF slag, converter slag, and AOD process slag with the same objectives as Teir et al. (2007).

Baldyga et al. (2011) compared the dissolution of wollastonite in acetic acid and dicarboxylic acids (adipic and succinic acids) and reported that the dicarboxylic acids accelerate wollastonite dissolution compared to monoprotic acetic acid. On the contrary, the results of Zhao et al. (2013) indicated that acetic acid showed greater acceleration than many other multiprotic acids. The study, however, did not test adipic acid and succinic acid. The study concluded that the acceleration is dependent on the initial pH, the activity of the chelating agent, the stability constant, and the solubility of the resultant Ca-salt in the solution. Further, oxalic acid was found to be slower than other organic acids due to poor solubility of calcium oxalate. Mun et al. (2017) reported similar results for oxalic acid leaching of waste cement. Ghoorah et al. (2014a) showed that

formic acid dissolved better than acetic acid and DL-lactic acid. Bao et al. (2010) used tributyl phosphate (TBP) along with acetic acid to produce PCC from steel slag. The process aimed at the recovering and recycling of acetic acid in addition to the improving of selectivity. The study reported selective leaching of calcium and magnesium with 75% and 30% efficiency when the acid-to-solid ratio was maintained below 0.5 g/g.

Precipitation of calcium carbonate was carried out either by direct injection of high-pressure CO_2 or low-pressure precipitation that was assisted by the addition of a basic solution to correct the pH. Kakizawa et al. (2001), who experimented with a calcium acetate solution under a 5–50 bar CO_2 pressure, showed that the calcium conversion to carbonate during crystallisation is less than 20%. Eloneva et al. (2008b) observed that bubbling CO_2 at atmospheric conditions into a calcium acetate solution yielded just 3% of the theoretical yield. Similarly, Jo et al. (2012) reported poor CO_2 absorption by leachate that was obtained from acetic acid dissolution of waste concrete. Thermodynamic calculation by Eloneva et al. (2008a) revealed that a maximum conversion of 4% or 22% is possible at 1 bar and 30 bar CO_2 pressure. Experiments with the addition of NaOH proved to be successful in achieving the maximum amount of precipitation albeit at a very high additional process cost. Alternatively, instead of carbonating by using CO_2, Zhao et al. (2013) attempted the use of potassium carbonate for precipitation, while Song et al. (2017) used CO_2 loaded MEA for PCC precipitation. Santos et al. (2014b) reported a case of the use of succinic acid to enhance dissolution, where calcium succinate was found to precipitate instead of calcium carbonate.

The cost of CO_2 capture was estimated to be $ 200/ton by Kakizawa et al. (2001), which translates to a PCC production cost of $ 88/ton without any purification cost. A more recent estimate of PCC production from steel slag by Eloneva et al. (2008b), was estimated to be €550/ton because of expensive NaOH, which was used for pH adjustment. In addition, separation of iron, magnesium and aluminium was needed to ensure PCC purity in the case of steel slag (Teir et al., 2007).

Table 2.2: Reported studies on indirect aqueous mineral carbonation using organic acids

Study	**Feedstock**	**Dissolution**				**Precipitation**	
		Organic acid	**Temp.** [°C]	**Acid conc.** [M]	**L/S** [ml/g]	**CO_2 press** [bar]	**Temp.** [°C]	**pH swing**
Kakizawa et al. (2001)	Wollastonite	Acetic acid	60	21 (wt%)	4.8	5–50	40–80	No
Teir et al. (2007)	GBFS, Converter slag, EAF slag, AOD slag, Wollastonite	Acetic acid	30–70	0-33.3(wt%)	59.5	-	-	-
Eloneva et al. (2008b)	GBFS	Acetic acid	70	20 vol%	20	atm, 30	30–70	No, NaOH
Eloneva et al. (2008a)	Steel converter slag	Acetic acid	30–70	0–8	NS	10–100% v/v	30	No, NaOH
Olsen and Donald Rimstidt (2008)	Forsterite olivine	Oxalic acid	25	0–0.35	20	-	-	-
Eloneva et al. (2009)	GBFS, desulphurized slag, converter slag	Acetic acid, propionic acid	20	0.1–2	50	-	-	-
Bao et al. (2010)	Steelmaking slag	Acetic acid with TBP	40–94	0.998, 1.466	NS	-	-	-
Ptáček et al. (2010)	Fibrous Wollastonite	Acetic acid	22–50	3	80	-	-	-
Baldyga et al. (2011)	Wollastonite	Acetic acid, adipic acid, succinic acid	40–80	3.66, 0.1–0.16, 0.5–0.7	4.85–149	30–70	60–100	No
Tinchana et al. (2012)	Steelmaking slag	Acetic acid	70	0–2	10	15% v/v	-	-
Jo et al. (2012)	Waste concrete, lime, portland cement	Acetic acid	25	1	5	1	RT	No
Zhao et al. (2013)	Wollastonite	Acetic acid, nitriloacetic acid, picolinic acid, iminodiacetic acid, EDTA, gluconic acid, pthalic acid, citric acid, ascorbic acid, glutamic acid, oxalic acid	22	0.0015–0.006, 1	-	NA	22, 82	K_2CO_3
Park et al. (2013)	Steel slag, Tail-wollastonite, waste cement, fly ash	Acetic acid	25–90	0–27 (wt%)	100	-	-	-
Santos et al. (2014b)	GBFS	Succinic acid, acetic acid	80	0.5	7.31	2–50	60, 120	No, NaOH, $NaHCO_3$
Ghoorah et al. (2014b)	Serpentines	Formic acid	80	0.1	200	-	-	-
Ghoorah et al. (2014a)	Wollastonite	Formic acid, DL-lactic acid, acetic acid	22–80	0.1, 5.0	172, 250	-	-	-
Chiang et al. (2014)	GBFS	Acetic acid	30	0.5–2.0	7.31	6–40	90–120	NaOH, $NaHCO_3$
Song et al. (2017)	Blast furnace slag	Acetic acid	10–30	0–30 %v/v	50	NA	RT	CO_2-MEA
Mun et al. (2017)	Waste cement, BF slag	Acetic acid, oxalic acid, citric acid	25	0.1	10	1	25	NaOH
Bilen et al. (2017)	Steelmaking slag	Acetic acid	22–80	0.1–1.0	9–26	1	30–70	NaOH

NS= Not specified; NA = Not applicable; Temp. = Temperature; Press. = Pressure; L/S = Liquid to solid ratio; RT = Room temperature; atm = atmospheric pressure; GBFS = Granulated BF slag

Table 2.3: pH-swing reaction chemistry along with the recovery of ammonia

Step	**Reaction**
CO_2 capture	$2\,NH_3 + CO_2 + H_2O \longrightarrow (NH_4)_2CO_3$
Mineral dissolution	$CaO \cdot SiO_2 + 2\,NH_4HSO_4 \longrightarrow CaSO_4 + SiO_2 + H_2O + (NH_4)_2SO_4$
	$FeO \cdot SiO_2 + 2\,NH_4HSO_4 \longrightarrow FeSO_4 + SiO_2 + H_2O + (NH_4)_2SO_4$
	$MgO \cdot SiO_2 + 2\,NH_4HSO_4 \longrightarrow MgSO_4 + SiO_2 + H_2O + (NH_4)_2SO_4$
pH adjustment	$NH_4HSO_4 + NH_4OH \longrightarrow (NH_4)_2SO_4 + H_2O$
Impurity precipitation	$(FeMg)SO_4 + 2\,NH_4OH \longrightarrow (FeMg)(OH)_2 + (NH_4)_2SO_4$
Carbonation	$CaSO_4 + (NH_4)_2CO_3 \longrightarrow CaCO_3 + (NH_4)_2SO_4$
Regeneration	$(NH_4)_2SO_4 \longrightarrow NH_4HSO_4 + NH_3$

pH-swing processes

Park and Fan (2004) proposed a pH-swing scheme in which multiple high-purity products such as iron oxide and magnesium carbonate could be recovered from the acid leachate. The process involves sequential precipitation of byproducts by increasing the pH of the acidic leachate through the addition of ammonia solution (NH_4OH). Subsequently, highly soluble alkaline earth metal ions are carbonated by injecting CO_2. Park and Fan (2004) studied the process using an organic acid and a strong-acid ammonium salt (NH_4HSO_4). Subsequently, Wang and Maroto-Valer (2011b,a, 2013); Dri et al. (2013, 2014) extended the use of NH_4HSO_4 as leaching agent and 35% ammonia in water (NH_4OH) as pH regulator that had an ammonia recovery scheme (Table 2.3). The process suggests precipitation of impurities such as $Fe(OH)_2$ and $Mg(OH)_2$ in the pH range of 8.2–8.3 (Dri et al., 2014). As apparent from the published results for steel slags, the calcium carbonated product obtained by this process contained significant Fe, Mg and Si impurities. Further, the carbonation was shown to be incomplete and had significant amounts of calcium sulphate in the product. Alternatively,Kodama et al. (2008) proposed a spontaneous pH-swing scheme that had a neutral ammonium salt NH_4Cl as opposed to acidic NH_4HSO_4. At the end of Ca leaching from steel slag, the pH of the leachate was 9.4 in the case of NH_4Cl in comparison to NH_4HSO_4, in which it remained highly acidic. Further, calcium forms a soluble chloride instead of the sparingly soluble calcium sulphate. The selectivity of calcium that was obtained after extraction step by using NH_4Cl was as high as 0.996 while the recovery was 59.5% (Kodama et al., 2008). A comparison of NH_4Cl as leaching agent with HCl and CH_3COOH shows the superiority of the NH_4Cl process in terms of fewer impurities, and high end-point pH that is suitable for spontaneous carbonate

precipitation at the cost of lower Ca recovery (Kodama et al., 2008). The process reported a predominantly calcite morphology and a 98% purity of the precipitate. Eloneva et al. (2012); Mattila et al. (2012); Said et al. (2013); Jo et al. (2014) made a comparative study of the efficiency of other ammonium salts such as CH_3COONH_4, and NH_4NO_3 in calcium extraction from steel slag and recycled concrete (refer to Table 2.4 for other pH-swing studies). All these studies suggest that extraction efficiency is higher in NH_4NO_3 and CH_3COONH_4 than in NH_4Cl. The process appears to be promising in the production of high-purity PCC; however, the recovery of ammonia from the extraction step remains a concern (Kodama et al., 2008). Although the estimated power requirement was shown to be lower than that of the conventional amine absorption process (Kodama et al., 2008), detailed economics for the process has not yet been worked out.

Table 2.4: Reported studies on indirect aqueous mineral carbonation using pH swing scheme

Study	**Feedstock**	**Dissolution**			**Precipitation**		
		Leaching agent	**Temp.** [°C]	**L/S** [ml/g]	**pH swing**	**Carbonation**	**Temp.** [°C]
Park and Fan (2004)	Serpentine	1 vol% orthophosphoric acid + 0.9 wt% oxalic acid + 0.1 wt% EDTA, 1.4 M NH_4HSO_4	70	NS	NH_4OH	1 atm CO_2	RT
Kodama et al. (2008)	Steel slag	NH_4Cl	40–90	NS	Spontaneous	13 vol% CO_2	80
Eloneva et al. (2009)	steel converter slag, BF slag, ladle slag, desulphurisation slag	CH_3COONH_4, NH_4NO_3, NH_4Cl	20	50	Spontaneous	1 atm CO_2	30, 70
Wang and Maroto-Valer (2011b)	Serpentine	1.4 M NH_4HSO_4	100	20	35 wt% NH_3 water	NH_4HCO_3	60
Wang and Maroto-Valer (2011a)	Serpentine	NH_4HSO_4	80–100	NS	35 wt% NH_3 water	NH_4HCO_3	85
Mulopo et al. (2012)	Steel slag	HCl	25	NS	NH_4OH	1 atm CO_2	25
Mattila et al. (2012)	Steel slag	NH_4Cl, NH_4NO_3	20–70	10–50	Spontaneous	1 atm CO_2	20–70
Eloneva et al. (2012)	Steel slag	CH_3COONH_4, NH_4NO_3, NH_4Cl	RT	1.6–50	-	-	-
Wang and Maroto-Valer (2013)	Serpentine	NH_4HSO_4	100	3.3, 5	35 wt% NH_3 water	NH_4HCO_3, $(NH_4)_2CO_3$	80
Dri et al. (2013)	Steel slag, recycled concrete	NH_4HSO_4	25–90	20	-	-	-
Said et al. (2013)	Steel slag	CH_3COONH_4, NH_4NO_3, NH_4Cl	30	10–200	Spontaneous	1 atm CO_2	30
Dri et al. (2014)	steel slag, GGBS, phosphorus slag	NH_4HSO_4	50	20–66.7	NH_4OH	$(NH_4)_2CO_3$	65
Jo et al. (2014)	Waste cement	CH_3COONH_4, NH_4NO_3, NH_4Cl, $(NH_4)_2SO_4$	20	20	Spontaneous	15 vol% CO_2	20
Hall et al. (2014)	Steel slags	NH_4Cl	RT	10	-	-	-
Teir et al. (2016)	Steel slag	NH_4Cl	60	NS	Spontaneous	22 vol% CO_2	60
de Carvalho Pinto et al. (2016)	Steel slag	NH_4Cl	85	20	Spontaneous	$NaHCO_3$, Na_2CO_3	25, 60
Mun et al. (2017)	Waste cement, BF slag	NH_4Cl	25	10	Spontaneous	1 atm CO_2	25
Van der Zee and Zeman (2017)	Waste concrete fines	HCl	NS	NS	$Ca(OH)_2$	Na_2CO_3	NS

NS= Not specified; NA = Not applicable; Temp. = Temperature; Press. = Pressure; L/S = Liquid to solid ratio; RT = Room temperature; atm = atmospheric pressure; GGBS = Ground granulated BF slag

Pressure-swing carbonation

Iizuka et al. (2004) proposed the pressure-swing carbonation route by which calcium from waste cement was first extracted into aqueous solution under CO_2 pressure, and then the obtained leachate was precipitated at a low pressure. Considering the higher solubility of calcium carbonate under high CO_2 pressure, significant amounts of calcium can be dissolved in an aqueous solution. However, the process requires a high water volume (L/S of 350 ml/g) or a large recycle of residual waste cement at a low liquid-to-solid ratio (L/S of 40 ml/g), which results in significant process cost (Katsuyama et al., 2005). The study reported only 80% of PCC in unseeded precipitation while precipitation with a large amount of seeding (2.5 wt%) resulted in 98% purity. The study did not characterise the PCC or report the nature of the impurities. Lee et al. (2012) experimented with air-cooled blast furnace slag by using a pressure up to 5 MPa CO_2. The calcium extraction efficiency was 30% and the precipitation efficiency was reported to be nearly 100%. The study, however, did not characterise any impurities in the precipitate, except for whiteness. Abe et al. (2013) compared the dissolution of calcium and magnesium from recycled concrete with naturally occurring minerals such as wollastonite, olivine, and phlogopite. The extraction of calcium from recycled concrete was 60.5%, while the fastest among the tested rock samples, wollastonite, yielded 12%. The extraction of magnesium from rocks under CO_2 pressure was very poor with less than 1% of total extraction.

2.3 Proposed reactors for mineral carbonation

Several reactor concepts have been proposed for the realisation of a commercial plant for *ex-situ* accelerated mineral carbonation process. Reddy et al. (2009) proposed a fluidised-bed reactor to capture and mineralise the point source CO_2 by using an industrial waste such as coal fly ash. A pilot study that was conducted by using the humidified stack gas of a power plant and coal fly ash showed 30% reduction in CO_2 at an approximate cost of \$11/t-CO_2. Stolaroff et al. (2005) proposed a spray chamber carbonation scheme by which alkaline water from a spray chamber that contains a steel slag bed is sprinkled back to facilitate CO_2 absorption from the air. The process is a derivative of the thin-film carbonation route and the study estimated \$8/t-CO_2 as the cost of CO_2 capture. Similarly, Morales-Flórez et al. (2011) suggested artificial weathering pools in which feedstock is

disposed as a film in shallow ponds for carbonation. The process involves the maintaining the solid-to-liquid ratio and the surface-to-volume ratio, which could lead to an efficiency that is high as 88% in the case of calcium hydroxide waste obtained from the acetylene industry. The progress of the reaction was, however, found to be limited by the formation of a floating calcite layer which resists CO_2 absorption. Penner et al. (2004) proposed a high-temperature, high-pressure pipeline flow-loop reactor for slurry carbonation. The process demonstrated enhanced reactivity in comparison to the stirred autoclave but had several design challenges such as clogging of the reactor and excessive wear and tear of components. Chang et al. (2012); Pan et al. (2013) proposed the use of a rotating packed bed for both the direct and indirect carbonation processes. A rotating packed bed is expected to improve the mass transfer rates due to high centrifugal forces and micro-mixing. With BOF slag as feedstock, Chang et al. (2012) reported that a very high conversion of 93% was achievable in the reactor. However, the energy requirement associated with the reactor rotation is high and is considered to be a drawback in the process (Pan, 2012). The total power requirement was 707 kWh/t-CO_2, which leads to a total capture cost of \$57/t-CO_2(Pan et al., 2013). Iizuka et al. (2012) demonstrated a bench-scale operation of a series of extraction and crystallisation reactors to produce high-purity calcium carbonate from the concrete sludge. The results indicated that it was necessary to improve the process parameters such as Ca extraction ratio (which was less than 30% after five series extractions), solid/liquid separation for scale-up to a commercial plant. Currently, the technological status of the *ex-situ* accelerated mineral carbonation process is in demonstration and at a pilot stage; the lack of proven reactor technology options is one of the major reasons for the absence of commercial deployment (Sanna et al., 2014).

2.4 Studies on dissolution kinetics of silicates

From the perspective of direct aqueous and indirect routes of mineral carbonation, the kinetics of metal ions leaching from oxides and silicates and the overall dissolution of the mineral were found to be important (Section 2.1). This section presents the literature that is related to the general characteristics of silicate dissolution, the experimentally determined rates of Ca/Mg leaching from oxides and silicates, and studies on the determining

of the controlling mechanism.

2.4.1 Dissolution behaviour of silicates

Silicates, which are the major constituents of alkaline industrial wastes and naturally occurring minerals, exist in multiple forms and have a varying number of bridging oxygens (number of oxygen atoms shared by silica tetrahedra), and structural arrangements such as chain, sheet, layered, cyclic etc., (Terry, 1983b). Depending on these two parameters, the acids dissolve the silicates either by a complete breakdown (congruent dissolution) or by the partial decomposition of the silicate structure by rapid leaching of cations leading to the formation of a leached layer (incongruent dissolution) (Terry, 1983b). For instance, orthosilicates in which silica tetrahedra are not directly linked by bridging oxygen bonds, dissolve completely by the breaking of metal-oxygen bonds without the necessity to break the stronger Si—O bonds. Further, Casey (1991) showed that the rate of dissolution of mineral oxides and corresponding orthosilicates are comparable. Also, the dissolution rates of various orthosilicates can be correlated to the rate of cation hydration, which indicates a direct influence of the cation-oxygen bond. Such a property was found to be true for most cations, which suggests the possibility to predict dissolution rates (Casey and Westrich, 1992). The dissolution of Si from silicates with bridging oxygen atoms, such as in chain-silicates, may occur incongruently and subsequently the resultant surface hydroxyl groups might undergo polymerisation reactions to form a porous silica layer (Casey et al., 1993). Though the formation and the role of such leached layers on the overall mineral dissolution continue to be debated (Schott et al., 2012), the rate of metal ions that are released by proton exchange from these silicates is expected to be comparable to the single oxides (Oelkers, 2001). In the next section, experimental data reported on leaching rates of Ca/Mg from silicates will be discussed.

2.4.2 Experimental studies on Ca/Mg dissolution rates

Thus far very few attempts have been made to compile the metal release rates from various minerals, whereas Si release rates were often examined in weathering studies. Kojima et al. (1997) experimentally determined the Ca/Mg leaching rates of various naturally occurring minerals in the presence of CO_2 under near neutral conditions (pH

range of 5–7). Wollastonite, a chain silicate that is known to show exceptionally high dissolution rates (Casey et al., 1993), was found to exhibit a rapid Ca leaching rate (log rate of -10.7 mol/cm^2/s) while Mg from talc (sheet silicate known for its poor reactivity) was observed to leach at rates lower by only an order of magnitude (log rate of -12.1 mol/cm^2/s). While the observed Ca release rate from wollastonite can be shown to be comparable to dissolution rates from orthosilicates (after extrapolating the rate data at pH of 2 reported by Casey and Westrich (1992) to pH 5–6), Mg release rates from talc and other minerals reported by Kojima et al. (1997) are greater by at least an order of magnitude—suggesting a large variation from the dissolution rates of orthosilicates. In another study on Wollastonite by Weissbart and Rimstidt (2000), Ca dissolution (log) rates in the pH range of 2–6 were found to be as low as -12.05 mol/cm^2/s. Similarly, an order of magnitude difference exists in MgO dissolution rates reported at pH 2 by Casey (1991) and Fedoročková and Raschman (2008), log rates of -7.2 and -8.8 mol/cm^2/s, respectively. In essence, it appears that a significant variation exists in the reported rate data. Additionally, as Rimstidt et al. (2012) suggested, the lack of ability to correlate the reactive sites to the geometric or to the BET surface could be the primary reason besides differences in sample preparation and solution composition, which is seen in various studies.

2.4.3 Determination of the rate controlling step

Early works on the dissolution of silicates led to the understanding that a rapid exchange of cations with proton results in the formation of a metastable surface layer (typically a hydrated layer) and product layers on the original reactant surface(Helgeson, 1971). Further, the observation of parabolic kinetics during mineral dissolution prompted the use of the shrinking core type models with product diffusion controlling the rate. However, further investigations using microscopy and spectroscopic techniques cast doubts over the existence and influence of such layers on the dissolution kinetics. In addition to these studies, experiments by Holdren and Berner (1979) showed that the presence of ultra-fine particles leads to parabolic trends instead of the expected linear dissolution curve for a surface reaction controlled system. This prompted a switch to surface reaction controlled models where the rate is thought to depend on solution pH and the effective surface area (Aagaard and Helgeson, 1982). Further evidence for and against the existence of a silica

passivating layer and consequently mass transport limitations continued to be reported in the literature (Chou and Wollast, 1984; Daval et al., 2011). In addition, a sustained effort is being made to decipher whether the silica layer forms due to incongruent dissolution or through dissolution coupled with the re-precipitation(Casey et al., 1993; Ruiz-Agudo et al., 2012; Hellmann et al., 2012).

In the mineral carbonation studies, determination of rate limiting process was largely carried out based on the integrated form of shrinking core models (Lekakh et al., 2008a; Dri et al., 2013; Nikolić et al., 2016), based on morphological changes observed through electron microscopy (Huijgen et al., 2005; Marini, 2006), and depending on the estimated activation energy values (Ghoorah et al., 2014a). As pointed out by Helgeson and Murphy (1983), owing to similarities in the form and within the experimental errors, the use of integrated rate equation allows for alternative interpretations of the rate determining step. Liddell (2005) also put forward a similar observation in a case study using shrinking core models. In the study on the dissolution of wollastonite using various organic acids, Ghoorah et al. (2014a) interpreted different control regimes (mass transfer limited and surface reaction limited kinetics) based on activation energy. However, the rate of wollastonite dissolution in the two cases varied by a factor of less than 2. Based on such small difference in rates for diffusion limited and surface limited kinetics, existence of a singular controlling regime is not conceivable as the assumption that one of these steps is fastest and the other do not influence rate would be invalid. When the complexity that is associated with the process, which could potentially involve precipitation of secondary phases, is taken into account, distinguishing whether the kinetics is controlled by mass transport or the surface reaction remains a difficult task in the absence of a definite methodology. As described by Brown et al. (2008), a surface reaction-controlled process may be dependent on multiple factors such as defect density, interaction among adsorbate molecules, intrinsic properties of minerals (for example, differences in isoelectric point), solution pH, types of functional groups, structural differences that are associated with various mineral surfaces, and influence of organic and bio-film coatings on the mineral surface. Models that have been proposed to describe the intrinsic kinetics of mineral dissolution are presented in the next section (2.5).

2.5 Models for intrinsic kinetics

Models that have been proposed to describe the surface reaction-controlled kinetics (equivalently described as proton-promoted or ligand-promoted dissolution) are discussed in this section.

2.5.1 Adsorption

One of the early intensive studies on the effect of strong acids on silicate dissolution was conducted by Kline and Fogler (1981). The study showed that the dissolution could be modelled as a sum of uncatalysed and acid catalysed reactions. Further, the acid catalysed dissolution was modelled using Langmuir–Hinshelwood kinetics where the overall reaction rate is given by Equation (2.1).

$$r = r_0(1 + P_C \frac{Ka_H}{1 + Ka_H}) \tag{2.1}$$

where r, r_0 are the overall reaction rate and the uncatalysed reaction rate, respectively. P_C is the maximum fraction by which the dissolution can be catalysed.

Wieland et al. (1988) observed that the surface protonation (represented by adsorbed H^+) on several oxides (MO) is non-Langmuirian in nature, possibly due to long range electrostatic interactions. Further, it was shown that the Frumkin–Fowler–Guggenheim isotherm (Frumkin equation) could better represent the surface protonation data. This equation was also shown to be similar to the constant capacitance surface complexation model that is described in the next section (2.5.3). Furthermore, at a pH lower than pH_{ZPC} by at least 1 unit, the Freundlich master isotherm (Equation 2.3) is shown to fit experimental data within a factor of 2.

$$\begin{aligned} [H^+] &= K^s_{a1} \frac{x_h}{1 - x_h} \exp(2w.x_h/RT) \\ x_h &= \{> MOH_2^+\}/S \\ r &= k_h \{> MOH_2^+\}^i \end{aligned} \tag{2.2}$$

$$r = k_h \frac{K^i_F [H^+]^n}{[H^+]^n_{ZPC}} \tag{2.3}$$

2.5.2 General model for mineral dissolution

Aagaard and Helgeson (1982) formulated the general rate equation which was based on the strong dependency of the mineral dissolution rate on the pH, temperature, and surface area. By using the transition state theory, the formulation (Equation 2.4) tried to explain the dissolution rates at both far-from-equilibrium conditions and the near-equilibrium condition by including the influence of chemical affinity.

$$r = ks(\prod_i a_i^{-n_{i,j}})(1 - \exp(-A/\sigma RT)) \tag{2.4}$$

Blum and Lasaga (1988) were not convinced by the use of the transition state theory to describe the kinetics because of the lack of a mechanistic description for variable and fractal reaction orders, which are very commonly encountered in silicate dissolution. Instead, rates were assumed to dependent on the surface-coordinated complex that formed due to the adsorption of reacting species. Dissolution under acidic conditions is described by the following equation (2.5),

$$r = kc_{2HX}^{1.0} \tag{2.5}$$

where c_{2HX} is the surface concentration of the exchange sites that are occupied by $2H^+$.

Wieland et al. (1988) combined the surface-coordination chemistry with lattice statistics and activated complex theory. This model answers the observed dependence of the rate on higher orders of the protonated surface. Lattice statistics was shown to provide a necessary framework for the estimation of probabilities of the geometric arrangement of the surface site. The rate of dissolution is given by,

$$r = kx_a P_j S \tag{2.6}$$

where, x_a denotes the mole fraction of the active sites, P_j is the probability of finding a specific site in the coordinative arrangement of the precursor complex, and S represents the surface concentration of sites.

Lasaga et al. (1994) further suggested that effect of deviation from equilibrium $f(\Delta G_r)$ may not be linear as obtained from the transition state theory and proposed a general

form for the overall dissolution equation.

$$r = k_0 A_{min} \exp\left(-Ea/RT\right) X_{H^+_{ads}}^{n_{H^+_{ads}}} \prod_i X_{i_{ads}}^{n_i} f(\Delta G_r) g(I) \tag{2.7}$$

where, $g(I)$ is the effect of ionic strength on the rate of mineral dissolution.

Largely, the concentration of adsorbed species was determined by using the Langmuir isotherm, which cannot account for electrostatic interactions and interaction among adsorbed species.

2.5.3 Surface complexation

Surface complexation models describe the equilibria of surface groups based on mass balance and mass-action equations. Based on the solution chemistry, the formation of surface complexes can be described and in turn explain the surface charging phenomenon observed in the oxides (Westall, 1980). These models essentially include long-range electrostatic interactions along with the short-range chemical potentials and explain phenomena such as adsorption, colloid stability and chemical reactions at surfaces (Westall, 1986). Different descriptions of surface complexation models arise with the differences in describing the surface/solution interface (description of the electric double layer) and relating the surface potential to surface charge (Westall, 1980).

Surface complexation for a diprotic surface group $>SOH_2{}^+$ is as follows,

Surface equilibrium reactions:

$$>SOH_2{}^+ \overset{K_{a1}}{\rightleftharpoons} >SOH + H^+$$
$$>SOH \overset{K_{a2}}{\rightleftharpoons} >SO^- + H^+$$

Surface charge:

$$\sigma = F\frac{V_L}{S}([>SOH_2{}^+] - [>SO^-]) \tag{2.8}$$

Surface equilibrium constants:

$$\begin{aligned} K_{a1} &= K^0_{a1} \exp\left(F\psi/RT\right) = \frac{[>SOH][H^+]}{[>SOH_2{}^+]} \\ K_{a2} &= K^0_{a2} \exp\left(F\psi/RT\right) = \frac{[>SO^-][H^+]}{[>SOH]} \end{aligned} \tag{2.9}$$

Balance of surface sites:

$$\frac{N_s S}{N_A V_L} = [>\mathrm{SOH_2}^+] + [>\mathrm{SOH}] + [>\mathrm{SO}^-] \tag{2.10}$$

Surface charge (σ)- surface potential (ψ) relationship based on electrostatic model:

$$\sigma = f(\psi) \tag{2.11}$$

Various electrostatic models for the oxide-solution interface have been described in detail by Westall and Hohl (1980). Among them, the triple-layer model that involves three planes (surface, inner-Helmotlz plane (IHP) and outer-Helmoltz plane (OHP)) is shown to describe a wide range of datasets, but requires large sets of data from surface titrations(Hayes et al., 1991). Alternatively, depending on the influence of ionic strength on the surface equilibrium, simpler models can be used. At high ionic strength (I), the triple-layer model collapses into the constant capacitance model where the diffuse layer does not play a role, and no effect of ionic strength is observed.

$$\sigma = C\psi \tag{2.12}$$

At a low ionic strength, where the role of the diffuse layer dominates, the ionic strength (I) influences the surface equilibrium and the Poisson–Boltzmann (PB) equation can be used to relate the surface charge (σ) and the potential (ψ_o) as follows:

$$\sigma = -(8\epsilon\epsilon_0 RTI)^{\frac{1}{2}} \sinh(F\psi_o/2RT) \tag{2.13}$$

At a very low surface potential $\psi_o < 25$ mV, the PB equation can be further simplified to,

$$\sigma = -(8\epsilon\epsilon_0 RTI)^{\frac{1}{2}} \frac{F\psi_o}{2RT} \tag{2.14}$$

The overall rate of dissolution under conditions at which a positive surface charge exists can be expressed as follows (Casey and Sposito, 1992):

$$r = k[>\mathrm{SOH_2}^+]^n \tag{2.15}$$

2.5.4 Pit nucleation

The dissolution model has been developed based on the crystal growth theory (Dixit and Carroll, 2007). The dissolution is expected to occur through retreat of steps with velocity ν. These steps originate either from existing dislocations or by nucleation of two-dimensional pits. However, such a 2-D pit formation from the smooth surface is only possible by overcoming free energy barrier, ΔG_{crit} which is dependent on the solution saturation state, Ω. As the dissolution progresses closer to equilibrium, the rate of dissolution is expected to show a transition from homogeneous nucleation to defect-assisted nucleation of pits. The dissolution rate, which is dependent on the step source; the nucleation rate (J); step height (h) and the retreat velocity (ν), is given by the following set of equations:

$$\nu = \omega\beta K_{eq}(\Omega - 1) \tag{2.16}$$

$$\Delta G_{crit} = -\frac{\pi a^2 \omega h}{kT \ln \Omega} \tag{2.17}$$

$$J = |\frac{1}{\ln \Omega}|^{1/2} n_S a h K_{T,eq} \beta \exp(-\frac{\pi \alpha_{T,i}^2 \omega h}{3(kT)^2} |\frac{1}{\ln \Omega}|) \tag{2.18}$$

$$r = h(\nu^2 J)^{(1/3)} \tag{2.19}$$

where, ω represents molar volume of molecule in crystal, β is the step kinetic coefficient, a is the lattice spacing, and n_S is the nucleation site density.

2.5.5 Proton-metal exchange

Based on the observation that all metal release reactions from single and multi-oxides involve the exchange of proton, Oelkers (2001) developed a proton-metal exchange model for multi-oxide dissolution assuming that the precursor complex to rate limiting step is formed post several proton-cation exchange reactions. Using the law of mass action on those proton-metal exchange reactions (not the rate limiting one) and balance of metal

sites on the surface, following equation is derived,

$$X_P = \prod_{i=1}^{\hat{i}} \left[\frac{K_i \left[\frac{a_{H+}^{z_i}}{a_{M_i^{z_i}+}} \right]^{n_i}}{1 + K_i \left[\frac{a_{H+}^{z_i}}{a_{M_i^{z_i}+}} \right]^{n_i}} \right] \tag{2.20}$$

$$r_+ = k_+ X_P \tag{2.21}$$

where, i refers to the first $\hat{i}$ metal ions leached before forming a precursor to rate determining step, a_{M_i} represents concentration of rapidly leaching metal ion i in solution and X_P refers to the surface concentration of precursor complex.

2.5.6 Crundwell Model (analogous to electron transfer mechanism)

Recently, Crundwell (2014) proposed a dissolution model to explain the fractal reaction orders frequently observed in mineral dissolution kinetics. The model assumes that dissolution of a mineral MA proceeds via release and transfer of M to outer Helmholtz plane after reaction with water molecules at the surface. This step is followed by reaction of H^+ with A at the Helmholtz plane resulting in the formation of an activated complex which further results in the product. Further, the model development involves an assumption that the rate of removal of anions and the rate of removal of the cations from the surface are equal.

The rate model for dissolution in an acid medium at conditions far from equilibrium is given by,

$$\vec{r} = \left(k_{a,+}[M_{lat}][H_2O^w]\right)^{(1-\vec{x})} \left(k_{a,-}[A_{lat}]\right)^{\vec{x}} \left[H^+\right]^{\vec{x}n} \tag{2.22}$$

$$\vec{x} = \frac{\alpha_+}{\alpha_+ + \alpha_-}; \tag{2.23}$$

where, $[M_{lat}]$, $[A_{lat}]$ are the concentrations of M and A on the surface; α is the transfer coefficient of the ion; n is the stoichiometric number of H^+ reacting for removal of an anion.

When constant terms are lumped, the model reduces to the familiar form with $\vec{x}n$ as reaction order,

$$\vec{r} = \vec{k}[H^+]^{\vec{x}n} \tag{2.24}$$

2.6 Models describing structural aspects

Models which have incorporated various structural aspects such as polydispersity, mineral phase inclusions and, mineral phases that are lumped as particles along with the surface reaction kinetics. These models in general describe the surface area evolution during dissolution.

2.6.1 Surface heterogeneity and surface roughness

Use of fractal dimensions

Avnir et al. (1985) showed that several particulate matter exhibit fractal geometry. For instance, experimental data considered in the study showed that periclase (MgO) has a fractal dimension D of ~ 2 indicating smooth surface while iron oxide (FeO) and silica gel (SiO_2) showed D of 2.59 and 3.0 respectively, indicating irregular geometry. Surface area can be expressed in surface-fractal dimension D as follows,

$$\frac{A}{m} \propto d^{D-3} \tag{2.25}$$

where, D assumes values in the range of 2.0–3.0.

On similar lines, Talman and Nesbitt (1988) showed that the effective surface area as proposed by Helgeson et al. (1984) (proportional to square of radius) cannot describe the dissolution of ultra-fines as reported by Holdren and Speyer (1985), instead the reactive surface area was shown to be proportional to the particle volume.

Two-layer shrinking-core model

Velardo et al. (2002) proposed a two-layer shrinking core model by introduction of a surface heterogeneity factor to account for the surface smoothing which occurs during dissolution. In addition, $\phi(r; R_i, R_o)$ was introduced as a scaling factor for surface area in the region between two layers with radii R_i and R_o.

Volume-surface area relation for a spherical particle with surface heterogeneity:

$$\frac{V(r)}{S(r)} = \frac{r}{3\alpha} \tag{2.26}$$

Model for surface reaction controlled conditions:

$$V(r) = 4\pi r^3/3 \tag{2.27}$$

$$S(r) = 4\pi r^2[(1 - \phi(r; R_i, R_o)) + \alpha\phi(r; R_i, R_o)] \tag{2.28}$$

$$\rho_s \frac{dV(r)}{dt} = -k_d S(r) \tag{2.29}$$

Scaling function, $\phi(r; R_i, R_o)$, is defined by a continuous C^∞ function as follows with adjustable steepness parameter β,

$$\phi(r; R_i, R_o) = \begin{cases} 0 & \text{for } r \leq R_i \quad (2.30) \\ \exp\left[\beta + \dfrac{\beta(R_o - R_i)^2}{(R_o - r)^2 - (R_o - R_i)^2}\right] & \text{for } R_i < r < R_o \quad (2.31) \\ 1 & \text{for } r = R_o \quad (2.32) \end{cases}$$

The model is expected to give good results even for a poly-disperse particle system.

2.6.2 Poly-disperse particle system

Influence of poly-disperse solids on reaction kinetics and errors associated with considering single particle size and determining the rate-determining step was apparent with the work of Holdren and Berner (1979) and Leblanc and Fogler (1987). Subsequent work by Gbor and Jia (2004) reiterated the errors associated when particle size distribution was neglected while using shrinking core model. In one of the early experimental studies on mineral dissolution, (Holdren and Berner, 1979) showed that parabolic kinetics was an artefact of preferential dissolution of ultra-fine particles adhered to the large grains.

Population balance model

Leblanc and Fogler (1987) used the following population balance model to incorporate the effect.

$$-\frac{\partial[R(D)F(D,t)]}{\partial D} = \frac{\partial[F(D,t)]}{\partial t} \tag{2.33}$$

where, $F(D,t)$ is particle size distribution and $R(D)$ is defined as follows,

$$R(D) = \frac{dD}{dt} = \begin{cases} \dfrac{-4\mathcal{D}C}{\rho_s D} & \text{mass transfer controlling} \quad (2.34) \\ \dfrac{-2kC}{\rho_s} & \text{surface reaction controlling} \quad (2.35) \end{cases}$$

Shrinking core modification

Considering the wide use of shrinking-core models for fluid-solid reactions, Gbor and Jia (2004) provided an objective approach to determining the associated errors with the assumption of mono-dispersion based on the initial particle size distribution (PSD) function and its coefficient of variance (CV). In the case of Gamma PSD, when CV was between 0.7 and 1.2, controlling step was observed to shift from chemical reaction to ash layer diffusion and similarly, a shift to chemical reaction control regime from liquid film diffusion when CV was in the range of 0.3–0.7. The study reported that ash layer controlled regime is not sensitive to particle size distribution. In the proposed model, PSD effect was coupled to the integrated shrinking-core model as shown below,

$$X_{unreacted} = \int_0^\infty f(D,t)p(D)dD \tag{2.36}$$

where, $p(D)$ is particle size distribution and $f(D,t)$ is given below,

$$f(D,t) = 1 - X_D = \begin{cases} \left(1 - \frac{k_{mn}t}{D}\right) & \text{liquid film diffusion control} \quad (2.37) \\ \left(1 - \frac{k_{rn}t}{D}\right)^3 & \text{surface reaction control} \quad (2.38) \end{cases}$$

for ash layer diffusion control, a simple analytical solution for $f(D,t)$ is not possible to arrive at (Gbor and Jia, 2004).

2.6.3 Particles present as inclusion and clusters

Mineral matter does exist in the form of clustered particles with other interstitial mineral matter or as inclusions within another mineral matrix. Two classes of models, sugar-lump dissolution model (Fletcher and Welham, 2000; Noiriel et al., 2009) and sporulation model(Adrover et al., 2004), were proposed to predict the surface area changes with the progression of dissolution.

Sugar-lump model

Fletcher and Welham (2000) proposed a sugar-lump model for mineral particle dissolution where the crystal grains of radius r_o are clustered together with the amorphous phase of the same mineral to form particles of radius R_o. Depending on the fraction of amorphous

content (F), the fraction of total material dissolved $D(t)$ under presumably reaction controlled regime is given by,

$$D(t) = F\left(1 - \frac{(R_o - Gt)^3}{R_o^3}\right) + (1 - F)\left(\frac{(r_o - Ht)^3}{r_o^3}\right) \tag{2.39}$$

where G, H are dissolution rates of amorphous and crystalline phases respectively.

Noiriel et al. (2009) reported a sugar-lump model for surface area evolution with the progression of dissolution. The model (Equation 2.40) is analogous to shrinking particle model with three empirical parameters n_1, n_2,n_3,

$$S(t) = \left(S_{r0} + S_{rm}\left(1 - \left(\frac{C(t)}{C_0}\right)^{n_1}\right)^{n_2}\right)\left(\frac{C(t)}{C_0}\right)^{n_3} \tag{2.40}$$

where, S_{r0}, S_{rm} represent the surface area of aggregate particles and the sum of individual particles (also the maximum surface area), respectively; and C_0, $C(t)$ are the concentration of the mineral at time 0 and t, respectively.

Sporulation model for dissolution of inclusions

Adrover et al. (2004) proposed the population-balance based sporulation model (Equation 2.41) where the dissolution or mechanical fragmentation of solid matrix is assumed to progressively release embedded reactive grains (spores) into the solution. The study validated the model with dissolution kinetics of manganiferous ores.

$$\frac{\partial n(r,t)}{\partial t} - \frac{\partial[R(r)n(r,t)]}{\partial r} = -N_p \frac{dV_p}{dt}\nu(r, r_p) \tag{2.41}$$

where, $n(r,t)$ is the distribution of spores released into the solution at any time t; $R(r)$ is the rate of shrinkage of spores in solution; $\nu(r, r_p)$ is the distribution of spores in aggregate particle with r_p to $r_p + dr_p$; $N_p \frac{dV_p}{dt}$ is the total rate of volume change of aggregate particles with dissolution.

2.7 Summary

An extensive review of mineral carbonation routes, reaction chemistry, and reactivity of feedstocks is presented. Further, dissolution characteristics, controlling mechanism and

relevant dissolution models for single and heterogeneous mineral phase residues reported in the literature are critically discussed. Also, a brief description on the current state-of-art of various reactor concepts for commercial plants is presented. Gaps observed in the literature are summarised below.

Among the indirect mineral routes, pH-swing, ammonia salts based processes and pressure-swing carbonation are promising options for PCC production. Although high calcium extraction efficiency and low impurities in PCC can be achieved via pH-swing processes, energy intensive processes such as recovery of acid and base reduce the CO_2 capture benefits and increase the PCC production cost. While ammonia salts-based leaching process demonstrates high calcium selectivity and the leachate readily carbonates without the need for pH adjustment, loss of ammonia is an added cost. On the other hand, CO_2 pressure-swing carbonation does not involve the use of any acids or bases except carbon dioxide itself. However, very little is understood about CO_2 pressure-swing process due to limited studies, and requirement of large water volume due to poor $CaCO_3$ solubility is a known drawback.

The major shortcomings for indirect mineral carbonation are associated with the extraction step, and include slow extraction rate, poor extraction efficiency and selectivity of calcium from slag. While the literature survey shows significant amount of experimental work on parametric studies in various acidic environments, several discrepancies exists in explaining the dissolution characteristics such as particle-size effect, liquid-to-solid ratio etc. So far, very little information is available about nature of impurities in leachate, factors that influence calcium selectivity during dissolution.

So far, based on apparent rates of calcium release, it has been speculated that the formation of a passive layer by Ca-depleted silica layer hinders the calcium extraction from residual slag and reduces the overall extraction potential. However, these observations on steel slags contradict two distinct findings based on pure mineral phases. Firstly, calcium predominantly exists as larnite and alite in most steel slags. These mineral phases, which belong to the orthosilicate family, are expected to dissolve congruently without leaving behind a Si-rich leached layer. Secondly, surface coverage by silica precipitation did not necessarily lead to passivation of several individual (pure) silicates present in steel slags, and complete carbonation was observed.

Generally, there are two problems associated with the understanding of dissolution

kinetics of steel slag, namely, identification of the rate controlling step, and a lack of kinetic models that consider the heterogeneous nature of steel slag. In several recent studies, identification of the controlling mechanism was attempted using integral forms of shrinking-core models, which are simplistic and often erroneous for several reasons. It has been shown in fluid-solid literature that different controlling mechanisms often fit conversion-time data equally well. Further, these models ignore the simultaneous release of other elements such as magnesium and iron and implicitly consider that the calcium extraction rate is independent of other elements. Thus, shrinking-core models reported so far were at best *effective* models as it is yet to be shown that the determined controlling mechanism and estimated kinetic parameters can provide reasonable predictions of various parametric effects (acid-to-solid ratio, particle size effect, liquid-to-solid ratio etc.).

Currently, the technological status of the ex situ accelerated mineral carbonation process is at a pilot stage. Besides low extraction efficiency and solid/liquid separation, lack of proven reactor technology is a major reason for the absence of commercial deployment.

Chapter 3

Materials and Methods

Basic oxygen furnace (BOF) slag, in granular form (>3 mm), was supplied by M/s JSW Steel Ltd. All the experiments were conducted using this BOF slag, which has henceforth been referred to as steel slag or slag, interchangeably. An extensive set of characterisation studies have been performed to estimate the chemical and mineral phase composition, morphology, particle-size distribution, and distribution of various elements in the slag. These studies were carried out using X-ray fluorescence, X-ray diffraction (XRD), environmental scanning electron microscopy (ESEM) equipped with energy dispersive spectroscopy (EDS). Batch leaching experiments were carried out to study the slag dissolution and precipitation characteristics in nitric, acetic and carbonic acids. The slag residues and carbonate precipitates obtained were characterised using XRD, Fourier transform infrared spectroscopy (FT-IR), X-ray photoelectron spectroscopy (XPS), Transmission electron microscopy (TEM) and ESEM with EDS.

3.1 Sample preparation

Slag was washed in acetone to remove surface impurities and dried overnight in oven at 100 °C. Dry slag was pulverised to fine powder using Herzog pulverizing mill (HSM100). The powdered slag was sieved to separate 212–355, 150–212, 90–125, 75–90 and <45 μm particle size fractions using standard test sieves. The sieved fractions were stored in airtight containers.

3.2 Slag, residue and product characterisation

The elemental, chemical, and mineral composition and morphological features of steel slag, leached and carbonated slag residue, and PCC have been characterised using the techniques described in this section.

3.2.1 X-ray Fluorescence spectroscopy of raw slag

Elemental composition (as oxides) of raw slag was determined using X-ray Fluorescence (XRF) spectroscopy. The sample analysis was carried out using Philips PW2404 with 4 kW x-ray power. Finely ground slag sample (<45 μm) was used for analysis. Four grams of overnight dried sample was thoroughly mixed with one gram of methylcellulose based binder using isopropanol solvent. Mixture was dried under infra red (IR) lamp to evaporate the solvent. Dried sample was pelletised at a pressure of 10 kg/cm^2. Instrument was calibrated with slag standards and sample analysis was carried out.

3.2.2 Sodium carbonate fusion of raw slag

Elemental composition of coarser particle size fractions was determined by sodium carbonate fusion. The objective of the study was to determine variation in elemental composition among finer and coarser particle size fractions (< 45, 90–125, and 150–212 μm). Sodium carbonate as a flux is known to fuse silicates at high temperature to glassy mass (Dulski, 1996), which can be easily dissolved in mineral acid solutions and analysed using techniques such as inductively coupled plasma atomic emission spectroscopy (ICP-AES).

In each experiment, 0.300 g of slag and 5.00 g of flux were mixed in a platinum crucible and fused at 900 °C for 45 min in a muffle furnace. After fusion, crucible was allowed to cool to room temperature. Fused mixture in the crucible was dissolved using dilute nitric acid and the aqueous solution was transferred to a glass beaker. Dilute hydrochloric acid was added to the beaker to form aqua-regia to dissolve suspended particles. The aqueous solution was diluted to one litre in a standard volumetric flask. Supernatant was sampled and filtered using 0.2 μm filter. Concentration of Ca, Fe, Si and Mg in liquid sample were analysed using ICP-AES analysis and elemental concentration in the slag was determined

as follows:

$$\%M = \frac{[M]_{ICP} \times \text{Atomic Weight} \times V_{liquid} \times \text{Dilution}}{\text{Slag mass}} \times 100 \tag{3.1}$$

3.2.3 X-ray diffraction

Powder x-ray diffraction (XRD) was carried out on raw slag, reacted slag and PCC for mineral phase identification and quantification. All samples were scanned from 5–60° of 2θ with a scan resolution of 0.026° using PANanalytical X'pert Pro (PW3050/60). XRD was also carried out for coarser raw slag particles to investigate the variation in the phase distribution in the coarser and finer particles.

Mineral phase quantification

Mineral phase identification was carried out by matching peaks with the standard XRD spectra available in ICSD database. Quantification of mineral phases was carried out using Maud, a Rietveld refinement software. Below mentioned methodology was adopted for fitting the raw slag and reacted slag spectra:

1. Background was modelled using polynomial with 3 (for raw slag) or 5 (for leached slag) adjustable parameters.

2. A sequential method of adding mineral phases was adopted to ensure unambiguous fit. Phases with unique and strong peaks were first fit by varying the scale parameters and basic parameters. Subsequently, mineral phases with overlapping peaks were added and fitted.

3. Scaling and basic parameters were modified during fitting. Crystal structure or micostructure parameters were fixed at default values.

4. Goodness of the fit was verified based on weighted profile R-factor (R_{wp}) value ($\leq 5\%$) and match with the oxide composition obtained from XRF analysis.

3.2.4 Scanning electron microscopy with energy dispersive spectroscopy

Raw slag, reacted slag, and PCC have been imaged under scanning electron microscope (SEM) to study morphological features. Energy dispersive spectroscopy was used to

determine distribution of elements in the sample. SEM studies have been performed using FEI Qanta 200 ESEM with EDAX® attachment. All samples were fixed on carbon tape and sputter-coated with Platinum before analysis. Morphological features were studied using secondary electron images. Back-scattered imaging has been used for Z-contrast imaging, elemental mapping in EDAX® and images for particle size distribution.

Particle size distribution by image analysis

Particle size distribution of various size fraction were analysed using back-scattered SEM images in ImageJ software. For each size fraction, projected area of particles were measured by tracing the particle boundary. Equivalent spherical diameter was calculated from the measured cross-section area. Distribution of particle size was determined using Distribution Fitter toolbox in MATLAB®.

3.2.5 X-ray photoelectron spectroscopy

Surface elemental composition, and chemical bonding of silicon was analysed using x-ray photoelectron spectroscopy (XPS). XPS was performed using Kratos analytical AXIS Supra model ESCA with monochromatic Al K-α (1486.6 eV) X-ray source. The analysis chamber pressure was $< 2 \times 10^{-9}$ Torr. Take off angle was 90°. XPS sample was prepared by drop-cast method. Powder samples (raw slag, reacted slag and PCC) were sonicated in methanol and drop-cast on aluminium or copper foil. In the case of coarse particles, particles were embedded in aluminium foil with mechanical pressure. Relative elemental composition was determined based on wide scan obtained at resolution of 1 eV. Chemical shifts were determined based on high-resolution scan obtained for C1s, O1s, Si2p at a scan resolution of 0.1 eV. Adventitious carbon at 284.7 eV is used an internal reference for charge correction. ESCApe software was used for data analysis.

3.2.6 Fourier transform infra red spectroscopy

Fourier transform infra red (FT-IR) spectroscopy has been carried out on PCC to distinguish silica from silicates and detect the presence of calcium carbonate in bulk sample. The procedure was carried out using Bruker Hyperion 3000. Powder sample were scanned in the wavenumber range of 4000–400 cm^{-1} at a scan resolution of 1.93 cm^{-1}.

3.2.7 Transmission electron microscopy

Transmission electron microscopy (TEM) was carried out on PCC for morphology, and diffraction pattern for phase identification. TEM imaging was carried out in bright-field mode using 300 kV FEI Tecnai G2, F30 microscope. Diffraction patterns were analysed using CrysTBox software.

3.2.8 Inductively coupled plasma

Inductively coupled plasma atomic emission spectroscopy (ICP-AES) and optical emission spectroscopy (ICP-OES) were used for determination of elemental concentrations of Ca, Si, Mg, Fe, Mn, and Al in liquid samples.

All leachate samples, except from pressure-swing experiments, were analysed using Spectro analytical instruments ICP-AES available at SAIF, IIT Bombay. The instrument has a detection limit of 10 pbb. Liquid samples were filtered using 0.2 μm syringe filter and diluted such that concentrations were in the range of 0–100 mg L^{-1}. Instrument was calibrated in the range of 0–100 mg L^{-1} using Sigma-Aldrich multi-element mixture 6 for ICP.

Leachate samples from pressure-swing carbonation study were analysed using PerkinElmer Avio200 ICP-OES, located at PerkinElmer facility, Monash University. Sample preparation and calibration standards were same as mentioned above for ICP-AES.

3.3 Chemical reactivity tests

Following tests were conducted to determine the alkalinity of the sample, understand phases which control dissolution, and assess the feedstock potential for mineral carbonation reaction.

3.3.1 Native pH test

Native pH test was conducted on raw slag to determine the alkalinity of sample (Huijgen et al., 2005). 5 g of slag in 50 ml of distilled water (L/S = 10 ml/g) was continuously stirred using magnetic stirrer in a air-tight bottle for 48 hours at room temperature. pH at the end of the test was recorded as native pH.

3.3.2 Selective extraction of C_2S and C_3S

The total amount of 'reactive' calcium present as dicalcium silicate (C_2S) and tricalcium silicate (C_3S) was determined by selective leaching in methanolic solution of salicylic acid (Runje and Bezjak, 1983). About 1.00 g of slag was dissolved in 100 ml of 30 g L^{-1} methanolic solution of salicylic acid for 60 min in a airtight bottle at room temperature. At the end of dissolution, liquid sample from slurry was filtered and diluted using dilute nitric acid for ICP-AES analysis. About 57% of Ca present in the slag was found to leach from the slag and the Ca/Si ratio in the leachate was found to be 2.1.

3.3.3 Neutralising capacity

Neutralising capacity was proposed as a surrogate for maximum amount of CO_2 sequestered as $CaCO_3$ by direct CO_2 absorption. The test involves determining the maximum moles of nitric acid added to the slag slurry above a pH of 8.2, above which $CaCO_3$ precipitation is feasible at atmospheric conditions. The test was conducted in a glass reactor by addition of 5 g of slag to 50 ml of distilled water (L/S of 10 ml/g) at room temperature. 1 M HNO_3 solution was slowly dosed into the slurry using Hanna auto-titrator till the slag slurry pH is above pre-set pH of 8.2. The experiment was stopped when the change in pH was negligible for 15 min.

3.3.4 Acid and base titrations

Acid titration has been carried out to study the acid uptake rates at various pH conditions and extents of dissolution. Experiments were also conducted to understand buffering phenomena in batch dissolution experiments. All experiments were conducted in batch reactor (Figure 3.1) along with auto-titrator for acid (HNO_3) dosing at predetermined rate. Base titration was carried out by titrating the acid leached slag slurry with NaOH to quantitatively determine the species which are susceptible for precipitation. Multiple cycles of acid and base titrations were carried out to determine reversible and irreversible buffering reactions.

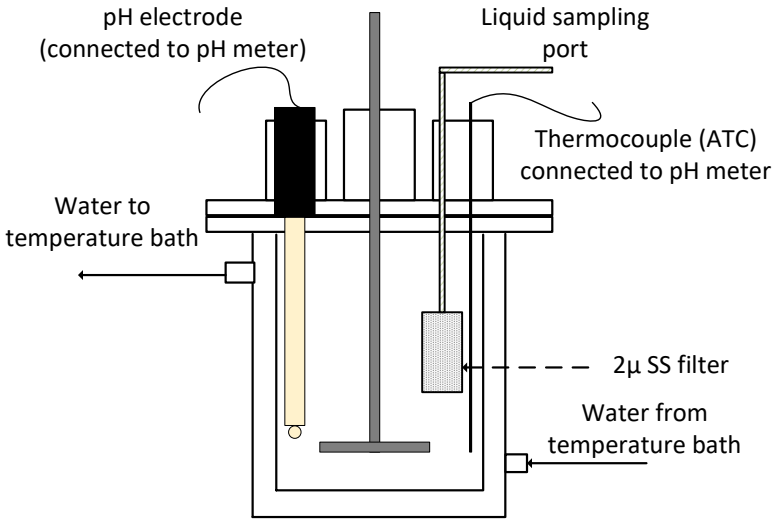

Figure 3.1: Batch reactor setup

3.4 Batch dissolution experiments

3.4.1 Parametric study

Batch dissolution experiments were conducted to study influence of parameters such as liquid-to-solid ratio, slag particle size, acid-to-solid ratio, temperature, leaching agent, ionic strength, and additives on calcium leaching characteristics. Batch experiments were carried out in a 500 ml jacketed glass reactor fitted with Orion 8190BW Ross pH electrode for continuous pH logging in Hanna HI-5222 dual pH meter or Hanna HI-901 autotitrator (shown in Figure 3.1). Reactor temperature was controlled using circulating water bath. pH measurements were temperature corrected using automatic temperature compensation (ATC) feature in pH meter. Before each experiments, pH meter was calibrated using pH 4.01 and pH 10.01 buffers and calibration slope was ensured to be within 100±0.5% of the theoretical slope.

In each experiment, reactor was filled with leaching solution and pH logging was started. Predetermined quantity of slag was measured and added to the solution. Samples were collected through sampling port after predetermined time intervals. Liquid samples were filtered using 0.2 μm syringe filter and acidified to avoid precipitation. Slag residue

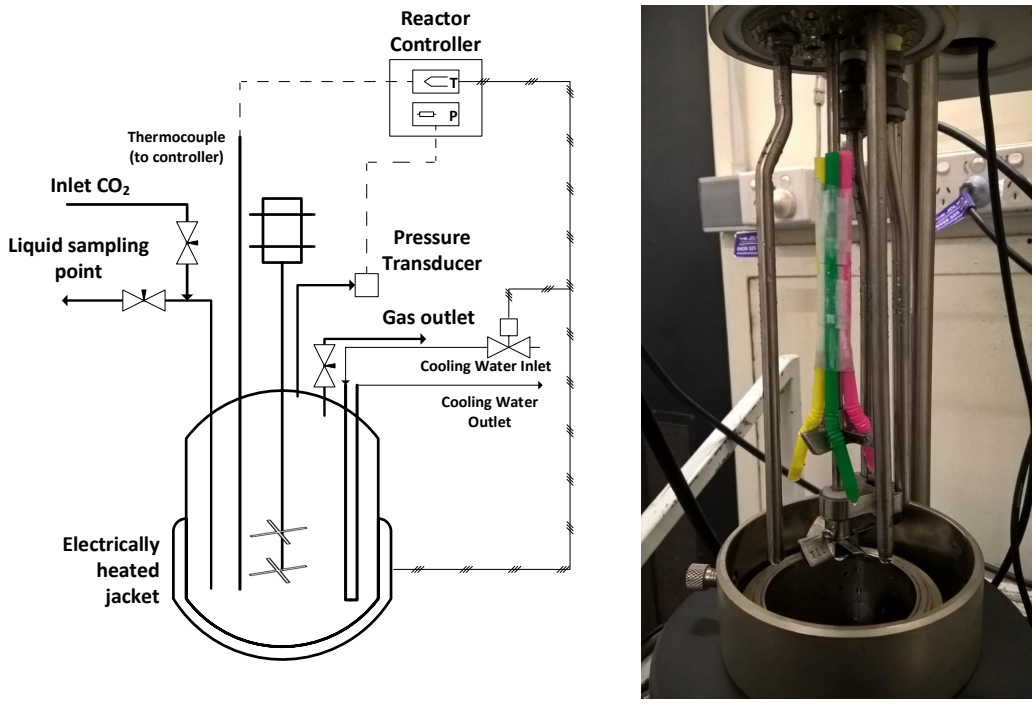

Figure 3.2: High pressure autoclave (Parr autoclave) setup

obtained at the end of experiment was filtered and dried overnight in the oven at 100 °C.

Leaching solution was either nitric acid or acetic acid. Experiments were also conducted by addition of analytical reagent grade sodium molybdate dihydrate (0–1.5 mmol/g of slag) as an additive in nitric acid leachate.

3.5 Pressure-swing dissolution and carbonation experiments

All high-pressure experiments were performed in a 600 ml bench top Parr autoclave (4568) equipped with Parr 4848 reaction controller (shown in Figure 3.2). The reactor temperature is maintained by electrically heated mantle and circulating cooling water. The reactor stirrer has two nos. of 4-blade impeller and has a maximum stirring speed of 800 rpm in water. Details of the setup with inlet and outlet ports are shown in Figure 3.2.

3.5.1 Mass transfer characterisation of the reactor

CO_2 absorption in water was studied to estimate the gas-liquid mass transfer characteristics in the reactor. The autoclave was filled with 250 ml of deionised water and air present in the reactor was purged out by performing three pressurizing-depressurizing cycles with CO_2. After air removal, reactor was pressurized to desired pressure of 8 bar. After achieving the desired reactor pressure, inlet valve was closed and the autoclave was stirred at 800 rpm. Changes in CO_2 pressure with time were recorded (recording time span was 10–30 seconds for first 3 minutes and then 1–5 minutes for the rest of the experiment). It was observed that it takes about 25 minutes before water is saturated with CO_2; the estimated k_La was found to be an order of magnitude lower than desired to avoid significant gas-liquid mass transport limitations. To overcome the problem, reactor stirrer was fitted with three thin plastic tubes with one end open to the gas space as shown in Figure 3.2. This would act like a self inducing impeller to improve the gas-liquid mass transfer. Absorption experiment under the same operating conditions with the aforesaid modification improved the k_La value significantly and reduced the saturation time to three minutes. This arrangement was continued for all further experimentation.

3.5.2 Calcium extraction experiments

All dissolution experiments were performed in 250 ml of deionised water. The slag was loaded into the reactor and the slurry was stirred for two minutes to avoid lump formation which was otherwise observed to form under CO_2 pressure. Liquid was sampled for elemental analysis before pressurizing the reactor. The reactor was then closed and rapidly pressurized to the desired pressure. The reaction mixture was stirred at 800 rpm and changes in pressure with time were recorded. About 2 ml of supernatant from the reaction slurry was sampled at 3, 10, 20, 60, 90, and 120 min by temporarily stopping (for about 30 seconds) the stirrer to avoid flow of thick slurry into the sampling line. The slurry was immediately filtered through 0.2 μm syringe filter and acidified using 0.1 M nitric acid for ICP-OES analysis. Also, part of the unacidified liquid sample was potentiometrically titrated with 0.01 M HNO_3 for alkalinity. Dissolution experiments were also repeated without intermittent liquid sampling to ensure a completely closed system for measurement of drop in CO_2 pressure (reactor pressure). Drop in reactor pressure,

with and without liquid sampling, were matching when pressure drop caused due to liquid sampling (as measured by the digital pressure transducer mounted on the autoclave) was discounted. At the end of the dissolution reaction, slag residue was filtered and dried overnight at 100 °C.

Reproducibility of experimental results was ensured by repeating the experiments at least twice. Firstly, the pressure drop profiles were found to be repeatable in each case. Secondly, concentrations at '90 min' in each experiment was at least measured twice using ICP-OES and found to be reproducible within 2.2% (max. error). In addition, for each measurement the total metal ion concentration from ICP-OES was found to be half the total alkalinity measured from the acid-base titration (expected due to predominance of divalent ions in leachate), which acts as a complimentary validation of measurements.

3.5.3 Precipitation kinetics of $CaCO_3$

At the end of dissolution step, leachate from the reactor obtained under CO_2 pressure was filtered using 0.2 μm filter. Filtered solution was stirred in a glass beaker at a stirring speed of 500 rpm. Precipitation was carried up to three hours by monitoring the progress by pH measurement and sampling for ICP-OES analysis. Calcium carbonate precipitate was filtered using Whatman filter paper and left for overnight drying in a hot air oven maintained at 100 °C.

Chapter 4

Slag characterisation and dissolution characteristics

4.1 Background

Currently, there are no definite methods available for *a priori* prediction of leaching behaviour and true calcium extraction (and hence carbonation) potential. For instance, the maximum extent of calcium extraction from a feedstock estimated based on the elemental composition is often not achievable. Several efforts are underway to understand the leaching characteristics based on the inherent minerological factors(Doucet, 2010; Engström et al., 2013; Bodor et al., 2013) and the solution chemistry(Mun et al., 2017). The prediction of true potential based on mineral phase composition and their susceptibility towards leaching has shown some promise and taking into account of morphological and rate controlling factors were thought to be necessary for better *a priori* predictions (Bodor et al., 2013).

Also, efforts to predict the elemental release rates from slags, which typically contain multiple mineral phases, have been largely unsuccessful. Batch leaching tests on steel slag along with the geochemical modelling (Windt et al., 2011) were useful for qualitative predictions of the influence of liquid-to-solid ratio and in turn, the solubility-controlled leaching. However, the approach is not suitable for understanding the influence of pH, especially in the acidic medium, on the rate of dissolution of primary minerals present in the slag. The understanding of leaching chemistry is especially important for interpretation of kinetic data from batch reactor, where in dissolution rates are influenced by the changes in solution chemistry with the time (Brantley, 2008). Thus, it is necessary to determine smallest reaction set that can adequately describe the slag leaching chemistry and subsequently formulate a rate model for reliable predictions. Alternatively, researchers

adopted pH-stat dissolution experiments to determine the influence of pH on relative extents of metal extraction, and also ascertain mineral phases which control the solubility of a species (Doucet, 2010; Huijgen and Comans, 2006). However, considering the formation of possible secondary precipitates and acid dissociation of aqueous species, these experiments provide little understanding of true metal release rates, corresponding acid uptake, and mechanism of primary mineral dissolution.

True elemental release rate information is essential for understanding the rate-controlling step, and the role of hydronium ion and complexing ligands concentrations in the leaching agent. So far, based on apparent rates of calcium release, some studies have speculated that the formation of a passive layer by Ca-depleted silica layer hinders the calcium extraction from residual slag and reduces the overall extraction potential (Lekakh et al., 2008b; Huijgen et al., 2005). However, these observations on steel slags contradict two distinct findings based on pure mineral phases. Firstly, calcium predominantly exists as larnite and alite in most steel slags (Yildirim and Prezzi, 2011). These mineral phases, which belong to the orthosilicate family, are expected to dissolve congruently without leaving behind a Si-rich leached layer (Terry, 1983b). Secondly, surface coverage by silica precipitation did not necessarily lead to passivation of several individual (pure) silicates present in steel slags, and complete carbonation was observed (Bodor et al., 2013).

Thus, in this chapter, it has been attempted to generate *a priori* information necessary to understand the carbonation potential, identify the controlling mechanism and develop dissolution kinetics model by determining the mineral composition and their susceptibility towards acid dissolution, determine the leaching chemistry, and identifying the morphological features that could affect the dissolution rates.

4.2 Characterisation studies

Steel slag has been characterised by various techniques to determine its elemental, and mineral compositions.

4.2.1 Elemental composition

Elemental composition of steel slag determined using X-ray fluorescence is reported in Table 4.1. The slag was found to have substantial amount of calcium ($\sim$ 43% as CaO)

Table 4.1: Elemental composition of slag determined using X-ray fluorescence

Oxide	CaO	MgO	SiO_2	FeO	Al_2O_3	MnO	Cr_2O_3	V_2O_5	SO_4	P_2O_5	TiO_2	LOI	Total
Wt%	42.9	9.2	17.4	21.7	2.15	2.25	0.12	0.25	0.22	2.32	0.68	< 0.1%	99.3
Std. deviation	0.5	-	1.1	2.8	0.25	0.34	0.01	0.02	0.25	0.71	0.10	-	-

along with iron, silica and magnesium. The slag composition was found to be similar to those reported in the literature (Yildirim and Prezzi, 2011). The high amount of calcium present in the slag makes it suitable for PCC production via mineral carbonation. Based on the elemental analysis, the theoretical potential for calcium carbonate production is estimated to be 766 kg/tonne of slag. In addition, recycling of iron-rich slag residue (post calcium and silica extraction) to iron and steel industry can reduce iron ore losses to the tune of 2–3%. Though these findings suggest that the current feedstock is promising for utilization by selective leaching, the actual potential is generally understood to be lower than that estimated based on elemental composition.

4.2.2 Mineral composition - quantification & phase distribution

The powder diffraction pattern of raw BOF slag with the mineral phase identification and deconvolution is shown in Figure 4.1. Mineral composition of the slag obtained from quantitative XRD is shown in Table 4.2. Slag was mainly found to contain dicalcium silicate (larnite: ICSD-963), tricalcium silicate (Hatrurite: ICSD-22501), dicalcium ferrite (brownmillerite: ICSD-9197), RO phase (MgO-MnO: ICSD-60710; Wuestite: ICSD-633036; MgO-FeO: ICSD-60697; FeO-MgO: ICSD-158105; FeO-MgO: ICSD-60696; FeO-MnO: ICSD-60687), and calcium magnesium silicate (merwinite; ICSD-26002). The total concentration of the identified phases has been normalized to 93.5 wt% based on the total weight percent for these elements (Ca, Fe, Mg, Si and Mn) obtained using XRF. As shown in Table 4.3, elemental composition determined based on quantitative XRD analysis shows a good match with the XRF analysis. The mineral composition indicates that about 77% of calcium in the slag exists in the form of orthosilicates, a family of silicates without bridging oxygen bond and known for high reactivity (illustrated in Figure 4.2). The remaining 23% of calcium is in the form of brownmillerite, which is not very reactive (Doucet, 2010; Bodor et al., 2013).

Based on the mineral composition, following assessment can be made about the carbonation potential and the mineral carbonation process when BOF slag is used as

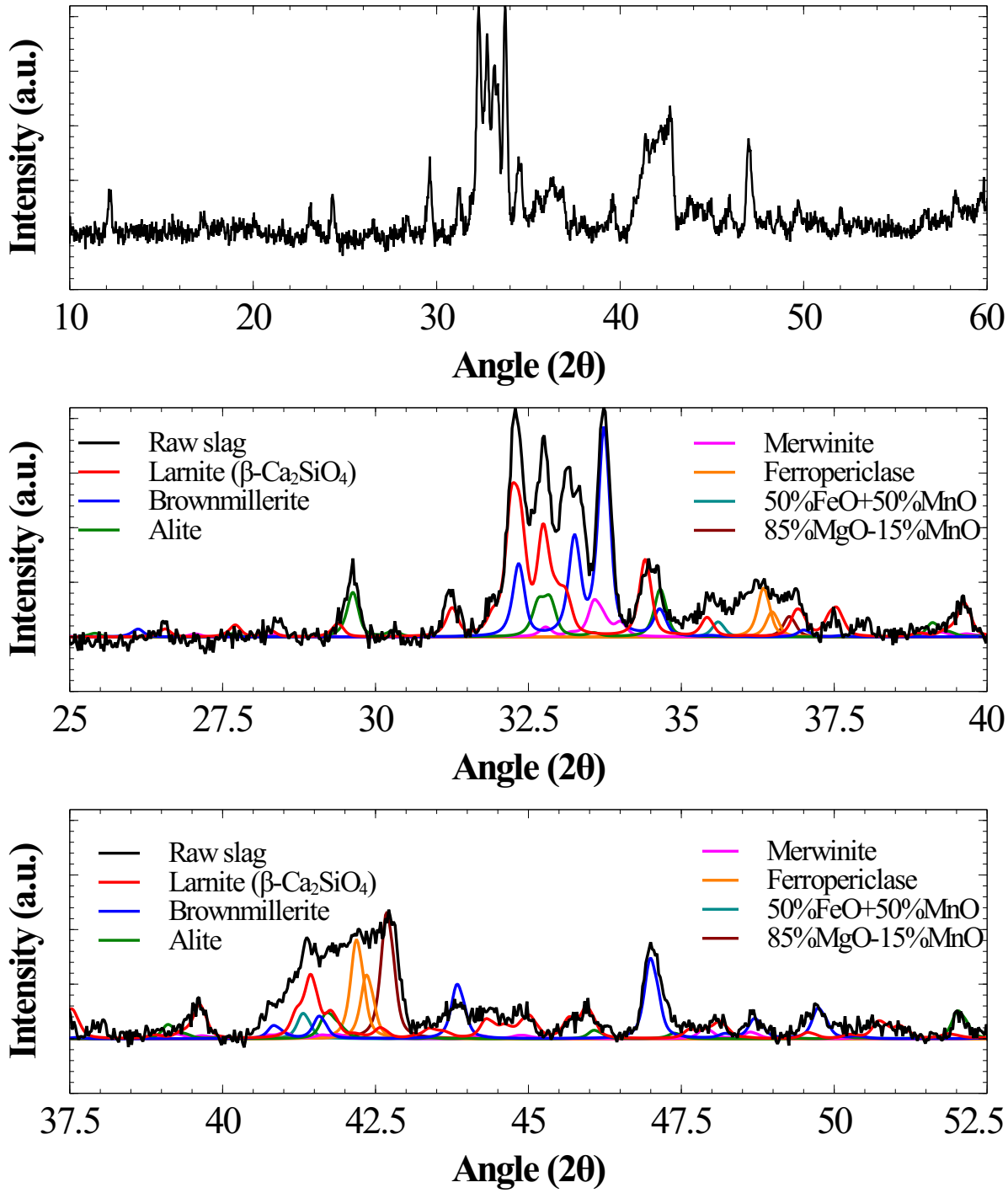

Figure 4.1: Deconvolution of mineral phases in XRD pattern of raw slag

Table 4.2: Quantification of mineral phases using XRD

Phase	**Formula**	**wt%**
Larnite	$2\,CaO \cdot SiO_2$	36.2
Brownmillerite	$2\,CaO \cdot Fe_2O_3$	23.5
Alite	$3\,CaO \cdot SiO_2$	9.1
Merwinite	$3\,CaO \cdot MgO \cdot 2\,SiO_2$	5.6
RO Phase	$(FeO_{0.28} - MgO_{0.66} - MnO_{0.12})$	20.4
Sum		93.5*

* Sum normalised according to XRF composition (refer Table 4.3)

Table 4.3: Comparison of slag composition obtained from XRD quantification with XRF analysis

Oxide	CaO	SiO_2	FeO	MgO	MnO	Sum
XRD fit	42.8	17.1	20.5	9.6	3.4	93.5
XRF	42.9	17.4	21.7	9.2	2.3	93.5

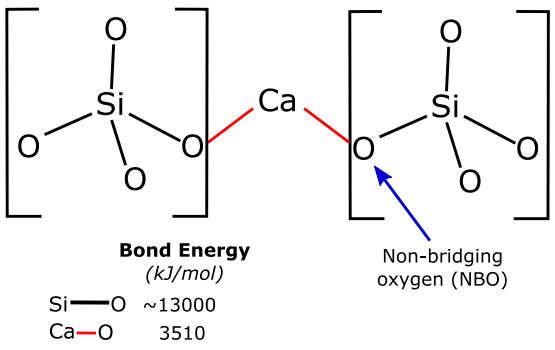

Figure 4.2: Silicate structure and non-bridging bond

a feedstock:

- Based on the calcium amount present as silicates, the potential for precipitated calcium carbonate production is estimated to be 589 kg per tonne of steel slag, with the corresponding CO_2 sequestration potential being 261 kg.

- Orthosilicates, the phases that contain 77% of the total calcium in slag, are known to dissolve by breaking Ca–O bonds and are as reactive as pure oxides (Casey and Westrich, 1992). In addition, these silicates undergo congruent dissolution without leaving any leached layer. It is expected that the congruent dissolution leads to release of Si as silica monomers, which can undergo polymerization and form a gel(Terry, 1983b). Contrary to what has been speculated by many (Lekakh et al., 2008b; Daval et al., 2011), rate and extent of calcium extraction may not be limited by surface passivation by amorphous silica. However, the formation of the gel can lead to filtration problems (Terry, 1983b), affecting the rate of transfer of filtered aqueous solution from dissolution to carbonate precipitation step.

- Iron present as Fe(II) has high solubility in aqueous solutions as compared to Fe(III). Significant amount of Fe(II) in the slag (XRD analysis) suggests that iron can potentially end up as an impurity in the leachate. Thus, removal of iron from the leachate is necessary to obtain high-purity precipitated calcium carbonate. Furthermore, inhibition of iron dissolution and efficient recovery of iron from leachate improves the potential to recycle the iron-rich slag residue to iron and steel industry.

Phase distribution

Figure 4.3 shows backscattered SEM imaging of raw slag sample with and without grinding using 2000 SiC grit. The phase distribution observed based on Z-contrast and EDS analysis (refer Table 4.4) corroborates with the observations from XRD analysis. Slag was found to be mainly made of three phases: calcium silicates, dicalcium ferrite and RO phase. While RO phase is present as inclusions (spores), calcium silicate and brownmillerite phases form the matrix of the slag particle. Based on the Z-contrast observable at the centre and periphery of RO phase particles in the Figure 4.3 and also evident from EDS composition, it can be concluded that the FeO (appears lighter in colour due to high

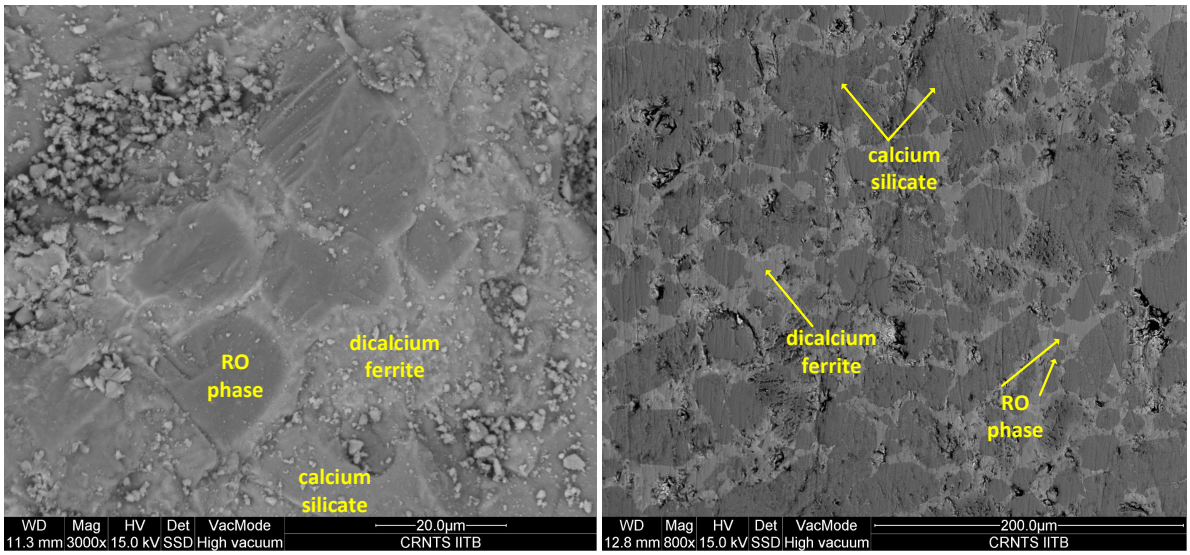

Figure 4.3: Backscattered SEM micrograph of raw steel slag showing phase distribution based on Z-contrast and EDS spectra shown in Table 4.4

Table 4.4: Relative elemental concentrations determined using standardless energy dispersive spectroscopy (EDS)

Phase (marked in Fig. 4.3)	**Ca** (At%)	**Si** (At%)	**Fe** (At%)	**Mg** (At%)
Calcium silicate	25.94	11.73	2.16	1.97
Dicalcium ferrite	25.37	1.54	19.70	0
RO phase	0.48	0	3.28	17.17

atomic weight) is concentrated on the periphery and MgO (appears darker in colour due to low atomic weight) is richer in the bulk.

4.3 Leaching characteristics of steel slag

4.3.1 Native pH and neutralising capacity

Native pH, which is a proxy to alkalinity, was found to be 12.50 ± 0.02. At this pH, the extent of calcium dissolution (measured to be 518 ± 62 ppm) into aqueous solution is expected to be controlled by calcium hydroxide solubility (809 ppm and pH of 12.5). Lower than maximum soluble concentration suggests that the slag has relatively small quantities of free lime and calcium hydroxide phases. Neutralising capacity of the slag was found to be 5.72 mol of acid/kg of slag or equivalently CO_2 sequestration capacity of

Table 4.5: CO_2 sequestration capacity based on calcium content and neutralising capacity

Method	**elemental Ca content**	**mineral phase quantification**	**neutralising capacity (all metal carbonates)**	**neutralising capacity (as $CaCO_3$)**
gCO_2/kg of slag	329	261	252	154

251 gCO_2/kg slag. Amount of calcium leached during the experiment was 0.14 g/g of slag while the maximum calcium content in the slag was 0.3 g/g of slag (refer Table 4.5 for corresponding CO_2 capture capacity). Thus, only 50% of the calcium could be sequestered to calcium carbonate when extraction is carried out at pH>8.2 (calcium carbonate native pH).

These results together indicate that the sample is highly alkaline and possesses high CO_2 sequestration potential, although direct carbonation under alkaline conditions may see a maximum of 50% calcium utilisation.

4.3.2 Susceptibility of mineral phases towards acid leaching

The maximum amount of Ca leached in the nitric acid was experimentally determined to be 81.8%. This shows a good match with the achievable calcium extraction efficiency (77%) predicted based on mineral composition. Powder diffraction patterns of the residual samples, shown in Figures 4.4 and 4.5, suggest leaching of silicate phase leaving behind poorly reactive brownmillerite phase, which concurs with the findings reported in the literature. Quantitative XRD analysis of the partially leached slag samples reveals that relative concentration of Fe(II) decreases in the residual slag (Figure 4.6), which suggests that Fe present in RO phase is susceptible to leaching unlike Fe(III) present in brownmillerite phase.

4.3.3 Stoichiometric acid consumption

Batch dissolution experiments suggest that the total acid uptake is twice the amount of total concentration of Ca, Mg, and Fe in the solution. Here, at the end of each addition, the solution was acidic and only divalent metal ions were found to leach (leaching of Fe(III) and Al(III) from brownmillerite phase is marginal). Based on these findings, the following

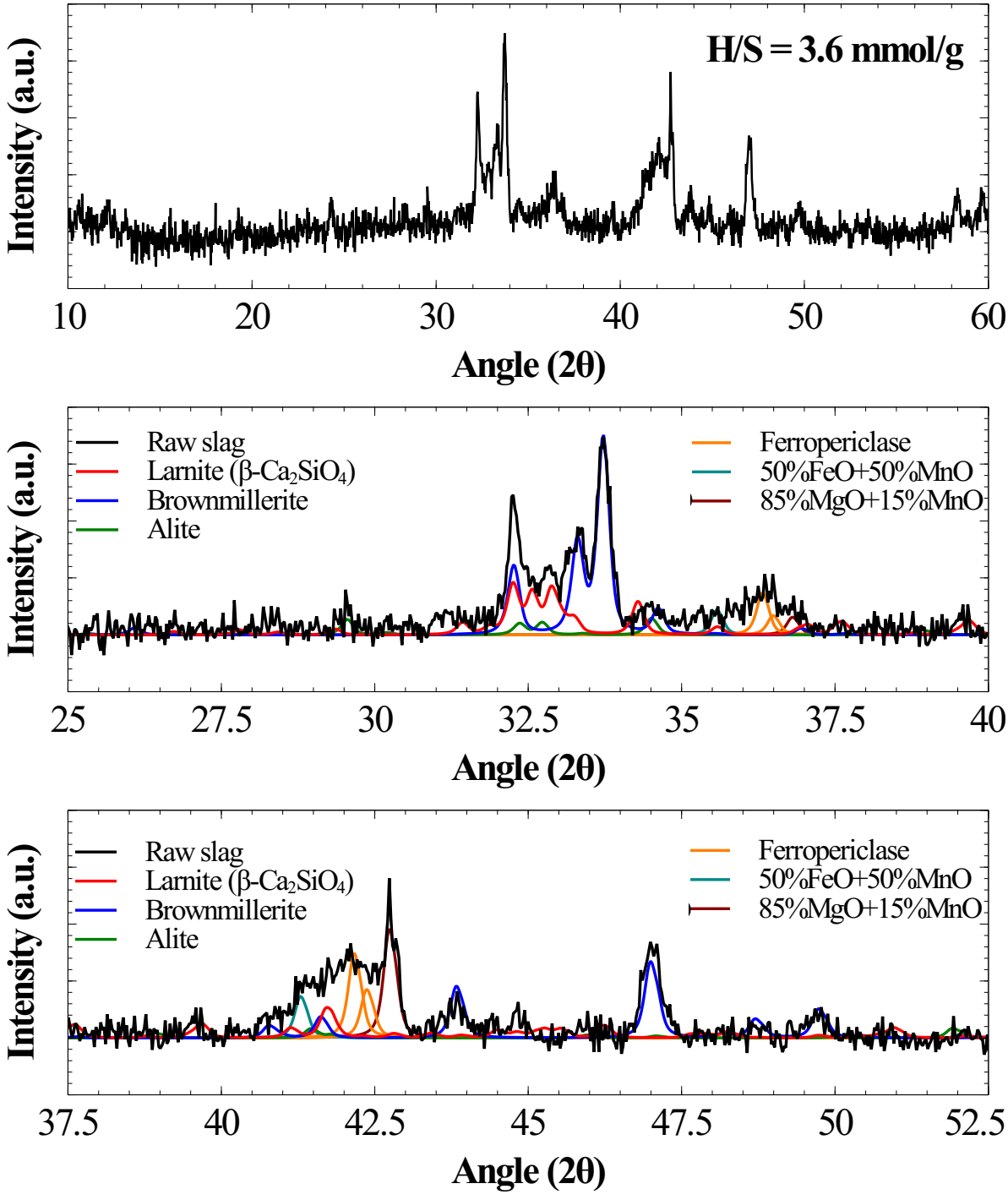

Figure 4.4: Deconvolution of mineral phases in XRD pattern of reacted slag (H/S=3.6 mmol/g)

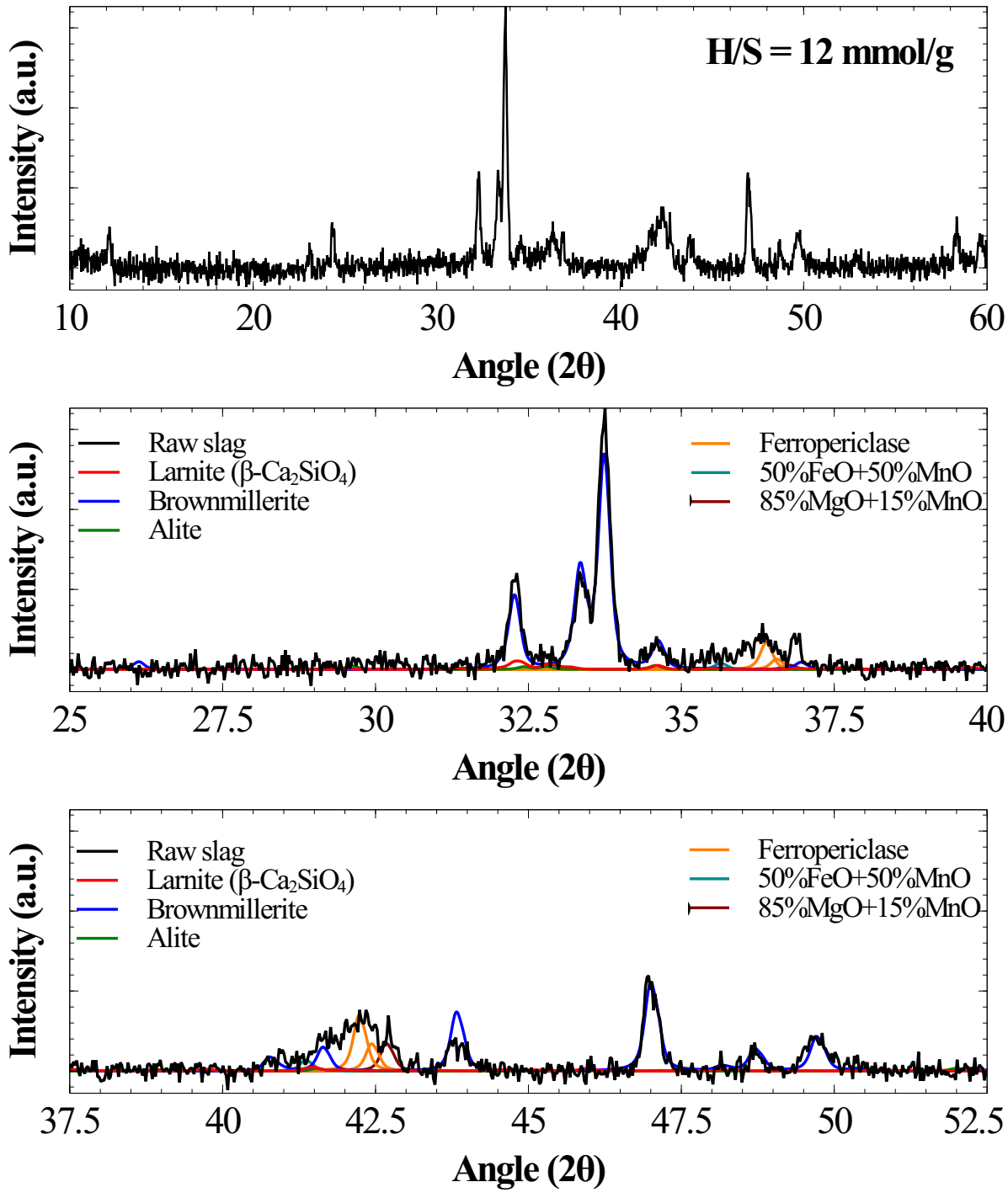

Figure 4.5: Deconvolution of mineral phases in XRD pattern of reacted slag (H/S=12 mmol/g)

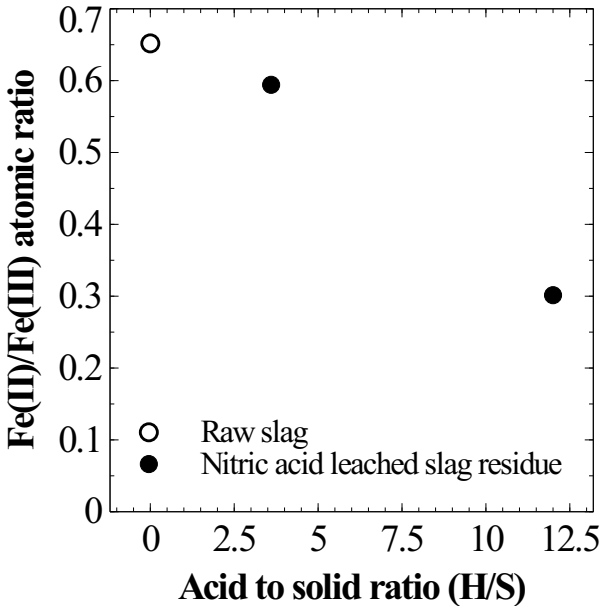

Figure 4.6: Relative amount of Fe(II) and Fe(III) mineral phases in the residual slag

slag dissolution reactions were deduced: $3\,CaO \cdot SiO_2 + 6\,H^+ \longrightarrow 3\,Ca^{+2} + H_4SiO_4 + H_2O$

$2\,CaO \cdot SiO_2 + 4\,H^+ \longrightarrow 2\,Ca^{+2} + H_4SiO_4$

$xFeO \cdot yMgO + 2\,(x+y)H^+ \longrightarrow xFe^{+2} + yMg^{+2} + (x+y)H_2O$

$H^+ + OH^- \longleftrightarrow H_2O$

4.3.4 Chemistry of aqueous solution

In addition to the the leaching reactions mentioned in previous section, it is necessary to determine the other proton consuming or generating reactions and the pH at which these reactions occur. Potentiometric titration has been used here to identify any acid consuming and generating reactions apart from slag dissolution. In each experiment, pH was measured after the addition of base to acidic slag slurry, wherein complete leaching was achieved. As shown in Figure 4.7A, two inflection points were noticed in the pH titration curve. These inflection points correspond to the following reactions (synthetic titrations obtained using Aqion PRO®[1] confirm these reactions as shown in Figure 4.8):

Speciation-precipitation reaction $Al^{+3} + H_2O \longrightarrow Al(OH)_3 + 3\,H^+$

[1] www.aqion.de

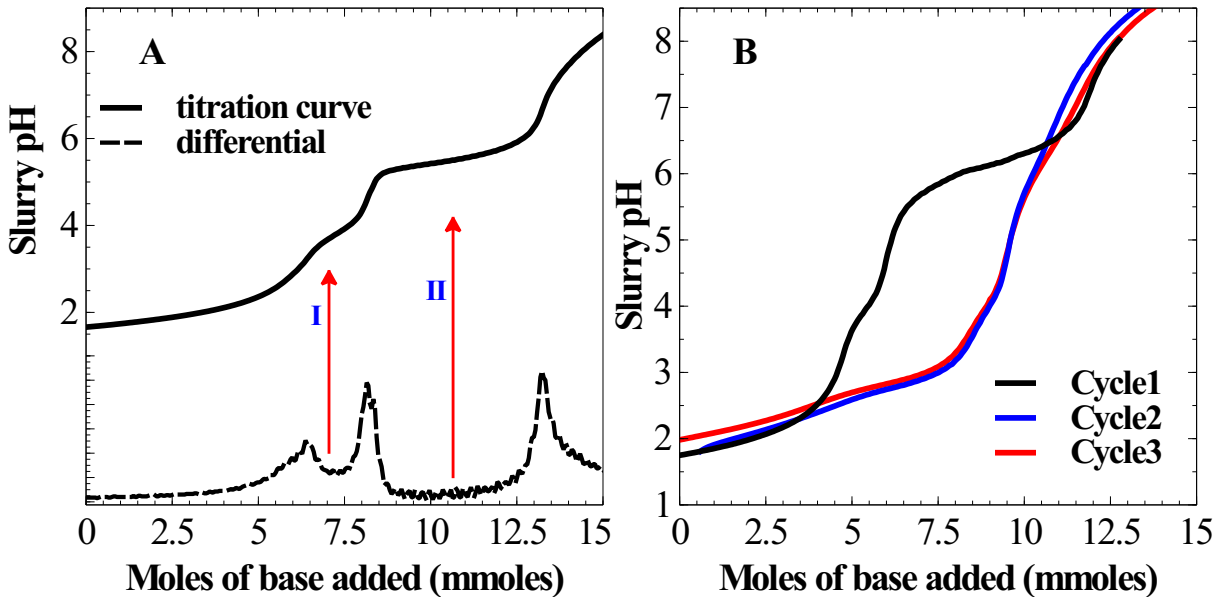

Figure 4.7: Acid-base titration to identify slag leaching chemistry A) Cyclic test to identify irreversible oxidation step; B) identification of acid dissociation steps based on acid-base titration

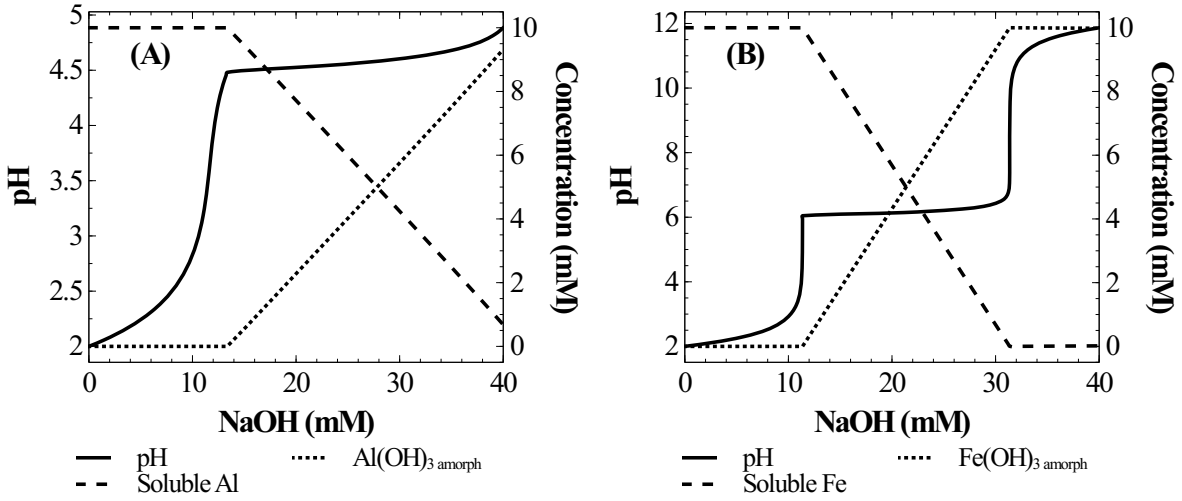

Figure 4.8: Simulated titration using Aqion shows (A) precipitation of aluminium hydroxide around pH of 4.5, and (B) precipitation of iron hydroxide around pH 6

Oxidation-precipitation reaction $Fe^{+2} + \frac{1}{4}O_2 + \frac{5}{2}H_2O \longrightarrow Fe(OH)_3 + 2H^+$

While speciation reactions are reversible with acid addition, oxidation is not. Cyclic titrations have been used to confirm that Fe-oxidation reaction is an irreversible oxidation reaction. As shown in Figure 4.7B, inflection point corresponding to Fe-oxidation reaction is missing in second and third cycles of titrations, which confirms that it is an irreversible reaction that can be attributed to the Fe oxidation and precipitation.

4.4 Implications for kinetic study

4.4.1 Leached layer formation and surface passivation

Mineral composition results from XRD and salicylic acid leaching tests indicate that silicates present in the steel slag are orthosilicates. As described elsewhere (Terry, 1983b), formation of siliceous residue which may protect the interior of silicate network is not expected in orthosilicates. Thus, formation of protective silica-rich leached layer is not expected as posited by many recent studies. Influence of re-precipitation of silica due to supersaturation on calcium extraction efficiency will be explored in next chapter.

4.4.2 Assessment of leaching agent

The results indicate a stoichiometric relation of 2:1 between acid uptake and metal ions release, concluding that metal ions are divalent (Figure 4.9A). In case of weak acids where acid dissociates partly, acid-metal exchange relation can be obtained using charge balance, law of mass action and mole balance, as shown below.

$$[H^+] + 2[M^{+2}] + [MA^+] - [OH^-] - [A^-] = 0 \tag{4.1}$$

$$[MA^+] + [A^-] + [HA] = [A_{tot}] \tag{4.2}$$

$$[MA^+] = \frac{[M^{+2}][A^-]}{K_{MA}} \tag{4.3}$$

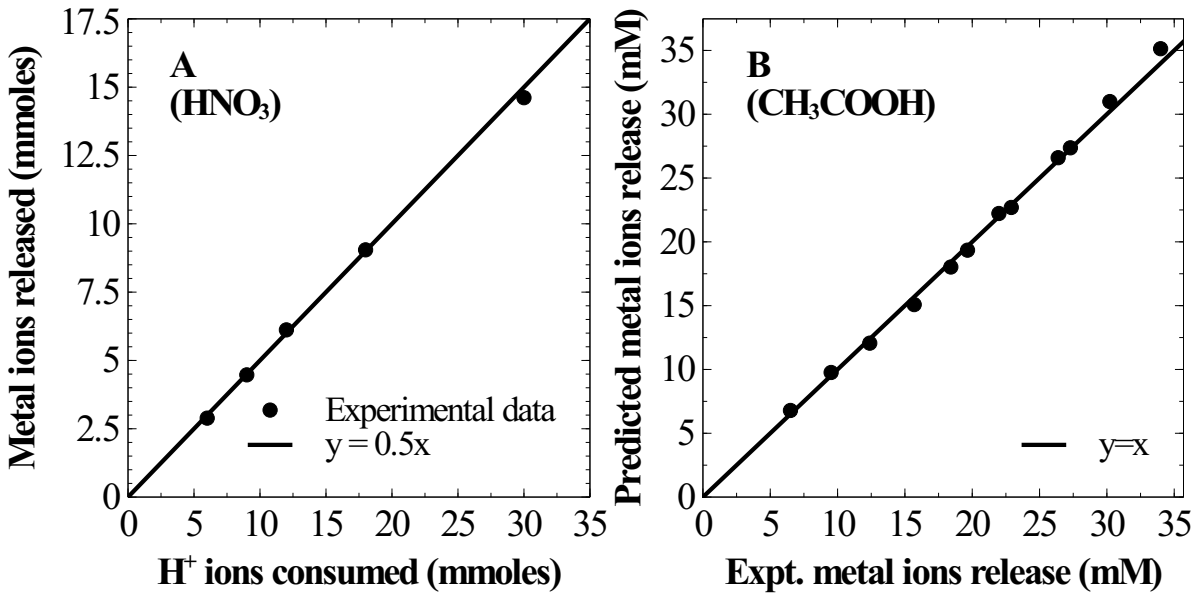

Figure 4.9: (A) Stoichiometric relation between acid uptake and metal ions release in nitric acid; (B) Prediction of metal ions release in acetic acid using pH data and Equations 4.1–4.4

$$[\mathrm{OH}^-] = \frac{[K_w]}{[\mathrm{H}^+]} \tag{4.4}$$

Batch dissolution experiments with acetic acid (weak acid) also revealed that the amount of metal ions released can be predicted based on pH change data using Equations 4.1–4.4 (shown in Figure 4.9B). These results suggest that the efficiency of a leaching agent in extraction of calcium from steel slag can be assessed by two parameters:

1. Ease of acid dissociation for proton-metal exchange reaction, and

2. Selectivity of acid towards calcium ions.

4.4.3 Proton-promoted dissolution

As shown by Terry (1983a) and Casey (1991), orthosilicates dissolve by breaking M—O bond as observed in the case of metal oxides; wherein orthosilicates exhibit similar dissolution trend as pure metal oxides. Thus, rates of metal ions leaching from steel slag is expected to agree with proton-promoted mechanism, which was shown to adequately describe metal oxides dissolution (Furrer and Stumm, 1986). Acceptability to such

Table 4.6: Elemental composition of various particle size fractions determined by sodium carbonate fusion

Particle size	**Ca**	**Fe**	**Mg**	**Si**
μm	wt%	wt%	wt%	wt%
< 45	28.3	19.6	4.8	4.2
75–90	27.1	18.9	3.1	5.5
150–212	28.5	21.4	3.8	5.3
(By XRF) < 45	30.7	16.9	5.5	8.0

Table 4.7: Coefficient of variation for various particle size distributions

Particle size	**Distribution**	**Mean** (μ)	**Standard deviation** (σ)	$\mathbf{C}_V = \sigma/\mu$
μm	-	μm	μm	-
90–125	Log-normal	192	52.8	0.28
150–212	Normal	212	32.4	0.15
212–355	Normal	376	67.3	0.18

mechanism will be explored by experimental kinetic study and mathematical modelling in subsequent chapters. Further, influence of organic acids and complexing ligands in catalysing or inhibiting leaching of various metal ions will be explored in the next chapter.

4.4.4 Homogeneity of samples

Previous investigations reported a decrease in overall calcium extraction efficiency with an increase in slag particle size. Mattila et al. (2012) attributed such differences to non-homogeneity of samples. Thus, chemical and mineral compositions have been investigated for various particle size fractions. The elemental composition among finer and coarser particles was investigated using sodium carbonate fusion method described in Section 3.2.2. Results, shown in Table 4.6, indicate that the elemental composition is similar among various particle size fractions. Also, a comparison with elemental composition obtained from XRF indicated a close match. Thus, there is no systematic change in calcium content with decrease in particle size in this steel slag; as speculated elsewhere (Mattila et al., 2012) for other steel slag. Also, XRD patterns of fine and coarse particles indicate that mineralogical composition is same for both (Figure 4.10).

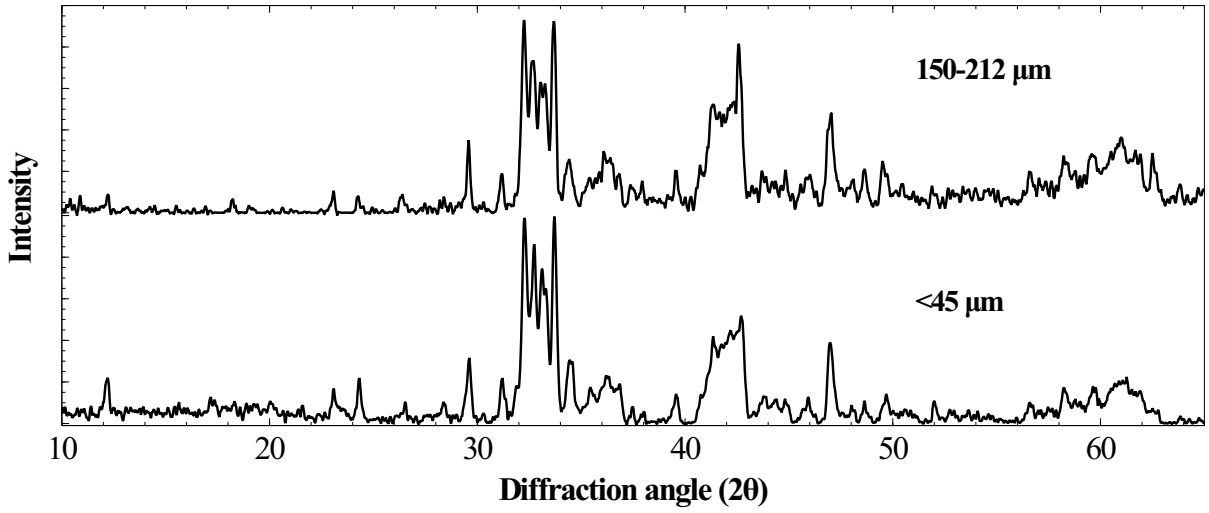

Figure 4.10: XRD pattern of steel slag (<45 μm and 150–212 μm)

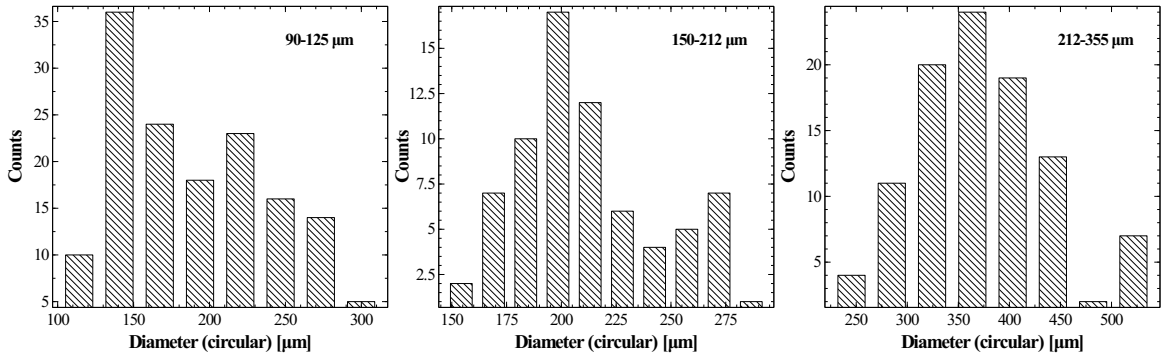

Figure 4.11: Particle size distribution obtained based on image analysis from SEM micrographs

4.4.5 Particle size distribution

Particle size distribution of coarser fractions of slag (90–125, 150–212 and 212–355 μm fractions) were obtained through image analysis of SEM micrographs (Figure 4.11). Dry grinding and sieving the steel slag sample resulted in a log-normal distribution for finer fractions and normal distribution for coarser fractions. Mean, variation and coefficient of variation (CV) for various particle size fractions are shown in Table 4.7. Results indicate that, CV is in the range of 0.15–0.28.

The particle size distribution analysis, however, did not account for the ultra-fine grains adhered to the particles. Presence of ultra-fine particles was shown to change linear kinetics to parabolic kinetics, leading to misinterpretation of controlling mechanism (Holdren and Speyer, 1985). Thus any role of ultra-fine grains in interpretation of controlling mechanism needs to be addressed separately.

4.4.6 Impurity removal

The concentration of Al in the solution is insignificant and its removal by spontaneous precipitation is not a concern. However, a significant amount of Fe(II) leaches (up to ~60% of Fe present in the slag) into the solution, which makes it a potential impurity. Its removal by spontaneous oxidation-precipitation is expected to be controlled by the increase in solution pH, which is expected to be a slow process as the rate of acid uptake by calcium silicate dissolution is expected to be slow around neutral pH. Impurity removal strategies will be explored in Chapter 5.

4.5 Summary

1. Elemental and mineral composition of steel slag shows that it has high calcium amount and mineral phases are very reactive. These results suggest that steel slag is a good feedstock for mineral carbonation. Mineral composition suggests that about 77% of the calcium which is present as silicates is extractable. Same was confirmed by acid leaching.

2. In the case of direct mineral carbonation, only 50% of the calcium in steel slag can be carbonated. This suggests that only indirect routes can maximise calcium

utilisation.

3. Amount of Fe, Mg and Si dissolved when calcium is completely dissolved in acidic media is significant and can potentially end up as impurities in PCC. Impurity removal steps must be considered for high-purity PCC production.

4. Gel formation is expected due to polymerisation of silica dissolved from silicates leading to filtration issues. Thus, filtration of calcium-rich aqueous solution from silica precipitated solution is concern.

5. Stoichiometric balance could be established between acid uptake and metal ions leached. Efficiency of any leaching agent can thus be correlated to extent of acid dissociation and calcium selectivity in that environment.

6. Characterisation studies suggest that silicate phases present in steel slag dissolve congruently and formation of leached layer is not expected. Further, slag dissolution kinetics in acidic media is expected to follow proton-promoted or ligand-promoted mechanisms in the absence of mass transfer limitations.

Chapter 5

Experimental investigation of slag dissolution kinetics

5.1 Background

The process of producing $CaCO_3$ using steel slag by indirect mineral carbonation is carried out in two steps (Baldyga et al., 2011; Sanna et al., 2014): 1) the selective dissolution of Ca from slag by a leaching agent followed by separation of leachate and 2) precipitation of calcium carbonate under CO_2 environment. Additionally, a purification step involving precipitation of iron and silica impurities by swinging the pH to alkaline conditions may be necessary (Park and Fan, 2004). It is well understood that the success of process is dependent on rapid, complete, and selective extraction of calcium. In order to improve the calcium leaching rate and overall carbonation efficiency several energy-intensive sub-processes such as grinding feedstock, use of strong acids and additives, addition on base for pH-swing and so on (Doucet, 2010; Romanov et al., 2015; Teir et al., 2016). These energy-intensive processes substantially reduce CO_2 capture benefits(Yuen et al., 2016) and increase the cost of PCC product. Currently, the process of selective leaching from slag is not clearly understood and lack of any *a priori* kinetic models for dissolution is a testimony for the same. It aimed in this chapter to identify independent parameters which influence leaching characteristics and aid in developing a kinetic model that provides insights into selection of leaching agent, tuning calcium selectivity, optimisation of overall process and reactor development.

5.1.1 Discrepancies in particle-size effect

Effect of particle size on Ca leaching characteristics has been reported in strong and weak acids in many studies(Stolaroff et al., 2005; Lekakh et al., 2008a; Said et al., 2015; Zhang et al., 2013; Mattila et al., 2012; Polettini et al., 2016). Besides the understandable influence of particle size on the rate of leaching, Ca extraction efficiency was also reported to increase with reduction of particle size. This was primarily attributed to surface passivation due to silica-rich layer, wherein bigger particle size particles passivate at lower extent of calcium extraction. A study by Mattila et al. (2012) attributed the effect to possible systematic variation in Ca concentration in particles of various size fractions. These hypotheses were speculative and inadequate to explain the effect of particle size as they necessitate the use of additional empirical parameter such as '*activity factor*' (Mattila et al., 2012) or use of variable diffusivity, which was in turn justified by assuming changes in product layer density with leaching) (Lekakh et al., 2008a). Moreover, the assumption of passive layer was based on SEM and simplistic models which assume surface area evolution to follow shrinking-core model. Further, the role of leaching chemistry and presence of Fe and Mg were ignored.

A conclusion such as diffusion limitation by passive layer formation had profound impact on choice of method for accelerating the process. For instance, it led to use of ultrasonic treatment (Said et al., 2015), inert grinding media (Park and Fan, 2004), and severe particle size reduction and so on to chip off passive layer. However, these energy-intensive processes also severely reduced particle size during dissolution and did not improve extraction efficiency in all cases. Thus, a better understanding of particle size effect and rate limiting processes are essential for prudent selection of techniques to accelerate the process.

5.1.2 Addition of base for pH-swing

As reported in section 2.2.4 of literature review chapter, NaOH or ammonical water is added to leachate to achieve the pH-swing to facilitate carbonation. Though pH-swing was proposed for removal of impurities by controlling pH, an inevitability of pH adjustment after dissolution step was observed even in cases where impurity removal is not attempted. The pH-swing step is nominally thought to be a consequence of dissimilar pH conditions

required for accelerated leaching and precipitation reactions (Kodama et al., 2008; Pan, 2012). In most cases, acidic/near neutral conditions were observed to prevail at the end of dissolution step. Such conditions were noticed even in those cases where weak acids such as organic acids were employed as leaching agents (Eloneva et al., 2008b; Santos et al., 2014b). In order to overcome the problem, recently, Kodama et al. (2008) proposed ammonium salt based process for spontaneous pH-swing. Though pH at the end of dissolution step was found to be favourable, loss of ammonia was observed.

The inevitability for pH-swing is intriguing as slag itself is highly alkaline (native pH of 12.5) and is expected to spontaneously increase the pH of the solution when the amount of acid supplied is less than maximum stoichiometric requirement. pH change during batch dissolution will be studied to determine the limit where pH-swing is spontaneous. Based on the improved understanding of leaching chemistry (described in Chapter 4), alternatives to base addition will be explored.

5.1.3 Kinetics of dissolution

There are two problems associated with the understanding of dissolution kinetics of steel slag, namely, identification of the rate controlling step, and a lack of kinetic models that consider the heterogeneous nature of steel slag. In several recent studies (Lekakh et al., 2008a; Dri et al., 2013; Mattila et al., 2012), identification of the controlling mechanism was attempted using integral forms of shrinking-core models, which are simplistic and often erroneous for several reasons (Gbor and Jia, 2004; Liddell, 2005). It has been shown in fluid-solid literature (Ghoroi and Suresh, 2007; Liddell, 2005) that different controlling mechanisms often fit conversion-time data equally well. Further, these models ignore the simultaneous release of other elements such as magnesium and iron and implicitly consider that the calcium extraction rate is independent of other elements. Thus, shrinking-core models reported so far were at best *effective* models as it is yet to be shown that the determined controlling mechanism and estimated kinetic parameters can provide reasonable predictions of various parametric effects (acid-to-solid ratio, particle size effect, liquid-to-solid ratio etc.).

In this chapter, an attempt has been made to systematically determine the rate controlling processes by identifying the independent parameters which influence the dissolution rate. Based on this understanding, development of mathematical model and comparison

of simulation results with parametric study will be presented in Chapter 7.

5.2 Parametric study

5.2.1 Effect of acid-to-solid ratio

Acid-to-solid ratio, expressed as the moles of acid added per gram of slag, has been varied to understand the influence of H^+ concentration on dissolution characteristics. In this study, we distinguish acid-to-solid ratio (H/S) from the liquid-to-solid ratio (L/S); the former parameter is expected to strongly influence the leaching rate and the extent of metal ions dissolved, while the latter parameter primarily provides a picture of primary or secondary mineral phases at their solubility limits.

Elemental release measured in the leachate during the leaching of slag, shown in Figure 5.1, demonstrates that both the rate of leaching (expressed as rate of conversion) and extent of leaching of all elements increase with an increase in the acid-to-solid ratio. A proportional increase in rates of release observed with an increase in acid concentration possible suggests that dissolution follows proton-promoted mechanism (Figure 5.2). Though a linear proportionality was observed, the intercept was found to be non-zero. This possibly indicates non-linear effect of proton adsorption, which will be systematically discussed in Section 5.3, where kinetic analysis is presented.

Although the initial rates of Ca, Fe and Mg increase proportionally with H/S, the enhancement in the extent of leaching has been observed to be higher in Fe and Mg, compared to Ca. As shown in Figure 5.3A, the selectivity of calcium (η_{Ca} defined in Equation 5.1) decreased with increase in calcium extraction, which suggests that the leaching is selective and selectivity varies with the extent of calcium extraction concomitantly leading to higher impurities. On the other hand, extraction of Si was found to be in stoichiometric proportion to Ca release (Figure 5.3B), which is expected as the slag is predominantly made up of orthosilicates.

$$\eta_{Ca} = \frac{[Ca](ppm)}{\{[Ca] + [Fe] + [Mg]\}(ppm)} \tag{5.1}$$

Experiments have also been done by varying the liquid-to-solid ratio and keeping the H/S constant. An increase in the leachate volume marginally reduced the initial

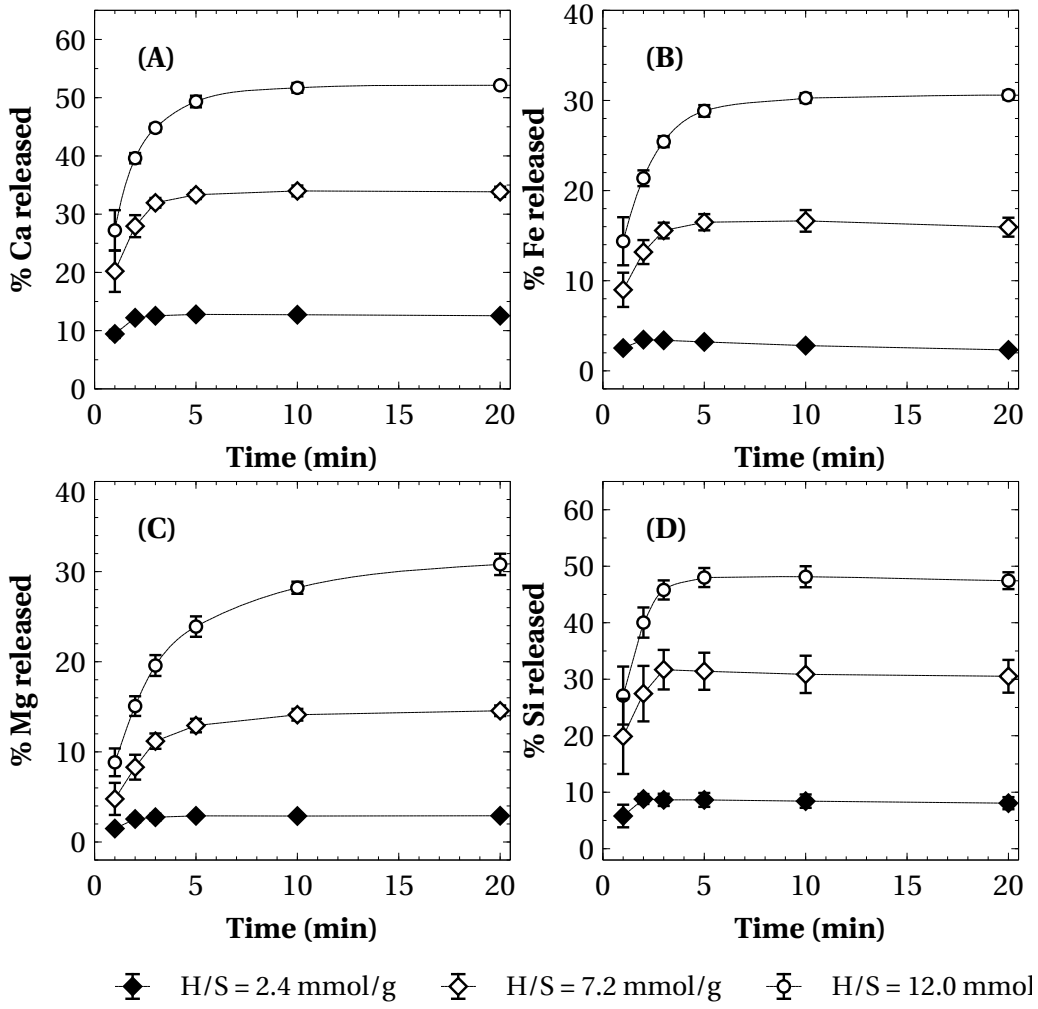

Figure 5.1: Effect of acid-to-solid (H/S) ratio on leaching characteristics of (A) Ca, (B) Fe, (C) Mg, and (D) Si in nitric acid (PS: 150–212 μm, L/S: 100 ml/g, T: 30 °C). Errors bars are standard deviations measured for at least three measurements; except for samples that were manually collected at t$\leq$1 min, where there is error in sample collection time by $\pm$5 seconds, error bars are comparable to marker sizes used in the plots.

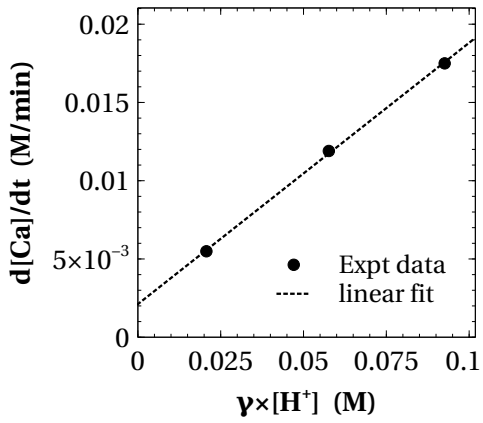

Figure 5.2: Dependence of initial release rate of calcium on H^+ activity

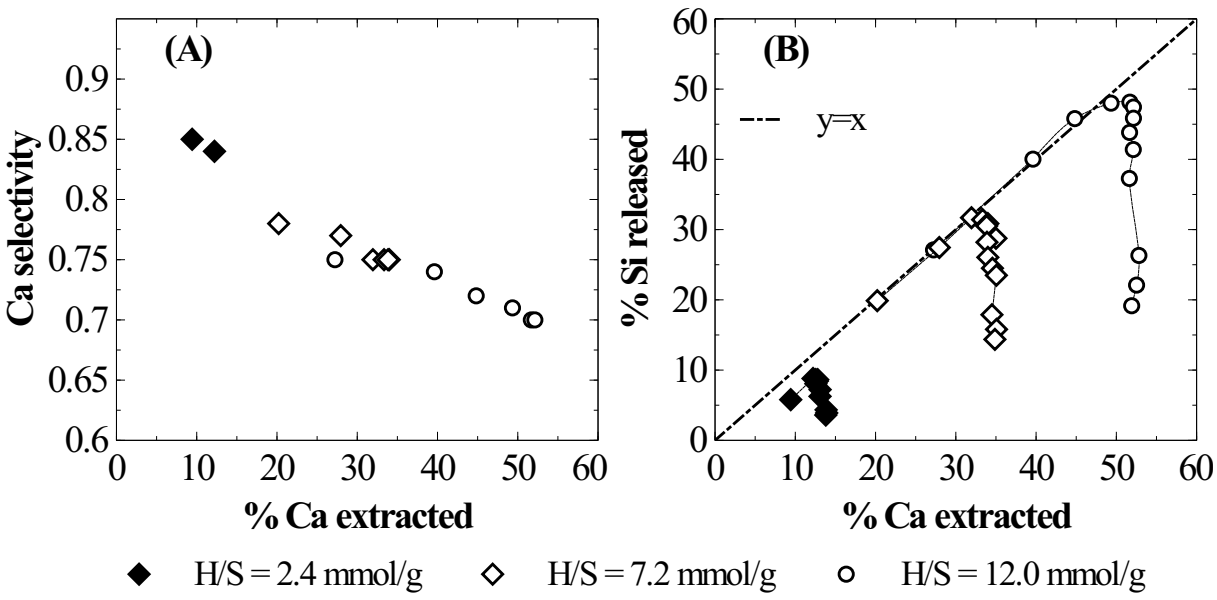

Figure 5.3: Relative extents of Ca and Si leaching (PS: 150–212 μm, L/S: 100 ml/g, T: 30 °C)

dissolution rate due to lower concentration (Figure 5.4). However, its influence on the extent of elemental release (Ca, Fe, and Mg) is insignificant. This suggests that the extraction efficiency is not limited by the solubility of corresponding primary or secondary mineral phases.

In case of Mg, while the effect on initial rate appears to be similar to that of Ca and Fe, a marginal enhancement in extent of dissolution was observed with an increase in L/S ratio. After the concentrations plateau (typically beyond pH of 5), there are secondary phenomena such as exchange of ions onto the surface of silica in bulk solution, formation of secondary precipitates etc. These secondary phenomena are affected by concentration of metal ions in the bulk solution (following changes in L/S) and have not been part of this study.

5.2.2 Effect of slag loading

The influence of solid loading on slag dissolution in nitric acid has been studied by keeping the acid concentration and liquid volume constant. The effect of solid loading can be distinguished from L/S effect based on the fact that the acid-to-slag ratio, and hence the total extent of metal ions release, is fixed in the latter case unlike the former case.

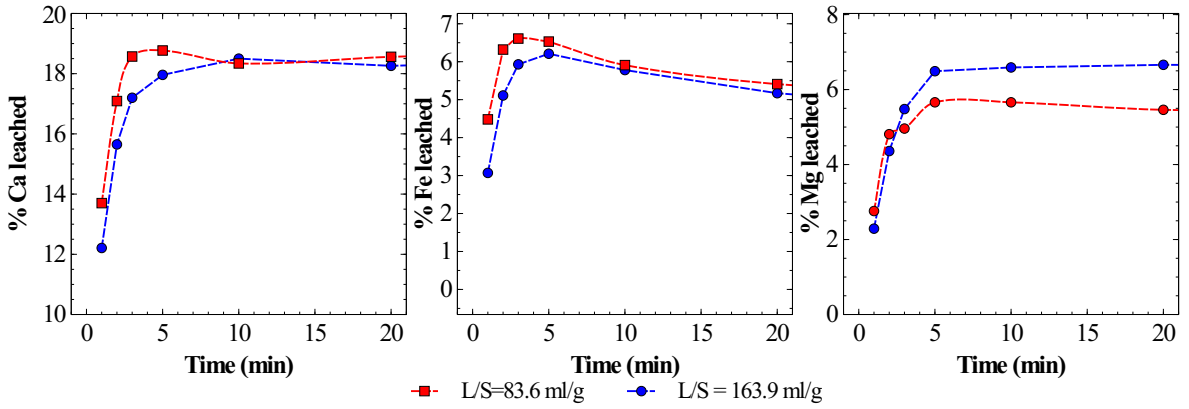

Figure 5.4: Effect of liquid-to-solid (L/S) ratio on leaching characteristics of (A) Ca, (B) Fe, and (C) Mg in nitric acid (PS: 150–212 μm, H/S: 7.2 mmol/g, T: 30 °C)

The results, shown in Figure 5.5, indicate that the initial rate of calcium leaching is proportional to amount of slag loaded (or surface area). Here, the extent of calcium leaching was found to increase with an increase in solid loading. On the other hand, the final concentration of magnesium and iron release decreased with increase in the solid loading. It is interesting to note that the initial rates of Fe and Mg release increased with increase in the solid loading, to an extent similar to that was observed in the case of calcium. As discussed in detail at a later stage (in Section 5.2.3), the effect can be attributed to strong geometrical influence on calcium leaching selectivity, where the amounts of Fe and Mg released could be related to effective calcium depth of leaching in the slag particle.

5.2.3 Effect of particle size

Effect of particle size was studied using five particle size fractions comprised of <45 μm, 75–90 μm, 150–212 μm, and 212–355 μm at an H/S of 7.2 mmol/g and L/S of 100 ml/g. Figure 5.6 shows the results. The effect of particle size on initial rate of calcium dissolution has been found to be proportional to geometrical surface area. The final concentration of calcium is observed to be higher in the case of finer particles compared to coarser particles. While previous studies associated this behaviour to passive layer formation or inhomogeneity of elemental concentration in various particle size fractions, in the current study, neither passive layer formation has been observed (due to congruent dissolution of silicates) nor is there any inhomogeneity of elemental or mineral phase composition

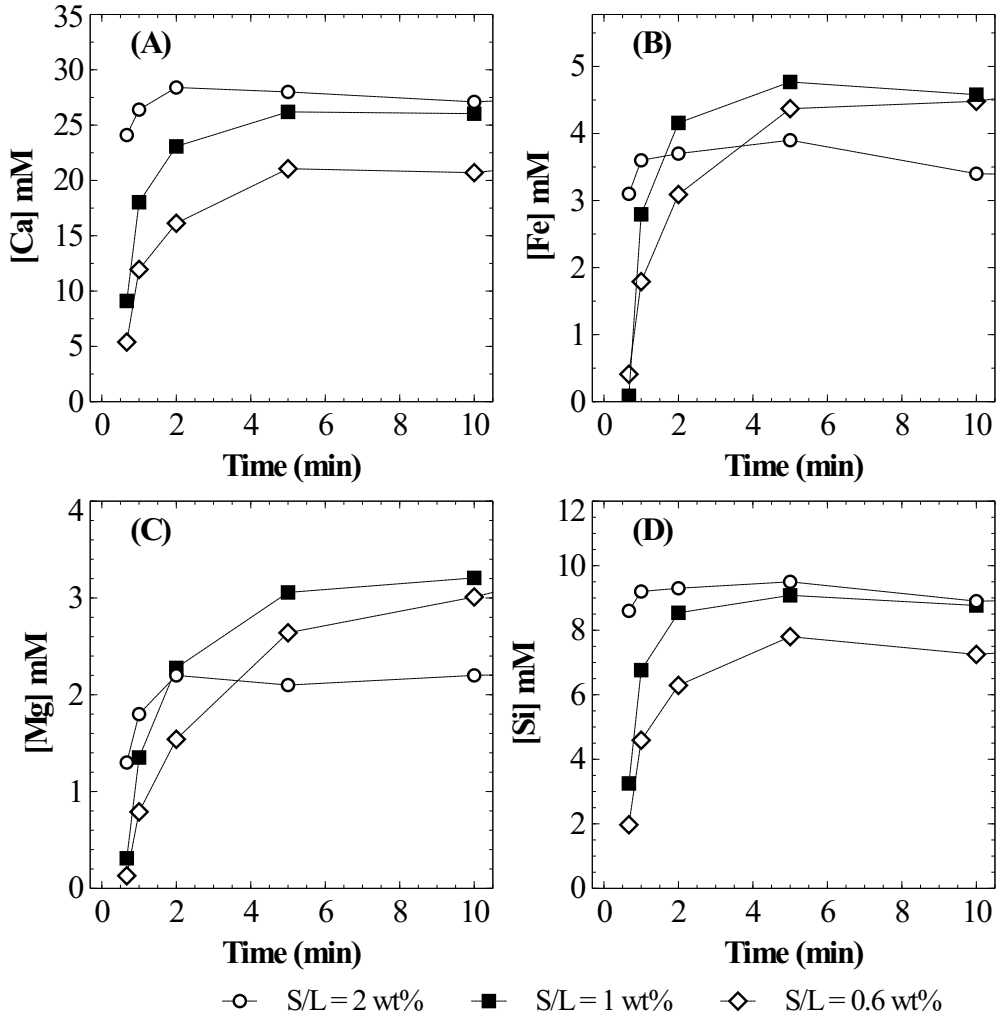

Figure 5.5: Effect of slag loading on leaching characteristics of (A) Ca, (B) Fe, (C) Mg, and (D) Si in HNO_3 (H/S: 7.2 mmol/g, T: 30 °C)

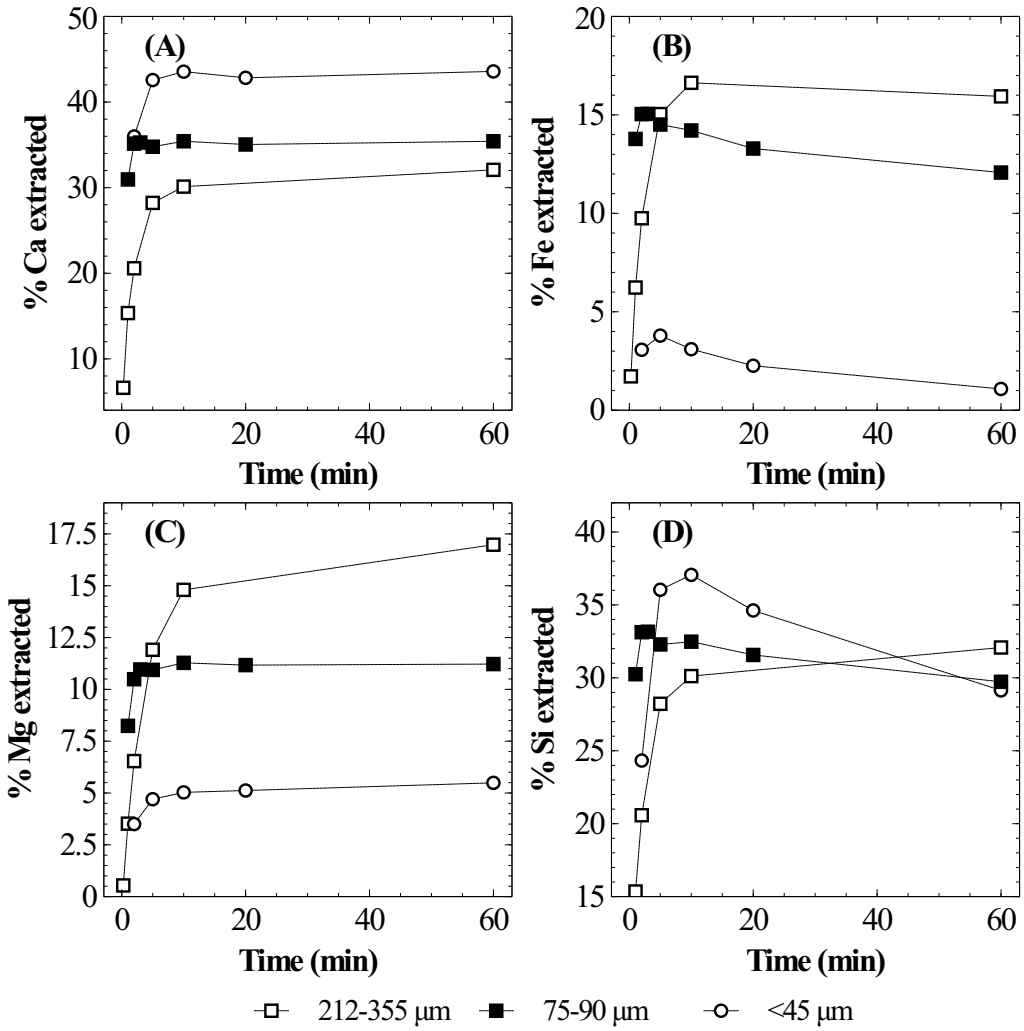

Figure 5.6: Effect of particle size (<45, 75–90, and 212–355 μm) on leaching characteristics of (A) Ca, (B) Fe, (C) Mg, and (D) Si in HNO_3 (H/S: 7.2 mmol/g, L/S: 87.2 ml/g, T: 30 °C)

among various particle size fractions (as shown in Section 4.4.4). On the other hand, seemingly similar to the effect of solid loading, despite an increase in initial release rates of Fe and Mg with a decrease in particle size, the extraction efficiencies of these elements were found to be lower for finer particle size fractions compared to coarser fractions (Figure 5.6). Further, the effect of particle size on elemental release characteristics in acetic acid media, shown in Figure 5.7, is similar to that observed in nitric acid, which suggests that the behaviour is independent of pH and the leaching agent.

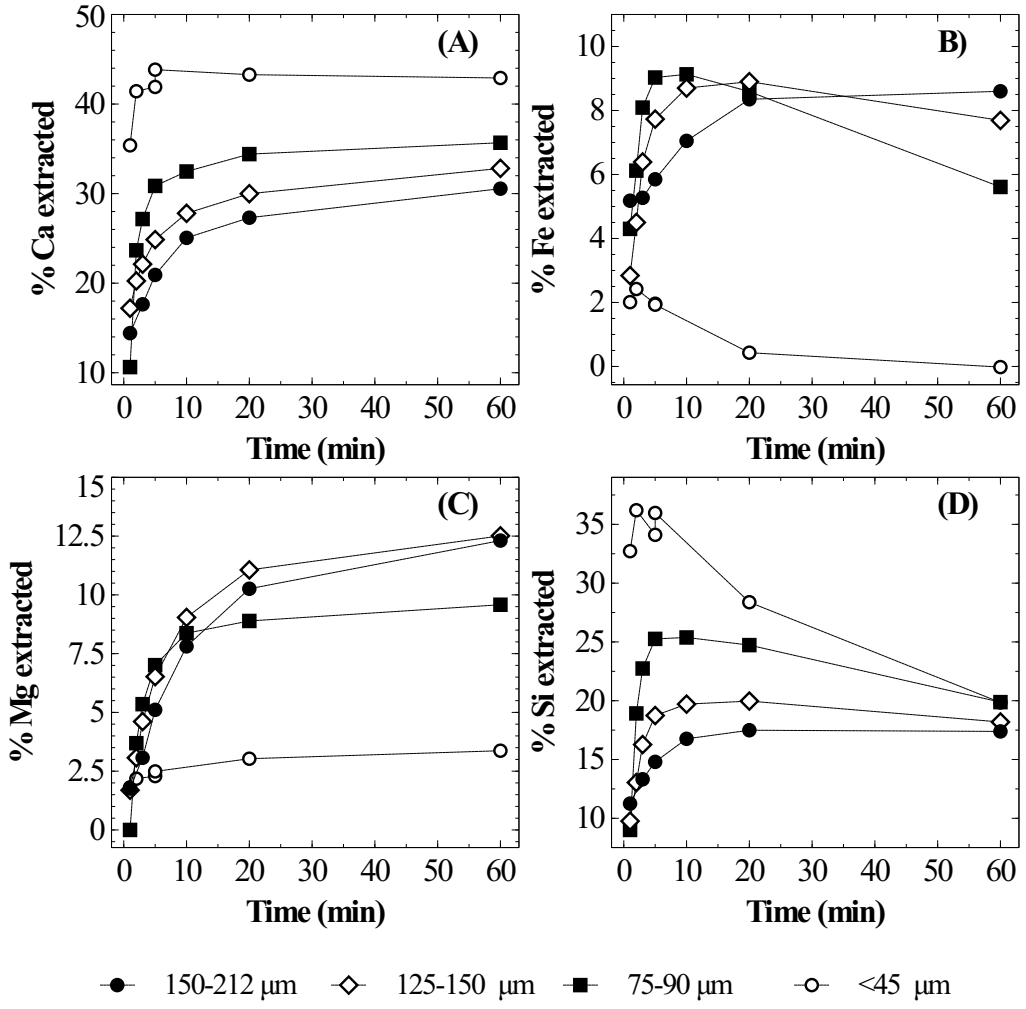

Figure 5.7: Effect of particle size on leaching characteristics of (A) Ca, (B) Fe, (C) Mg, and (D) Si in acetic acid (H/S: 7.2 mmol/g, L/S: 87.2 ml/g, T: 30 °C)

5.2.4 Effect of temperature

The influence of dissolution temperature on rate and extent of calcium dissolution was studied in acetic acid medium. The results, shown in Figure 5.8, suggest a marginal increase in initial rate of calcium dissolution at 52 °C as compared to 32 °C, while there is no appreciable difference between 52 °C and 70 °C. The extent of calcium leaching at the end of 60 min was found to be higher in the case of 70 °C, largely due to lower release of Fe into the solution. Fe was observed to precipitate rapidly with an increase in temperature leading to higher calcium selectivity. Under acidic conditions, solubility of Fe(III) hydroxide (ferrihydrite) is known to reduce with an increase in temperature (Liu and Millero, 1999), which explains the observed trend of Fe precipitation. Also, the precipitation of silica, whose polymerisation rate is known to accelerate with an increase in temperature (Chan, 1989), and expected to co-precipitate with ferrihydrite was found to be faster at higher temperatures. It can be concluded that improvement in extraction rate is marginal and higher temperature may assist in impurity removal.

5.2.5 Effect of ionic strength

As the kinetic analysis is attempted based on batch dissolution experiments, where the ionic strength (I) of the solution is expected to increase with the progression of dissolution, it is necessary to investigate the influence. During the course of slag dissolution in nitric acid, the maximum increase in ionic strength of the solution was found to be 0.1 M. Accordingly, its effect on the rate of calcium dissolution was investigated by adjusting the ionic strength of leaching solution to 0.1 M by addition of sodium nitrate salt. The results, shown in Figure 5.9, indicate that within the experimental conditions the influence of ionic strength is negligible. Hence, for the purpose of kinetic analysis, ionic strength effect will be neglected.

5.3 Controlling mechanism and independent parameters

The results from the parametric studies (discussed in the previous section) reveal that the rate of calcium release depends on the surface area per unit volume of the slag and acid concentration. Further, orthosilicates present in slag dissolve congruently without

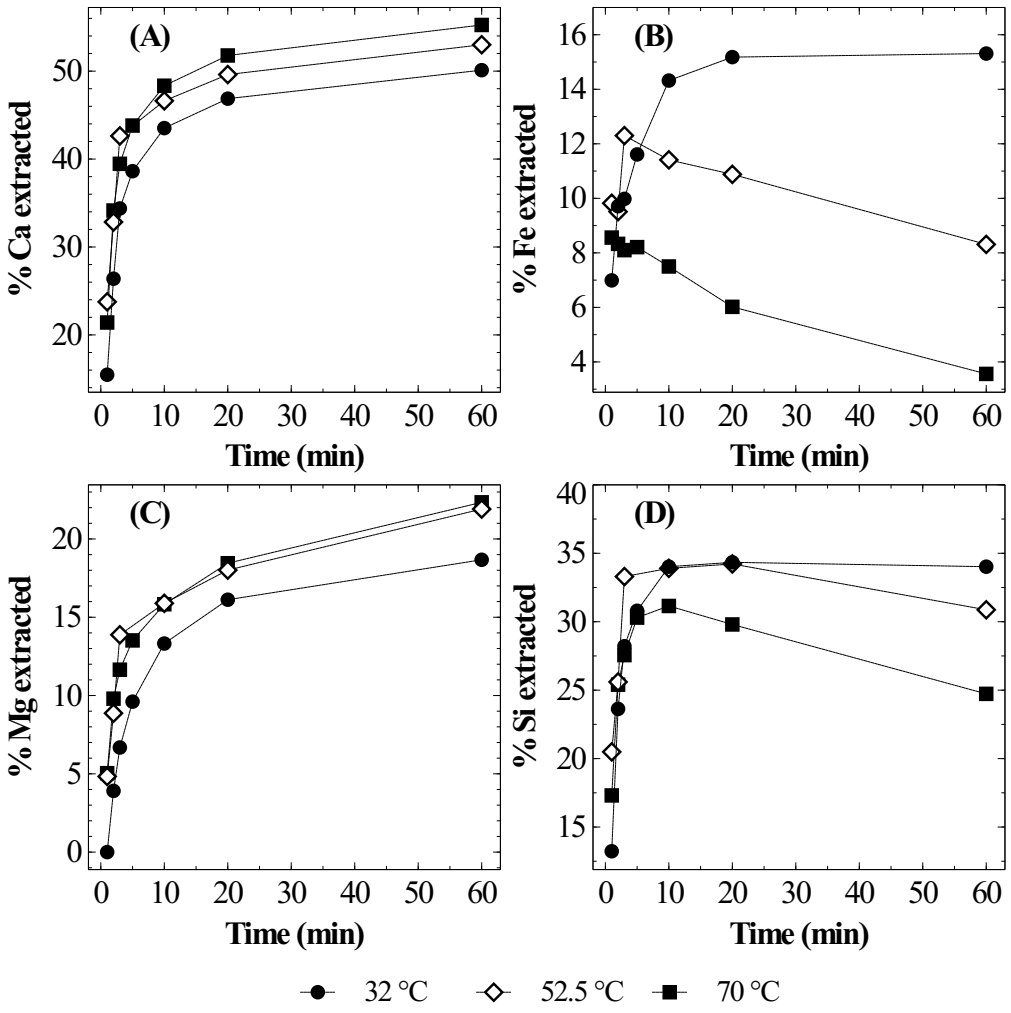

Figure 5.8: Effect of temperature on leaching characteristics of (A) Ca, (B) Fe, (C) Mg, and (D) Si in acetic acid (H/S: 7.2 mmol/g, L/S: 87.2 ml/g, PS: 150–212 μm)

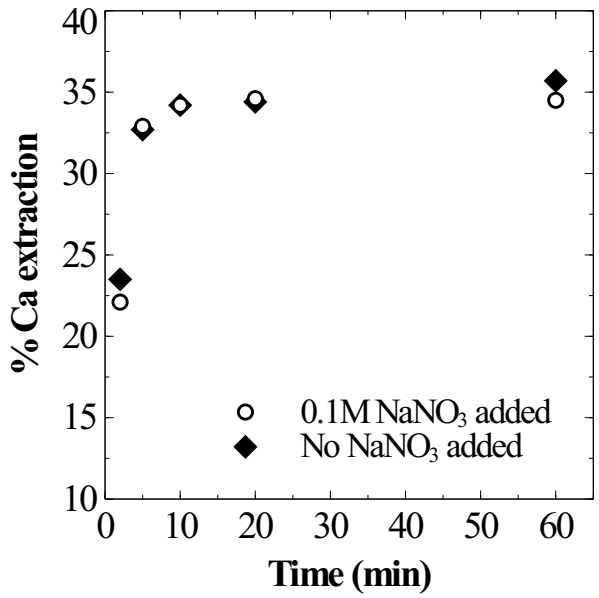

Figure 5.9: Effect of ionic strength on Ca leaching characteristics in HNO_3 (H/S: 7.2 mmol/g, L/S: 100 ml/g, PS: 150–212 μm)

leaving a leached layer. Also, the effect of stirring rate was found to be negligible on dissolution rate. Together, these results suggest little influence of external mass transport or surface passivation effects on the dissolution rate and surface reaction appears to be the rate controlling process. Accordingly, here, it is attempted to quantitatively describe the influence of independent parameters on dissolution kinetics controlled by surface reaction.

5.3.1 Proton-promoted dissolution

From data such as shown in Figure 5.1, rates of Ca extraction were calculated. Figure 5.10A shows the initial rates plotted against proton activity $\{H^+\}$ using data from acid-to-solid ratio experiments in nitric acid. The proton activity (in the bulk solution) was measured using pH electrode. Figure 5.10A shows a linear dependency of initial calcium leaching rate proton activity. However, linear regression yields a non-zero intercept, which probably indicates a non-linear behaviour. In general, leaching of metals from single silicate minerals are expected to depend on the surface concentration of H^+ and are satisfactorily expressed by the rate equation (5.2)(Stumm and Wollast, 1990).

$$r_M \propto [> SOH_2{}^+]^n \tag{5.2}$$

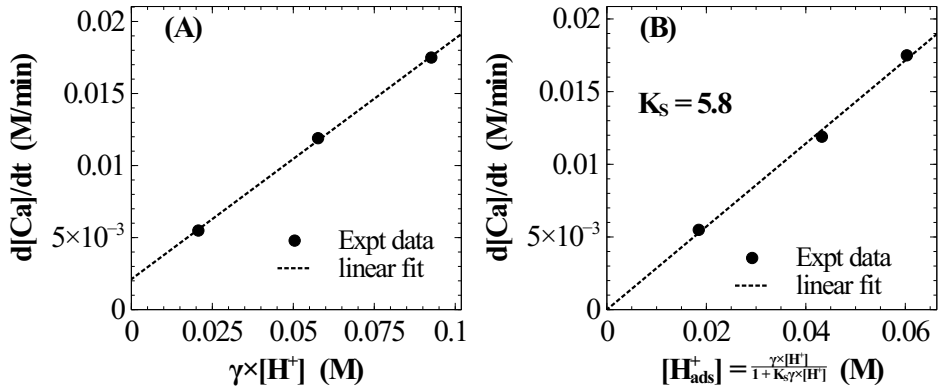

Figure 5.10: Dependence of initial calcium leaching rate on (A) $\{H^+\}$ and (B) $[H^+{}_{ads}]$ described by Langmuir isotherm given in Equation 5.3; The value of K_S was determined by linear regression as shown in (B).

where, $[> SOH_2{}^+]$ is the concentration of H^+ adsorbed on the surface. The formation of surface hydroxyls by adsorption of proton on a single site is given by following reaction scheme.

$$>SOH_2{}^+ \overset{K_{a1}}{\rightleftharpoons} >SOH + H^+$$
$$>SOH \overset{K_{a2}}{\rightleftharpoons} >SO^- + H^+$$

In general, a surface complexation model is deemed to be necessary to rigorously describe the adsorption of charged species (H^+) at the mineral-water interface. A simpler, yet satisfactory, approach would be to use an adsorption isotherm, say Langmuir or Freundlich for describing surface adsorption of H^+ in a narrow pH range, which is the case in current study. In addition, two distinct reasons make such isotherms suitable for the current experimental dataset. Firstly, the pH in current experiments was far from the isoelectric point (pH_{ZPC}) of dissolving minerals ($pH_{ZPC} - pH > 2$). Extrapolation of isotherm predictions to the neighbourhood of isoelectric point were previously found to be poor(Stumm and Wollast, 1990). Secondly, the effect of ionic strength, which is known to influence the sorption characteristics of charged species, was observed to be negligible. Hence, choosing the Langmuir formalism, we relate the adsorbed H^+ concentration to activity in solution as:

$$[H^+_{ads}] = \frac{K_S\{H^+\}}{1 + K_S\{H^+\}} \tag{5.3}$$

Here, as shown in Figure 5.10B, *single parameter* Langmuir adsorption isotherm

(Equation 5.3) was found to be sufficient to describe the influence of H^+ on initial calcium release rate. Further, the validity of Langmuir isotherm at pH values other than the initial point in a batch reaction has been verified as follows. The relevant pH range (2.5–3.5) has been chosen such that the surface area changes were expected to be minimal (extent of leaching in this pH range is expected to be small) and there is no secondary precipitation of dissolved species, thus allowing an independent analysis of acid concentration on dissolution rate. Further, $[H^+]$ data obtained from continuous pH measurement has been used instead of sparse metal analysis from ICP-AES in the chosen pH range. The relation 5.4 between rate of acid consumption and metal ion release is based on the experimentally determined stoichiometric relation of metal-proton exchange reaction.

$$\frac{\mathrm{d}[M^{2+}]}{\mathrm{d}t} = \frac{-1}{2} \times \frac{\mathrm{d}[H^+]}{\mathrm{d}t} \tag{5.4}$$

$$\frac{-1}{2} \times \frac{\mathrm{d}[H^+]}{\mathrm{d}t} = r_{Ca} + r_{Mg} + r_{Fe} \approx k \times [H^+_{ads}] \tag{5.5}$$

Here, it has been assumed that the Langmuir constants for various calcium silicate phase and RO phase are of similar magnitude and rate equations for metal ions release can be added to obtain acid uptake. The validity of the same will be examined using numerical simulations discussed in Section 7.2.3 of Chapter 7.

As shown in Figure 5.11, a linear correlation (with a slope of 1) between the logarithmic rate of H^+ consumption and the logarithm of $H^+{}_{ads}$ validates the applicability of the Langmuir isotherm. Based on this preliminary analysis, a detailed model is presented in Chapter 7.

5.3.2 Surface area evolution

Based on the experimental observations from solid-loading and particle-size effects, it is evident that the relative rate of release of calcium with respect to iron and magnesium decreases with the progression of leaching, that is, the calcium selectivity drops with the progression of leaching. Considering that the Langmuir constants for Ca-rich phases, and Mg- and Fe-rich phases are expected to be similar in magnitude (will be shown in Section 7.2.3), a significant change in selectivity with an increase in pH is not expected.

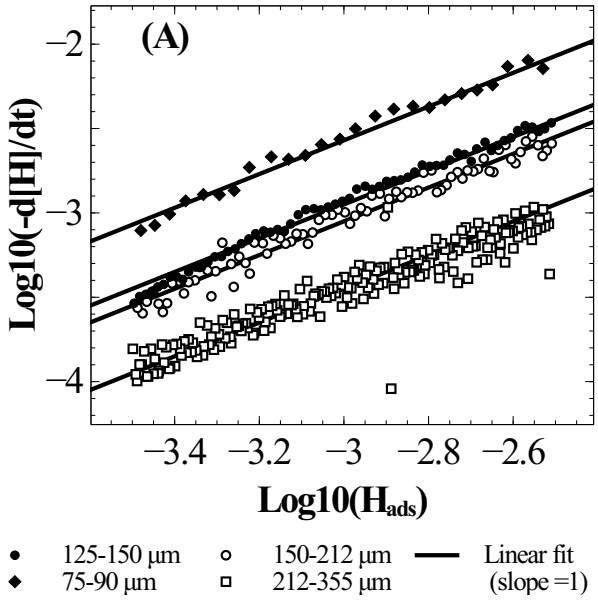

Figure 5.11: Linear relation between acid uptake and $[H^+_{ads}]$ described by Langmuir isotherm in the pH range of 2.5–3.5 for various particle size fractions

Consequently, it has been hypothesised that the observed reduction in calcium selectivity is due to surface area evolution, which is the other dominant factor that affects the rate of dissolution. An analysis of overall Ca selectivity (Equation 5.6) with the *depth of calcium leaching* d_{Ca} (Equation 5.7), a proxy geometrical parameter for surface area of Ca-rich phase in the slag, has been shown in Figure 5.12. It is evident that the influence of solid loading and particle size variations on calcium selectivity are similar, which confirms the role of geometrical factors in the observed dissolution characteristics.

$$\eta_{Ca} = \frac{[\mathrm{Ca}]}{[\mathrm{Ca}] + [\mathrm{Fe}] + [\mathrm{Mg}]} \tag{5.6}$$

$$d_{\mathrm{Ca}} = \frac{d_{0,\mathrm{slag}}}{2} \times \left(1 - (1 - X_{\mathrm{Ca}})^{1/3}\right) \tag{5.7}$$

where, $d_{0,\mathrm{slag}}$ is the initial diameter of slag particle, X_{Ca} is the fraction of calcium extracted.

Here, it is hypothesised that the relative surface area of Fe and Mg, which are part of the RO phase, increases with the progression of dissolution. The increase in surface area can be attributed to the release of RO phase globular inclusions (which were previously inaccessible to leaching solution) due to the dissolution of calcium silicate matrix, as illustrated in Figure 5.13A. Observation of a typical leached slag grain under scanning

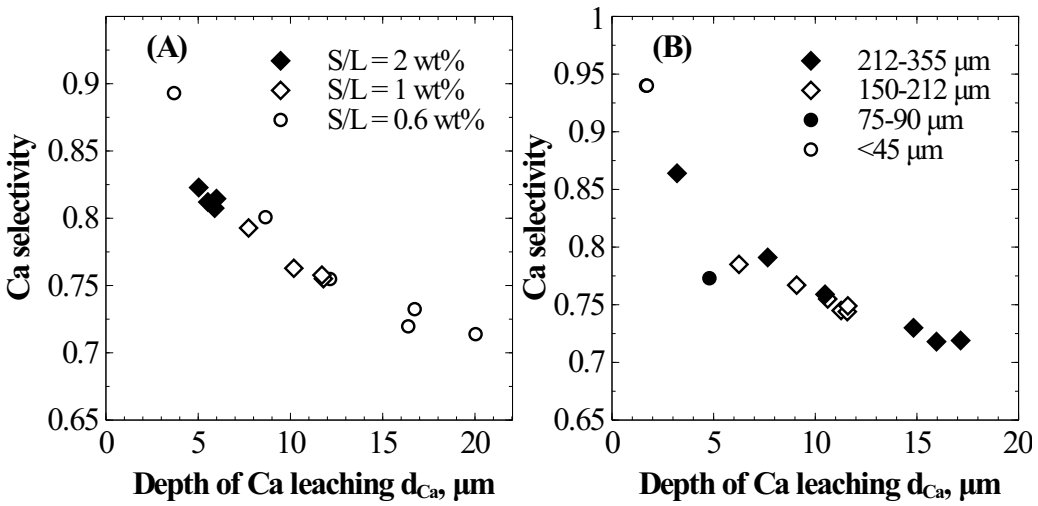

Figure 5.12: Dependence of calcium selectivity on depth of leaching for (A) solid loading case, and (B) particle size effect case in nitric acid (H/S: 7.2 mmol/g, T: 30 °C)

electron microscopy, shown in Figure 5.13B, corroborates the hypothesis. With the assumption that the RO phase particles are homogeneously distributed in the slag matrix, for the same extent of dissolution i.e. same volume of slag dissolved, the number of RO phase particles exposed to the leaching agent is expected to be same for coarser and finer particle size fractions. On the contrary, for the same sample mass per unit liquid volume, the number of slag particles and in turn the calcium silicates matrix surface area are lower for coarser particles compared to the finer particles. Thus, the relative surface area of RO phases particles is higher in the case of coarser particle which leads to lower calcium selectivity observed in the experiment. The mathematical model for the same has been developed using population balance method in Chapter 7, in similar lines to the *sporulation* model (Adrover et al., 2004).

5.3.3 Role of silica in calcium extraction kinetics

Several studies have speculated on the formation of a residual silica layer on the surface of the slag and posited that rate of metal ion release into the aqueous solution is controlled by the diffusion across the silica layer. The evidence is mainly based on the effect of particle size, microscopy and goodness of fit observed in shrinking core modelling. Although the observations on particle size effect concur with the literature, the results show there is no formation of a leached layer as the dissolution of silicates is congruent.

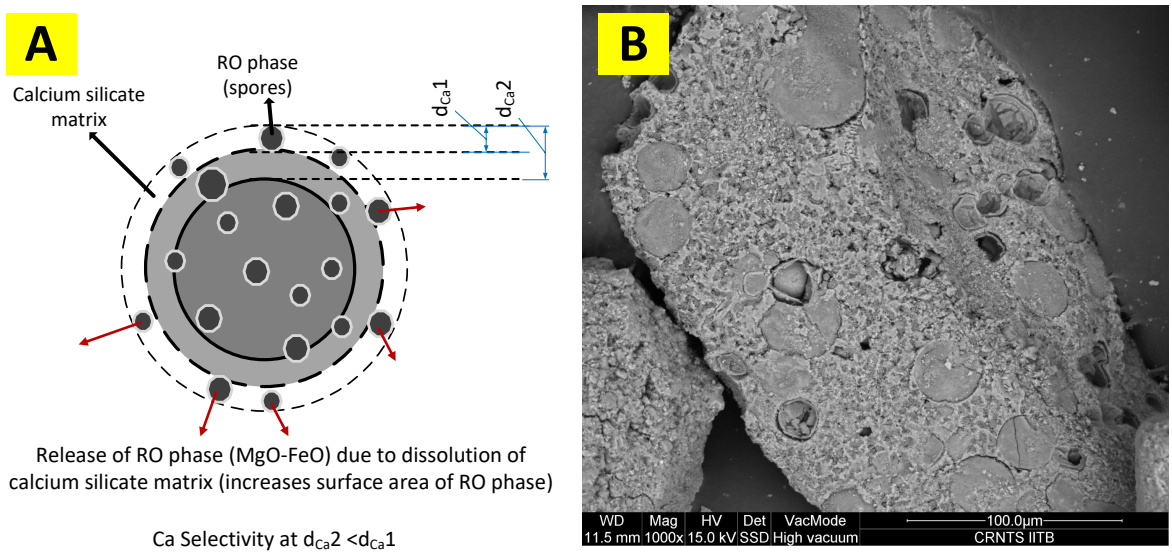

Figure 5.13: (A) Geometric model to explain reduction of Ca selectivity with depth of calcium leaching (B) SEM micrograph of leached slag showing release of RO phase from calcium silicate matrix

The silicon concentration, however, has been found to be supersaturated by an order of magnitude. Thus, it of interest to investigate the possibility of simultaneous dissolution and precipitation and its influence on calcium extraction efficiency. For this, semi-batch dissolution experiments, as done in the case of pH-stat experimentation that were widely employed to study kinetics, were conducted to measure the apparent rates of Si release at different rates of acid addition. Figure 5.14 shows the results. In Figure 5.14A, the rate of acid addition was more than that required to maintain constant pH, leading to a progressive decrease in pH. Figure 5.14B shows that the relative extraction efficiency of Si leaching reduces with a decrease in the rate of acid addition. At the slowest rate of addition, the net Si released was found to correspond to the solubility of silica (1.9 mmol/L, which corresponds to 5.8% extraction efficiency). These results suggest that the rate of silica polymerization, under pH-stat conditions, would be comparable or faster than the observed dissolution rate. Considering that the silica has lower pH_{zpc} of ~2.5(Carroll-Webb and Walther, 1988) and carries a negative surface charge in the near-neutral pH environment, it is possible that (a) it precipitates on positively charged residual slag, or (b) the silica surface charge is neutralized by calcium ions present in solution(Belton et al., 2012). The latter case appears to be more dominant as the formation of gel was observed with the progression of leaching. In any case, it is to be noted that the overall calcium

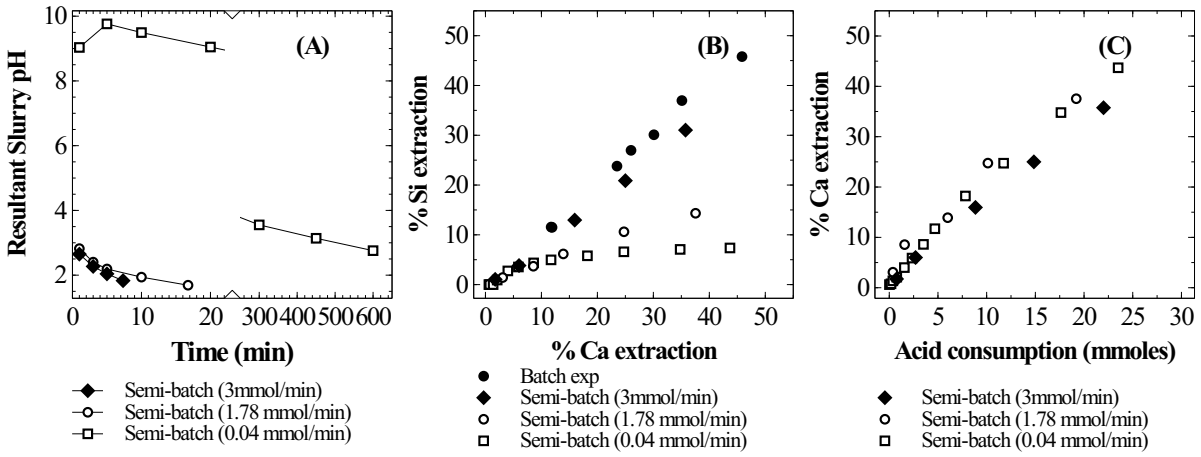

Figure 5.14: (A) Resultant slurry pH at various acid addition rates in semi-batch slag leaching experiments; (B) Influence of acid addition rate on Si release characteristics; (C) influence of acid addition rate on calcium extraction efficiency

extraction remained the same without affecting the calcium selectivity (Figure 5.14C). These findings suggest that observations reported in the case of slags with orthosilicates, are artefacts and interpretation of dissolution kinetics based on apparent release rates may lead to an erroneous interpretation of the controlling mechanism. Also, as shown in the previous section, Fe(II) oxidation-precipitation and Al precipitation also contribute to net acid consumption. Thus, in multi-element systems such as slag, rates evaluated by maintaining a constant pH may not be the true rate observed at that pH.

5.4 Impurity removal

Batch dissolution experiments conducted for 60 min (see inset of Figure 5.15) showed that end pH remains stable in the range of 5–6 for cases where H/S was greater than 2.4 mmol/g. The H/S of 2.4 mmol/g corresponds to just 20% of the stoichiometric requirement of acid for complete metal extraction. Here, we observe the inability of residual alkalinity present in the steel slag, which is 80% of the initial amount, to spontaneously increase the slurry pH in this time. However, extending the dissolution time to 24 hours reveals a second period of spontaneous increase in pH after a plateau (Figure 5.15). Figure 5.16 shows the pH-time profile compared with the time course of iron extraction. As seen in this figure, the second phase of pH increase occurs after complete precipitation of iron in the solution. Based on leaching chemistry described in Sections 4.3.3 and 4.3.4

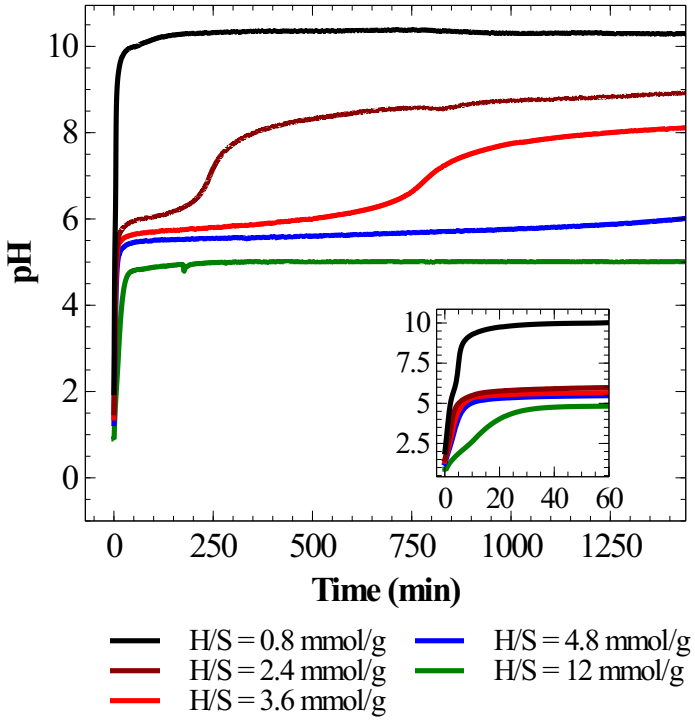

Figure 5.15: Experimental pH data observed during 24 hour leaching experiments. Inset shows the slurry pH evolution for first 60 minutes of dissolution

of Chapter 4, the pH plateau can be attributed to the Fe(II) oxidation to Fe(III) and spontaneous precipitation of as ferrihydrite (FeOOH), as also observed during cyclic acid-base titrations. Here, the rate of oxidation and subsequent precipitation appears to be limited by the rate of leaching of calcium and magnesium, whose dissolution controls the hydroxyl ion generation in the slurry.

For production of high purity PCC, it is necessary to reduce the [Fe(II)] either by oxidation and precipitation as Fe(III) hydroxide or to inhibit the dissolution of Fe(II). In subsequent Sections 5.4.2 and 5.4.3, induced precipitation and dissolution inhibition of iron by additives are investigated.

5.4.1 pH plateau

5.4.2 Addition of base for pH-swing

Teir et al. (2007) reported a low leachate pH at the end of the dissolution step for slag in acetic acid. However, the reason for the same was not commented upon in the study. These authors subsequently adopted the addition of NaOH to increase the pH, which

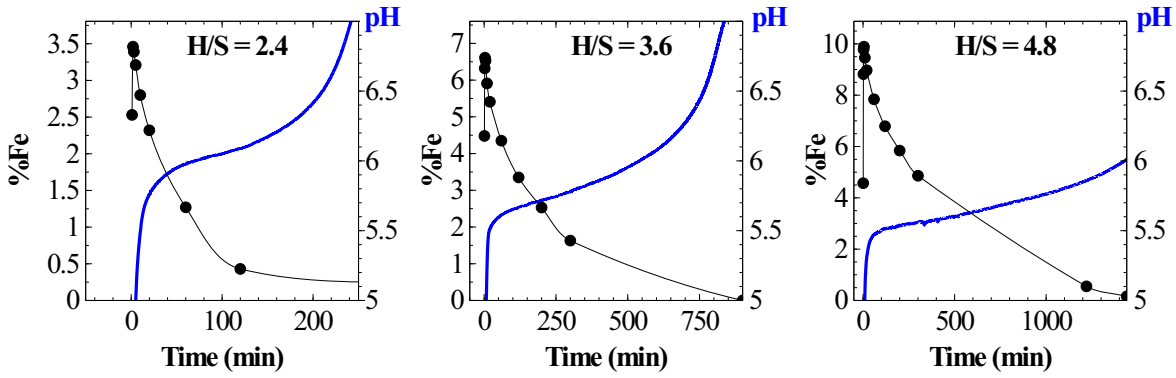

Figure 5.16: Correlation between Fe precipitation and slurry pH change

is required for carbon dioxide absorption and carbonate precipitation. Similarly, the addition of NaOH to increase the slurry pH has been investigated. Figure 5.17 shows the results. As shown in Figure 5.17B, iron was observed to spontaneously precipitate with the addition of NaOH, which corroborates the observation that the rate of iron oxidation is limited by hydroxyl concentration. However, the addition of NaOH was found to reduce the concentration of Ca and Mg in the leachate, reducing the overall extraction efficiency. This shows that addition of NaOH not only results in an additional cost, but also in a penalty on calcium extraction. Further, the addition of sodium hydroxide resulted in spontaneous gelation of silica that made filtration difficult. Based on these findings, it can be concluded that the addition of sodium hydroxide results in many drawbacks both in terms of energy efficiency and operational efficiency.

5.4.3 Inhibition of Fe leaching using chemical additives

As an alternative to pH-swing to remove iron impurity, we explored the possibility of reducing the iron leaching from the slag by surface complexation by sodium molybdate. Molybdate ion is a known deterrent of iron oxides dissolution and widely applied in corrosion studies (Armour and Robitaille, 1979; Huang et al., 2012). It is understood that the pH_{ZPC} (pH corresponding to zero surface charge) of iron molybdate complex is lower than that of iron oxide(Tian et al., 2011); lowering the difference between slurry pH and pH_{ZPC} reduces the surface concentration of H^+, which lowers the rate of dissolution

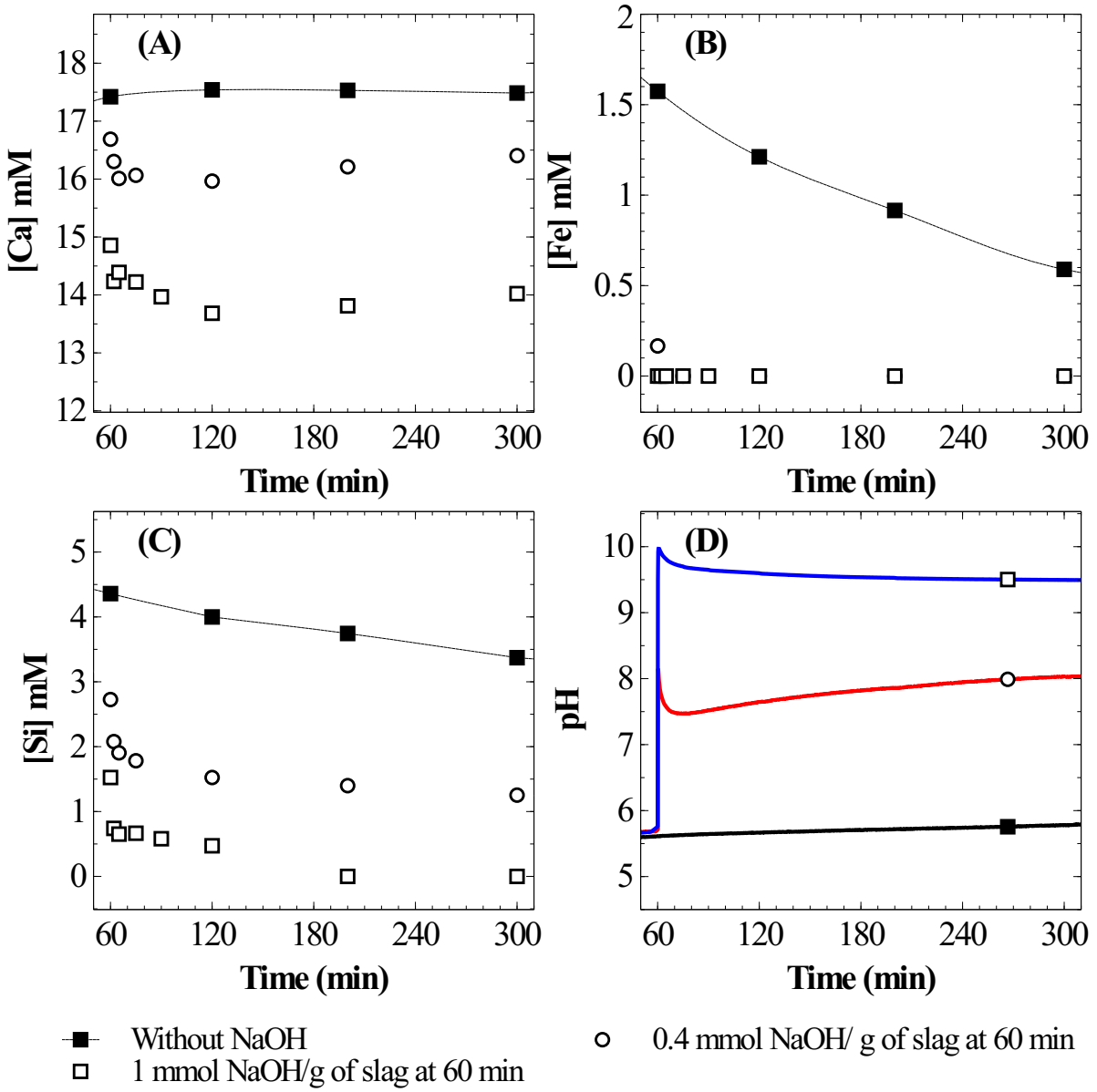

Figure 5.17: Effect of addition of NaOH into slag slurry after 60 minutes of dissolution in HNO_3 for pH-swing on (A) Ca, (B) Fe, (C) Si, and (D) pH (H/S: 3.6 mmol/g, L/S: 83.6 ml/g, PS: 150–212 μm)

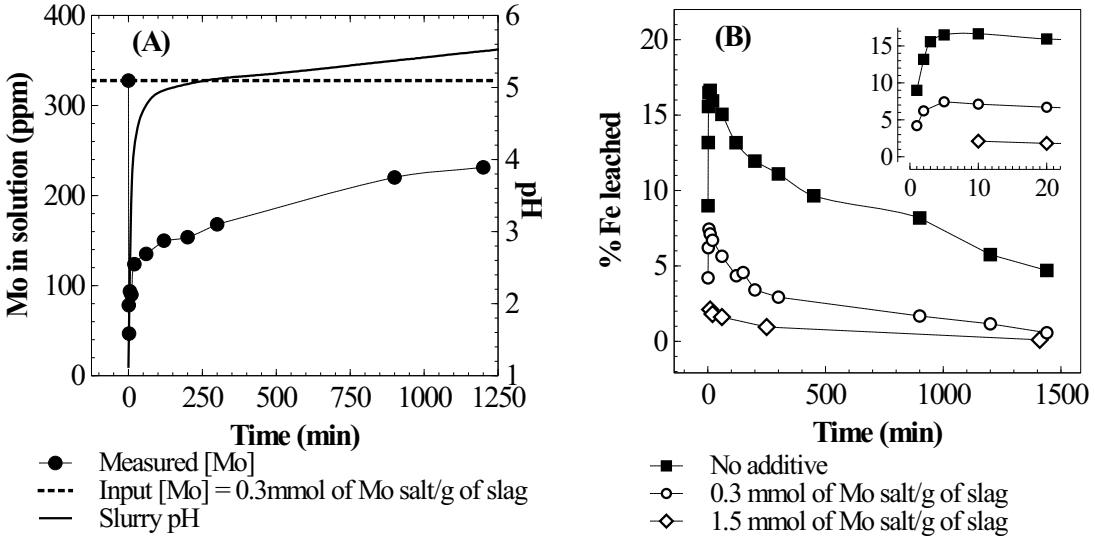

Figure 5.18: (A) Molybdenum adsorption and desorption by slag and evolution of pH (B) Fe leaching with and without sodium molybdate addition in HNO_3 (H/S: 7.2 mmol/g, L/S: 87.2 ml/g, PS: 150–212 μm). Inset shows dissolution data for short time period.

of oxides. As shown in Figure 5.18B, the addition of sodium molybdate resulted in only 2% Fe leaching as compared to 20% without the additive. Figure 5.19 shows the effect of molybdate addition on the leaching of Ca and Mg; a decrease is observed in Mg leaching (as in the case of Fe) while Ca release increased marginally after 90 minutes. Consequently, there is a significant improvement in calcium selectivity (0.97 compared to 0.75 without additive after 60 min of dissolution) and a marginal improvement in calcium extraction efficiency. An increase in calcium leaching (after 90 min of dissolution) can be attributed to the reversal of molybdate condensation (below reactions) which releases H^+ ions into the solution (Strickland, 1952) in the pH range of 4–5 (determined by potentiometric titration).

$$4\,{MoO_4}^{2-} + 6\,H^+ \longleftrightarrow {Mo_4O_{13}}^{-2} + 3\,H_2O$$
$$5\,{MoO_4}^{2-} + 4\,{Mo_4O_{13}}^{-2} \longleftrightarrow 3\,{Mo_7O_{24}}^{6-}$$

The effect of molybdate addition on pH variation is shown in Figure 5.20, for two size fractions. A spontaneous increase in pH, more than in the absence of molybdate, is seen for both sizes. These results show that molybdate addition is a promising approach, which can also reduce the cost of pulverizing the slag to fine fractions. The evolution of molybdate concentration in a batch reaction is shown in Figure 5.18A. This figure shows that an increase in pH results in desorption of molybdate ions from the surface into the

aqueous solution, which makes it possible to recover and recycle the same. Similar decrease in molybdate adsorption with an increase in pH has been previously reported(Huang et al., 2012). Unlike widely adopted sodium hydroxide addition, here it is possible to spontaneously recover the additive for recycling.

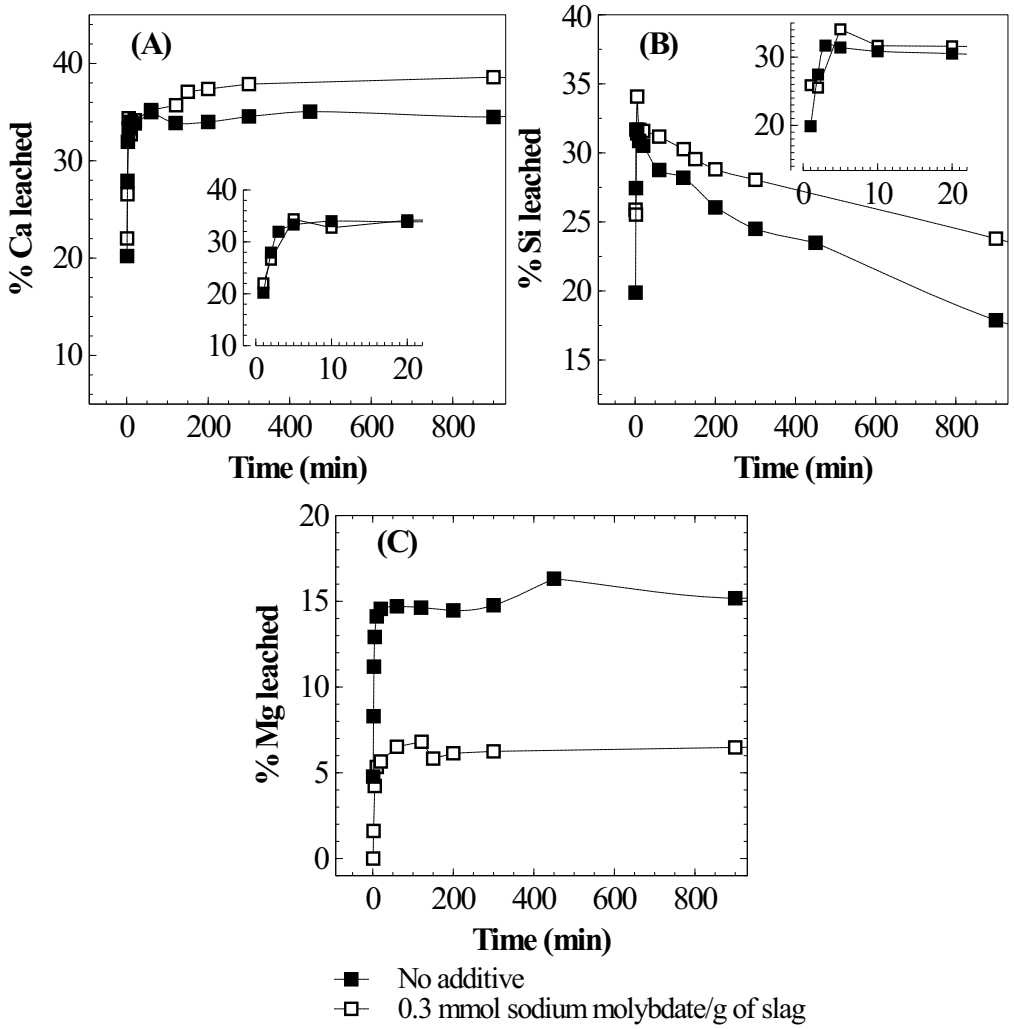

Figure 5.19: Effect of addition of sodium molybdate on leaching characteritsics of (A) Ca, (B) Si, and (C) Mg in HNO_3 (H/S: 7.2 mmol/g, L/S: 87.2 ml/g, PS: 150–212 μm)

5.5 Summary

Experimental investigation was carried out to understand the influence of operating parameters such as acid-to-solid ratio, solid loading, particle size, ionic strength, and temperature on calcium leaching characteristics. Following observations and conclusions were made from the study:

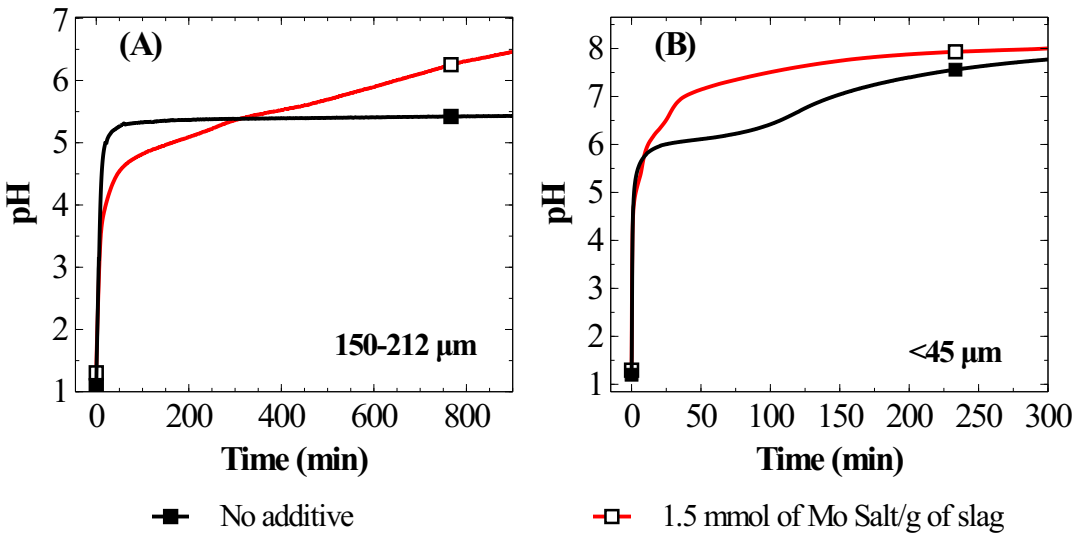

[H]

Figure 5.20: Effect of sodium molybdate addition on pH in the case of (A) PS: 150–212 μm (B) PS: <45 μm in HNO_3 (H/S: 7.2 mmol/g, L/S: 87.2 ml/g)

- In general, slag dissolution behaviour was found to be similar in the case of nitric acid and acetic acid.
- The selectivity of calcium was found to decrease with the depth of calcium leaching, while the influence of acid concentration and solution chemistry was found to be insignificant. It is hypothesised that sporulation model can explain this phenomenon.
- Slow oxidation and precipitation of Fe(II), possibly limited by [OH^-] concentration, resulted in pH plateau. Addition of base to accelerate the precipitation led to loss of calcium. Instead, addition of sodium molybdate during dissolution step substantially reduced Fe and Mg leaching and improved the calcium selectivity.
- The influence of temperature, ionic strength were found to be insignificant, while acid concentration and surface area evolution were found to be the main independent parameters which influence dissolution kinetics.
- Preliminary kinetic analysis suggested that the rate of calcium dissolution and acid uptake can be modelled using proton-promoted mechanism.

Chapter 6

PCC production via pressure-swing carbonation

6.1 Background

Among various PCC generating processes, carbon dioxide pressure-swing technique proposed by Iizuka et al. (2004) appears to be promising as it does not involve use of any acids or bases except carbon dioxide gas. Pressure-swing carbonation has been devised to take advantage of the increase in calcium carbonate solubility at high CO_2 partial pressure. The dissolution stage of the process involves leaching of Ca in aqueous solution under high-pressure of carbon dioxide. Post dissolution, Ca rich aqueous solution is filtered and precipitated at low partial pressure of CO_2. Studies on waste cement (Iizuka et al., 2004; Katsuyama et al., 2005), showed potential for high Ca extraction rate and Ca extraction efficiency. The purity of calcium carbonate, however, was found to be 80% in unseeded precipitation; synthesis of high-purity (98 wt%) PCC required a large amount (2.5 wt%) of calcium carbonate seed material, an amount which is comparable to the expected precipitate weight. The nature of impurities and influence of dissolution conditions on carbonate characteristics have also not been reported. Further, in the case of Ca extraction from waste cement, the process required either high water volume (liquid-to-solid ratio of 350 ml/g) or large recycle of residual waste cement at a low liquid-to-solid ratio (L/S of 40 ml/g), which resulted in a significant process cost(Katsuyama et al., 2005).

In terms of the mechanisms involved, multi-oxide/silicates dissolution and carbonate precipitation under CO_2 pressure appears to be complex and not clearly understood. For instance, precipitation of carbonate and silica preferentially occur on the surface of the slag (Huijgen et al., 2005) leading to speculation about surface passivation. However, such passivation has not been conclusively established (Daval et al., 2009a). Iizuka

et al. (2004) reported supersaturation of calcium during the dissolution step. However, reasons for the same are not clear. Calcium extraction beyond calcite solubility limit can significantly reduce the water volume required for complete calcium extraction, an aspect which has not yet been explored. Also, some direct mineral carbonation experiments (Huijgen et al., 2005; Fernández Bertos et al., 2004a; Ukwattage et al., 2013) showed better overall conversion at very low liquid-to-solid ratios, which was deduced as an enhancement in Ca dissolution efficiency. However, these studies are in contradiction to a few other studies (Iizuka et al., 2004; Ukwattage et al., 2017) where better Ca dissolution efficiency was obtained at high L/S. To a large extent, the problem of not being able to understand the dissolution and precipitation mechanisms is due to limited data (Marini, 2006), inconsistency in methodology and incomplete evidence. In most high-pressure mineral dissolution and carbonation studies, researchers relied upon either inductively coupled plasma (ICP) analysis of filtered liquid samples or carbonate quantification of solid samples obtained after de-pressurisation of the system to interpret the kinetics. It must be noted that precipitation of carbonate is spontaneous when the system is de-pressurised and estimated carbonate content in the residues after filtration and drying does not therefore reflect the true process efficiency. Thus, it is impossible to resolve true rate of dissolution from apparent rates without the knowledge of in situ carbonation. In addition to these shortcomings in existing data, there are specific complexities arising due to the nature of feedstock. For instance, in the case of mineral carbonation of steel slag, the influence of Mg and Fe which can potentially influence carbonate morphology (Rodriguez-Blanco et al., 2012; Reddy and Nancollas, 1976; Chen et al., 2006a) and form secondary precipitates are yet to be explored.

This chapter attempts to address the above-mentioned gaps in experimentation and determine true calcium dissolution rate. High-pressure batch dissolution experiments have been carried out in a closed system after eliminating CO_2 mass transfer limitations. Calcium leaching characteristics from steel slag under CO_2 pressure have been studied to probe surface passivation and its influence on dissolution kinetics. The study further attempts to understand the mechanism behind calcium supersaturation and the possibility to reduce the water requirement. To investigate these aspects, dissolution experiments were performed at moderate CO_2 pressure, temperature and liquid-to-solid ratio (0.6–1.25 MPa, 25–60 °C, and 50–100 ml/g, respectively) using fine (<75 μm) and coarse particle

size fractions (90–125 μm, and 212–355 μm) of the steel slag. A study has also been carried out on carbonate precipitation characteristics at atmospheric pressure by pressure-swing and PCC characterisation to determine the PCC purity and overall calcium conversion.

6.2 Methodology of the study

The present methodology involves the use of a closed system to study the existence and extent of calcium supersaturation in the liquid and surface passivation of slag particles by calcium carbonate precipitation. The rationale behind the choice of a closed system is to follow CO_2 pressure change with time, in addition to the elemental concentration in the aqueous solution by ICP analysis. As shown below, based on these measurements in a closed system, wherein CO_2 moles, gas phase volume, and temperature are constant (constant NVT), it is possible to determine the state of solution (pH, supersaturation). This is based on a calculation, from the experimental data, of the moles of CO_2 fixed as bicarbonate and carbonate per unit mole change of M^{+2} ions in solution ($\Delta C_s/\Delta[M]$). Relations between $\Delta C_s/\Delta[M]$ and solution state are obtained using an overall carbon balance (equation given below) and the condition that the aqueous solution is saturated with CO_2.

$$[\mathrm{CO_2}]_{tot} = \frac{P_{\mathrm{CO_2}} V_G}{RTV_L} + [\mathrm{CO_2}]_{aq} + [\mathrm{HCO_3}^-] + [\mathrm{CO_3}^{-2}] \tag{6.1}$$

where $[\mathrm{CO_2}]_{tot}$ is the total moles of CO_2 per unit liquid volume (V_L), $P_{\mathrm{CO_2}}$ is the CO_2 partial pressure, $[\mathrm{CO_2}]_{aq}$ is the concentration of undissociated CO_2 absorbed in the liquid (H_2CO_3 is usually negligible under these conditions), V_G is the volume of gas, R is the universal gas constant.

Under CO_2 saturated conditions (using Henry's law $[\mathrm{CO_2}]_{aq} = k_H \times P_{\mathrm{CO_2}}$), the change in the concentration of CO_2 fixed as carbonate and bicarbonate in aqueous solution is, from Equation 6.1,

$$\Delta C_s = \Delta([\mathrm{HCO_3}^-] + [\mathrm{CO_3}^{-2}]) = -\Delta P_{\mathrm{CO_2}} \Big(\frac{V_G}{RTV_L} + k_H \Big) \tag{6.2}$$

Table 6.1 shows the reactions involved. Based on the reaction chemistry and charge balance equation, depending on the solution state, different conditions for $\Delta C_s/\Delta[M]$

Table 6.1: Reaction chemistry of slag-CO_2-H_2O system

Step	Reactions
CO_2 absorption & speciation	$CO_2(g) \xleftrightarrow{k_H} CO_2(aq)$
	$CO_2(aq) + H_2O \xleftrightarrow{K_{a0}} H_2CO_3$
	$H_2CO_3 \xleftrightarrow{K_{a1}} HCO_3^- + H^+$
	$HCO_3 \xleftrightarrow{K_{a2}} CO_3^{-2} + H^+$
Slag dissolution	$C_3S + H_2O \longrightarrow C_2S + Ca(OH)_2$
	$C_2S + 4\,H^+ \longrightarrow 2\,Ca^{+2} + H_4SiO_4$
	$MgO + 2\,H^+ \longrightarrow Mg^{+2} + H_2O$
	$FeO + 2\,H^+ \longrightarrow Fe^{+2} + H_2O$
Overall dissolution	$C_2S + 4\,H_2CO_3 \longrightarrow 2\,Ca^{+2} + 4\,HCO_3^- + H_4SiO_4$
PCC precipitation	$Ca^{+2} + CO_3^{-2} \longrightarrow CaCO_3$
Charge balance	$2\,M^{+2} + H^+ + MHCO_3^+ - OH^- - HCO_3^- - 2\,CO_3^{-2} = 0$

$[M^{+2}]=[Ca^{+2}]+[Mg^{+2}]+[Fe^{+2}]$; PCC: Precipitated calcium carbonate

exist (as shown below). Based on the saturation state of solution, these conditions are categorised into two cases.

Case I: *Ionic activity product (IAP) less than solubility product (K_{sp}) for $CaCO_3$*

During the dissolution step (under acidic and circumneutral pH conditions, where $[CO_3^{-2}] \ll [HCO_3^-]$),

$$\Delta C_s/\Delta[M] \approx 2 \tag{6.3}$$

On the other hand, when dissolution takes place in mildly basic environment ($8 < pH < 10$) where $[CO_3^{-2}]$ and $[HCO_3^-]$ are comparable,

$$1 < \Delta C_s/\Delta[M] < 2 \tag{6.4}$$

In the case of dissolution in very basic conditions (pH>10) where $[CO_3^{-2}] \gg [HCO_3^-]$,

$$\Delta C_s/\Delta[M] \approx 1 \tag{6.5}$$

Case II: *IAP greater than K_{sp} for $CaCO_3$* Here, three possibilities exist—(a) the solution may remain supersaturated with respect to $CaCO_3$, or (b) the supersaturation may be discharged as precipitate that remains suspended and does not show up in the liquid samples, or (c) the supersaturation is discharged as a colloidal precipitate that passes through the sampling filter and shows up in the liquid sample. These cases may be distinguished by defining $\Delta C_s'$, the moles of CO_2 consumed to dissolve Ca^{+2} ions into the

solution[1], as Equation 6.6.

$$\Delta C_s' = \Delta C_s - 2 \times \Delta[\mathrm{Mg}] \tag{6.6}$$

(a) In the case of acidic pH (Equation 6.3) and true solution supersaturated with respect to $CaCO_3$, we have,

$$\Delta C_s'/\Delta[\mathrm{Ca}] \approx 2 \tag{6.7}$$

(b) In the case where supersaturation is discharged as a $CaCO_3$ precipitate and the precipitate is not passed into the liquid sample (precipitate size > filter pore size),

$$\Delta[\mathrm{Ca}] \leq 0 \tag{6.8}$$

(c) In the case where $CaCO_3$ precipitate exists in colloidal form, which passes through sampling filter and dissolves upon acidification of the sample[2], if calcium dissolution rate from the slag is negligible,

$$\Delta[\mathrm{Ca}] = 0 \tag{6.9}$$

On the other hand, when calcium dissolution and $CaCO_3$ precipitation rates are comparable,

$$1 < \Delta C_s'/\Delta[\mathrm{Ca}] < 2 \tag{6.10}$$

Thus, by measuring the ΔP_{CO_2} under CO_2 saturated condition, it is possible to distinguish Ca dissolution reaction from carbonate precipitation reaction, and a true supersaturated solution from colloidal precipitate.

Though the above methodology is limited by the sensitivity of pressure loss measurement and ability to maintain the system at constant temperature, the concept is useful to gain insights into various regimes of dissolution and precipitation. A detailed discussion on such limitations and numerical methods to overcome them are presented in the results and discussion section 6.4.

[1]In the current study, the reaction slurry is undersaturated with respect to $MgCO_3$ and Fe^{+2} leaching is negligible at the operating CO_2 pressure

[2]standard practice to store the sample for ICP analysis

6.3 Elimination of gas-liquid mass transfer limitation

To understand the rate of CO_2 absorption in the autoclave, absorption experiments were performed in a closed system (Figure 3.2) with 250 ml of distilled water and 350 ml of gas volume at 25 °C. As described in experimental section, experiment was stopped when CO_2 pressure remained constant. Since, the absorption is performed in a constant NVT and variable pressure system, the following equation is used to determine mass transfer coefficient (k_La),

$$\frac{\mathrm{d}[\mathrm{CO_2}]_{aq}}{\mathrm{d}t} = k_La \times ([\mathrm{CO_2}]^* - [\mathrm{CO_2}]_{aq}) \tag{6.11}$$

where, $[\mathrm{CO_2}]^*$ is the saturation concentration of CO_2 (at gas-liquid interface) and $[\mathrm{CO_2}]_{aq}$ is the concentration of CO_2 in the bulk liquid.

Using Equation 6.1, Henry's law ($[\mathrm{CO_2}]^* = k_H \times P_{\mathrm{CO_2}}$), and neglecting $[\mathrm{HCO_3}^-] + [\mathrm{CO_3}^{-2}]$ which is $\ll [\mathrm{CO_2}]_{aq}$ under CO_2 pressure greater than 1 bar in distilled water, following equation was arrived at.

$$\frac{\mathrm{d}P_{\mathrm{CO_2}}}{\mathrm{d}t} = \frac{-V_G}{V_L RT} \times k_La \times \left(k_H P_{\mathrm{CO_2}} - [\mathrm{CO_2}]_{tot} + \frac{P_{\mathrm{CO_2}} V_G}{RTV_L}\right) \tag{6.12}$$

Integrating the above equation, we get

$$\chi(T, P_{\mathrm{CO_2}}, [\mathrm{CO_2}]_{total}) = -k_La \times t + C \tag{6.13}$$

where C is a constant, and

$$\chi(T, P_{\mathrm{CO_2}}, [\mathrm{CO_2}]_{total}) = \frac{\ln\left\{\left(k_H + \frac{V_G}{RTV_L}\right) \times P_{\mathrm{CO_2}} - [\mathrm{CO_2}]_{total}\right\}}{\left(\frac{k_H RTV_L}{V_G} + 1\right)}$$

Using Equation 6.13, mass transfer coefficient (k_La) is estimated as the slope of linear fit as illustrated in Fig. 6.1B.

Absorption experiments showed that the time required to reach constant pressure (CO_2 saturation time) with the existing reactor configuration was about 25 min (Fig. 6.1A). Since this time was comparable to the estimated dissolution time of 1–2 hours Iizuka et al. (2004); Huijgen et al. (2005), it was anticipated that external mass transfer limitations would be influencing the reaction rate. To overcome the problem, the reactor

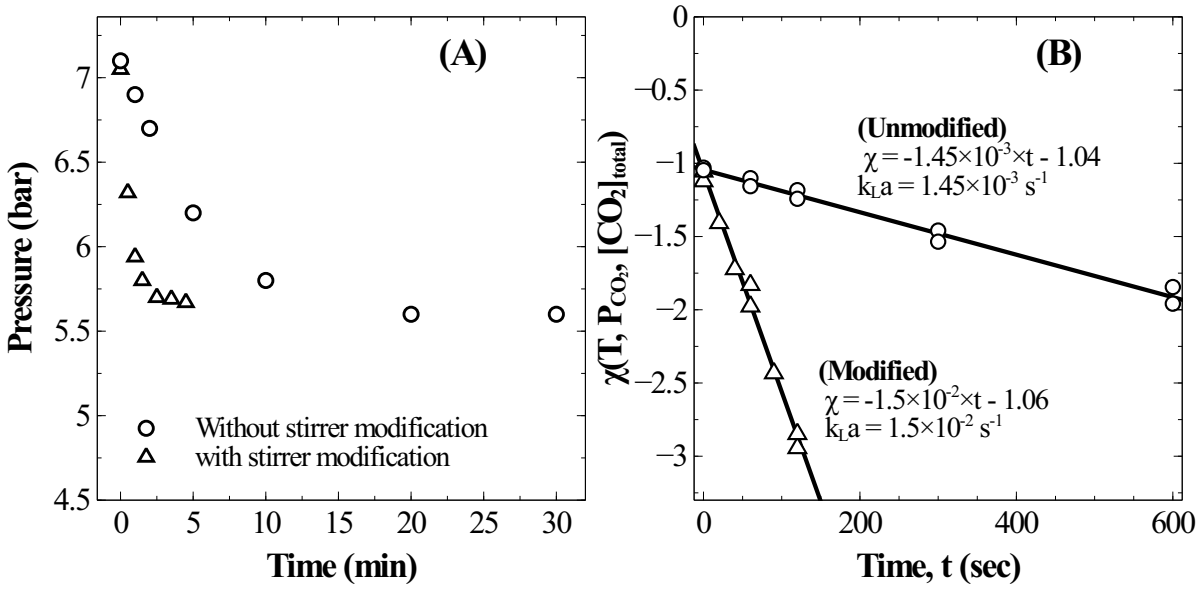

Figure 6.1: (A) Drop in reactor pressure during absorption in distilled water without (◯) and with (△) stirrer modification, and (B) corresponding $k_L a$ estimation.

stirrer was modified to act like a self-inducing impeller. As demonstrated in Fig.6.1, mass transfer coefficient improved by an order of magnitude from $1.45 \pm 0.07 \times 10^{-3}\text{s}^{-1}$ to $1.50 \pm 0.01 \times 10^{-2}\text{s}^{-1}$, reducing the saturation time to three minutes. Pressure data in slag carbonation experiments (to be discussed later) showed that the fall in pressure in the post saturation phase was much more gradual than in the initial saturation phase. Thus, it can be stated that the rate of CO_2 absorption is much faster than slag dissolution reactions and does not influence the dissolution kinetics.

6.4 Temperature sensitivity of pressure loss measurement

In a closed system, reactor pressure is expected to be influenced by fluctuation in reactor temperature, mainly due to changes in CO_2 solubility, and in turn influence the pressure loss measurements. An analysis has therefore been carried out to understand the influence of temperature fluctuations on observed reactor pressure.

A total CO_2 balance in the slag carbonation system with solid phase gives,

$$[\text{CO}_2]_{total} = \frac{P_{\text{CO}_2} V_G}{RTV_L} + [\text{CO}_2]_{aq} + [\text{HCO}_3^{-}] + [\text{CO}_3^{-2}] + [\text{CaCO}_3] \qquad (6.14)$$

In pure water, under CO_2 pressure, concentration of $[\text{HCO}_3^{-}]$ and $[\text{CO}_3^{-2}]$ are insignificant

compared to $[CO_2]_{aq}$. On the other hand, in the case of slag carbonation, concentration of these species is strongly dependent on concentration of metal ions (for charge balance) and expected to show negligible influence with small temperature changes. Hence, Equation 6.15 can be used for further analysis under saturated conditions, where $[CO_2]_{aq}$ can be described by Henry's law.

$$\frac{P_{CO_2} V_G}{RTV_L} + k_H \times P_{CO_2} = n_{CO_2}(P,T) \tag{6.15}$$

where, $k_H = 0.035 \times e^{2400\times(\frac{1}{T}-\frac{1}{298.15})}$mol/L/bar (Sander, 2015).

Differentiating the above equation with respect to P and T; we get, $dn_{CO_2} = 0$ and,

$$\left(\frac{V_G}{RTV_L} + k_H\right) \times \frac{\Delta P_{CO_2}}{P_{CO_2}} - \left(\frac{V_G}{RT^2V_L} + k_H \times \frac{2400}{T^2}\right) \times \Delta T = 0 \tag{6.16}$$

Equation 6.16 is rearranged as follows to estimate the changes in reactor pressure due to a small magnitude of change in reactor temperature,

$$\Delta P_{CO_2} = \left(\frac{V_G}{RT^2V_L} + k_H \times \frac{2400}{T^2}\right)\left(\frac{V_G}{RTV_L} + k_H\right)^{-1} \times P_{CO_2} \times \Delta T \tag{6.17}$$

Under typical experimental conditions of V_G =0.35 L, V_L = 0.25 L, T = 298.5 K and $P_{(CO_2)}$ =800 kPa, a change in 1 °C of reaction temperature influences pressure measurement by $\sim$ 10 kPa (Fig. 6.2A). Though this temperature change induced error in pressure is insignificant when compared to the total reactor pressure, it is large enough to introduce noise in reaction induced pressure loss estimates. Ideally, temperature fluctuation less than 0.1 °C is desired to contain errors in pressure measurement to less than 1 kPa. However, reactor used for the current study is electrically heated and PID controller often resulted in fluctuations of about 1–2 °C due to reaction exothermicity and changes in cooling water temperature. As the observed accuracy in pressure loss measurement is lower than the desired value, recorded pressure was corrected based on the temperature changes using Equation 6.17. Changes in reactor pressure observed with a change in reactor temperature in a closed system were experimentally determined at typical experimental conditions of V_G =0.35 L, V_L = 0.25 L, T = 2981.5 K and $P_{(CO_2)}$ =885 kPa and compared

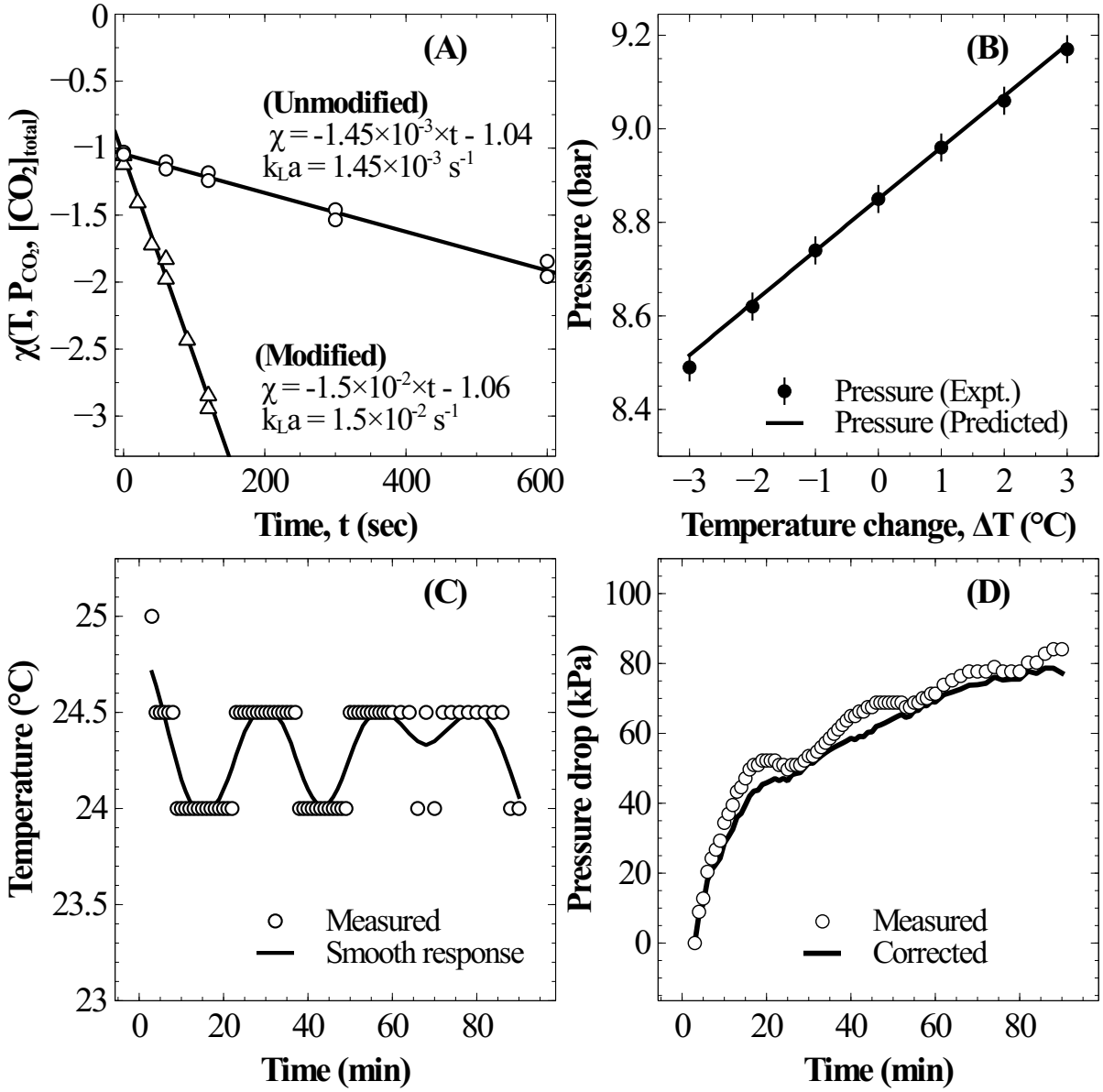

Figure 6.2: (A) Sensitivity of pressure with temperature change during CO_2 absorption in distilled water at 25 °C; (B) Typical temperature fluctuation during slag carbonation experiment, and (C) fluctuations in corresponding pressure loss measurement during slag dissolution and the numerically corrected response using Equation 6.17

with the predictions of Equation 6.17. As shown in Fig. 6.2A, corrections in pressure predicted by Equation 6.17 are in excellent match with experimental observations. Further, as shown in Fig. 6.2B and 6.2C, corrections using Equation 6.17 significantly reduced the noise in pressure loss measurements, which allowed to accurately determine the relation between ΔC_s and $\Delta[M]$.

6.5 Calcium leaching characteristics from slag — parametric study

A parametric study was conducted to understand the influence of various operating parameters such as liquid-to-solid ratio, particle size, temperature and carbon dioxide pressure on dissolution characteristics of slag. Based on these results, an attempt has been made to identify optimal conditions for mineral carbonation.

6.5.1 Effect of liquid-to-solid ratio

Influence of liquid-to-solid ratio (L/S) on extent of calcium dissolution was studied in the range of 50–100 ml/g using < 75 μm particles at 25 °C and initial CO_2 pressure of 12.4 bar. In these experiments, slag weight was varied while keeping water volume constant to obtain desired L/S ratio. This procedure was chosen over other option to vary the liquid volume since the gas-liquid interfacial area is nearly constant in this procedure, and hence the gas-liquid mass transfer rate. As shown in Fig. 6.3A, rate of CO_2 pressure loss was found to increase with an increase in solid loading suggesting that rate of CO_2 absorption is not limiting the dissolution. As shown in Fig. 6.3B, increasing solid loading (low L/S ratio) resulted in higher initial rates of Ca release and higher final concentration of dissolved calcium. As shown in Figure 6.4, initial calcium release rates are proportional to the mass of slag (also surface area). As dissolution proceeds, Ca release rate per unit mass of slag at L/S of 50 ml/g decelerated faster compared to L/S of 100 ml/g, understandably due to lower CO_2 pressure in the reactor and higher alkalinity of the solution which reduce rate of leaching. Consequently, %Ca dissolved from slag reduced from 57.1% to 40.2% (after 120 min of dissolution) as L/S ratio was lowered from 100 to 50 ml/g.

The current experimental observations on the influence of L/S on calcium dissolution

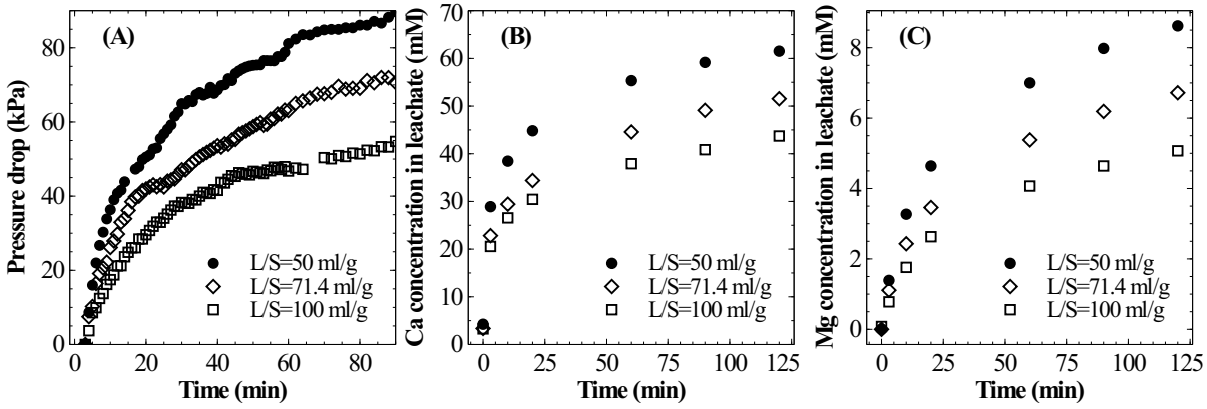

Figure 6.3: Effect of liquid-to-solid ratio (T=25 °C, PS=< 75 μm, $P_{CO_2,intial}$=12.4 bar) on (A) pressure loss during dissolution step (B) Ca leaching characteristics, and (C) Mg leaching characteristics

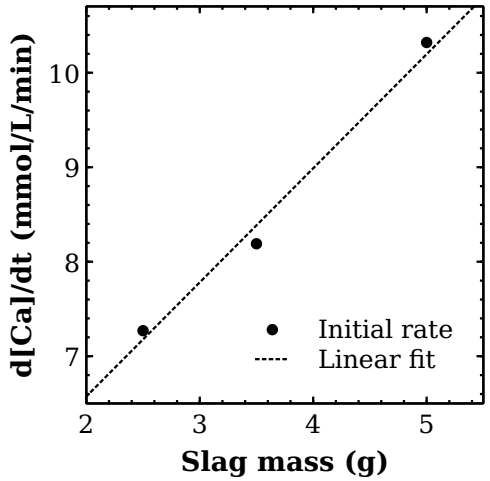

Figure 6.4: Effect of slag loading on initial calcium release rate

rates are in contrast with the previously reported works. For instance, Huijgen et al. (2005) reported that the overall calcium carbonate yield monotonically increased with a decrease in liquid-to-solid ratio. It was hypothesised that ionic strength improved the dissolution of Ca. Also, some works (Fernández Bertos et al., 2004a; Ukwattage et al., 2013) reported presence of an optimal L/S ratio for unstirred systems and rather weakly stirred system(Tamilselvi Dananjayan et al., 2015). These works hypothesised that too much of water hindered CO_2 permeability into the material. Together, these hypotheses that dissolution step accelerates when L/S is reduced contradict current experimental results and those reported by a few others(Iizuka et al., 2004). Further, all these works determined extent of carbonation by measuring the weight gain of the carbonated residue which does not provide direct insights into Ca dissolution characteristics. Possible reasons for these contradicting observations are i) varying liquid volume reduced the liquid surface-area-to-volume ratio which in turn reduces gas-liquid absorption rates, and ii) incomplete carbonation precipitation at higher L/S ratio (due to low supersaturation) leading to low overall efficiency. Under CO_2 saturated conditions, it is clear from the current experimental observations that higher L/S improves the calcium extraction efficiency.

Similar to Ca leaching behaviour, initial rate of Mg dissolution was observed to proportionally increase with increasing mass of slag owing to higher surface area (Fig. 6.3C). However, the deceleration in dissolution of Mg with progression of leaching at low L/S ratio is comparatively lower than that of Ca. This resulted in a marginal increase in Mg/Ca ratio from 0.11 to 0.14 when L/S was varied from 100 to 50 ml/g.

The influence of L/S on Si dissolution characteristics is very similar to Ca dissolution behaviour. As shown in Fig. 6.5A, a stoichiometric relation exists between temporal evolution of dissolved Si and Ca. This can be explained by the mineralogy of the slag where extractable Ca and Si are present in dicalcium silicate and tricalcium silicate phases (calcium present in dicalcium ferrite phase is not susceptible for leaching(Bodor et al., 2013)). These phases belong to orthosilicate group containing no bridging oxygen (Si–O–Si) and dissolution is expected to occur in two-steps where, breaking of Ca–O bonds is followed by liberation of SiO_4 tetrahedra without any need to break Si–O bond(Marini, 2006). The overall dissolution step from calcium silicate phase present in the slag can be considered as follows with soluble silica (present as silicic acid) as a stable intermediate which is further expected to undergo polymerization to form silica particles.

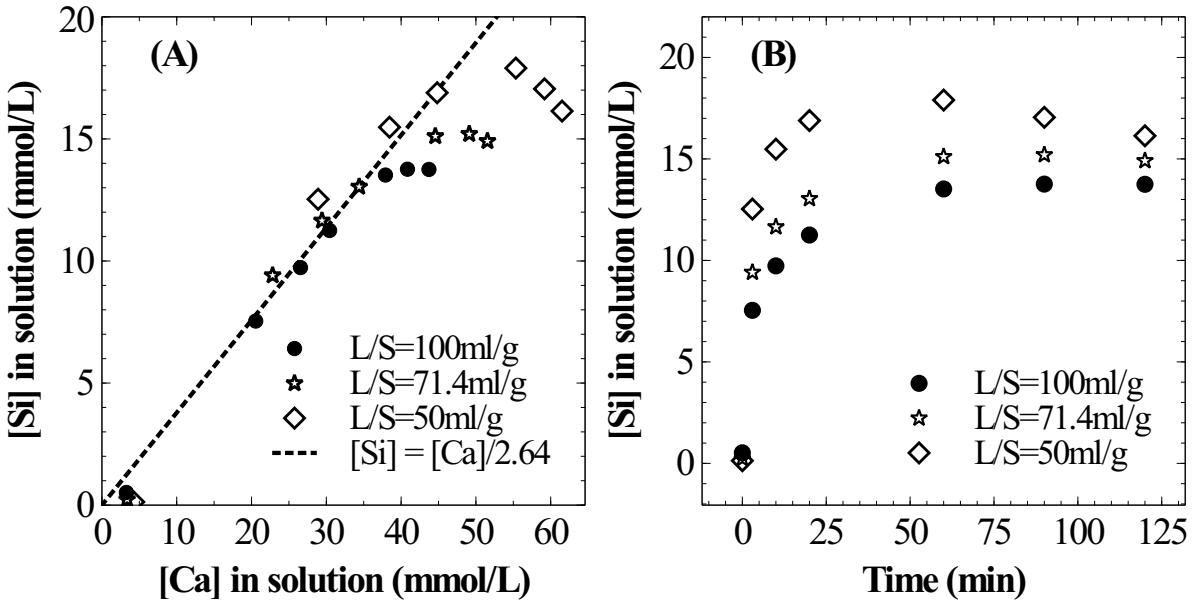

Figure 6.5: (A) Relative dissolution of calcium and silicon; (B) Effect of L/S on Si release

In all three cases, Si concentration reached a plateau within the two-hour period of dissolution time (Fig. 6.5B). And, maximum Si concentration (18 mmol/L) was significantly higher than its expected solubility (1.9 mmol/L) under prevailing reaction conditions. Given the extremely high apparent supersaturation, it is highly likely that silica exists as colloidal particles of size less than 0.2 μm (filter pore size) instead of a true solution. Under the prevailing pH (4–6), nano-colloid silica demonstrates uncharacteristic stability with a lifetime ranging from few hours to days(Conrad et al., 2007). This behaviour is expected due to strong repulsion among nano-colloid silica particle due to negative surface charge. However, increase in ionic strength(Gorrepati et al., 2010) and presence of divalent cations(Crerar et al., 1981) could accelerate the growth of particles, possibly due to reduction or cancellation of negative surface charge (Belton et al., 2012). As observed by Iler (1975), a critical concentration calcium ion concentration is necessary for coagulation of colloidal silica where critical concentration is higher for smaller colloidal silica particles. Thus, silica precipitation is induced with further Ca dissolution as shown in Fig. 6.5B. As the slag loading was increased, understandably, the rate of Si precipitation increased because of higher Ca concentration in the solution.

From the current investigation, it may thus be concluded that higher L/S is desirable for maximum utility of calcium in the slag. Further, slower polymerisation of silica at high L/S allows easy filtration as polymerised silica from orthosilicates is gelatinous and

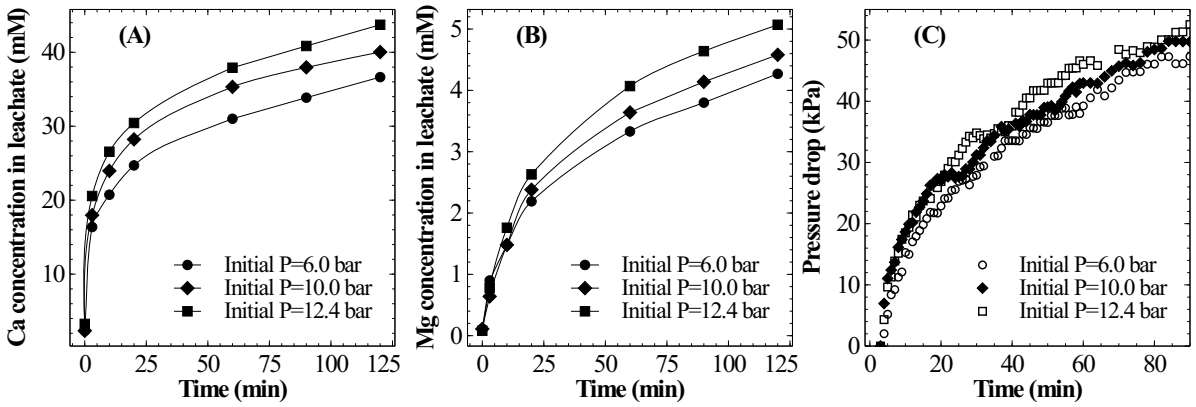

Figure 6.6: Effect of CO_2 pressure (T=25 °C, PS=< 75 μm, L/S = 100 ml/g) on (A) Ca leaching characteristics, (B) Mg leaching characteristics, and (C) on pressure loss during dissolution step

makes filtration difficult(Terry, 1983b).

6.5.2 Effect of CO_2 pressure

The influence of carbon dioxide pressure on Ca dissolution characteristics was studied by varying the initial reactor pressure (CO_2 partial pressure) from 6 to 12.4 bar using $<$ 75 μm particles at 25 °C and L/S of 100 ml/g. As shown in Fig. 6.6, an increase in the initial CO_2 pressure resulted in a higher extent of Ca dissolution at the end of 120 min. In both the regimes where CO_2 is under-saturated (<3 min) and saturated (>3 min), increasing pressure showed a positive influence on the rate of Ca dissolution. The influence of pressure on Ca dissolution rate is estimated to be higher in the first three minutes of dissolution compared to that in the CO_2 saturated region. This can be attributed to rapid rate of acidification of slurry under higher CO_2 pressure. On the other hand, in the CO_2 saturated regime, enhancement at higher CO_2 pressure can be attributed to a smaller change in pH as compared to lower CO_2 pressure. CO_2 pressure has a similar influence on Mg leaching. An increase in pressure led to a marginal increase in the net CO_2 pressure loss indicating a higher rate of overall elemental dissolution (Figure 6.6). Overall, CO_2 partial pressure has a positive and noticeable influence on mineral dissolution kinetics.

6.5.3 Effect of particle size

Effect of particle size on Ca release and Mg release was studied using $< 75\ \mu$m, 90–125 μm and 212–355 μm at L/S of 100 ml/g, 25 °C and 12.41 bar of initial CO_2 pressure. As shown in Fig. 6.7, Ca and Mg elemental release showed a parabolic trend for both fine and coarse particles in the first 10 min of dissolution. However, beyond 10 min of dissolution time, the rate of dissolution was observed to be constant for coarser particles while the finer particles continued to exhibit parabolic concentration profile. In fact, coarser particles (90–125 μm) continued to exhibit the linear concentration profile even when reaction time was extended up to 240 min. The difference, however, does not appear to have origins in non-homogeneity of sample or changes in reaction chemistry as ratios of release of elements (Ca/Si and Ca/Mg) remained same for both cases. It is likely that the parabolic trend prevalent in the finer particle-size fraction ($<75\ \mu$m) is due to the presence of ultra-fine particles and broader particle-size distribution in the sample(Holdren and Berner, 1979), wherein high initial rate corresponds to rapid dissolution of ultra-fine particles and the progressive change to coarser particle-size distribution reduces the dissolution rate.

Surface passivation by Si rich layer or precipitated calcium carbonate layer has been widely suspected as the reason for the reduction in overall Ca leaching/carbonation efficiency when particle size is increased (Huijgen et al., 2005; Lekakh et al., 2008a). Extended dissolution experiments with 90–125 μm particles for 240 min showed that Ca extraction efficiency can reach as high as finer particles without showing any sign of surface passivation. These results suggest that high Ca extraction efficiency from coarser particles can be achieved, which can bring down the need for energy-intensive particle-size reduction.

6.5.4 Effect of temperature

The effect of temperature on dissolution kinetics was studied at 100 ml/g of L/S and initial CO_2 pressure of 12.4 bar using $<75\ \mu$m particles. As shown in Fig. 6.8A, the overall extent of calcium dissolution was observed to decrease with an increase in temperature. During the initial stage of dissolution (at 3 min), Ca extraction efficiency is higher at 25 °C. This observation is consistent with the finding that the rate of CO_2 absorption in water reduces with an increase in temperature (Lívanský, 1982). After 3 minutes of

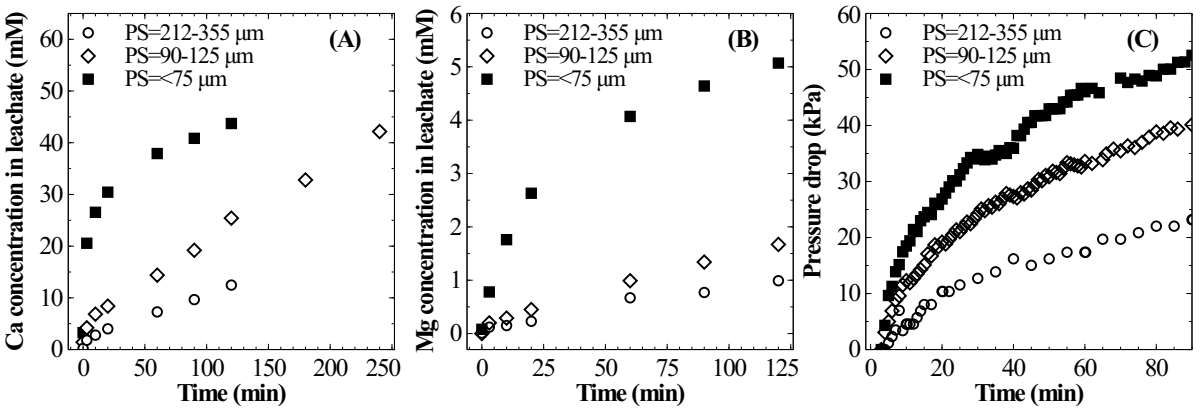

Figure 6.7: Effect of particle size (T=25 °C, L/S=100 ml/g, $P_{CO_2,intial}$=12.4 bar) on (A) Ca leaching characteristics, (B) Mg leaching characteristics, and (C) on pressure loss during dissolution step

dissolution, the net rate of Ca dissolution marginally increased when temperature was increased from 25 to 40 °C. It is to be noted that $[CO_2]$ in the solution is lower at 40 °C owing to lower solubility and a negative influence on Ca dissolution kinetics is expected based on observations at lower CO_2 partial pressure. Thus, a net marginal increase in Ca dissolution rate reflects a considerable influence of temperature which overwhelmed the effect of lower CO_2 concentration. This is a consequence of positive influence of temperature on mass transfer or surface reaction rates. However, increase in temperature strongly influenced $CaCO_3$ solubility in the solution and led to precipitation after 60 min when the dissolution was carried out at 60 °C.

As shown in Fig. 6.8B, temperature has only a marginal influence on dissolution of Mg. It appears that the rate of Mg dissolution increases with an increase in temperature, however, due to very small changes and low concentration it could not be clearly resolved. The drop in reaction pressure, which is shown in Fig. 6.8C, was found to be higher at 25 °C as compared to higher temperatures; this is due to higher overall extraction of calcium at low temperature. Thus, in view of complete extraction of Ca from slag, lower temperature appears to be optimal for mineral carbonation through pressure-swing route.

6.6 Supersaturation of calcite

Iizuka et al. (2004) reported up to three times supersaturation of calcium in dissolution

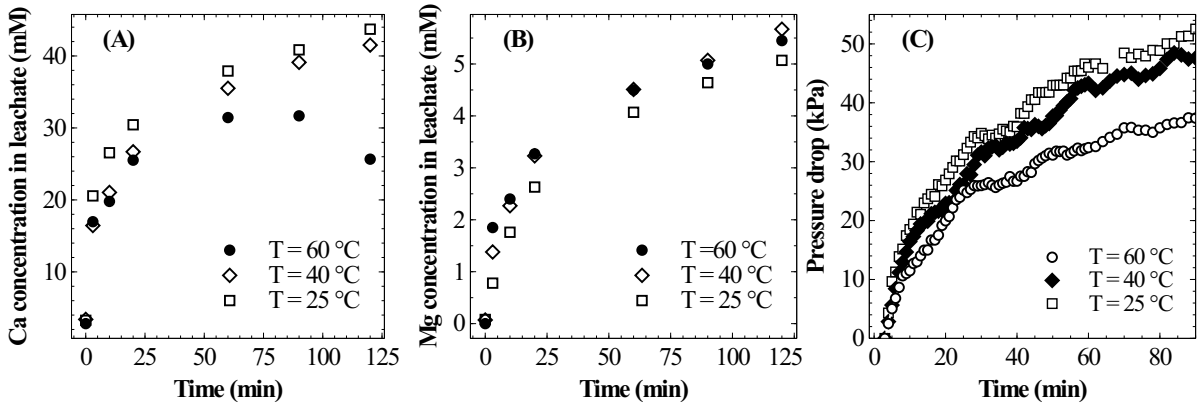

Figure 6.8: Effect of temperature (PS=< 75 μm, L/S = 100 ml/g, $P_{CO_2,intial}$=12.4 bar) on (A) Ca leaching characteristics, (B) Mg leaching characteristics, and (C) on pressure loss during dissolution step

Table 6.2: Estimation of saturation indices for $CaCO_3$ polymorphs

Experimental Condition	$[Ca]_{total}$	$[Mg]_{total}$	P_{CO_2}	pH	$[Ca^{+2}]$	$[CO_3{}^{-2}]$	$\frac{[Ca^{+2}]}{[CO_3{}^{-2}]}$	IAP	Ω_{CA}	Ω_{AR}	Ω_{VA}	Ω_{ACC}
	mM	mM	bar	-	mM	mM	-	M^2	-	-	-	-
L/S = 100 ml/g, 120 min	43.7	5.1	8.05	5.71	31.6	4.5E-03	7022	1.7E-08	4.5	3.8	1.4	0.04
L/S = 71.4 ml/g, 120 min	51.5	6.7	7.85	5.78	36.0	6.5E-03	5538	2.6E-08	6.8	5.7	2.2	0.07
L/S= 50 ml/g, 120 min	61.5	8.6	7.38	5.88	41.2	9.9E-03	4162	4.2E-08	10.9	9.2	3.5	0.11
T=60 °C, 60 min†	31.4	4.5	9.31	5.82	22.9	6.3E-03	3635	1.8E-08	9.4	7.1	3.0	0.15

IAP: Ionic activity product; Ω: saturation index (IAP/K_{sp}); CA: Calcite; AR: Aragonite; VA:Vaterite; ACC: amorphous calcium carbonate; † Precipitation was noticed during dissolution; K_{sp} values for various polymorphs reported by Brečević and Nielsen (1989) were used; Davies equation(Brečević and Nielsen, 1989) was used for estimation of activity coefficient for ionic species

experiments with waste cement. As shown in Table 6.2, similar observations were made in the current study where all the fine particle experiments, depending on the L/S ratio, showed an ionic activity product (IAP) 4–10 times higher than the solubility product of calcite. Since such an observation has implications to obtain high Ca dissolution at lower CO_2 (reaction) pressure than thermodynamically predicted, it is worth exploring the reasons for the same. Further, understanding reasons for the observed remarkable solution stability for long time periods can pave the way for complete extraction of calcium without surface passivation posing a limitation as posited by many researchers. Also, even if the apparent supersaturation is due to colloidal nature of precipitated calcium carbonate formed in solution (which pass through a syringe filter during sampling), it is worth understanding the reason behind nucleation in bulk solution so that surface precipitation can be avoided.

Firstly, to determine if the apparent supersaturation is a true solution or a colloidal

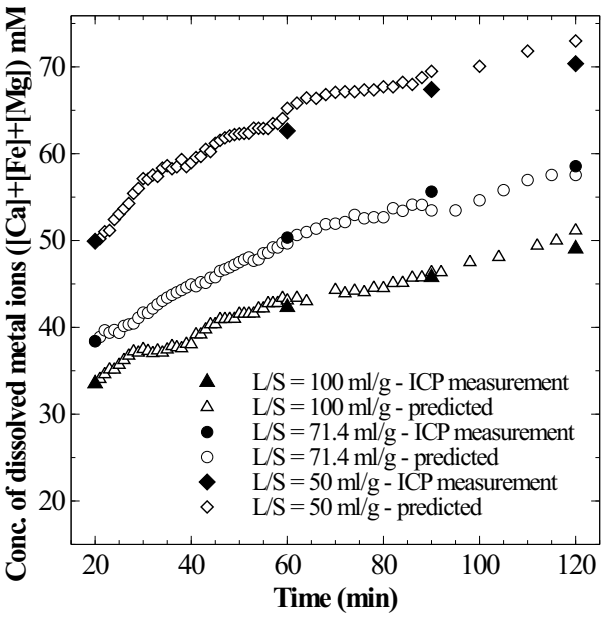

Figure 6.9: Total concentration of metal ions in super saturated solutions - measured (solid symbols) and predicted (open symbols) assuming true solution ($\Delta[M] = \Delta C_S/2$)

suspension, the moles of CO_2 consumed per mole of metal ions released into the solution is estimated. Theoretical formulation based on which solution status could be interpreted is presented in section 6.2. Since the observed supersaturation levels are as high as 4–10 times ($[Ca]_{total} - [Ca]_{saturated} > 20$ mM), sensitivity of pressure loss measurement was found to be suitable to distinguish a true solution from a saturated colloidal suspension. For all the datasets where supersaturation was evident ($\Omega_{calcite} > 1$) and Ca concentration was monotonously increasing, an excellent prediction of total metal ions concentration could be made from pressure loss data when the ratio of CO_2 moles consumed per moles of metal ions was assumed as 2 (Fig. 6.9). This shows that the solution is a true solution and disproves formation of any measurable colloidal precipitation or formation of non-recoverable precipitate. Further, in the case of coarse particle size (90–125 μm) experiment, where rapid filtration was possible to avoid further $CaCO_3$ precipitation on residual slag after reactor de-pressurisation, the thermogravimetric analysis (TGA) on slag residue obtained after 240 min dissolution ($\Omega_{calcite} = 4.5$) showed insignificant weight loss corresponding to carbonate decomposition (Figure 6.10). This corroborates that there is no precipitation of calcium carbonate on the slag surface during dissolution stage.

High supersaturation compared to calcite appears to be a consequence of calcite precipitation being kinetically unfavourable compared to other less-stable polymorphs such as amorphous calcium carbonate (ACC) or vaterite which subsequently transform

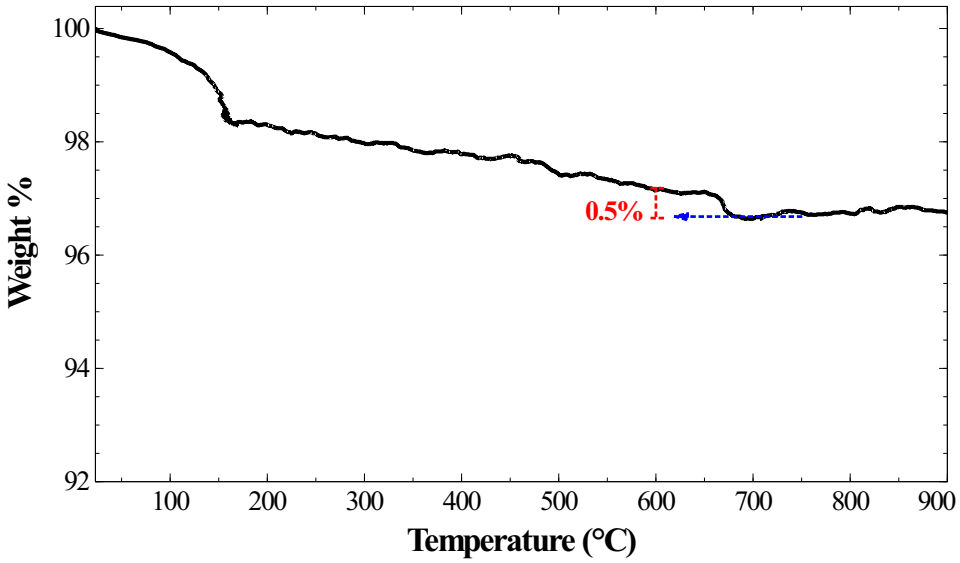

Figure 6.10: Thermogravimetric analysis (TGA) curve for slag residue (90–125 μm) obtained after 240 min of dissolution (L/S = 10 mml/g, initial CO_2 Pressure = 12.4 bar)

to calcite. As the more stable calcite grows, the solution becomes undersaturated with respect to less-stable polymorphs leading to their dissolution and complete transformation to calcite. Multiple studies (Ogino et al., 1987; Rieger et al., 2007) agree that amorphous calcium carbonate is the preferred nucleating polymorph when the supersaturation is sufficient to produce ACC. However, in the current study all the solutions, including where precipitation occurred, were undersaturated with respect to ACC (Table 6.2). Under circumstances where ACC cannot be produced, several studies (Ogino et al., 1987; Spanos and Koutsoukos, 1998; Lakshtanov and Stipp, 2010) agree that the first formed solid is metastable vaterite with the exception of Clarkson et al. (1992) who reported it to be calcite when there are no calcite inhibiting species. Vaterite also appears to be the kinetically preferred polymorph because of very high $[Ca^{+2}]/[{CO_3}^{-2}]$ (Lakshtanov and Stipp, 2010), a parameter which significantly affects the calcite growth rate (Larsen et al., 2010). Also, condensation of supersaturated silica (>10 mM) on carbonate particles especially under acidic conditions can potentially stabilize the growth and transformation of carbonate particles to calcite (Kellermeier et al., 2013). Though it is difficult to precisely conclude the reason for the remarkable stability of supersaturated solution, low pH and very high $[Ca^{+2}]/[{CO_3}^{-2}]$ appear to be important factors.

6.7 Surface passivation

Several previous works (Huijgen et al., 2005; Lekakh et al., 2008a) reported passivation of residual slag surface due to precipitation of silica and calcium carbonate. In the current study calcium carbonate precipitated during dissolution step only at high temperature and very high supersaturation. Accordingly, as shown in Figure 6.11A, no calcium carbonate precipitate was observed on the surface where supersaturated aqueous solution was determined to be a true solution. Thus, it can be concluded that calcium carbonate does not passivate the surface under current experimental conditions. As reported in Section 6.5.1, Si releases as monomeric units of silica and does not polymerise even at high supersaturation. For instance, in the case of coarse particle dissolution, Si was found to remain stable in solution for 240 minutes of dissolution time. Overall, about 57% of the calcium could be extracted from fine and coarse particles in 120 minutes and 240 minutes, respectively, without any sign of surface passivation.

In the case where precipitation occurred (60 °C), as shown in Figure 6.11B, micron-sized calcite crystals were observed as agglomerates along with silica, with the slag surface still being exposed. On the contrary, Huijgen et al. (2005) reported that the precipitation was exclusively on the surface and no carbonate crystals were observed in the bulk. The study also reported presence of silica rich layer on the surface of residual slag. Based on the current experimental results, it appears that calcite and silica co-precipitated as agglomerates in the bulk rather than precipitating as individual layers on the slag surface. This may be because of the acidic slurry pH, under which conditions, calcium silicate surface and calcite nuclei are generally expected to be positively charged and more so because of high $Ca^{+2}/CO_3{}^{-2}$ ratio (> 4000) (Chibowski et al., 2003). Thus, calcite is expected to co-precipitate with negatively charged silica. Smaller calcite crystals which appear to partly cover the slag surface might have precipitated after depressurisation when the saturation index increases multi-fold along with slurry pH.

Based on these results, it can be concluded that surface passivation is not significant with steel slag as feedstock under current experimental conditions.

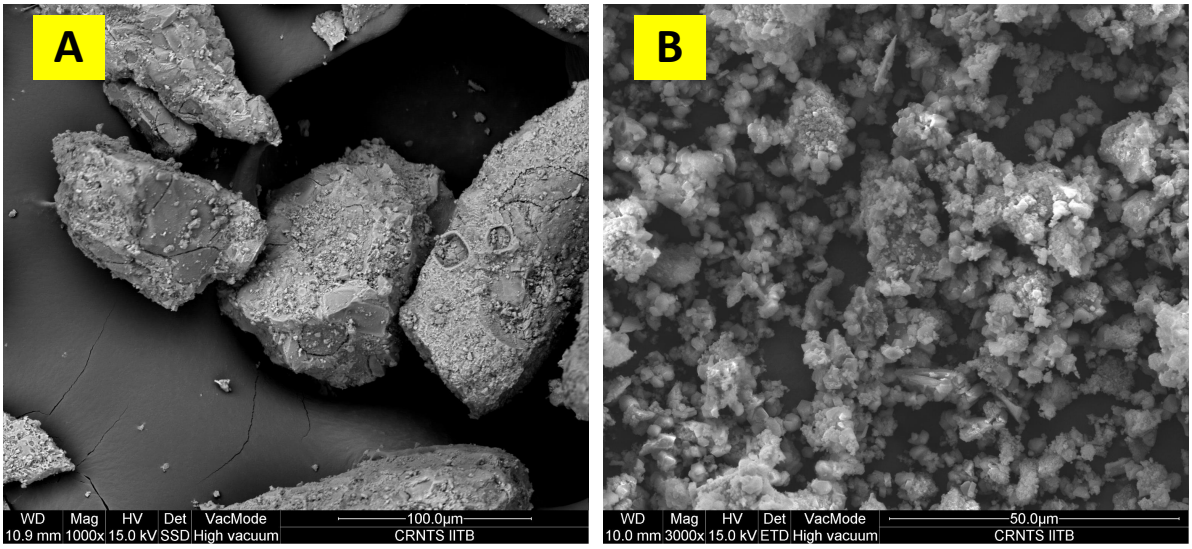

Figure 6.11: SEM image of (A) slag residue after 240 minutes of leaching at 25 °C (PS:212–355 μm), and (B) slag residue after 120 minutes of leaching at 60 °C (PS:<75 μm)

6.8 Precipitation

Unseeded precipitation of $CaCO_3$ was carried out under atmospheric CO_2 pressure using the filtrate (through 0.2 μm filter) from dissolution experiments conducted using <75 μm particles at 75 °C, initial pressure of 12.41 bar and varying L/S in the range of 50–100 ml/g. A reduction in CO_2 pressure from 7.38–8.05 bar to atmospheric conditions increased the supersaturation by more than an order of magnitude (even after considering that the solution is not completely free of dissolved CO_2). After 2–5 minutes of stirring, clear solution turned turbid which indicates the onset of precipitation. During this induction period, a rapid increase in pH to 7.5 was noticed (Figure 6.12). This probably indicates degassing of excess dissolved CO_2. After 60 minutes of precipitation the solution pH reached 8.45 and turbidity was completely lost with suspension of calcium carbonate particles in clear solution. Beyond this point, solution pH continued to increase at slower rate until it stabilized in the range of 8.5–8.6.

As shown in Figure 6.12, calcium concentration reached a plateau after rapidly decreasing for first 30 minutes. The silicon concentration, however, continued to decrease at the constant rate for 120 minutes. These results suggest that very high calcium recovery as carbonate is possible, however, amount of silicon as impurity increases exponentially

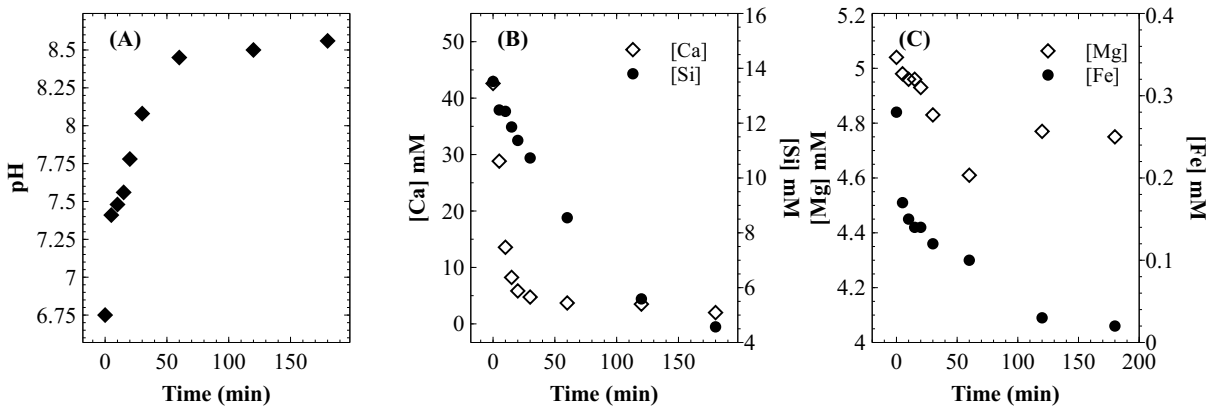

Figure 6.12: (A) Change in pH during precipitation step; (B) Change in concentration of Ca and Si during precipitation step

with calcium recovery. The combined maximum concentration of Mg and Fe as impurity (determined based on elemental concentrations in mother liquor) was found to be less than 1.5 wt% as magnesium carbonate and Fe(III) hydroxide. Silicon is the major secondary constituent with a maximum concentration of 16.6 wt% as SiO_2, as estimated based on Si concentration change in mother liquor. Calcium carbonate content determined by thermal decomposition of PCC samples up to 900 °C showed a weight loss of 36%, which is equivalent to 81.5 wt% purity. This is in close agreement with the elemental analysis where other constituents were estimated to be ∼18 wt%. Si is known to co-precipitate as silica along with calcium carbonate without formation of silicate (Kitano et al., 1979). As shown in Figure 6.13, the morphology of precipitated calcium carbonate under all experimental conditions was found to be rhombohedral indicating calcite polymorph (also confirmed using XRD spectra shown in Figure 6.14). Additionally, globular amorphous phase rich in silicon was also observed in SEM-EDS analysis (Figure 6.13B). FT-IR analysis was performed to investigate the chemical form of Si in the PCC sample. FT-IR spectra shown in Fig. 6.15, show peaks corresponding to symmetric (794 cm^{-1}), anti-symmetric (1082 cm^{-1}), and bending vibration (475 cm^{-1}) of Si-O-Si group. Additionally, peaks corresponding to anti-symmetric (1418 cm^{-1}), out-plane bending (871 cm^{-1}), and planar bending (713 cm^{-1}) vibrations of CO_3 group were noticed. No shoulder or peaks corresponding to Si-O-Ca which are expected at (950 cm^{-1})Pappas et al. (2008) were noticed. This result suggests the absence of silicate and existence of Si as silica. Silica is also a paper-filler with similar optical and ink adsorption properties as PCCGill (1995).

These observation suggest that further purification of PCC is not required for use as a filler in writing and printing papers.

6.9 Surface modified PCC

Recently, it was shown by Lourenço et al. (2013) that silica-PCC composite filler provides better mechanical strength to the paper without affecting the optical properties of PCC. The work used organic salt of orthosilicate as precursor for surface modification of PCC by sol-gel method. Considering that silicates in the steel slag are orthosilicates and Si leaches into solution to form monomeric units of H_4SiO_4, PCC obtained from pressure-swing route is expected to show surface encapsulation by silica and possible formation of composite PCC. FT-IR analysis suggests that Si exists in silica form and relatively slow precipitation rate of silica compared to $CaCO_3$ hints at condensation of silica on calcium carbonate. For further evidence of enrichment of silica on PCC surface, XPS and TEM analyses have been carried out.

6.9.1 Surface concentration by XPS

XPS was carried out to study the relative concentration of silica and calcium on PCC surface. The quantification analysis suggested that Si/Ca wt%/wt% of ≈10, which is more than an order of magnitude higher than the bulk (Si/Ca ≈ 0.2 wt%/wt%). This clearly indicates that the PCC surface is enriched with silica.

6.9.2 Imaging of PCC using TEM

TEM imaging has been done to confirm the presence of silica on the PCC surface. As shown in Figure 6.16A, precipitate existed as clusters of calcite and silica which are greater than 300 nm in size. At higher magnification, the edge of calcite crystal showed globular particles whose size is less than 50 nm (Figure 6.16B). High resolution TEM imaging showed short-range order without definite orientation indicating amorphous content (Figure 6.16C). This can be further confirmed based on the diffuse rings observed in selected area diffraction shown in Figure 6.16D. Diffuse rings were observed to match with silica.

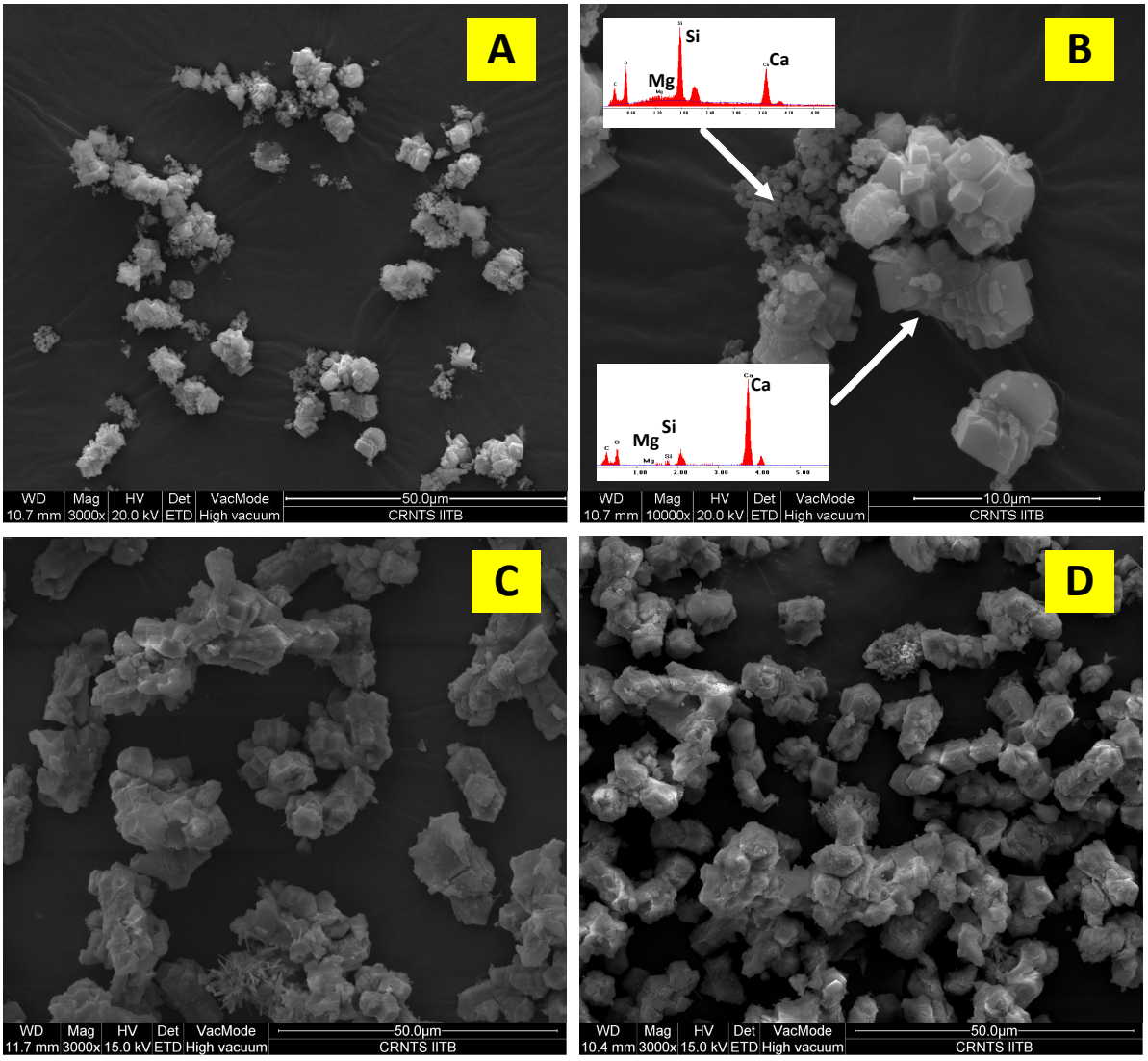

Figure 6.13: SEM micrographs of PCC produced at (A) L/S=100 ml/g, 60 min of precipitation - 3000x magnification, and (B) 10000x magnification with EDS spectra; (C) L/S=71.4 ml/g, 120 min of precipitation; (D) L/S=50 ml/g, 120 min of precipitation

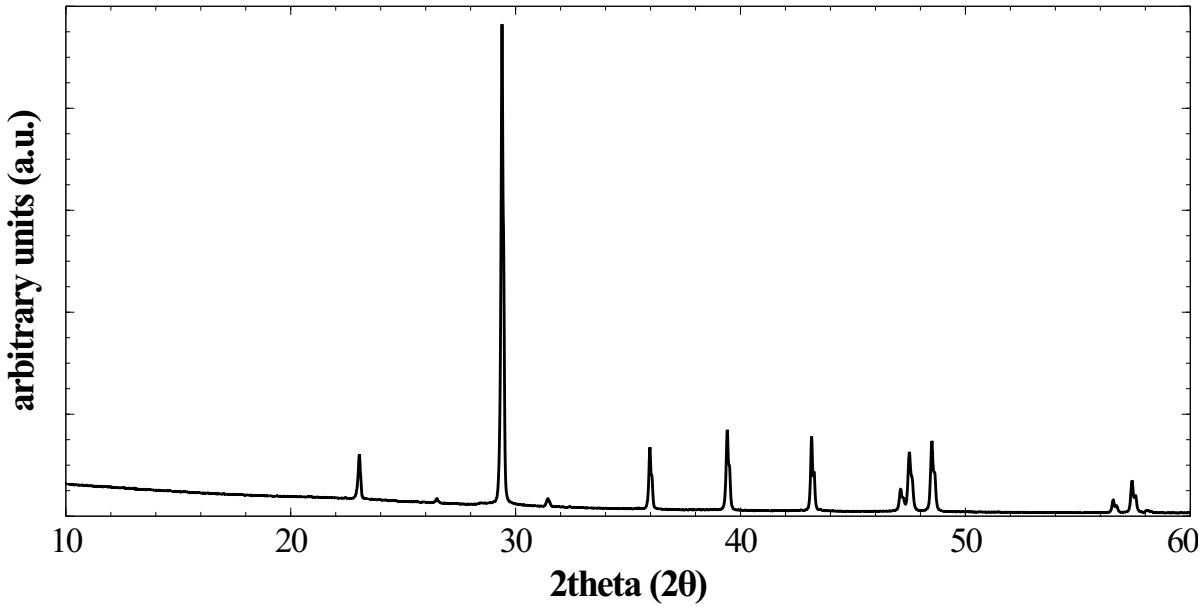

Figure 6.14: XRD spectra of PCC sample obtained from BOF slag

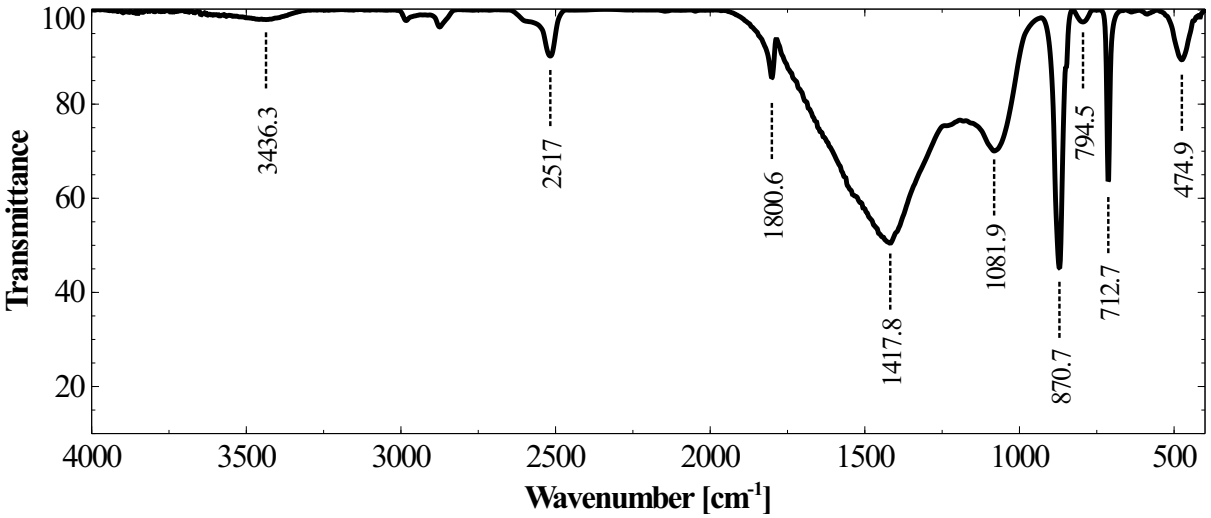

Figure 6.15: FT-IR spectra of PCC sample

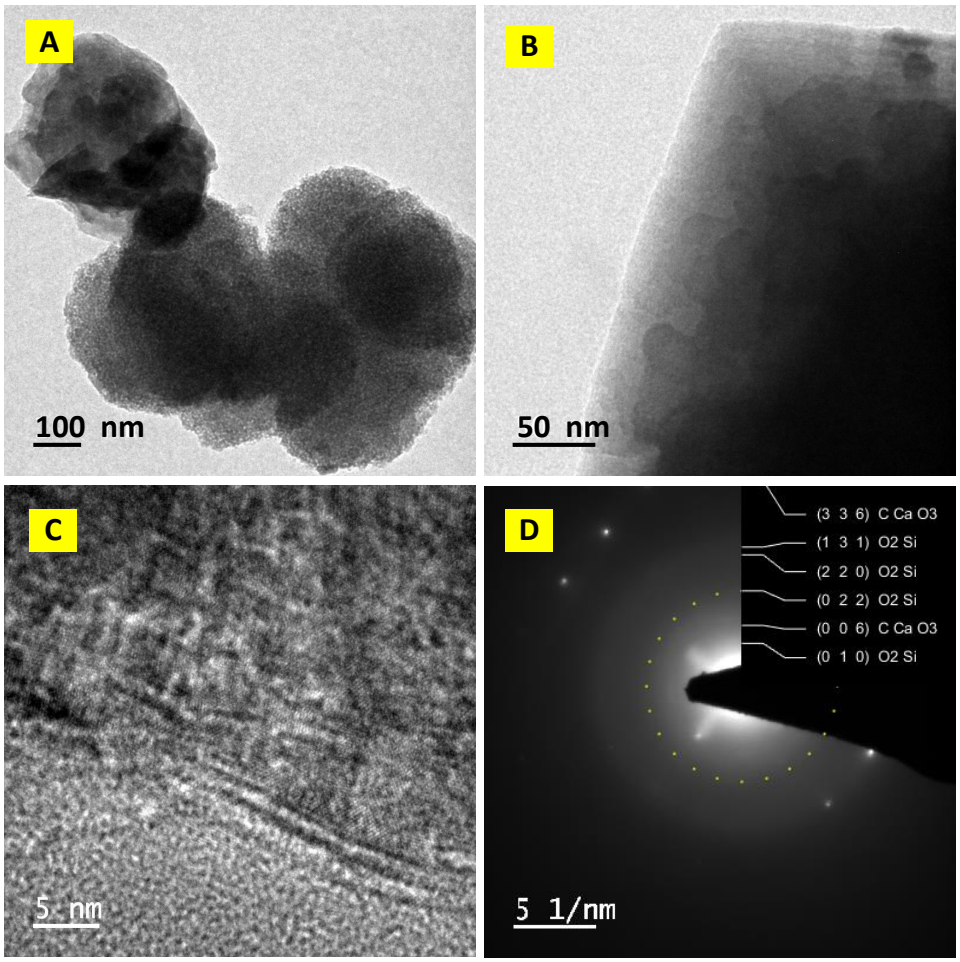

Figure 6.16: Bright-field TEM images of (A) Cluster of calcite and silica, and (B) Calcite edge showing surface modification; (C) HR-TEM image showing short-range order; (D) Diffraction pattern showing diffuse rings of silica in reciprocal space

Based on FT-IR, TEM and XPS analyses it is conclusive that the surface of PCC is enriched with SiO_2. Thus, PCC obtained from pressure-swing carbonation shows scope for production of silica-PCC composite from steel slag.

6.10 Summary

In this chapter, pressure-swing carbonation as a potential route for production of PCC using steel slag to sequester CO_2 has been investigated. Simple stirrer modification allowed us to increase the gas-liquid mass transfer coefficient and perform studies on mineral carbonation under CO_2 saturated condition, which in turn permitted to perform carbon balance and determine that the solution is truly supersaturated during dissolution stage. Precipitation of calcite is not kinetically favoured possibly due to low slurry pH and high calcium to carbonate ion ratio. Precipitation of silica or calcium carbonate on the residual slag surface which could lead to surface passivation was not observed in this study. Thus, the overall recovery of Ca as calcium carbonate is an order of magnitude higher than equilibrium estimate based on calcite solubility. Within the investigated parametric space, dissolution at low temperature, high-pressure and high liquid-to-solid ratio are favourable conditions for PCC production. Silica which has similar optical and ink adsorption characteristics as PCC co-precipitated with calcite; wherein further purification may not be required for use as a filler in paper industry. Under all conditions investigated, rhombohedral calcite was the product. Overall extraction efficiency obtained after 120 minutes of dissolution was 57% leading to a production of 535 kg of PCC per tonne of steel slag. Further extension of dissolution time can enhance the PCC production and CO_2 sequestration to 720 kg and 260 kg per tonne of steel slag, respectively.

The study shows significant scope for process-intensification of pressure-swing carbonation, especially to reduce the water requirement. Further investigations on dissolution step to achieve high and stable calcium concentration in the leachate, up to the solubility limit of amorphous calcium carbonate, are necessary. Also, investigations to obtain various morphologies of PCC and to control the particle size distribution are necessary for taking the process a step closer to commercialisation.

Chapter 7

Modelling dissolution kinetics of steel slag

A general framework for mathematical modelling of dissolution kinetics of multi-component aggregates such as steel slag is illustrated in Figure 7.1. Based on the experimental investigation presented in Chapter 5, leaching of elements confirm to be controlled by surface reaction. Thus, rate of leaching of elements from slag is expected to be a function of surface area of the mineral phase under consideration and concentration of dissolution promoting species in the solution (proton or ligands). As observed in experimental investigation, selectivity of calcium varies based on the leaching chemistry and thus, surface concentration of elements and surface area dynamically evolve by enrichment or depletion of species during the process of dissolution. Additionally, several reactions such as precipitation of secondary phases, re-adsorption of dissolved species on to residual slag or precipitated phases may alter the concentration of dissolution promoting species. In batch reactor system, with continuous evolution of species concentration, these steps add to complexity.

The complexity associated with slag dissolution was systematically addressed by evaluating mineral composition (discussed in Chapter 4), deducing leaching chemistry (discussed in Chapter 4), identifying rate controlling mechanism (discussed in Chapter 5), modelling surface area evolution and determination of kinetic parameters.

7.1 Dissolution model

The temporal evolution of metal ions concentration in a batch reactor has been modelled by considering two independent parameters, proton concentration and reactive surface area, which were found from experimental parametric investigations. Here, the general

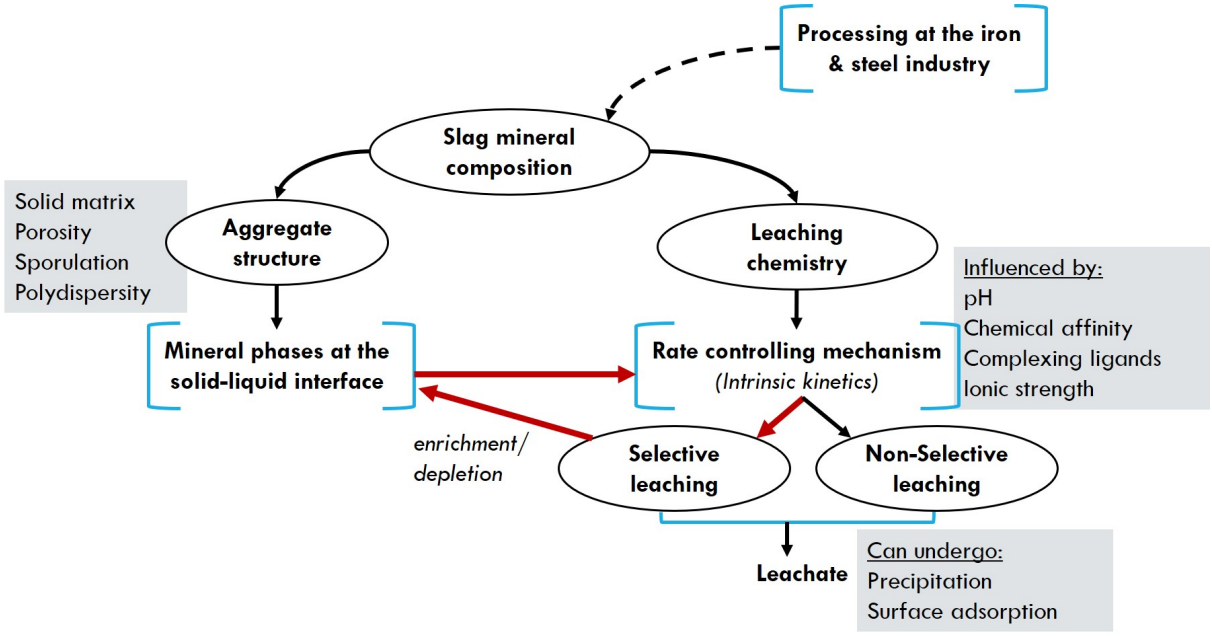

Figure 7.1: Framework of kinetic model

dissolution model (Equation 2.7)—a widely applied rate-model for dissolution of single minerals by surface reaction—has been used. The model development is restricted to far-from-equilibrium conditions (in tune with the experimental data where chemical affinities of dissolving minerals C_3S ($>$ 134 kJ/mol) and C_2S ($>$ 76 kJ/mol) are very high ($\gg \sigma RT \approx$ 7.5 kJ/mol)[1], where the influence of saturation state on dissolution rate can be neglected. The general assumptions in deriving the model are: (a) considering the acidic pH, concentration of CO_2 in the leaching agent has been assumed to be zero, (b) partial pressure of oxygen has been assumed to be constant, (c) based on experimental observations and dissolution characteristics of orthosilicates, formation of Si-rich leached layer on residual slag has been neglected, (d) Fe(III) rich phase is considered to be inert, (e) dissolution of Mg and Fe(II) from the slag is considered to be predominantly from the RO phase, and (f) considering the non-porous nature of slag and absence of stirring rate (above 350 rpm) influence on dissolution rate, mass transport effects have been neglected.

[1]Chemical affinities have been calculated using solubility product values given in literature(Nicoleau et al., 2013).

7.1.1 Rate equations

The general dissolution model after neglecting the influences of ionic strength, chemical affinity, catalytic and inhibitory effects of species other than H^+ is given in Equation 7.1.

$$\begin{aligned} \frac{\mathrm{d}m}{\mathrm{d}t} &= -k \times S_{area} \times g\left([\mathrm{H}^+_{ads}]\right) \\ \frac{\mathrm{d}[\mathrm{M}]}{\mathrm{d}t} &= \frac{k}{V \times A_{\mathrm{M}}} \times S_{area} \times g\left([\mathrm{H}^+_{ads}]\right) \end{aligned} \tag{7.1}$$

where m is the residual mass of mineral (MX) during leaching, [M] is the concentration of metal M in the leachate, S_{area} is the reactive mineral surface area, k is the rate constant, V is the leachate volume, A_{M} is the atomic weight of metal M, and $[\mathrm{H}^+_{ads}]$ is the activity of H^+ on the mineral surface.

Based on Equation 7.1, rate equations for leaching of calcium, magnesium, and iron can be written as below. Here, the activity of H^+ on the mineral surface is modelled using Langmuir–Hinshelwood isotherm.

$$\frac{\mathrm{d}[\mathrm{Ca}]}{\mathrm{d}t} = \frac{k_{\mathrm{Ca}}}{V \times A_{\mathrm{Ca}}} \times S_{\mathrm{Ca}} \times \left(\frac{\{\mathrm{H}^+\}}{1 + K_{S\mathrm{Ca}}\{\mathrm{H}^+\}}\right) \tag{7.2}$$

$$\frac{\mathrm{d}[\mathrm{Mg}]}{\mathrm{d}t} = \frac{k_{\mathrm{Mg}}}{V \times A_{\mathrm{Mg}}} \times S_{\mathrm{Mg}} \times \left(\frac{\{\mathrm{H}^+\}}{1 + K_{S\mathrm{Mg}}\{\mathrm{H}^+\}}\right) \tag{7.3}$$

where $\{H^+\}$ is the activity of H^+ in the aqueous solution, $K_{S\mathrm{Ca}}$ and $K_{S\mathrm{Mg}}$ are surface stability constants.

As described in Chapter 5, Fe(II) oxidised to Fe(III) and precipitates as ferrihydrite (FeOOH). Thus, net dissolution of Fe(II) and Fe(III) into leachate is given as follows.

$$\frac{\mathrm{d}[\mathrm{Fe(II)}]}{\mathrm{d}t} = \frac{k_{\mathrm{Fe(II)}}}{V \times A_{\mathrm{Fe}}} \times S_{\mathrm{Fe}} \times \left(\frac{\{\mathrm{H}^+\}}{1 + K_{S\mathrm{Fe}}\{\mathrm{H}^+\}}\right) - k'_{\mathrm{Fe(III)}} \times \{\mathrm{Fe(II)}\}\{\mathrm{OH}^-\}^2 \tag{7.4}$$

$$\frac{\mathrm{d}[\mathrm{Fe(III)}]}{\mathrm{d}t} = k'_{\mathrm{Fe(III)}} \times \{\mathrm{Fe(II)}\}\{\mathrm{OH}^-\}^2 - k_{\mathrm{FeOOH}} \times \{\mathrm{Fe(III)}\}\{\mathrm{OH}^-\} \tag{7.5}$$

where, $k'_{\mathrm{Fe(III)}} = k_{\mathrm{Fe(III)}} \times p\mathrm{O}_2$.

The rate of re-precipitation of iron as ferrihydrite is give as follows.

$$\frac{\mathrm{d}[\mathrm{FeOOH}]_{ppt}}{\mathrm{d}t} = k_{\mathrm{FeOOH}} \times \{\mathrm{Fe(OH)_3}\} \times hf(SI) \tag{7.6}$$

where SI is the saturation index of ferric hydroxide, $hf()$ is the Heaviside step function.

Charge balance and speciation

In the above set of equations (7.2–7.6), the unknown species concentration, $[H^+]$ and $[OH^-]$, can be calculated by solving charge balance and equilibrium relation for water dissociation, as given below.

$$\sum_{j=\text{Ca,Fe,Mg}} z_j[M_j^{z_j}] + [H^+] - [OH^-] - [NO_3{}^-] = 0 \tag{7.7}$$

$$\{H^+\}\{OH^-\} = K_w \tag{7.8}$$

Speciation calculation has been performed based on leaching chemistry described in Chapter 4 and summarised in Appendix B.

Estimation of activity coefficient

Since the ionic strength (I) of the leachate was observed to be lower than 0.1 M in the current experimental investigations, Davies equation(Davies and Shedlovsky, 1964) (Equation 7.10) has been used to determine the activity coefficients of various ionic species.

$$I = \frac{1}{2}\left(\sum_{j=\text{Ca,Fe,Mg}} z_j^2[M_j^{z_j}] + [H^+] + [OH^-] + [NO_3{}^-]\right) \tag{7.9}$$

$$\log \gamma^{+z} = \log \gamma^{-z} = -Az_j^2\left(\frac{\sqrt{I}}{1+\sqrt{I}} - 0.3I\right) \tag{7.10}$$

Activity of an ion M^{+z} in the solution can be related to its concentration by,

$$\{M^{+z}\} = \gamma^{+z} \times [M^{+z}]. \tag{7.11}$$

7.1.2 Surface area evolution of Ca-rich phases

Slag is a non-porous solid and modelling the surface area evolution was attempted by following considerations:

Solid matrix analysis

Based on the mineral composition and microscopy studies, it was understood that calcium silicates and dicalcium ferrite phases form the matrix of the slag particle while RO phase is distributed as spores in the matrix. Considering the fact that dicalcium ferrite is inert, dissolution of two mineral phases—calcium silicate and RO phase—that control the release of Ca, Si and Fe, Mg, respectively. Thus, it is sufficient to consider surface area evolution of the matrix (calcium silicates) and spores (RO phase) present in it.

Polydispersity and fractal geometry

It was well recognised that surface area evolution of poly-disperse spherical particles differs from uniformly-sized particle system and that, if this is not taken into account, it can potentially lead to wrong interpretation of the rate controlling process. In order to understand the effect of polydispersity on surface area evolution and conversion, numerical simulations based on the population balance model have been carried out (for model equations and results refer supplementary information). Surface area evolution with conversion was simulated for two commonly encountered distribution functions namely Gaussian and log-normal distributions with varying coefficients of variation C_V, defined as the ratio of standard deviation to the mean. The simulation results (refer Appendix A) indicate that a wider distribution (high C_V) results in a surface area evolution that changes linearly with conversion, that is, surface area follows changes in particle volume. Although C_V determined for the samples used for experimentation in the current study using image analysis is about 0.15–0.28, because of the presence of the ultra-fine particles which could not be measured, the actual distribution is expected to be wider. In addition, slag surface exhibited severe etching with the dissolution of calcium silicate phases in nitric acid and probably dissolving inter-crystalline material, thus exhibiting rough and irregular surface (Figure 7.2). A study on fractal surfaces(Avnir et al., 1985) suggested that the surface area evolution of rough and irregular surfaces can be better explained

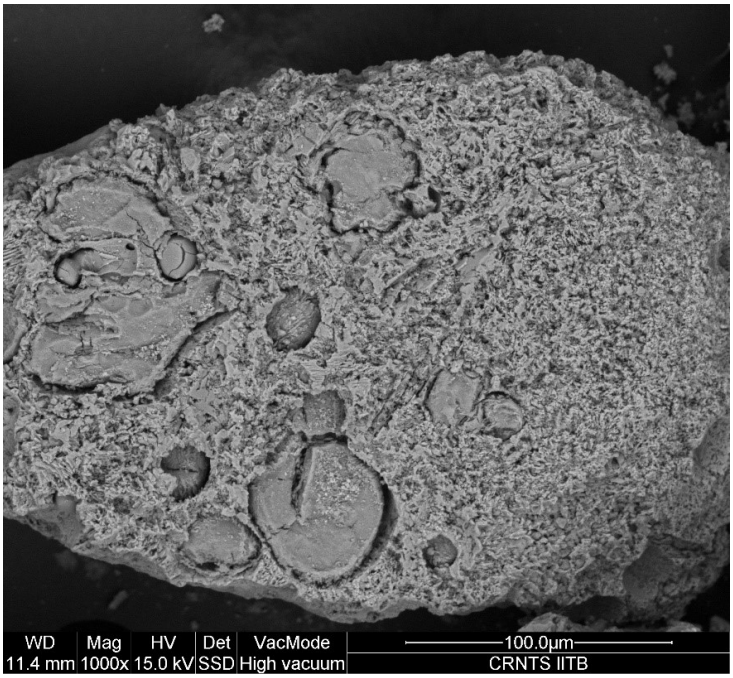

Figure 7.2: Typical slag particle after dissolution in acid media showing surface etching

by fractal geometry, where surface area evolution follows changes in particle volume for highly irregular surfaces. Considering the above two aspects, Equation 7.12 has been considered to model the surface area evolution of the matrix containing calcium silicate phases.

$$S_{\mathrm{Ca}}(t) = S_{\mathrm{Ca}}(t_0) \times (1 - X_{\mathrm{Ca}}) \tag{7.12}$$

where conversion X_{Ca} is $[\mathrm{Ca}]/[\mathrm{Ca}]_{max}$ and $[\mathrm{Ca}]_{max}$ is $x_{\mathrm{Ca}} m_{i,slag}/VA_{\mathrm{Ca}}$; $m_{i,slag}$ is the initial slag mass used in the experiment.

Inert calcium mineral phases

The matrix which is predominantly formed of calcium silicates also contains dicalcium ferrite which was found to be inert. In order to account for the volume occupied by inert material, an additional parameter b was introduction in Equation 7.12 to obtain Equation 7.13.

$$S_{\mathrm{Ca}}(t) = S_{\mathrm{Ca}}(t_0) \times (1 - bX_{\mathrm{Ca}}) \tag{7.13}$$

$$= S_{\mathrm{Ca}}(t_0) \times \left(1 - b\frac{[\mathrm{Ca}]A_{\mathrm{Ca}}V}{x_{\mathrm{Ca}}m_{i,slag}}\right) \tag{7.14}$$

7.1.3 Surface area evolution of Mg- and Fe-rich phases

The Mg- and Fe-rich phases which are part of RO phase have been modelled as regular and uniformly dispersed spherical inclusions (or globules) which become accessible with the leaching of the matrix material (calcium silicates). Here, modelling the surface area of those RO phase particles, which are in contact with the aqueous solution, has been done in similar lines to *sporulation* model Adrover et al. (2004). Given a particle-size distribution $F(D,t)$ of RO phase particles in contact with the aqueous phase, the surface area S_{RO} can be estimated using the following equation.

$$S_{RO}(t) = \int_0^{D_\infty} \pi D^2 F(D,t) \mathrm{d}D \tag{7.15}$$

The reactive surface of Mg and Fe phases, which are part of RO phase, have been approximated based on the relative composition of these elements.

$$\begin{aligned} S_{\mathrm{Mg}}(t) &= \left(\frac{x_{\mathrm{Mg}}}{x_{\mathrm{Mg}} + x_{\mathrm{Fe}}}\right) \int_0^{D_\infty} \pi D^2 F(D,t) \mathrm{d}D \\ S_{\mathrm{Fe}}(t) &= \left(\frac{x_{\mathrm{Fe}}}{x_{\mathrm{Mg}} + x_{\mathrm{Fe}}}\right) \int_0^{D_\infty} \pi D^2 F(D,t) \mathrm{d}D \end{aligned} \tag{7.16}$$

Population balance

The particle size distribution of globules released into the aqueous solution $F(D,t)$ has been modelled using population balance method with the following assumptions:

1. Volumetric distribution of RO phase inclusions in the slag particle is homogeneous.

2. Particles may not fall off into the leachate in all instances. Nevertheless, dissolution around these inclusions creates gaps providing access to the acidic solution.

3. Density of inclusions is assumed to be same as matrix material.

4. Breakage of slag particles to smaller size during reaction because of agitation and collisions are ignored.

The net accumulation of particles sized D to (D+ΔD) in solution can be expressed as a sum of net rate of particle growth into the size interval D to (D+ΔD) and rate of release of globules with size D to (D+ΔD) leading to following equations.

$$\frac{\partial F(D,t)\Delta D}{\partial t} = F(D,t)R(D)_D - F(D,t)R(D)_{D+\Delta D} + r_{sp}(D,t)\Delta D \tag{7.17}$$

$$\frac{\partial F(D,t)}{\partial t} = \frac{F(D,t)R(D)_D - F(D,t)R(D)_{D+\Delta D}}{\Delta D} + r_{sp}(D,t) \tag{7.18}$$

as $\Delta D \to 0$,

$$\frac{\partial [F(D,t)]}{\partial t} + \frac{\partial [R(D)F(D,t)]}{\partial D} = r_{sp}(D,t) \tag{7.19}$$

where, $R(D)$ is the rate of growth of particle diameter, $r_{sp}(D,t)$ is the rate of sporulation.

Particle growth rate

The rate of diminution (negative growth rate, $-R(D)$) of a non-porous and spherical RO phase particle of diameter D due to acid dissolution can be derived as follows using the Equations 7.1. Here, the rate of change of RO phase mass is taken as sum of the rates of leaching of Mg- and Fe-rich phases.

$$\frac{\mathrm{d}m_{RO}}{\mathrm{d}t} = -\frac{\pi D^2\{\mathrm{H}^+\}}{x_{\mathrm{Mg}} + x_{\mathrm{Fe}}} \times \left(\frac{k_{\mathrm{Mg}} x_{\mathrm{Mg}}}{1 + K_{S\mathrm{Mg}}\{\mathrm{H}^+\}} + \frac{k_{\mathrm{Fe}} x_{\mathrm{Fe}}}{1 + K_{S\mathrm{Fe}}\{\mathrm{H}^+\}} \right) \tag{7.20}$$

$$\rho \frac{\pi D^2}{2} \frac{\mathrm{d}D}{\mathrm{d}t} = -\frac{\pi D^2\{\mathrm{H}^+\}}{x_{\mathrm{Mg}} + x_{\mathrm{Fe}}} \times \left(\frac{k_{\mathrm{Mg}} x_{\mathrm{Mg}}}{1 + K_{S\mathrm{Mg}}\{\mathrm{H}^+\}} + \frac{k_{\mathrm{Fe}} x_{\mathrm{Fe}}}{1 + K_{S\mathrm{Fe}}\{\mathrm{H}^+\}} \right) \tag{7.21}$$

$$\frac{\mathrm{d}D}{\mathrm{d}t} = R(D) = -\frac{2\{\mathrm{H}^+\}}{\rho(x_{\mathrm{Mg}} + x_{\mathrm{Fe}})} \times \left(\frac{k_{\mathrm{Mg}} x_{\mathrm{Mg}}}{1 + K_{S\mathrm{Mg}}\{\mathrm{H}^+\}} + \frac{k_{\mathrm{Fe}} x_{\mathrm{Fe}}}{1 + K_{S\mathrm{Fe}}\{\mathrm{H}^+\}} \right) \tag{7.22}$$

Sporulation rate

The sporulation rate of RO particles which are of diameter D from the slag, $r_{sp}(D,t)$, can be expressed as the product of RO particle density in the slag matrix and volumetric rate of matrix leaching ($\mathrm{d}V_{matrix}/\mathrm{d}t$).

$$r_{sp}(D,t) = n_{RO} \times f(D) \times \left(-\frac{\mathrm{d}V_{matrix}}{\mathrm{d}t} \right) \tag{7.23}$$

where, $f(D)$ is the PSD density function of RO phase particles in the slag. The number of RO particles present per unit volume of the slag can be expressed as,

$$n_{RO} = \frac{\left[\frac{x_{RO} m_{slag}}{1/6\rho\pi D^3}\right]}{\left[\frac{m_{slag}}{\rho}\right]} \tag{7.24}$$

$$= \frac{x_{RO}}{1/6\pi D^3} \tag{7.25}$$

where, x_{RO} is the mass fraction of RO phase present in the slag. The volumetric rate of matrix leaching $\mathrm{d}V_{matrix}/\mathrm{d}t$ is given by,

$$\begin{aligned} \frac{\mathrm{d}V_{matrix}}{\mathrm{d}t} &= -V_{i,matrix}\frac{\mathrm{d}X_{Ca}}{\mathrm{d}t} \\ &\approx -\frac{m_{i,slag}}{\rho}\frac{\mathrm{d}X_{Ca}}{\mathrm{d}t} \\ &= -\frac{A_{\mathrm{Ca}}V}{x_{\mathrm{Ca}}\rho}\frac{\mathrm{d}[\mathrm{Ca}]}{\mathrm{d}t} \end{aligned} \tag{7.26}$$

Using Equations 7.23–7.26, sporulation rate can be expressed in known terms as,

$$r_{sp}(D,t) = \frac{x_{RO}}{1/6\pi D^3} \times f(D) \times \left(\frac{A_{\mathrm{Ca}}V}{x_{\mathrm{Ca}}\rho}\frac{\mathrm{d}[\mathrm{Ca}]}{\mathrm{d}t}\right) \tag{7.27}$$

The surface area of calcium silicate (Equation 7.12) and RO phases (Equation 7.16) can be simultaneously solved along with the population balance model (Equation 7.19) and the rate equations (7.2–7.6).

7.2 Numerical methods

7.2.1 Discretisation and ODE solution

The population balance model (Equation 7.19), which is a hyperbolic PDE with source term, has been approximated using forward difference scheme to obtain following set of finite ordinary differential equations (ODE).

$$\frac{F(D_j,t_{i+1}) - F(D_j,t_i)}{\Delta t} = \frac{R(D_{j+1})F(D_{j+1},t_i) - R(D_j)F(D_j,t_i)}{\Delta D} + r_{sp}(D_j,t_i) \tag{7.28}$$

where, $j = 1$ to J; $\Delta D = (D_J - D_1)/J$; function value beyond the end point, $F(D_{J+1}, t_i)$, has been taken as $2 \times F(D_J, t_i) - F(D_{J-1}, t_i)$; D_J is taken as $D_\mu \times 1.2$, $J = 500$, and $D_1 = 0$ for numerical simulation.

The above equation (7.28) has been solved as a set of J ODEs, which are a function of time t, uniformly discretised over space domain (D). The J time dependent ODE functions have been solved simultaneously along with rate equations using *ode15s* of MATLAB®. The grid spacing ΔD for the space domain was maintained uniform, while that of time domain (Δt) has been allowed to be determined by *ode15s* function in MATLAB®.

7.2.2 Initial conditions

The set of ordinary differential equations, which include the rate equations (7.2–7.6) and discretised partial differential equation (7.28), can be solved using following initial conditions. The initial concentration of product species are [Ca] = [Mg] = [Fe] = [Si] = 0, and of acid is $[H^+] = [NO_3{}^-] = C_0$. The initial PSD of RO phase particles $F(D, 0)$ exposed at time $t = 0$, required to solve population balance equations, is estimated as,

$$F(D,0) = y_0 \times \left(n_{RO} \frac{m_{i,slag}}{\rho} \right) f(D) \tag{7.29}$$

$$= y_0 \times \left(\frac{x_{RO}}{1/6\pi D^3} \frac{m_{i,slag}}{\rho} \right) f(D) \tag{7.30}$$

where, y_0 is the fraction of RO particles which are initially exposed to the aqueous solution. For the same sample mass, y_0 varies with the particle size, where the maximum fraction is exposed in the case of finely pulverised sample and the least for single large coarse slag particle. Assuming that the exposed particles are located in a volume $\Delta V_{surface}$ beneath the exposed slag surface, the following parametric relation between slag particle size and y_0 can be established.

$$\begin{aligned} y_0 &= \Delta V_{surface}/V_{slag} \\ &= \delta \times S_{area}/V_{slag} \end{aligned} \tag{7.31}$$

With the idealisation of spherical surface, one can arrive at following relation.

$$y_0 = \frac{6\delta}{d_{slag}} = \frac{\delta'}{d_{slag}} \tag{7.32}$$

where, δ' is an adjustable parameter.

In the current study, the dissolution behaviour was studied for $C_0 = 0.024$, 0.072, and 0.12 M. Volume of aqueous solution was fixed at 0.25 L for all studies. The dissolution behaviour was studied for $m_{i,slag} = 1.5$, 2.5, and 5.0 g, and for slag particle diameter $d_{slag} = \leq$45, 90–125, 150–212, 212–355 μm. The values used for the fixed parameters in the model are given in the Table 7.1. Discretisation scheme for partial differential equation (Equation 7.19) and the methodology for numerical simulation of the model are given in supporting information.

Table 7.1: Fixed parameters and their numerical values

Parameter	Value	Parameter	Value	Parameter	Value	Parameter	Value
x_{Ca}	0.307	x_{Mg}	0.0553	b	1.25	$\log(K_w)$	-14
x_{Fe}	0.101	x_{RO}	0.219	ρ (kg/m3)	4000	$f(D)$	$\frac{1}{D_\sigma\sqrt{2\pi}} \exp -\frac{1}{2}\left(\frac{D-D_\mu}{D_\sigma}\right)^2$

where $D_\mu = 14 \times 10^{-6}$ m; D_σ is assumed to be equal to step-size ΔD; b, which is the ratio of total calcium content to extractable calcium content is 1.25 owing to 20% inert calcium associated with brownmillerite phase.

7.2.3 Parameter Estimation

The adjustable parameters in the model are rate constants, $k_{Ca}, k_{Mg}, k_{Fe(II)}$ and $k'_{Fe(III)}$, Langmuir–Hinshelwood equilibrium constant, K_{SFe}, and geometrical parameter δ'. K_{SCa} has been fixed to 5.8 and K_{SMg} has been assigned the same value as K_{SFe}.

The above set of six parameters were estimated by least square error method (Equation 7.33), where square of errors in concentrations of Ca, Fe and Mg have been minimised using *lsqcurvefit* function available in MATLAB®. The error minimisation has been carried out with the constraint that the parameters are non-negative.

$$err = \min \sum_{i=Ca,Mg,Fe} \Big([\mathrm{M_{i,exp}}] - [\mathrm{M_{i,model}}]\Big)^2 \tag{7.33}$$

The estimated values for the adjustable parameters obtained from error minimisation are $K_{SFe} = K_{SMg} = 5.65$, $k_{\mathrm{Ca}} = 10.89$, $k_{\mathrm{Fe(II)}} = 80.67$, $k_{\mathrm{Mg}} = 38.12$, $k'_{Fe(III)} = 1E18$, and

$\delta' = 52.5$. The obtained results validate the assumption made in Section 5.3.1 that the Langmuir constants for Ca-rich and Fe, Mg rich phases are similar and there is negligible effect of $[H^+]$ on the Ca selectivity.

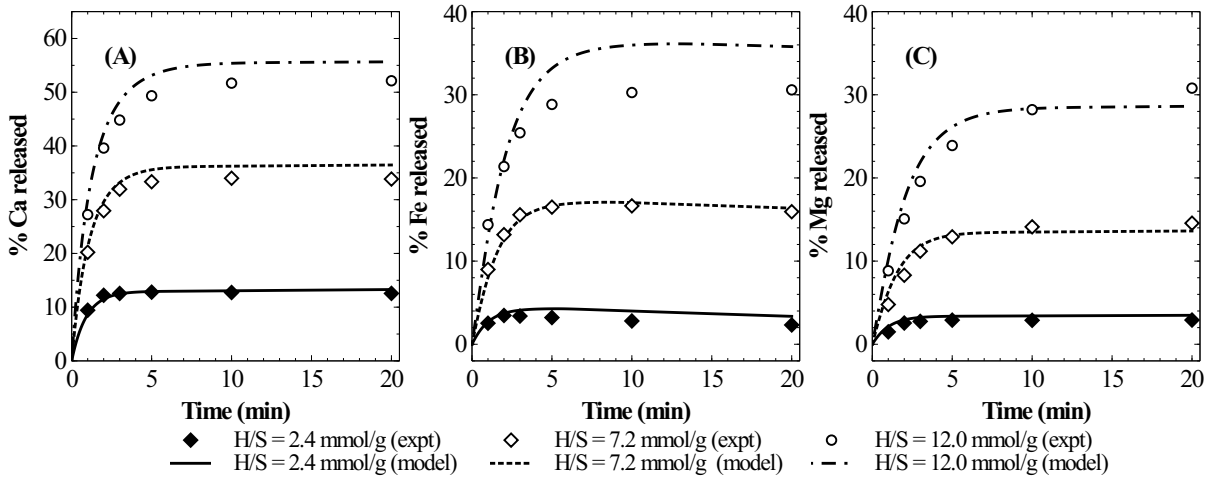

Figure 7.3: Effect of acid-to-solid ratio (H/S) on the release of (A) Calcium, (B) Iron, (C) Magnesium from the slag in dilute nitric acid.

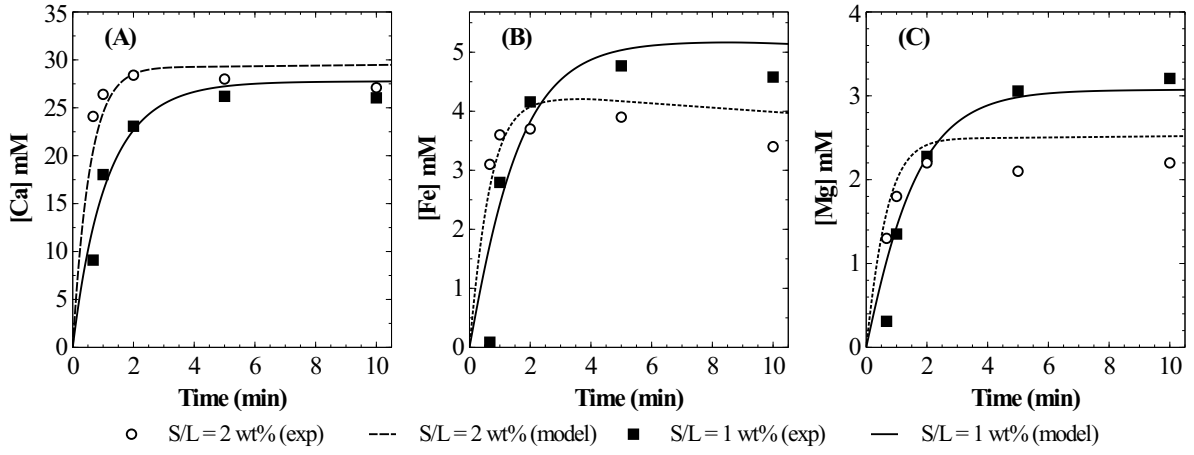

Figure 7.4: Effect of slag loading on leaching characteristics of (A) Ca, (B) Fe, and (C) Mg in HNO_3 (H/S: 7.2 mmol/g, T: 30 °C)

7.3 Simulation results

The simulation results, with the best-fit parameters, are compared against experimental data in Figures 7.3–7.5. As seen in these figures, the model results are in good agreement with the experimental data. A typical simulation of particle size distribution of RO phase

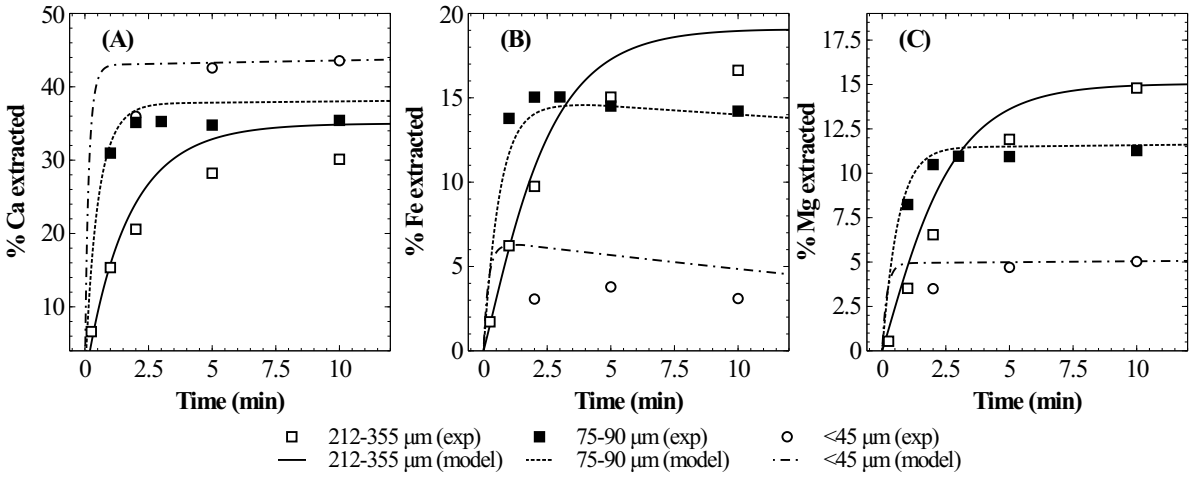

Figure 7.5: Effect of particle size on leaching characteristics of (A) Ca, (B) Fe, (C) Mg in nitric acid(H/S: 7.2 mmol/g, L/S: 87.2 ml/g, T: 30 °C)

spores, which are exposed to the aqueous solution, is shown in Figure 7.6A. As expected, the monodisperse particle size at time t=0 min becomes polydisperse with the progression of leaching. As shown in Figure 7.6B, the particle size decreased from the initial 14 μm to about 10.8 μm after 60 minutes of dissolution. The skewness is initially negative owing to rapid sporulation compared to dissolution rate. Subsequently, the skewness is positive due to slower sporulation rate compared to the rapid dissolution of finer particles. The temporal evolution of the surface area of MgO (normalised to the initial value), simulated for various parametric studies, is presented in Figure 7.7. As hypothesised, the surface area was found to increase with the progress of dissolution. While the increase in surface area was found to be maximum for coarse particle size fractions, the surface area was observed to decrease for finer particle size fraction of slag, where all RO phase spores are initially exposed and no sporulation is anticipated. The model fits and simulation results conclusively show that geometrical considerations in the model are sufficient to explain the dissolution characteristics without the need to invoke mechanisms such as surface passivation with variable diffusivity or the use of hypothetical activity factor.

7.4 Summary

A mathematical model to describe kinetics of slag dissolution has been developed by considering the heterogeneous morphology. The dissolution model considering Langmuir–

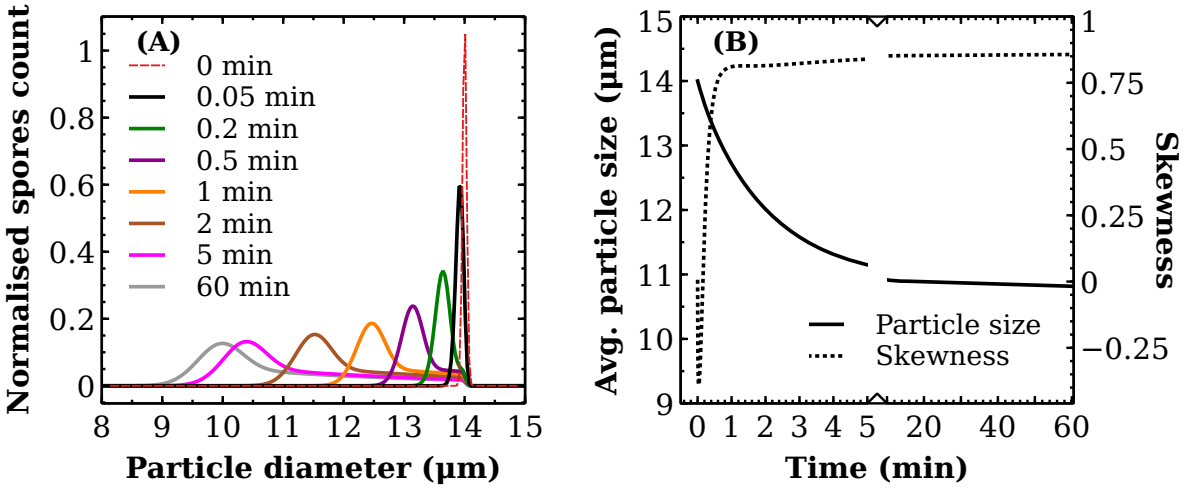

Figure 7.6: (A) Typical simulation result (for PS:150–212μm, H/S=30 mmol/g, LS=100 ml/g) showing temporal evolution of particle size distribution of RO phase spores exposed to aqueous solution, (B) corresponding changes in average particle size and skewness (third moment)

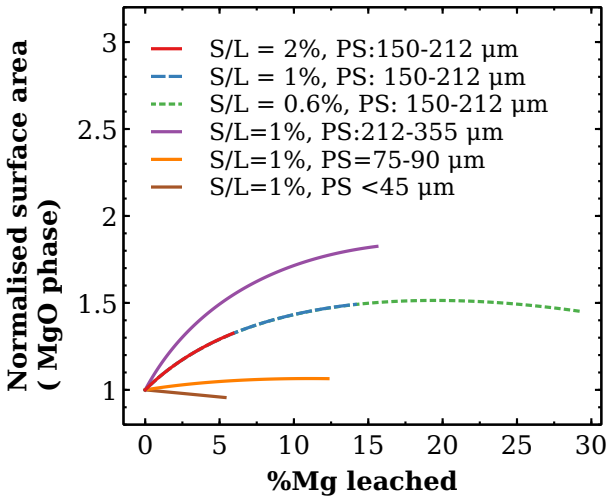

Figure 7.7: Surface area evolution of MgO phase with the extent of Mg dissolution corresponding to particle size (PS) and solid loading (S/L) variations

Hinshelwood kinetics and RO phase surface area evolution by sporulation has been found to explain the dissolution characteristics observed in parametric studies. The reduction in the extent of calcium extraction with the increase in particle size, which in earlier literature was explained using assumptions such as surface passivation and hypothetical activity factors, is shown to be a consequence steel slag morphology and competitive dissolution of RO phase and silicate matrix.

Although the current dissolution model is limited to acidic pH conditions and large

chemical affinity, it appears to be a promising start for scientific investigations on two distinct fronts. Firstly, the model shows that dissolution kinetics of non-homogeneous residues such as slag can be modelled as a combination of dissolution of pure single mineral phases. This allows a logical extension of the model to predict the release of trace metals which are homogeneously distributed within a dissolving phase. Secondly, the success of the bottom-up approach to develop the model based on mineral phase characterisation and morphology study brings us one step closer to *a priori* modelling of dissolution characteristics. Understanding of dissolution and precipitation kinetics of primary and secondary mineral phases in the circumneutral and alkaline pH leaching solutions is required for further advancements towards *a priori* modelling. Further, the model can be used to resolve the effects of potentially accelerating/inhibiting ligands on metal ion leaching rates from proton-promoted dissolution.

Chapter 8

Conclusions

A systematic investigation of steel slag utilisation through mineral carbonation was carried out. Overall, steel slag was found to be a suitable feedstock based on the high-reactivity of calcium-rich mineral phases and high calcium amount for precipitated calcium carbonate production.

The study demonstrates the importance of leaching chemistry, surface reaction kinetics and geometrical aspects which govern surface area evolution during dissolution process. These aspects were found to determine the extent of calcium leaching and calcium selectivity during dissolution process. In addition, Fe and Si were found to be primary impurities during dissolution in acidic media. Removal of Fe impurity as precipitate is controlled by rate of oxidation of Fe(II), which accelerates in neutral and basic conditions. The dependency of Fe precipitation on $[OH^-]$ and pH buffering phenomenon associated with Fe(III) precipitation, necessitates additional of alkaline solutions such as NaOH or NH_4OH for pH-swing. Addition of base also leads to operational problems in addition to input cost. For instance, precipitation of Fe by addition of base leads to co-precipitation of ferrihydrite and silica. Silica formed from orthosilicates is known to be gelatinous and causes filtration problems. Addition of sodium molybdate to the leaching agent was found to reduce Fe leaching and improve spontaneity in pH-swing. However, input cost and recycling efficiency of such additives is yet to be evaluated.

Alternatively, pressure-swing carbonation was found to be better for mineral carbonation of steel slag for two distinct reasons: 1) leaching of Fe was found to be minimal at circumneutral pH conditions observed under CO_2 pressure, and 2) silica precipitation was found to be slow and presence of smaller units of silica during calcium carbonate precipitation was found to condense on PCC particles. Recently, such surface modified

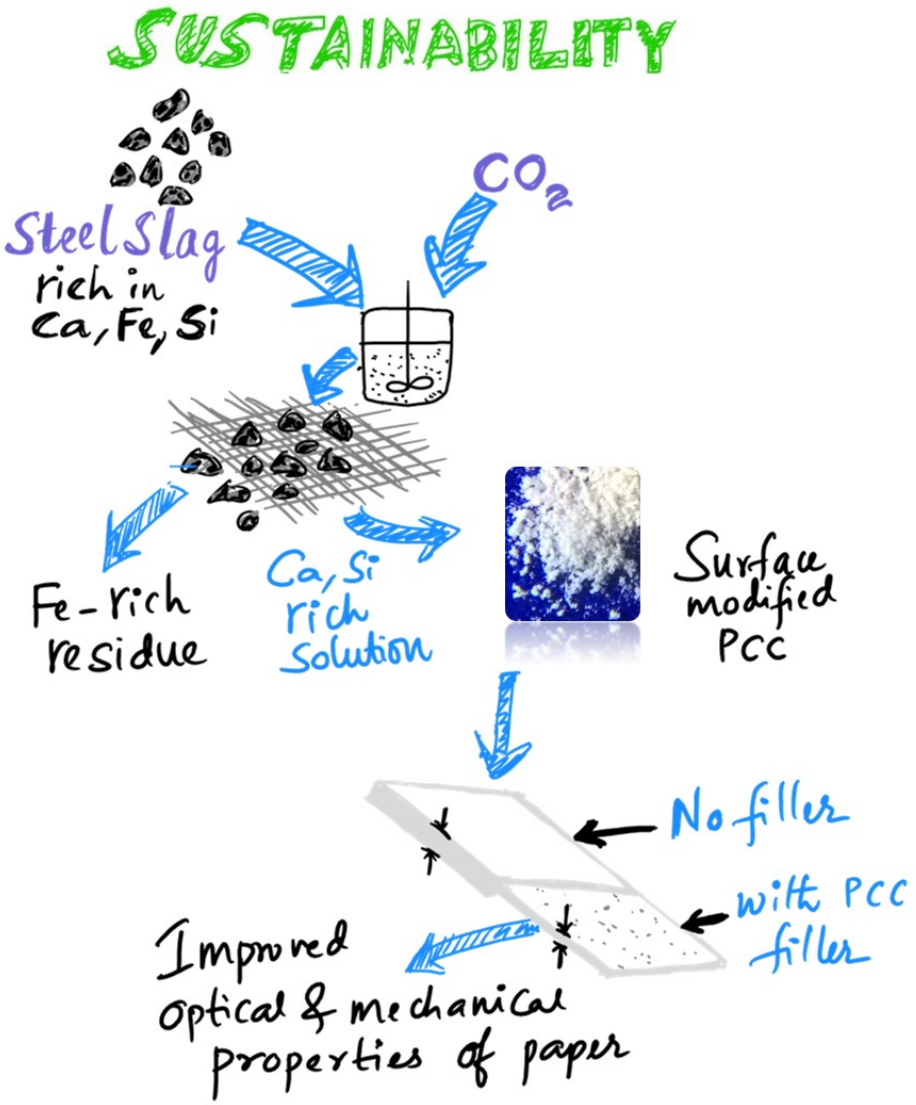

Figure 8.1: Waste utilisation, recycling, and less-resource consumption by mineral carbonation of steel slag demonstrating sustainability

PCC filler material produced from different route was shown to improve mechanical properties of paper without affecting its optical properties.

Existence of stable $CaCO_3$ supersaturation during pressure-swing carbonation which is fundamental to understanding the dissolution and precipitation process has been confirmed in this investigation. This suggests that maximum theoretical carbonation potential via pressure-swing carbonation is higher than previously suggested. Furthermore, it is hypothesised that rapid calcium dissolution and presence of monomeric silica may allow calcium dissolution until saturation of amorphous calcium carbonate (ACC). ACC is the amorphous polymorph of calcium carbonate whose solubility is two orders of magnitude higher than calcite. Achieving this step would open new avenues for development of PCC in variety of morphologies. In addition, high solubility reduces the water requirement for pressure-swing carbonation which was seen as a major drawback compared to other indirect processes where low pH dissolution is carried out.

Overall 57% of calcium in steel slag could be recovered as PCC during 120 minutes of dissolution under 12.5 bar CO_2 pressure, 25 °C, and liquid-to-solid ratio of 100 ml/g. These results demonstrate that higher recovery of calcium is possible at less severe conditions than proposed earlier. Further, it was observed that similar extents of dissolution were possible in the case of coarse and fine particles without any sign of surface passivation as has been speculated by many studies. In addition, the process allows recycling of Fe-enriched slag residue and production of thin paper with high mechanical strength paper using surface-modified PCC by reducing fibre content. As illustrated in Figure 8.1, the process can lead to sustainability by recycling, re-utilisation and less-resource consumption.

A parametric mathematical model was developed using characterisation data and leaching chemistry as *a priori* information to describe dissolution kinetics of complex aggregates such as steel slag. The influence of surface area evolution on Ca leaching characteristics was demonstrated experimentally and through simulations using sporulation model. The model predictions were closely matching with experimental observations and demonstrated that calcium leaching characteristics can be described by surface reaction and surface area evolution. The model can be extended to predict dissolution of heavy metals, which is necessary for environmental assessment, based on elemental mapping and understanding of dissolution congruency.

Future work would involve further investigations into CO_2 pressure-swing carbonation

with an aim to control the stability of calcium carbonate and silica supersaturation during dissolution step and produce composite silica-PCC from the leachate on similar line to sol-gel method. Another future objective is to extend the dissolution model to trace metal leaching (Cr, V etc.) and leachates that contain complexing ligands.

Appendices

Appendix A

Effect of particle size distribution on surface area evolution with conversion

Consider that the initial particle size distribution density of spherical particles is $P(D,0)$ and the rate of reduction of particle size due to leaching is $-R(D)$. The population balance of particles in the interval of D to $D+\Delta D$ leads to following equation (A.1),

$$\frac{\partial P(D,t)}{\partial t} = -\frac{\partial P(D,t)R(D)}{\partial D} \tag{A.1}$$

For any given proton activity $\{H^+\}$, $R(D)$ is given as,

$$\frac{\mathrm{d}m}{\mathrm{d}t} = \rho\frac{\pi D^2}{2}\frac{\mathrm{d}D}{\mathrm{d}t} = -k_{\mathrm{Ca}}\pi D^2\{H^+\} \tag{A.2}$$

$$R(D) = \frac{\mathrm{d}D}{\mathrm{d}t} = -\frac{2k_{\mathrm{Ca}}}{\rho}\{H^+\} \tag{A.3}$$

Surface area of the particles $S_A(t)$ can be estimated using,

$$S_A(t) = \int_0^{D_\infty} \pi D^2 P(D,t)dD \tag{A.4}$$

Conversion $X(t)$ is defined as,

$$X(t) = \frac{m_0 - m}{m_0} = 1 - \frac{V(t)}{V_0} = 1 - \frac{\int_0^{D_\infty} \pi D^3 P(D,t)dD}{\int_0^{D_\infty} \pi D^3 P(D,0)dD} \tag{A.5}$$

A numerical simulation of above population balance equation was carried out using

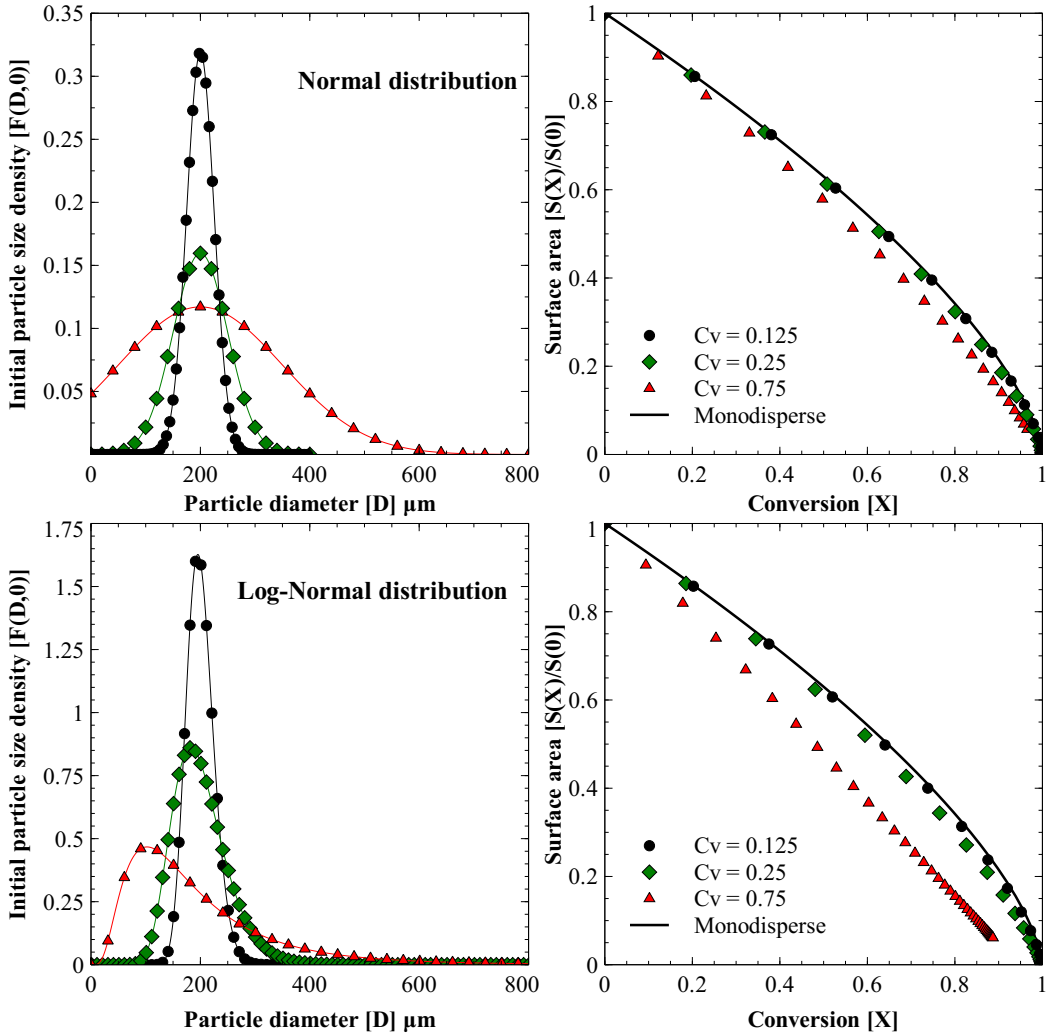

Figure A.1: Influence of particle size distribution on surface area evolution with conversion

two common distribution functions as initial condition (with arbitrary average diameter D_μ and varying Coefficient of variation C_V). Numerical results are shown in Figure A.1.

Normal distribution: $P(D,0) = \frac{1}{D_\sigma\sqrt{2\pi}} e^{-\frac{(D-D_{mu})^2}{2D_\sigma^2}}$

where, $D_\sigma = C_V \times D_\mu$

Log-normal distribution: $P(D,0) = \frac{1}{\ln D \times D_\sigma\sqrt{2\pi}} e^{-\frac{(\ln D-D_{mu})^2}{2D_\sigma^2}}$

The results shown in Figure A.1 suggest that surface area evolution of wide particle size distribution is better described by volumetric model, where surface area change is proportional to volume change (also conversion).

Appendix B

Slag aqueous Chemistry

B.1 Leaching reactions

$3\,CaO \cdot SiO_2 + 6\,H^+ \longrightarrow 3\,Ca^{+2} + H_4SiO_4 + H_2O$

$2\,CaO \cdot SiO_2 + 4\,H^+ \longrightarrow 2\,Ca^{+2} + H_4SiO_4$

$xFeO \cdot yMgO + 2\,(x+y)H^+ \longrightarrow xFe^{+2} + yMg^{+2} + (x+y)H_2O$

B.2 Oxidation reaction

$Fe^{+2} + \frac{1}{4}\,O_2 + \frac{5}{2}\,H_2O \longrightarrow Fe(OH)_3 + 2\,H^+$

B.3 Speciation reactions

$H^+ + OH^- \xleftrightarrow{K_w} H_2O \;\; K_w = 10^{-14}$

$Fe^{+3} + OH^- \xleftrightarrow{K_{eq}} Fe(OH)^{+2} \;\; K_{eq} = 10^{11.30}$

$Fe(OH)^{+2} + OH^- \xleftrightarrow{K_{eq}} Fe(OH)_2{}^{+} \;\; K_{eq} = 10^{9.965}$

$Fe(OH)_2{}^{+} + OH^- \xleftrightarrow{K_{eq}} Fe(OH)_3 \;\; K_{eq} = 10^{6.808}$

$Fe(OH)_3 \xleftrightarrow{K_{sp}} FeOOH_{ppt} \;\; K_{sp} = 10^{-13.581}$

LogK values for Fe(III) speciation were taken from Hydra database(Puigdomenech, 2004).

B.4 In CO_2 environment

$CO_2(gas) \xleftrightarrow{k_H} CO_2(aq) \;\; k_H = 0.035 \times e^{2400\times(\frac{1}{T}-\frac{1}{298.15})}$mol/L/bar (Sander, 2015)

$CO_2(aq)\cdot + H_2O \overset{K_{a1,app}}{\rightleftharpoons} HCO_3^- + H^+$ $K_{a1,app} = 4.448 \times 10^{-7}$ estimated from Plummer and Busenberg (1982)

$HCO_3 \overset{K_{a2}}{\rightleftharpoons} CO_3^{-2} + H^+$ $K_{a2} = 4.69 \times 10^{-11}$ estimated from (Plummer and Busenberg, 1982)

B.5 $CaCO_3$ precipitation

$Ca^{+2} + CO_3^{-2} \overset{K_{sp}}{\longleftrightarrow} CaCO_3$

$K_{\text{sp, calcite}} = 3.90\times10^{-09}$; $K_{\text{sp, aragonite}} = 4.61\times10^{-09}$; $K_{\text{sp, vaterite}} = 1.22\times10^{-08}$; $K_{\text{sp, amorphous}} = 4.00 \times 10^{-07}$ (Brečević and Nielsen, 1989)

† All the equilibrium constants are at 25°C.

References

P. Aagaard and H. C. Helgeson. Thermodynamic and kinetic constraints on reaction rates among minerals and aqueous solutions. I. Theoretical considerations., 1982. ISSN 00029599.

Yoshinobu Abe, Atsushi Iizuka, Hiroki Nagasawa, Akihiro Yamasaki, and Yukio Yanagisawa. Dissolution rates of alkaline rocks by carbonic acid: Influence of solid/liquid ratio, temperature, and CO_2 pressure. *Chemical Engineering Research and Design*, 91(5):933–941, 2013. ISSN 02638762.

Alessandra Adrover, Antonio Velardo, Massimiliano Giona, Stefano Cerbelli, Francesca Pagnanelli, and Luigi Toro. Structural modelling for the dissolution of non-porous ores: Dissolution with sporulation. *Chemical Engineering Journal*, 99(2):89–104, 2004. ISSN 13858947.

M Andreani, L Luquot, P Gouze, M Godard, E Hoisé, and B Gibert. Experimental Study of Carbon Sequestration Reactions Controlled by the Percolation of CO_2-Rich Brine through Peridotites. *Environmental Science & Technology*, 43(4):1226–1231, feb 2009. ISSN 0013-936X.

Paris K. Araizi, Colin D. Hills, Alan Maries, Peter J. Gunning, and David S. Wray. Enhancement of accelerated carbonation of alkaline waste residues by ultrasound. *Waste Management*, 2016. ISSN 0956053X.

Alan W. Armour and D.R. Robitaille. Corrosion inhibition by sodium molybdate. *Journal of Chemical Technology Biotechnology*, 29(1):619–628, 1979. ISSN 00225088.

David Avnir, Dina Farin, and Peter Pfeifer. Surface geometric irregularity of particulate materials: The fractal approach. *Journal of Colloid And Interface Science*, 103(1):112–123, 1985. ISSN 00219797.

R Baciocchi, G Costa, M Di Gianfilippo, A Polettini, R Pomi, A Stramazzo, M Di Gianfilippo, A Polettini, R Pomi, and A Stramazzo. Thin-film versus slurry-phase carbonation of steel slag: CO_2 uptake and effects on mineralogy. *Journal of Hazardous Materials*, 283:302–313, feb 2015. ISSN 1873-3336.

Renato Baciocchi, Alessandra Polettini, Raffaella Pomi, Valentina Prigiobbe, Viktoria Nikulshina Von Zedwitz, and Aldo Steinfeld. CO_2 sequestration by direct gas-solid carbonation of air pollution control (APC) residues. *Energy and Fuels*, 20(5):1933–1940, 2006. ISSN 08870624.

Renato Baciocchi, Giulia Costa, Alessandra Polettini, and Raffaella Pomi. Influence of particle size on the carbonation of stainless steel slag for CO_2 storage. *Energy Procedia*, 1(1):4859–4866, 2009. ISSN 1876-6102.

Renato Baciocchi, Giulia Costa, Elisabetta Di, Bartolomeo Alessandra, and E Di Bartolomeo. Carbonation of Stainless Steel Slag as a Process for CO_2 Storage and Slag Valorization. pages 467–477, 2010.

Renato Baciocchi, Giulia Costa, and E Di Bartolomeo. Wet versus slurry carbonation of EAF steel slag. *Greenhouse Gases: Science and Technology*, pages 312–319, 2011. ISSN 21523878.

Jerzy Baldyga, Marek Henczka, and Katarzyna Sokolnicka. Mineral carbonation accelerated by dicarboxylic acids as a disposal process of carbon dioxide. *Chemical Engineering Research and Design*, 89(9):1841–1854, sep 2011. ISSN 02638762.

Weijun Bao, Huiquan Li, and Yi Zhang. Selective leaching of steelmaking slag for indirect CO_2 mineral sequestration. *Ind. Eng. Chem. Res.*, 49(5):2055–2063, mar 2010.

Hamdallah Béarat, Michael J McKelvy, Andrew V G Chizmeshya, Deirdre Gormley, Ryan Nunez, R W Carpenter, Kyle Squires, and George H Wolf. Carbon sequestration via aqueous olivine mineral carbonation: role of passivating layer formation. *Environmental science & technology*, 40(15):4802–8, aug 2006. ISSN 0013-936X.

David J. Belton, Olivier Deschaume, and Carole C. Perry. An overview of the fundamentals of the chemistry of silica with relevance to biosilicification and technological advances. *FEBS Journal*, 279 (10):1710–1720, 2012. ISSN 1742464X.

S. K. Bhatia and D. D. Perlmutter. Effect of the product layer on the kinetics of the CO_2-lime reaction. *AIChE Journal*, 29(1):79–86, 1983. ISSN 0001-1541.

Muhammet Bilen, Mahmut Altiner, and Mehmet Yildirim. Evaluation of steelmaking slag for CO_2 fixation by leaching-carbonation process. *Particulate Science and Technology*, 36(3):1–10, 2017. ISSN 15480046.

Alex Blum and Antonio Lasaga. Role of surface speciation in the low-temperature dissoltion of minerals. *Nature*, 331(4):431–433, 1988. ISSN 0028-0836.

F. Bodénan, F. Bourgeois, C. Petiot, T. Augé, B. Bonfils, C. Julcour-Lebigue, F. Guyot, a. Boukary, J. Tremosa, a. Lassin, E. C. Gaucher, and P. Chiquet. Ex situ mineral carbonation for CO_2 mitigation: Evaluation of mining waste resources, aqueous carbonation processability and life cycle assessment (Carmex project). *Minerals Engineering*, 59:52–63, 2014. ISSN 08926875.

Marius Bodor, Rafael M. Santos, Lubica Kriskova, Jan Elsen, Maria Vlad, and Tom Van Gerven. Susceptibility of mineral phases of steel slags towards carbonation: mineralogical, morphological and chemical assessment. *European Journal of Mineralogy*, 25(4):533–549, aug 2013. ISSN 09351221.

Danielle Bonenfant, Lynda Kharoune, Robert Hausler, Patrick Niquette, Sébastien Sauvé, Robert Hausler, Patrick Niquette, Murielle Mimeault, and Mourad Kharoune. CO_2 Sequestration Potential of Steel Slags at Ambient Pressure and Temperature. *Industrial and Engineering Chemistry Research*, 47(20):7610–7616, oct 2008. ISSN 0888-5885.

Benjamin Bonfils, Florent Bourgeois, Carine Julcour, François Guyot, and Pierre Chiquet. Understanding the chemistry of direct aqueous carbonation with additives through geochemical modelling. *Energy Procedia*, 4:3809–3816, 2011. ISSN 18766102.

Benjamin Bonfils, Carine Julcour-Lebigue, François Guyot, Françoise Bodénan, Pierre Chiquet, and Florent Bourgeois. Comprehensive analysis of direct aqueous mineral carbonation using dissolution enhancing organic additives. *International Journal of Greenhouse Gas Control*, 9:334–346, jul 2012. ISSN 17505836.

Paulo H R Borges, Juliana O. Costa, Neil B. Milestone, Cyril J. Lynsdale, and Roger E. Streatfield. Carbonation of CH and C-S-H in composite cement pastes containing high amounts of BFS. *Cement and Concrete Research*, 40(2):284–292, 2010. ISSN 00088846.

Susan L. Brantley. *Kinetics of Water-rock interaction*. 2008. ISBN 9780387735627.

Ljerka Brečević and Arne Erik Nielsen. Solubility of amorphous calcium carbonate. *Journal of Crystal Growth*, 98(3):504–510, 1989. ISSN 00220248.

Gordon E Brown, Thomas P. Trainor, and Anne M Chaka. Geochemistry of mineral surfaces and factors affecting their chemical reactivity. In *Chemical Bonding at Surfaces and Interfaces*. 2008. ISBN 9780444528377.

Anne Carpenter. CO_2 abatement in the iron and steel industry. 2012.

Susan A. Carroll-Webb and John V. Walther. A surface complex reaction model for the pH-dependence of corundum and kaolinite dissolution rates. *Geochimica et Cosmochimica Acta*, 52(11):2609–2623, 1988. ISSN 00167037.

William H Casey. On the relative dissolution rates of some oxide and orthosilicate minerals. *Journal of Colloid and Interface Science*, 146(2):586–589, 1991. ISSN 00219797.

William H. Casey and Henry R. Westrich. Control of dissolution rates of orthosilicate minerals by divalent metal-oxygen bonds. *Nature*, 355:472–475, 1992. ISSN 0028-0836.

William H. Casey, Henry R. Westrich, Jillian F. Banfield, Giulio Ferruzzi, and Geroge W. Arnold. Leaching and reconstruction at the surfaces of dissolving chain-silicate minerals. *Nature*, 366(6452): 253–256, 1993. ISSN 0028-0836.

William H WH Casey and Garrison Sposito. On the temperature dependence of mineral dissolution rates. *Geochimica et Cosmochimica Acta*, 56(10):3825–3830, 1992.

S H Chan. A Review on solubility and polymerization of silica. *Geothermics*, 18(1):49–56, 1989.

S. Chand, B. Paul, and M. Kumar. Sustainable Approaches for LD Slag Waste Management in Steel Industries: A Review. *Metallurgist*, 60(1-2):116–128, 2016. ISSN 15738892.

E-E Chang, Shu-Yuan Pan, Yi-Hung Chen, Hsiao-Wen Chu, Chu-Fang Wang, and Pen-Chi Chiang. CO_2 sequestration by carbonation of steelmaking slags in an autoclave reactor. *Journal of hazardous materials*, 195:107–14, nov 2011a. ISSN 1873-3336.

E. E. Chang, Shu Yuan Pan, Yi Hung Chen, Chung Sung Tan, and Pen Chi Chiang. Accelerated carbonation of steelmaking slags in a high-gravity rotating packed bed. *Journal of Hazardous Materials*, 227-228:97–106, 2012. ISSN 03043894.

E-E E.-E. Chang, Chung-Hua Chen, Yi-Hung Chen, Shu-Yuan Pan, and Pen-Chi Chiang. Performance evaluation for carbonation of steel-making slags in a slurry reactor. *Journal of hazardous materials*, 186(1):558–64, feb 2011b. ISSN 1873-3336.

Tao Chen, Anne Neville, and Mingdong Yuan. Influence of Mg^{2+} on $CaCO_3$ formation-bulk precipitation and surface deposition. *Chemical Engineering Science*, 61(16):5318–5327, 2006a. ISSN 00092509.

Zhong-Ying Chen, William K. O'Connor, S.J. J Gerdemann, William K O Connor, and S.J. J Gerdemann. Chemistry of aqueous mineral carbonation for carbon sequestration and explanation of experimental results. *Environmental Progress*, 25(2):161–166, jul 2006b. ISSN 0278-4491.

Yi Wai Chiang, Rafael M. Santos, Jan Elsen, Boudewijn Meesschaert, Johan A. Martens, and Tom Van Gerven. Towards zero-waste mineral carbon sequestration via two-way valorization of ironmaking slag. *Chemical Engineering Journal*, 249:260–269, aug 2014. ISSN 13858947.

E. Chibowski, L. Hotysz, and A. Szcześ. Time dependent changes in zeta potential of freshly precipitated calcium carbonate. *Colloids and Surfaces A: Physicochemical and Engineering Aspects*, 222(1-3):41–54, 2003. ISSN 09277757.

Lei Chou and Roland Wollast. Study of the weathering of albite at room temperature and pressure with a fluidized bed reactor. *Geochimica et Cosmochimica Acta*, 48(11):2205–2217, nov 1984. ISSN 00167037.

John R. Clarkson, Timothy J. Price, and Christopher J. Adams. Role of metastable phases in the spontaneous precipitation of calcium carbonate. *Journal of the Chemical Society, Faraday Transactions*, 88(2):243, 1992. ISSN 0956-5000.

Christine F. Conrad, Gary A. Icopini, Hideaki Yasuhara, Joel Z. Bandstra, Susan L. Brantley, and Peter J. Heaney. Modeling the kinetics of silica nanocolloid formation and precipitation in geologically relevant aqueous solutions. *Geochimica et Cosmochimica Acta*, 71(3):531–542, 2007. ISSN 00167037.

David A Crerar, Ellen V Axtmann, and Robert C Axtmann. Growth and ripening of silica polymers in aqueous solutions. 1981.

F.K. K Crundwell. The mechanism of dissolution of minerals in acidic and alkaline solutions: Part I — A new theory of non-oxidation dissolution. *Hydrometallurgy*, 149:252–264, oct 2014. ISSN 0304386X.

B. Das, S. Prakash, P.S.R. S R Reddy, and V.N. N Misra. An overview of utilization of slag and sludge from steel industries. *Resources, Conservation and Recycling*, 50(1):40–57, mar 2007. ISSN 09213449.

Damien Daval, Isabelle Martinez, Jérôme Corvisier, Nathaniel Findling, Bruno Goffé, and François Guyot. Carbonation of Ca-bearing silicates, the case of wollastonite: Experimental investigations and kinetic modeling. *Chemical Geology*, 265(1–2):63–78, jul 2009a. ISSN 0009-2541.

Damien Daval, Isabelle Martinez, Jean Michel Guigner, Roland Hellmann, Jérôme Corvisier, Nathaniel Findling, Christian Dominici, Bruno Goffé, and François Guyot. Mechanism of wollastonite carbonation deduced from micro- To nanometer length scale observations. *American Mineralogist*, 94(11-12):1707–1726, 2009b. ISSN 0003004X.

Damien Daval, Olivier Sissmann, Nicolas Menguy, Giuseppe D Saldi, Francois Guyot, Isabelle Martinez, Jerome Corvisier, Bruno Garcia, Imene Machouk, Kevin G Knauss, and Roland Hellmann. Influence of amorphous silica layer formation on the dissolution rate of olivine at 90 °C and elevated pCO_2. *Chemical Geology*, 284(1-2):193–209, may 2011. ISSN 0009-2541.

Cecil Whitfield Davies and Theodore Shedlovsky. Ion association. *Journal of The Electrochemical Society*, 111(3):85C–86C, 1964.

P. C. de Carvalho Pinto, T. R. da Silva, F. M. Linhares, F. V. de Andrade, M. M. de Oliveira Carvalho, and G. M. de Lima. A integrated route for CO_2 capture in the steel industry and its conversion into $CaCO_3$ using fundamentals of Solvay process. *Clean Technologies and Environmental Policy*, 2016. ISSN 1618-954X.

R. Dippenaar. Industrial uses of slag (the use and re-use of iron and steelmaking slags). *Ironmaking & Steelmaking*, 32(1):35–46, 2005. ISSN 0301-9233.

Suvasis Dixit and Susan A Carroll. Effect of solution saturation state and temperature on diopside dissolution. *Geochemical transactions*, 8(1):3, jan 2007. ISSN 1467-4866.

Frédéric J. Doucet. Effective CO_2-specific sequestration capacity of steel slags and variability in their leaching behaviour in view of industrial mineral carbonation. *Minerals Engineering*, 23(3):262–269, feb 2010. ISSN 08926875.

Marco Dri, Aimaro Sanna, and M. Mercedes Maroto-Valer. Dissolution of steel slag and recycled concrete aggregate in ammonium bisulphate for CO_2 mineral carbonation. *Fuel Processing Technology*, 113: 114–122, sep 2013. ISSN 03783820.

Marco Dri, Aimaro Sanna, and M. Mercedes Maroto-Valer. Mineral carbonation from metal wastes: Effect of solid to liquid ratio on the efficiency and characterization of carbonated products. *Applied Energy*, 113:515–523, jan 2014. ISSN 03062619.

Thosmas R. Dulski. *A Manual for the Chemical Analysis of Metals*. ASTM International, 100 Barr Harbor Drive, PO Box C700, West Conshohocken, PA 19428-2959, mnl25-eb edition, mar 1996. ISBN 978-0-8031-2066-2.

Espen Eikeland, Anders Bank Blichfeld, Christoffer Tyrsted, Anca Jensen, and Bo Brummerstedt Iversen. Optimized Carbonation of Magnesium Silicate Mineral for CO_2 Storage. *ACS Applied Materials & Interfaces*, 7(9):5258–5264, feb 2015. ISSN 19448244.

Sanni Eloneva, Sebastian Teir, Justin Salminen, Carl-Johan Fogelholm, and Ron Zevenhoven. Fixation of CO_2 by carbonating calcium derived from blast furnace slag. *Energy*, 33(9):1461–1467, sep 2008a. ISSN 03605442.

Sanni Eloneva, Sebastian Teir, Justin Salminen, Carl-Johan Johan Fogelholm, and Ron Zevenhoven. Steel converter slag as a raw material for precipitation of pure calcium carbonate. *Industrial and Engineering Chemistry Research*, 47(18):7104–7111, sep 2008b. ISSN 08885885.

Sanni Eloneva, Sebastian Teir, Hannu Revitzer, Justin Salminen, Arshe Said, C J Fogelholm, and Ron Zevenhoven. Reduction of CO_2 Emissions from steel plants by using steelmaking slags for production of marketable calcium carbonate. *Steel Research International*, 80(6):415–421, 2009. ISSN 16113683.

Sanni Eloneva, Arshe Said, Carl-Johan Fogelholm, and Ron Zevenhoven. Preliminary assessment of a method utilizing carbon dioxide and steelmaking slags to produce precipitated calcium carbonate. *Applied Energy*, 90(1):329–334, feb 2012. ISSN 03062619.

Fredrik Engström, Margareta Lidström Larsson, Caisa Samuelsson, Åke Sandström, Ryan Robinson, and Bo Björkman. Leaching Behavior of Aged Steel Slags. *steel research int.*, 85(4):607–615, sep 2013. ISSN 16113683.

Alena Fedoročková and Pavel Raschman. Effects of pH and acid anions on the dissolution kinetics of MgO. *Chemical Engineering Journal*, 143(1-3):265–272, 2008. ISSN 13858947.

M Fernández Bertos, X Li, S J R Simons, C D Hills, and P J Carey. Investigation of accelerated carbonation for the stabilisation of MSW incinerator ashes and the sequestration of CO_2. *Green Chemistry*, 6(8):428–436, 2004a. ISSN 1463-9262.

M. Fernández Bertos, S. J R Simons, C. D. Hills, and P. J. Carey. A review of accelerated carbonation technology in the treatment of cement-based materials and sequestration of CO_2. *Journal of Hazardous Materials*, 112(3):193–205, 2004b. ISSN 03043894.

N. H. Fletcher and N. J. Welham. Enhanced dissolution following extended milling. *AIChE Journal*, 46 (3):666–669, 2000. ISSN 00011541.

Gerhard Furrer and Werner Stumm. The coordination chemistry of weathering: I. Dissolution kinetics of δ-Al2O3 and BeO. *Geochimica et Cosmochimica Acta*, 50(9):1847–1860, sep 1986. ISSN 00167037.

Philip K Gbor and Charles Q Jia. Critical evaluation of coupling particle size distribution with the shrinking core model. *Chemical Engineering Science*, 59(10):1979–1987, may 2004. ISSN 00092509.

S. J. Gerdemann, D. C. Dahlin, and W. K. O'Connor. Carbon Dioxide Sequestration by Aqueous Mineral Carbonation of Magnesium Silicate Minerals. *Proceedings of the Sixth International Conference on Greenhouse Gas Control Technologies, October 1-4, Kyoto, Japan*, I:677–682, 2003.

Stephen J. Gerdemann, William K. O'Connor, David C. Dahlin, Larry R. Penner, and Hank Rush. Ex Situ Aqueous Mineral Carbonation. *Environmental Science & Technology*, 41(7):2587–2593, apr 2007. ISSN 0013-936X.

Alia Ben Ghacham, Louis-césar Pasquier, Emmanuelle Cecchi, Jean-françois Blais, and Guy Mercier. CO_2 sequestration by mineral carbonation of steel slags under ambient temperature : parameters influence , and optimization. *Environmental Science and Pollution Research*, 2016. ISSN 0944-1344.

Manisha Ghoorah, Bogdan Z. Dlugogorski, Reydick D. Balucan, and Eric M. Kennedy. Selection of acid for weak acid processing of wollastonite for mineralisation of CO_2. *Fuel*, 122:277–286, 2014a. ISSN 00162361.

Manisha Ghoorah, Bogdan Z. Dlugogorski, Hans C. Oskierski, and Eric M. Kennedy. Study of thermally conditioned and weak acid-treated serpentinites for mineralisation of carbon dioxide. *Minerals Engineering*, 59:17–30, may 2014b. ISSN 08926875.

Chinmay Ghoroi and A. K. Suresh. Intermediate conversion kinetics in ticalcium aluminate formation. *AIChE Journal*, 53(9):2399–2410, sep 2007. ISSN 00011541.

R.A. Gill. Applications of Wet-End Paper Chemistry. In Che On Au and Ian Thorn, editors, *Paper Chemistry*, chapter Fillers, pages 1–8. Springer Netherlands, Dordrecht, 1 edition, 1995. ISBN 978-94-017-0758-9. doi: 10.1007/978-94-017-0756-5. URL `http://advances.sciencemag.org/lookup/doi/10.1126/sciadv.1602285http://link.springer.com/10.1007/978-94-017-0756-5`.

Elizabeth A. Gorrepati, Pattanapong Wongthahan, Sasanka Raha, and H. Scott Fogler. Silica precipitation in acidic solutions: Mechanism, pH effect, and salt effect. *Langmuir*, 26(13):10467–10474, 2010. ISSN 07437463.

Peter J Gunning, Colin D Hills, and Paula J Carey. Accelerated carbonation treatment of industrial wastes. *Waste management (New York, N.Y.)*, 30(6):1081–90, jun 2010. ISSN 1879-2456.

Jianlong Guo, Yanping Bao, and Min Wang. Steel slag in China: Treatment, recycling, and management. *Waste Management*, 78:318–330, 2018. ISSN 18792456.

C. Hall, D.J. Large, B. Adderley, and H.M. West. Calcium leaching from waste steelmaking slag: Significance of leachate chemistry and effects on slag grain mineralogy. *Minerals Engineering*, 65: 156–162, oct 2014. ISSN 08926875.

Du Re Han, Hueon Namkung, Ha Min Lee, Dae Gee Huh, and Hyung Taek Kim. CO_2 sequestration by aqueous mineral carbonation of limestone in a supercritical reactor. *Journal of Industrial and Engineering Chemistry*, 21:792–796, 2014. ISSN 1226086X.

Kim F Hayes, George Redden, Wendell Ela, and James O Leckie. Surface complexation models: An evaluation of model parameter estimation using FITEQL and oxide mineral titration data. *Journal of Colloid and Interface Science*, 142(2):448–469, mar 1991. ISSN 00219797.

Harold C. Helgeson. Kinetics of mass transfer among silicates and aqueous solutions. *Geochimica et Cosmochimica Acta*, 35(5):421–469, 1971. ISSN 00167037.

Harold C Helgeson, William M. Murphy, and Per Aagaard. Thermodynamic and kinetic constraints on reaction rates among minerals and aqueous solutions. II. Rate constants, effective surface area, and the hydrolysis of feldspar. *Geochimica et Cosmochimica Acta*, 48(12):2405–2432, 1984. ISSN 00167037.

HC Helgeson and WM Murphy. Calculation of mass transfer among minerals and aqueous solutions as a function of time and surface area in geochemical processes. I. Computational approach. *Mathematical Geology*, 15(1):19–30, 1983.

Roland Hellmann, Richard Wirth, Damien Daval, Jean-paul Barnes, Jean-michel Penisson, Delphine Tisserand, Thierry Epicier, Brigitte Florin, and Richard L Hervig. Unifying natural and laboratory chemical weathering with interfacial dissolution – reprecipitation : A study based on the nanometer-scale chemistry of fl uid – silicate interfaces. *Chemical Geology*, 294-295:203–216, 2012. ISSN 0009-2541.

George R. Holdren and Robert A. Berner. Mechanism of feldspar weathering-I. Experimental studies. *Geochimica et Cosmochimica Acta*, 43(8):1161–1171, 1979. ISSN 00167037.

George R. Holdren and Patricia M. Speyer. Reaction rate-surface area relationships during the early stages of weathering-I. Initial observations. *Geochimica et Cosmochimica Acta*, 49(3):675–681, 1985. ISSN 00167037.

Yong H. Huang, Cilai Tang, and Hui Zeng. Removing molybdate from water using a hybridized zero-valent iron/magnetite/Fe(II) treatment system. *Chemical Engineering Journal*, 200-202:257–263, 2012. ISSN 13858947.

WJJ Wouter J J Huijgen and RNJ Rob N J Comans. Carbonation of steel slag for CO_2 sequestration: leaching of products and reaction mechanisms. *Environmental science & technology*, 40(8):2790–2796, apr 2006. ISSN 0013936X.

Wouter J. J. Huijgen, Geert-Jan Witkamp, and Rob N. J. Comans. Mineral CO_2 Sequestration by Steel Slag Carbonation. *Environmental science & technology*, 39(24):9676–9682, dec 2005. ISSN 0013-936X.

Wouter J.J. Huijgen, Geert-Jan Witkamp, and Rob N.J. Comans. Mechanisms of aqueous wollastonite carbonation as a possible CO_2 sequestration process. *Chemical Engineering Science*, 61(13):4242–4251, jul 2006. ISSN 00092509.

Deborah N. Huntzinger, John S. Gierke, S. Komar Kawatra, Timothy C. Eisele, and Lawrence L. Sutter. Carbon Dioxide Sequestration in Cement Kiln Dust through Mineral Carbonation. *Environmental Science & Technology*, 43(6):1986–1992, mar 2009. ISSN 0013-936X.

Atsushi Iizuka, Minoru Fujii, Akihiro Yamasaki, and Yukio Yanagisawa. Development of a New CO_2 Sequestration Process Utilizing the Carbonation of Waste Cement. *Industrial & Engineering Chemistry Research*, 43(24):7880–7887, nov 2004. ISSN 0888-5885.

Atsushi Iizuka, Yuka Sakai, Akihiro Yamasaki, Masato Honma, Yasuyuki Hayakawa, and Yukio Yanagisawa. Bench-scale operation of a concrete sludge recycling plant. *Industrial and Engineering Chemistry Research*, 51(17):6099–6104, 2012. ISSN 08885885.

Ralph K. Iler. Coagulation of colloidal silica by calcium ions, mechanism, and effect of particle size. *Journal of Colloid And Interface Science*, 53(3):476–488, 1975. ISSN 00219797.

Karalee Jarvis, R. W. Carpenter, Todd Windman, Youngchul Kim, Ryan Nunez, and Firas Alawneh. Reaction Mechanisms for Enhancing Mineral Sequestration of CO_2. *Environmental Science & Technology*, 43(16):6314–6319, aug 2009. ISSN 0013-936X.

Karalee Ann Jarvis. *Reaction mechanisms for enhancing carbon dioxide mineral sequestration.* PhD thesis, 2008.

Hwanju Jo, Ho Young Jo, and Young Nam Jang. Effect of extraction solutions on carbonation of cementitious materials in aqueous solutions. *Environmental Technology (United Kingdom)*, 33(12): 1391–1401, 2012. ISSN 09593330.

Hwanju Jo, So-Hee Park, Young-Nam Jang, Soo-Chun Chae, Pyeong-Koo Lee, and Ho Young Jo. Metal extraction and indirect mineral carbonation of waste cement material using ammonium salt solutions. *Chemical Engineering Journal*, 254:313–323, oct 2014. ISSN 13858947.

Carine Julcour, Florent Bourgeois, Benjamin Bonfils, Imane Benhamed, François Guyot, Françoise Bodénan, Charlotte Petiot, and Éric C Gaucher. Development of an attrition-leaching hybrid process for direct aqueous mineral carbonation. *Chemical Engineering Journal*, 262(0):716–726, feb 2015. ISSN 1385-8947.

M Kakizawa, A Yamasaki, and Y Yanagisawa. A new CO_2 disposal process via artificial weathering of calcium silicate accelerated by acetic acid. *Energy*, 26(4):341–354, apr 2001.

A.M. Kalinkin, E. V. Kalinkina, O. A. Zalkind, and T. I. Makarova. Chemical interaction of Calcium Oxide and Calcium Hydroxide with CO_2 during Mechanical Activation. *Journal of the American Ceramic Society*, 41(10):1073–1079, dec 2005. ISSN 00027820.

Yasuro Katsuyama, Akihiro Yamasaki, Atsushi Iizuka, Minoru Fujii, Kazukiyo Kumagai, and Yukio Yanagisawa. Development of a process for producing high-purity calcium carbonate ($CaCO_3$) from waste cement using pressurized CO_2. *Environmental Progress*, 24(2):162–170, 2005. ISSN 02784491.

Matthias Kellermeier, Fabian Glaab, Regina Klein, Emilio Melero-García, Werner Kunz, and Juan Manuel García-Ruiz. The effect of silica on polymorphic precipitation of calcium carbonate: an on-line energy-dispersive X-ray diffraction (EDXRD) study. *Nanoscale*, 5(15):7054, 2013. ISSN 2040-3364.

Yasushi Kitano, Minoru Okumura, and Masatoshi Idogaki. Behavior of dissolved silica in parent solution at the formation of calcium carbonate. *GEOCHEMICAL JOURNAL*, 13(6):253–260, 1979. ISSN 0016-7002.

W. E. Kline and H. S. Fogler. Dissolution kinetics: Catalysis by strong acids. *Journal of Colloid And Interface Science*, 82(1):93–102, 1981. ISSN 00219797.

Ming-Sheng Ko, Ying-Liang Chen, and Jhih-Hua Jiang. Accelerated carbonation of basic oxygen furnace slag and the effects on its mechanical properties. *Construction and Building Materials*, 98:286–293, 2015. ISSN 09500618.

S Kodama, T Nishimoto, N Yamamoto, K Yogo, and K Yamada. Development of a new pH-swing CO_2 mineralization process with a recyclable reaction solution. *Energy*, 33(5):776–784, may 2008. ISSN 03605442.

T Kojima, A Nagamine, N Ueno, and S Uemiya. Absorption and fixation of carbon dioxide by rock weathering. *Energy Conversion and Management*, 38, Supple(0):S461–S466, 1997. ISSN 01968904.

Samuel C Krevor and Klaus S Lackner. Enhancing process kinetics for mineral carbon sequestration. *Energy Procedia*, 1(1):4867–4871, feb 2009.

Klaus S Lackner. A Guide to CO_2 Sequestration. *Sience*, 300(2):1677–1678, 2003. ISSN 1095-9203.

Klaus S. Lackner, Christopher H. Wendt, Darryl P. Butt, Edward L. Joyce, and David H. Sharp. Carbon dioxide disposal in carbonate minerals. *Energy*, 20(11):1153–1170, jan 1995. ISSN 03605442.

Klaus S Lackner, Darryl P Butt, and Christopher H Wendt. Progress on binding CO_2 in mineral substrates. *Energy Conversion and Management*, 38:S259–S264, 1997. ISSN 01968904.

L. Z. Lakshtanov and S. L S Stipp. Interaction between dissolved silica and calcium carbonate: 1. Spontaneous precipitation of calcium carbonate in the presence of dissolved silica. *Geochimica et Cosmochimica Acta*, 74(9):2655–2664, 2010. ISSN 00167037.

K. Larsen, K. Bechgaard, and S. L S Stipp. The effect of the Ca^{2+} to CO_3^{2-} activity ratio on spiral growth at the calcite $\{1\ 0\ \overline{1}\ 4\}$ surface. *Geochimica et Cosmochimica Acta*, 74(7):2099–2109, 2010. ISSN 00167037.

Antonio C Lasaga, Josep M Soler, Jiwchar Ganor, Timothy E Burch, and Kathryn L Nagy. Chemical weathering rate laws and global geochemical cycles. *Geochimica et Cosmochimica Acta*, 58(10):2361–2386, 1994.

S. E. Leblanc and H. S. Fogler. Population balance modeling of the dissolution of polydisperse solids: Rate limiting regimes. *AIChE Journal*, 33(1):54–63, 1987. ISSN 15475905.

Seong-Ho Lee, Joobeom Seo, Kwang-Suk You, Thenepalli Thriveni, and Ji-Whan Ahn. Synthesis of calcium carbonate powder from air-cooled blast furnace slag under pressurized CO_2 atmosphere. *Geosystem Engineering*, 15(4):292–298, 2012. ISSN 1226-9328.

S.N. N Lekakh, C.H. H Rawlins, D.G.C. G C Robertson, V.L. L Richards, and K.D. D Peaslee. Kinetics of Aqueous Leaching and Carbonization of Steelmaking Slag. *Metallurgical and Materials Transactions B*, 39(1):125–134, jan 2008a. ISSN 1073-5615.

S.N. N Lekakh, D.G.C. G C Robertson, C.H. H Rawlins, V.L. L Richards, and K.D. D Peaslee. Investigation of a Two-Stage Aqueous Reactor Design for Carbon Dioxide Sequestration Using Steelmaking Slag. *Metallurgical and Materials Transactions B*, 39(3):484–492, jun 2008b. ISSN 1073-5615.

KNona C. Liddell. Shrinking core models in hydrometallurgy: What students are not being told about the pseudo-steady approximation. *Hydrometallurgy*, 79(1-2):62–68, sep 2005. ISSN 0304386X.

Qi Liu and M. Mercedes Maroto-Valer. Investigation of the pH effect of a typical host rock and buffer solution on CO_2 sequestration in synthetic brines. *Fuel Processing Technology*, 91(10):1321–1329, oct 2010. ISSN 03783820.

Xuewu Liu and Frank J. Millero. The solubility of iron hydroxide in sodium chloride solutions. *Geochimica et Cosmochimica Acta*, 63(19-20):3487–3497, 1999. ISSN 00167037.

K. Lívanský. Effect of temperature and pH on absorption of carbon dioxide by a free level of mixed solutions of some buffers. *Folia Microbiologica*, 27(1):55–59, 1982. ISSN 00155632. doi: 10.1007/BF02883839.

Ana F. Lourenço, José A F Gamelas, Christin Zscherneck, and Paulo J. Ferreira. Evaluation of silica-coated PCC as new modified filler for papermaking. *Industrial and Engineering Chemistry Research*, 52(14):5095–5099, 2013. ISSN 08885885.

Mehrdad Mahoutian, Yixin Shao, Alfonso Mucci, and Benoit Fournier. Carbonation and hydration behavior of EAF and BOF steel slag binders. *Materials and Structures*, pages 3075–3085, 2014. ISSN 1359-5997.

L Marini. *Geological Sequestration of Carbon Dioxide - Thermodynamics, Kinetics, and Reaction Path Modeling*, volume 11 of *Developments in Geochemistry*. Elsevier, 2006. ISBN 9780444529503.

Hannu-Petteri Mattila, Inga Grigaliūnaitė, and Ron Zevenhoven. Chemical kinetics modeling and process parameter sensitivity for precipitated calcium carbonate production from steelmaking slags. *Chemical Engineering Journal*, 192:77–89, jun 2012. ISSN 13858947.

Michael J. McKelvy, Andrew V.G. Chizmeshya, Kyle Squires, Ray W Carpenter, and Hamdallah Béarat. A novel approach to mineral carbonation: enhancing carbonation while avoiding mineral pretreatment process cost. Technical Report 480, Arizona State University, 2006.

Govt. of India Ministry of Steel. National Steel Policy, 2017. URL `http://steel.nic.in/national-steel-policy-nsp-2017`.

Liwu Mo and Daman K. Panesar. Accelerated carbonation – A potential approach to sequester CO_2 in cement paste containing slag and reactive MgO. *Cement and Concrete Composites*, 43:69–77, oct 2013. ISSN 09589465.

G. Montes-Hernandez, R. Chiriac, F. Toche, and F. Renard. Gas-solid carbonation of Ca(OH)2 and CaO particles under non-isothermal and isothermal conditions by using a thermogravimetric analyzer: Implications for CO_2 capture. *International Journal of Greenhouse Gas Control*, 11:172–180, 2012. ISSN 17505836.

V. Morales-Flórez, A. Santos, A. Lemus, and L. Esquivias. Artificial weathering pools of calcium-rich industrial waste for CO_2 sequestration. *Chemical Engineering Journal*, 166(1):132–137, jan 2011. ISSN 13858947.

J Mulopo, M Mashego, and J N Zvimba. Recovery of calcium carbonate from steelmaking slag and utilization for acid mine drainage pre-treatment. *Water Science & Technology*, 65(12):2236, may 2012. ISSN 0273-1223.

Myoungwook Mun, Heechan Cho, and Jihoe Kwon. Study on Characteristics of Various Extractants for Mineral Carbonation of Industrial Wastes. *Journal of Environmental Chemical Engineering*, 2017. ISSN 22133437.

L. Nicoleau, A. Nonat, and D. Perrey. The di- and tricalcium silicate dissolutions. *Cement and Concrete Research*, 47:14–30, 2013. ISSN 00088846.

Irena Nikolić, Ana Drinčić, Dijana Djurović, Ljiljana Karanović, Vuk V. Radmilović, and Velimir R. Radmilović. Kinetics of electric arc furnace slag leaching in alkaline solutions. *Construction and Building Materials*, 108:1–9, 2016. ISSN 09500618.

V. Nikulshina, M. E. Gálvez, and A. Steinfeld. Kinetic analysis of the carbonation reactions for the capture of CO_2 from air via the $Ca(OH)_2$–$CaCO_3$–CaO solar thermochemical cycle. *Chemical Engineering Journal*, 129(1-3):75–83, 2007. ISSN 13858947.

Catherine Noiriel, Linda Luquot, Benoît Madé, Louis Raimbault, Philippe Gouze, and Jan van der Lee. Changes in reactive surface area during limestone dissolution: An experimental and modelling study. *Chemical Geology*, 262(3-4):353–363, 2009. ISSN 00092541.

W.K. O'Connor, D C Dahlin, D N Nilsen, R P Walters, and P C Turner. Carbon dioxide sequestration by direct aqueous mineral carbonation. In *25 th International Technical Conference on Coal Utilization & Fuel Systems, Coal Technology Association, Clear Water, FL*, 2001.

Eric H EH Oelkers. General kinetic description of multioxide silicate mineral and glass dissolution. *Geochimica et Cosmochimica Acta*, 65(21):3703–3719, 2001.

Takeshi Ogino, Toshio Suzuki, and Kiyoshi Sawada. The formation and transformation mechanism of calcium carbonate in water. *Geochimica et Cosmochimica Acta*, 51(10):2757–2767, 1987.

Amanda Albright Olsen and J. Donald Rimstidt. Oxalate-promoted forsterite dissolution at low pH. *Geochimica et Cosmochimica Acta*, 72(7):1758–1766, apr 2008. ISSN 00167037.

Kai Pan, Hui Quan Li, Chen Ye Wang, Wei Jun Bao, Ke Lin Huang, and Dan Kui Liao. Enhanced Steelmaking Slag Mineral Carbonation in Dilute Alkali Solution. *Advanced Materials Research*, 878: 244–253, jan 2014. ISSN 1662-8985.

Shu-Yuan Pan. CO_2 Capture by Accelerated Carbonation of Alkaline Wastes: A Review on Its Principles and Applications. *Aerosol and Air Quality Research*, pages 770–791, 2012. ISSN 16808584.

Shu-Yuan Pan, Pen-Chi Chiang, Yi-Hung Chen, Chun-Da Chen, Hsun-Yu Lin, and E-E E.-E. Chang. Systematic approach to determination of maximum achievable capture capacity via leaching and carbonation processes for alkaline steelmaking wastes in a rotating packed bed. *Environmental science & technology*, 47(23):13677–85, dec 2013. ISSN 1520-5851.

Shu-Yuan Pan, Hsing-Lu Liu, E.-E. Chang, Hyunook Kim, Yi-Hung Chen, and Pen-Chi Chiang. Multiple model approach to evaluation of accelerated carbonation for steelmaking slag in a slurry reactor. *Chemosphere*, 154:63–71, 2016. ISSN 00456535.

G. S. Pappas, P. Liatsi, I. A. Kartsonakis, I. Danilidis, and G. Kordas. Synthesis and characterization of new SiO_2-CaO hollow nanospheres by sol-gel method: Bioactivity of the new system. *Journal of Non-Crystalline Solids*, 354(2-9):755–760, 2008. ISSN 00223093.

Ah-Hyung Alissa Park and Liang-Shih Fan. mineral sequestration: physically activated dissolution of serpentine and pH swing process. *Chemical Engineering Science*, 59(22-23):5241–5247, nov 2004. ISSN 00092509.

Hyun Kyu Park, Myung Won Bae, Ik Hyun Nam, and Sun Geon Kim. Acid leaching of CaO–SiO_2 resources. *Journal of Industrial and Engineering Chemistry*, 19(2):633–639, 2013. ISSN 1226086X.

Larry Penner, William K O Connor, David C Dahlin, Steve Gerdemann, and Gilbert E Rush. Mineral Carbonation: Energy Costs of Pretreatment Options and Insights Gained from Flow Loop Reaction Studies Larry Penner, William K. O'Connor, David C. Dahlin, Steve Gerdemann, Gilbert E. Rush Albany Research Center, Office of Fossil Energy, US DOE. Technical report, 2004.

L N Plummer and E Busenberg. The solubilities of calcite, aragonite and vaterite in CO_2-H_2O solutions between 0 and 90 C, and an evaluation of the aqueous model for the system CaCO 3-CO_2-H .... *Geochimica et Cosmochimica Acta*, 46(6):1011–1040, 1982. URL `http://linkinghub.elsevier.com/retrieve/pii/0016703782900564{%}5Cnpapers3://publication/doi/10.1016/0016-7037(82)90056-4`.

A Polettini, R Pomi, and A Stramazzo. Carbon sequestration through accelerated carbonation of BOF slag : influence of particle size characteristics. *Chemical Engineering Journal*, 2016. ISSN 1385-8947.

Valentina Prigiobbe. *Mineral Carbonation for CO_2 storage*. PhD thesis, ETH Zurich, 2010.

Valentina Prigiobbe, Alessandra Polettini, and Renato Baciocchi. Gas-solid carbonation kinetics of Air Pollution Control residues for CO_2 storage. *Chemical Engineering Journal*, 148(2-3):270–278, 2009. ISSN 13858947.

Petr Ptáček, Magdaléna Nosková, Jiří Brandštetr, František Šoukal, and Tomáš Opravil. Dissolving behavior and calcium release from fibrous wollastonite in acetic acid solution. *Thermochimica Acta*, 498(1-2):54–60, 2010. ISSN 00406031.

Ignasi Puigdomenech. Hydra/medusa chemical equilibrium database and plotting software. *KTH Royal Institute of Technology*, 2004.

Katta J Reddy, Argyle Morris, A Viswatej, and DT Taylor. A novel method to capture and store flue gas carbon dioxide (CO_2): Accelerated mineral carbonation. *Climate Change: Global Risks, Challenges and Decisions*, 172021:8–10, 2009. ISSN 1755-1315.

Katta J Reddy, Hollis Weber, Pradip Bhattacharyya, Argyle Morris, David Taylor, Mikol Christensen, Thomas Foulke, and Paul Fahlsing. Instantaneous Capture and Mineralization of Flue Gas Carbon Dioxide: Pilot Scale Study. *Nature Precedings*, pages 1–11, 2010. ISSN 1756-0357.

M. M. Reddy and G. H. Nancollas. The crystallization of calcium carbonate. IV. The effect of magnesium, strontium and sulfate ions. *Journal of Crystal Growth*, 35(1):33–38, 1976. ISSN 00220248.

J. Rieger, T. Frechen, G. Cox, W. Heckmann, C. Schmidt, and J. Thieme. Precursor structures in the crystallization/precipitation processes of $CaCO_3$ and control of particle formation by polyelectrolytes. *Faraday Discussions*, 136:265, 2007. ISSN 1359-6640.

J Donald Rimstidt, Susan L Brantley, and Amanda A Olsen. Systematic review of forsterite dissolution rate data. *Geochimica et Cosmochimica Acta*, 99:159–178, 2012.

J. D. Rodriguez-Blanco, S. Shaw, P. Bots, T. Roncal-Herrero, and L. G. Benning. The role of pH and Mg on the stability and crystallization of amorphous calcium carbonate. *Journal of Alloys and Compounds*, 536(SUPPL.1):S477–S479, 2012. ISSN 09258388.

Vyacheslav Romanov, Yee Soong, Casey Carney, Gilbert E. Rush, Benjamin Nielsen, and William O'Connor. Mineralization of Carbon Dioxide: A Literature Review. *ChemBioEng Reviews*, (4):231–256, 2015. ISSN 21969744.

Encarnación Ruiz-Agudo, Christine V. Putnis, Carlos Rodriguez-Navarro, and Andrew Putnis. Mechanism of leached layer formation during chemical weathering of silicate minerals. *Geology*, 40 (10):947–950, aug 2012. ISSN 00917613.

Encarnación Ruiz-Agudo, Krzysztof Kudłacz, Christine V Putnis, Andrew Putnis, and Carlos Rodriguez-Navarro. Dissolution and carbonation of Portlandite [Ca(OH)2] single crystals. *Environmental science & technology*, 47(19):11342–9, oct 2013. ISSN 1520-5851.

V Runje and A Bezjak. Kinetic analysis of extraction of calcium silicates with methanolic solution of salicylic acid. I. Theoretical part. *Cement and Concrete Research*, 13(2):186–196, 1983. ISSN 00088846.

Arshe Said, Hannu-Petteri Mattila, Mika Järvinen, and Ron Zevenhoven. Production of precipitated calcium carbonate (PCC) from steelmaking slag for fixation of CO_2. *Applied Energy*, 112:765–771, dec 2013. ISSN 03062619.

Arshe Said, Olli Mattila, Sanni Eloneva, and Mika Järvinen. Enhancement of calcium dissolution from steel slag by ultrasound. *Chemical Engineering and Processing: Process Intensification*, 89:1–8, 2015. ISSN 02552701.

Muhammad Salman, Özlem Cizer, Yiannis Pontikes, Rafael M. Santos, Ruben Snellings, Lucie Vandewalle, Bart Blanpain, and Koen Van Balen. Effect of accelerated carbonation on AOD stainless steel slag for its valorisation as a CO_2-sequestering construction material. *Chemical Engineering Journal*, 246:39–52, 2014. ISSN 13858947.

R. Sander. Compilation of Henry's law constants (version 4.0) for water as solvent. *Atmospheric Chemistry and Physics*, 15(8):4399–4981, 2015. ISSN 16807324.

a Sanna, M Uibu, G Caramanna, R Kuusik, and M M Maroto-Valer. A review of mineral carbonation technologies to sequester CO_2. *Chemical Society reviews*, 43(23):8049–80, dec 2014. ISSN 1460-4744.

A. Santos, M. Ajbary, V. Morales-Flórez, A. Kherbeche, M. Piñero, and L. Esquivias. Larnite powders and larnite/silica aerogel composites as effective agents for CO_2 sequestration by carbonation. *Journal of Hazardous Materials*, 168(2-3):1397–1403, 2009. ISSN 03043894.

Rafael Santos, Marius Bodor, Jens Van Bouwel, Lubica Kriskova, Jan Elsen, Maria Vlad, and Tom Van Gerven. Mineralogical effects on the intensified mineral carbonation of steel slags: kinetics, conversion, basicity and products. In *European Mineralogical Conference*, 2012a.

Rafael M. Santos, Da Ling, Amin Sarvaramini, Muxing Guo, Jan Elsen, Faïçal Larachi, Georges Beaudoin, Bart Blanpain, and Tom Van Gerven. Stabilization of basic oxygen furnace slag by hot-stage carbonation treatment. *Chemical Engineering Journal*, 203:239–250, sep 2012b. ISSN 13858947.

Rafael M. Santos, Davy François, Gilles Mertens, Jan Elsen, Tom Van Gerven, and Tom Van Gerven. Ultrasound-intensified mineral carbonation. *Applied Thermal Engineering*, 57(1-2):154–163, aug 2013a. ISSN 13594311.

Rafael M. Santos, Jens Van Bouwel, Ellen Vandevelde, Gilles Mertens, Jan Elsen, Tom Van Gerven, Jens Van Bouwel, Ellen Vandevelde, Gilles Mertens, Jan Elsen, and Tom Van Gerven. Accelerated mineral carbonation of stainless steel slags for CO_2 storage and waste valorization: Effect of process parameters on geochemical properties. *International Journal of Greenhouse Gas Control*, 17:32–45, sep 2013b. ISSN 17505836.

Rafael M. Santos, Marius Bodor, Paul N. Dragomir, Andreea G. Vraciu, Maria Vlad, Tom Van Gerven, and Tom Van Gerven. Magnesium chloride as a leaching and aragonite-promoting self-regenerative additive for the mineral carbonation of calcium-rich materials. *Minerals Engineering*, 59:71–81, may 2014a. ISSN 08926875.

Rafael M. Santos, Yi Wai Chiang, Jan Elsen, and Tom Van Gerven. Distinguishing between carbonate and non-carbonate precipitates from the carbonation of calcium-containing organic acid leachates. *Hydrometallurgy*, 147-148:90–94, aug 2014b. ISSN 0304386X.

Jacques Schott, Oleg S. Pokrovsky, Olivier Spalla, François Devreux, Alexandre Gloter, and Jerzy A. Mielczarski. Formation, growth and transformation of leached layers during silicate minerals dissolution: The example of wollastonite. *Geochimica et Cosmochimica Acta*, 98:259–281, dec 2012. ISSN 00167037.

W. Seifritz. CO_2 disposal by means of silicates. *Nature*, 345:486–486, 1990. ISSN 0028-0836.

Huiting Shen and E. Forssberg. An overview of recovery of metals from slags. *Waste Management*, 23 (10):933–949, 2003. ISSN 0956053X.

Olga Shtepenko, Colin Hills, Adrian Brough, and Mike Thomas. The effect of carbon dioxide on β-dicalcium silicate and Portland cement. *Chemical Engineering Journal*, 118(1-2):107–118, may 2006.

Kyungsun Song, Sangwon Park, Wonbaek Kim, Chi Jeon, and Ji-Whan Ahn. Effects of Experimental Parameters on the Extraction of Silica and Carbonation of Blast Furnace Slag at Atmospheric Pressure in Low-Concentration Acetic Acid. *Metals*, 7(6):199, 2017. ISSN 2075-4701.

Nikos Spanos and Petros G. Koutsoukos. Kinetics of Precipitation of Calcium Carbonate in Alkaline pH at Constant Supersaturation. Spontaneous and Seeded Growth. *The Journal of Physical Chemistry B*, 102(34):6679–6684, 1998. ISSN 1520-6106.

Gabrielle J. Stockmann, Domenik Wolff-Boenisch, Nicolas Bovet, Sigurdur R. Gislason, and Eric H. Oelkers. The role of silicate surfaces on calcite precipitation kinetics. *Geochimica et Cosmochimica Acta*, 135:231–250, jun 2014. ISSN 00167037.

Joshuah K Stolaroff, Gregory V Lowry, and David W Keith. Using CaO- and MgO-rich industrial waste streams for carbon sequestration. *Energy Conversion and Management*, 46(5):687–699, mar 2005.

J D H Strickland. The Preparation and Properties of Silicomolybdic Acid. III. The Combination of Silicate and Molybdate. *Journal of the American Chemical Society*, 74(4):872–876, 1952. ISSN 8756-8160.

Werner Stumm and James J Morgan. *Aquatic chemistry: chemical equilibria and rates in natural waters*, volume 126. John Wiley & Sons, 2012.

Werner Stumm and Roland Wollast. Coordination chemistry of weathering: Kinetics of the surface-controlled dissolution of oxide minerals. *Reviews of Geophysics*, 28(1):53, 1990. ISSN 8755-1209.

S. J. Talman and H. W. Nesbitt. Dissolution of populations of ultrafine grains with applications to feldspars. *Geochimica et Cosmochimica Acta*, 52(6):1467–1471, 1988. ISSN 00167037.

Rushendra Revathy Tamilselvi Dananjayan, Palanivelu Kandasamy, and Ramachandran Andimuthu. Direct mineral carbonation of coal fly ash for CO_2 sequestration. *Journal of Cleaner Production*, 2015. ISSN 09596526. doi: 10.1016/j.jclepro.2015.05.145.

Sebastian Teir, Sanni Eloneva, and Ron Zevenhoven. Production of precipitated calcium carbonate from calcium silicates and carbon dioxide. *Energy Conversion and Management*, 46(18):2954–2979, nov 2005. ISSN 01968904.

Sebastian Teir, Sanni Eloneva, Carl-Johan Fogelholm, and Ron Zevenhoven. Dissolution of steelmaking slags in acetic acid for precipitated calcium carbonate production. *Energy*, 32(4):528–539, apr 2007. ISSN 03605442.

Sebastian Teir, Tuukka Kotiranta, Jouko Pakarinen, and Hannu-Petteri Mattila. Case study for production of calcium carbonate from carbon dioxide in flue gases and steelmaking slag. *Journal of CO_2 Utilization*, 14:37–46, 2016. ISSN 2212-9820.

B. Terry. The acid decomposition of silicate minerals part II. Hydrometallurgical applications. *Hydrometallurgy*, 10(2):151–171, 1983a. ISSN 0304386X.

B. Terry. The acid decomposition of silicate minerals part I. Reactivities and modes of dissolution of silicates. *Hydrometallurgy*, 10(2):135–150, 1983b. ISSN 0304386X.

S. H. Tian, Y. T. Tu, D. S. Chen, X. Chen, and Y. Xiong. Degradation of Acid Orange II at neutral pH using $Fe_2(MoO_4)_3$ as a heterogeneous Fenton-like catalyst. *Chemical Engineering Journal*, 169(1-3): 31–37, 2011. ISSN 13858947.

Si-cong Tian, Jian-guo Jiang, Kai-min Li, Feng Yan, and Xue-jing Chen. Performance of steel slag in carbonation–calcination looping for CO_2 capture from industrial flue gas. *RSC Advances*, 4(14):6858, 2014. ISSN 2046-2069.

Sicong Tian, Jianguo Jiang, Xuejing Chen, Feng Yan, and Kaimin Li. Direct gas-solid carbonation kinetics of steel slag and the contribution to in situ sequestration of flue gas CO_2 in steel-making plants. *ChemSusChem*, 6(12):2348–55, dec 2013. ISSN 1864-564X.

Sudarat Tinchana, Juntima Chungsiriporn, and Charun Bunyakan. Leaching of Steelmaking Slag using Acetic Acid Solution and Deionized Water for CO_2 Sequestration. pages 45–48, 2012.

Mai Uibu, Rein Kuusik, Lale Andreas, and Kalle Kirsimäe. The CO_2 -binding by Ca-Mg-silicates in direct aqueous carbonation of oil shale ash and steel slag. *Energy Procedia*, 4:925–932, 2011. ISSN 18766102.

N. L. Ukwattage, P. G. Ranjith, and S. H. Wang. Investigation of the potential of coal combustion fly ash for mineral sequestration of CO_2 by accelerated carbonation. *Energy*, 52:230–236, 2013. ISSN 03605442.

N. L. Ukwattage, P. G. Ranjith, and X. Li. Steel-making slag for mineral sequestration of carbon dioxide by accelerated carbonation. *Measurement: Journal of the International Measurement Confederation*, 97:15–22, 2017. ISSN 02632241.

N.L. Ukwattage, P.G. Ranjith, M. Yellishetty, H.H. Bui, and T. Xu. A laboratory-scale study of the aqueous mineral carbonation of coal fly ash for CO_2 sequestration. *Journal of Cleaner Production*, 103:665–674, 2014. ISSN 09596526.

N.L. Ukwattage, P.G. Ranjith, and L. Xin. Steel-making slag for mineral sequestration of Carbon dioxide by accelerated carbonation. *Measurement*, 2016. ISSN 02632241.

Sterling Van der Zee and Frank Zeman. Recovery and carbonation of 100% of calcium in waste concrete fines: Experimental results. *Journal of Cleaner Production*, 2017. ISSN 09596526.

Antonio Velardo, Massimiliano Giona, Alessandra Adrover, Francesca Pagnanelli, and Luigi Toro. Two-layer shrinking-core model: Parameter estimation for the reaction order in leaching processes. *Chemical Engineering Journal*, 90(3):231–240, 2002. ISSN 13858947.

Xiaolong Wang and M Mercedes Maroto-Valer. Integration of CO_2 capture and mineral carbonation by using recyclable ammonium salts. *ChemSusChem*, 4(9):1291–1300, 2011a. ISSN 18645631.

Xiaolong Wang and M. Mercedes Maroto-Valer. Optimization of carbon dioxide capture and storage with mineralisation using recyclable ammonium salts. *Energy*, 51:431–438, 2013. ISSN 03605442.

Xiaolong Wang and Mercedes Maroto-Valer. Integration of CO_2 capture and storage based on pH-swing mineral carbonation using recyclable ammonium salts. *Energy Procedia*, 4:4930–4936, 2011b. ISSN 18766102.

Erich J. Weissbart and J. Donald Rimstidt. Wollastonite: Incongruent dissolution and leached layer formation. *Geochimica et Cosmochimica Acta*, 64(23):4007–4016, 2000. ISSN 00167037.

John Westall. Chemical Equilibrium Including Adsorption on Charged Surfaces. In *Advances in Chemistry*, pages 33–44. 1980. ISBN 0841204993.

John Westall and Herbert Hohl. A comparison of electrostatic models for the oxide/solution interface. *Advances in Colloid and Interface Science*, 12(4):265–294, 1980. ISSN 00018686.

John C Westall. Reactions at the oxide-solution interface: chemical and electrostatic models. In *Geochemical Processes at Mineral Surfaces*, volume 323, pages 54–78. 1986. ISBN 0-8412-1004-7.

Erich Wieland, Bernhard Wehrli, and Werner Stumm. The coordination chemistry of weathering: III. A generalization on the dissolution rates of minerals. *Geochimica et Cosmochimica Acta*, 52(8):1969–1981, aug 1988. ISSN 00167037.

Laurent De Windt, Perrine Chaurand, Jerome Rose, Laurent De Windt, Perrine Chaurand, and Jerome Rose. Kinetics of steel slag leaching: Batch tests and modeling. *Waste management (New York, N.Y.)*, 31(2):225–35, feb 2011. ISSN 1879-2456.

Zhao Jin Wu, Bei Feng Jiang, Wei Ming Liu, Fa Bin Cao, Xing Rong Wu, and Liao Sha Li. Selective recovery of valuable components from converter steel slag for preparing multidoped $FePO_4$. *Industrial and Engineering Chemistry Research*, 50(24):13778–13788, 2011.

Heng Yan, JunYing Zhang, YongChun Zhao, and ChuGuang Zheng. CO_2 Sequestration from flue gas by direct aqueous mineral carbonation of wollastonite. *Science China Technological Sciences*, 56(9): 2219–2227, 2013. ISSN 1674-7321.

Heng Yan, Junying Zhang, Yongchun Zhao, and Rui Liu. CO_2 Sequestration by Direct Aqueous Mineral Carbonation under Low-Medium Pressure Conditions. *Journal of Chemical Engineering of Japan*, 48 (11):937–946, 2015.

Irem Zeynep Yildirim and Monica Prezzi. Chemical, Mineralogical, and Morphological Properties of Steel Slag. *Advances in Civil Engineering*, 2011:1–13, 2011. ISSN 1687-8086.

Juan Yu and Kaibin Wang. Study on characteristics of steel slag for CO_2 capture. *Energy & Fuels*, 25: 5483–5492, 2011.

Yeo Tze Yuen, Paul N Sharratt, and Bu Jie. Carbon dioxide mineralization process design and evaluation : concepts , case studies , and considerations. *Environmental Science and Pollution Research*, 2016. ISSN 0944-1344.

Ron Zevenhoven and Inga Kavaliauskaite. Mineral carbonation for long-term CO_2 storage: An exergy analysis. *International Journal of Thermodynamics*, 7(1):23–31, 2004. ISSN 13019724.

Ron Zevenhoven, Jens Kohlmann, and A Mukherjee. Direct dry mineral carbonation for CO_2 emissions reduction in Finland. In *Proc. of the 27th Int. Conf. on Coal Utilization & Fuel Systems*, volume 127, 2002.

Hui-ning Zhang, An-jun Xu, Dong-feng He, and Jian Cui. Alkaline extraction characteristics of steelmaking slag batch in NH_4Cl solution under environmental pressure. *Journal of Central South University*, 20(6):1482–1489, jun 2013. ISSN 2095-2899.

Huangjing Zhao, Youngjune Park, Dong Hyun Lee, and Ah-Hyung Alissa Park. Tuning the dissolution kinetics of wollastonite via chelating agents for CO_2 sequestration with integrated synthesis of precipitated calcium carbonates. *Physical chemistry chemical physics : PCCP*, 15(36):15185–92, sep 2013.

Daniela Zingaretti, Giulia Costa, and Renato Baciocchi. Assessment of Accelerated Carbonation Processes for CO_2 Storage Using Alkaline Industrial Residues. *Industrial & Engineering Chemistry Research*, 53(22):9311–9324, jun 2014.

List of publications

Peer-reviewed Journals

- **Raghavendra Ragipani**, Sankar Bhattacharya, and Akkihebbal K. Suresh, "Towards efficient calcium extraction from steel slag and carbon dioxide utilisation via pressure-swing mineral carbonation" *Reaction Chemistry & Engineering*, 2018, DOI: 10.1039/C8RE00167G
- **Raghavendra Ragipani**, Sankar Bhattacharya, Akkihebbal K. Suresh, "Kinetics of steel slag dissolution - from experiments to modelling" *Proceeding of Royal Society A: Mathematical, Physical and Engineering Sciences*, 2019, DOI: 10.1098/rspa.2018.0830

Acknowledgement

I express my sincere gratitude to my guides, **Prof. A. K. Suresh** & **Prof. Sankar Bhattacharya** for their valuable suggestions, constant encouragement and personal guidance during the course of this work. I would like to take this opportunity to thank **M/s JSW** & industry supervisor **Dr. Suman Majumdar** for project funding and providing steel slag samples for experimentation.

My sincere thanks to all my lab mates and friends for their constant support and advice.

Raghavendra Ragipani